ÉCOLE POLYTECHNIQUE DE BRUXELLES
UNIVERSITÉ LIBRE DE BRUXELLES

VRIJE UNIVERSITEIT BRUSSEL

Characterization of a light petroleum fraction produced from automotive shredder residues

Thesis presented by Steven TIPLER

with a view to obtaining the PhD Degree in Engineering Sciences and Technology (ULB - "Docteur en Sciences de l'Ingénieur et Technologie") and in Doctor of Engineering Sciences (VUB)

Année académique 2020-2021

Supervisors : Professor Axel COUSSEMENT (Université libre de Bruxelles)
Aero-Thermo-Mechanics Laboratory
and Professor Francesco CONTINO (Vrije Universiteit Brussel)
Fluid Mechanics and Thermodynamics research group

Avec le soutien de la Wallonie

ABSTRACT

Wastes have a real potential as being players in the energy mix of tomorrow. They can have a high heating value depending on their composition, which makes them good candidates to be converted into liquid fuel via pyrolysis. Among the different types of wastes, automotive residues are expected to rocket due to the increasing number of cars and the tendency to build cars with more and more polymers. Moreover, the existing regulations concerning the recycling of end-of-life vehicles become more and more stringent.

Unconventional fuels such as those derived from automotive shredder residues (ASR) have a particular composition which tends to increase the amount of pollutants comparing with conventional fuels. Relying on alternative combustion modes, such as reactivity controlled compression ignition (RCCI), is a solution to cope with these pollutants.

In RCCI, two types of fuels are burned simultaneously, namely a light fraction with a low reactivity, and a heavy fraction with a high reactivity. The heavy fraction governs the ignition as it is injected directly in the cylinder close to the end of compression. A variation of its ignition delay could impact the quality of the combustion. Nevertheless, this issue can be tackled by adjusting the injection timing.

As long as the low reactivity fuel is concerned, such a solution cannot be adopted as its reactivity depends on the initial parameters (equivalence ratio, inlet temperature, exhaust gas recirculation ratio). However, if the fuel is too reactive, it could create knock that have a dramatic impact on the engine, leading to damages. Thus, being able to predict its features is a key aspect for a safe usage. Predicting methods exist but had never been tested yet with fuels derived from automotive residues.

With petroleum products, usual prediction methods stand at three different levels: the chemical composition, the properties, and the reactivity in an appliance. The fuel is studied at these three levels. First, the structure gives a good overview of the fuel auto-ignition. For instance, aromatics tend to have higher ignition delay time (IDT) than paraffins. Second, the octane numbers are good indicators of the fuel IDT and of the resistance toward knock. Precisely, the octane numbers depict the resistance of a fuel towards an end-gas auto-ignition. Last, the IDT was studied in a rapid compression machine and a surrogate fuel was formulated. Surrogate fuels substitute real fuels during simulations because real fuels cannot be modelled by kinetic mechanisms due to their complexity.

The existing methods to estimate the composition were updated to predict the n-paraffin, iso-paraffin, olefin, napthene, aromatic and oxygenate (PIONAOx) fractions. A good accuracy was achieved compared with the literature. This new method requires the measurement of the specific gravity, of the distillation cut points, of the CHO atom fractions, of the kinematic viscosity and of the refractive index.

Two methods to predict the octane numbers were developed based on Bayesian inference, principal component analysis (PCA) and artificial neural network (ANN). The first is a Bayesian method which modifies the pseudo-component (PC) method. It introduces a correcting factor which corrects the existing formulation of the PC method to increase its accuracy. A precision of more than 2% is achieved. The second method is based on PCA and ANN.

41 properties are studied among which reduced set of principal variables are selected to predict the octane numbers. 10 properties calculated only with the distillation cut points, the CHO atom fraction and the specific gravity were selected to accurately predict the octane numbers.

Measurements of the IDT in a rapid compression machine (RCM) of a fuel produced from ASR were realized. They are the first measurements in such a machine ever made. This provide experimental data to the literature. Moreover, these experimental data were used to formulate a surrogate fuel. Surrogate fuels can be used to realize simulations under specific conditions.

The current thesis investigates fuels derived from ASR. It was showed that this fuel can be burnt in engines as long as their properties are carefully monitored. Among others, the IDT is particularly important. Nevertheless, additional experimental campaigns and simulations in engine are required in order to correctly assess all of the combustion features of such a fuel in an engine.

Science has not yet taught us if madness is or is not the sublimity of intelligence.

— Edgar Allan Poe [1]

ACKNOWLEDGMENTS

First of all, I would like to thank Prof. Axel Coussement and Prof. Francesco Contino for giving me this opportunity of conducting a PhD thesis and who plan a route to success. Thank you for your human and scientific skills. You believed in me and you were always positive, giving a vision and keeping me on track. Additionally, it was always interesting to discuss with you about research. Thanks also to Prof. Alessandro Parente with who I initially started this journey. Thanks to all of you, to Prof. Gérard Degrez and Prof. Patrick Hendrick for giving me the opportunity to teach, which was another appreciable aspect of my work.

Research is not possible without appropriate funding. I thank the Walloon region without which nothing would had been possible. I also thank the Fonds Renard which allowed me to carry out experimental campaign.

I thank the jury members for having accepted to review the current thesis and for their insightful comments and questions.

A single person is nothing without a team. I would like to thank all the colleagues in the Aero-Thermo-Mechanics department and in the FLOW research group. I always appreciated crossing your paths and discussing with you. Special thoughts to the technical team, Adrien Fita-Codina, Pascal Beine, Lionel Lambert, Yves Simon, Narcisse Yoppa, Florent Biname, Abdelouahid Tarhach, with whom I spend my days especially during my first years. Thank you Adrien Fita-Codina, I now tend to have a right hand, instead of having two left ones. I also appreciated these philosophical discussions of which you have the secret. Thank you to Olivier Berten for his encouragement and his enthusiasm and to Shirley Wayne, Joëlle Humbert and Anne De Gelas for their administrative support and their kindness. Additionally, I enjoyed my later years as a teaching assistant with Maryam Khaji and Rafi Malik. Thank you for having integrated me along to your sides. I cannot talk about the research team without mentioning my room mates, Dr. Marco Ferrarrotti, Dr. Praskovia Milova, Mayo Abeyo and Maxime Remacle. I owe Dr. Magnus Fürst and Giuseppe D'Alessio for having introduced me to the world of uncertainty quantification and machine learning. I thank Dr. Maxime Pochet for the discussions and lights he gave me on power-to-fuel and on HCCI piston engine, Dr. Nicolas Bourgeois for having supported

me when dealing with rapid compression machine, and Dr. Subir Bhaduri for having introduced me to experimental uncertainty quantification and experimental testing.

International exchange is of major importance in research. I thank the PC2A department from the University of Lille without who the experimental campaign could not have been possible. I thank Pr. Guillaume Vanhove for his knowledge and his confidence. Thank you for being such a perfect host. I also thank Carolina Mergulhao who mastered the rapid compression machine installation and lead the experimental campaign. Thank you to the rest of the PC2A department including Dr. Hwasup Song and the technical staff. Thanks are also due to Dr. Steffen H. Symoens, Dr. Marko R. Djokic, and Prof. Kevin M. Van Geem from the Laboratory for Chemical Technology of Ghent University, for the measurements in comprehensive two-dimensional gas chromatography and who also provided their precious knowledge on this technology. My adventure as a PhD student also brought me to the Physikalisch-Technische Bundesanstalt where Pr. Ravi Fernandes received me together with Dr. Kai Moshammer. Thank you also to Sonal Vallabhuni for the experimental campaign that was carried out.

Engineering comes with project management and teaching. Then, I also have to mention and thanks master students – Julien Schiltz, Simon Judée and Taici Botelho – who undertook their master thesis along with me and my research subject, and interns – Martin Pascal, Loïc Coriton, Nathan Gil and Aymane Bensalimane – who contributed to numerical and experimental work. Thanks are also due to the Teaching in English for Academics (TEA) project, more specifically to Nell Foster and to Kelsey Hull, for supporting me with English speaking and writing. This kind of project supported by the Fonds d'Encouragement pour l'Enseignement (FEE) is a real chance for Academics.

Finally, nothing would had been possible without my loved ones. Thank you mum and dad for having tough me the taste of effort. Thank you Carl, for having developed my curiosity towards science. Finally, thank you Eléonore who supported me and who always believed in me.

CONTENTS

LIST OF FIGURES

LIST OF TABLES

ABS	acrylonitrile butadiene styrene
AD	Anno Domini
AF_s	air-to-fuel ratio under stoichiometric conditions
AKI	antiknock index
ANN	artificial neural network
API	American Petroleum Institute
AP	Aniline point
ASR	automotive shredder residues
ASTM	American Society for Testing and Materials
BC	before Christ
BON	blending octane number (ON)
BMON	blending MON
BRON	blending RON
CAI	controlled auto-ignition
CCI	Calculated cetane index
CFR	cooperative fuel research
CHP	combined heat and power
CI	compression ignition
CN	cetane number
CNG	compressed natural gas
CO	carbon monoxide
COP	conference of the parties
CR	compression ratio
DCN	derived cetane number
DI	direct injection
DI	diesel index
DME	dimethyl ether
EA	elemental analyzer
ECU	electronic control unit
EGR	exhaust gas recirculation
ELV	end-of-life vehicle
EPDM	ethylene propylene diene monomer
CG	Coryton gasoline
FACE	fuels for advanced combustion engines
FAME	fatty acid methyl esters
FID	flame ionization detector
GC	gas chromatography
GC × GC	comprehensive two dimensional gas chromatography
H/C	hydrogen to carbon ratio
HCCI	homogeneous charge compression ignition
HG	Halterman gasoline
HRR	heat release rate
HSN	Haltermann straight naphtha
HTC	high temperature chemistry
IDT	ignition delay time

IEA international energy agency

IQT ignition quality tester

IMEP indicated mean effective pressure

KLSA knock limited spark advance

K_W Watson K factor

LHS latin hypercube sampling

LPG Liquefied petroleum gases

LTC low temperature chemistry

MABP molal average boiling point

MeABP mean average boiling point

Mm molar mass

MS mass spectrometry

MON motor octane number

MSE mean squared error

MW molecular weight

NCD nitrogen chemiluminescence detector

NMR nuclear magnetic resonance

NOx nitrogen oxides

NTC negative temperature coefficient

O/C oxygen to carbon ratio

OI octane index

PBT polybutylene terephthalate

OECD Organisation for Economic Cooperation and Development

ON octane number

OS octane sensitivity

PA polyamide

PC polycarbonate

PC pseudo-component

PC principal component

PCA principal component analysis

PC2A Physico-Chimie des Processus de Combustion et de l'Atmosphère

PDF probability density function

PE polyethylene

PIONA n-paraffin, iso-paraffin, olefin, napthene, aromatic

PIONAOx n-paraffin, iso-paraffin, olefin, napthene, aromatic and oxygenate

PNA n-paraffin, napthene and aromatic

PP polypropylene

PPRR peak pressure rise rate

PRF primary reference fuel

PS polystyrene

PVC polyvinyl chloride

PUR polyurethane

RCCI reactivity controlled compression ignition

RCM rapid compression machine

RF response factor

Ri refractivity intercept

RI ringing intensity

RON research octane number

SALN Saudi Aramco light naphtha

SARA	saturates, aromatics, resins and asphalthenes
SCD	sulfur chemiluminescence detector
SG	specific gravity
SI	spark ignition
SOAOx	saturate, olefin, aromatic, oxygenate
SOC	substance of concern
TDC	top dead center
TEL	tetraethyllead
TOF	time of flight
TRF	toluene reference fuel
VABP	volume average boiling point
VGC	viscosity gravity constant
VGF	viscosity gravity function
WABP	weight average boiling point
WDF	waste derived fuel
WEO	world energy outlook

1 INTRODUCTION

1.1 CONTEXT

1.1.1 *Energy mix*

Global warming is one of the most central issues of our century. It is a consequence of emissions from human activities, which depend mainly on our energy mix. To control emissions adequate energy policies must be implemented to limit global warming. To reach this objective a scenario and an ecological aim must be defined.

One such energy policy is the Paris agreement which is an universal agreement made during the 21st conference of the parties (COP). Its purpose is to limit the global temperature from increasing below 2°C in 2100 compared with the pre-industrial levels.

The world energy outlook (WEO) provides scenarios that assess the consequences of different energy policies. Three scenarios are studied: New Policies, Current Policies, and Sustainable Development. The New Policies Scenario takes into account the ambitions of today according to the Nationally Determined Contribution of the Paris Agreement by including announced policies. The aim of this scenario is to provide the direction in which existing policy frameworks and today's policy ambitions would take the energy sector out to 2040. In the Current Policies Scenario, the existing laws and regulations are considered so that there is no change in policies from today. This scenario gives a picture of how global energy markets would evolve if governments make no changes to their existing policies. In the Sustainable Development Scenario, the objective of the Paris Agreement are considered achievable so then calculations are made to define how this objective could be achieved. The objective being to outlines a major transformation of the global energy system to meet goals related to climate change. More information on the three scenarios are available in the WEO-2018 [35].

The New Policies Scenario and the Sustainable Development Scenario are particularly interesting as the difference between them corresponds to the missing part of renewables between the expected policies and the objective, which is staying well below 2°C. To reach this objective, the energy mix must allow the greenhouse gas emissions to fall to zero by 2065 [35, 36].

It is evident that the energy mix questions the way we produce energy. The energy mix between 2010 and 2019 is reported on Figure 1. One of these potential energy sources, namely wastes, will be further explored.

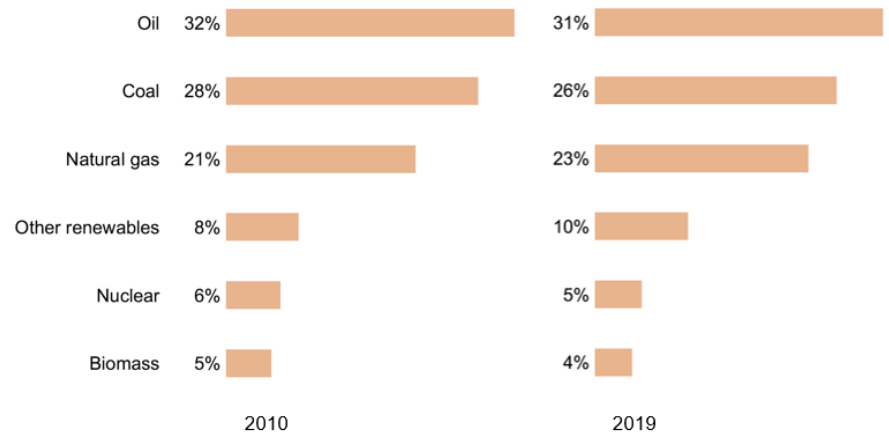

Figure 1: Evolution of the fuel share between 2010 and 2019 [2]. The energy mix remains almost constant although there is a slight increase in renewable energies.

1.1.2 *The potential of wastes*

The heating value of wastes ranges between 7300 and 10000 kJ/kg [37] which makes them a very good candidate to be burnt to recover their energy content. Although there is a potential in producing energy from waste, only 1.2% (almost 130 000 GWh [38]) of the electricity was produced from wastes in 2018 in the Organisation for Economic Cooperation and Development (OECD) countries [39]. The production of energy from wastes, or waste-to-energy, remains thus marginal.

Managing wastes is one of the key challenges of the Twenty First century [40]. Wastes come from materials that are considered useless. At first, the disposal of waste was not an issue as plenty of space was available. Nevertheless, the population growth and the consumerist society has led to an increasing amount of waste that has to be handled. In 2016, 2.01 billion tonnes of municipal wastes were generated in the world of which 242 million tonnes was plastic wastes [3]. Waste generation is expected to reach 3.40 billion tonnes by 2050. The repartition of wastes by region is reported on Figure 2.

Samples of garbage can be sorted into categories to define their composition. While the composition of wastes vary depending on the income level of the country, food and greens always compose the highest part. Moreover, it is noteworthy that the plastic content increases with the income level of the country.

For disposing of wastes, several methods exist such as open dump, landfill, composting, recycling, anaerobic digestion and incineration. Recycling tends to be used more in developed countries while open dump is still present in countries with lower income levels. Wastes contribute about 5 percent to global warming due to the emission of greenhouse gases (mainly CH_4) when they are disposed of in open dumps or landfills without a gas collection system.

Today, the field of waste usage is particularly evolving to reuse old matter. Additionally, biomass and municipal waste are sectors that are particularly dynamic. Municipal solid waste is a type of biomass which is mainly composed of food waste, paper, wood, plastics, textiles, metals and glass. Improper management of municipal wastes causes hazards to inhabitants,

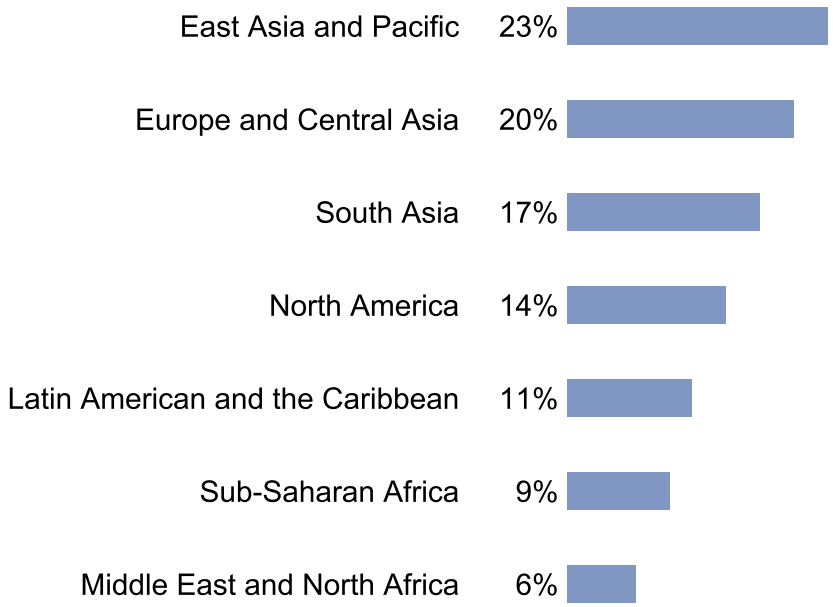

Figure 2: Waste generation by region[3]. High income countries account for only 16 percent of the population in the world but generate 34 percent of the wastes.

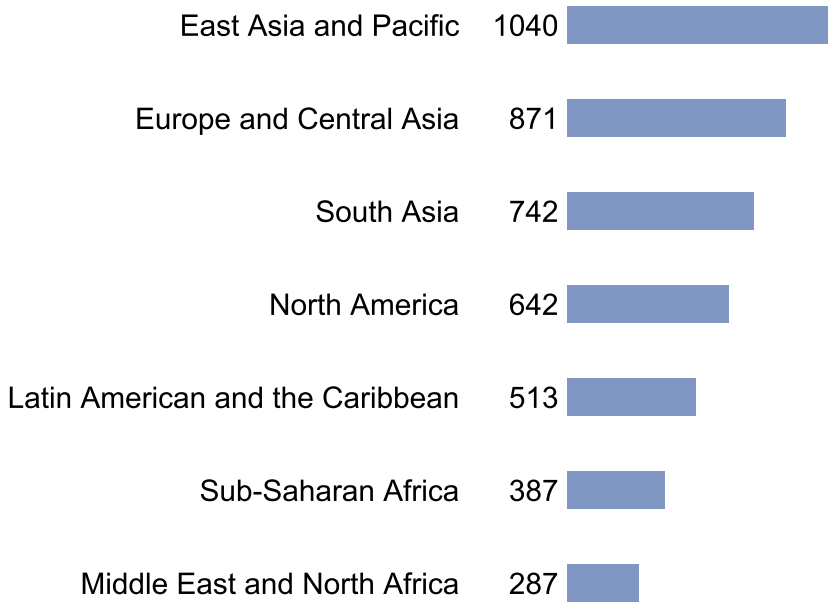

Figure 3: Energy content (in Million of MWh) of wastes calculated with a heating value of 8000 kJ/kg [3]. There is a real potential in exploiting waste as an energy source.

which explains the recent interest in this type of wastes. For example, recent studies evaluate the status and identify the major problems of waste management in several cities in India [41] and Kenya [42]. As a solution, these wastes could be turned into fuels by gasification. Mathematical models were recently developed to simulate the gasifier of municipal wastes to produce syngas [43].

To conclude, up until now dumping has been the first choice as waste processing has a high economical and financial cost. Nonetheless, the conventional and conservative perceptions towards wastes are being challenged as they are synonymous to financial losses, and, moreover, impact the environment, leading to subsequent sanitation and financial costs. In addition, the perceived benefits are numerous, including social, economical and environmental security. Thus, waste recycling has promoted an optimistic public opinion [44–46].

1.1.3 *Wastes from automotive residues*

Among the different types of wastes, the number of end-of-life vehicle (ELV) increased over the years until 2012 with a rate estimated at 2.25 %/y [5]. From 2012 to 2015, this number converged and remained nearly constant with an average of six million units [47]. To limit the environmental impact of ELV, Europe enforced new policies (European Directive 2000/53/EC [47]). For example, the reprocessing of wastes into new products and the use of wastes to replace raw matters are enhanced by the European objectives for the ELV: the recycling mass rate (85%) and the recovery mass rates (95%), respectively. Recycling means the reprocessing in a production process of the waste materials for the original purpose or for other purposes but excluding energy recovery. A list of recovery operation is summarized in Annex IIB of Directive 75/442/EEC. Some of these operations are listed thereafter. They are the use of the waste to produce energy, regeneration of solvent, acids or bases, recycling of organic substances, metals, inorganic materials, recovery of components used for pollution abatement, recovery of components from catalysts, oil re-refining and land treatment. Today, according to the end-of-life vehicle statistics published by the European Commission, the mean recycling mass rate in Europe has reached 85.7% but the mean recovery mass rate has reached only 91.3% [4]. Moreover, some countries do not fulfil their recycling and recovery rates (Figure 4).

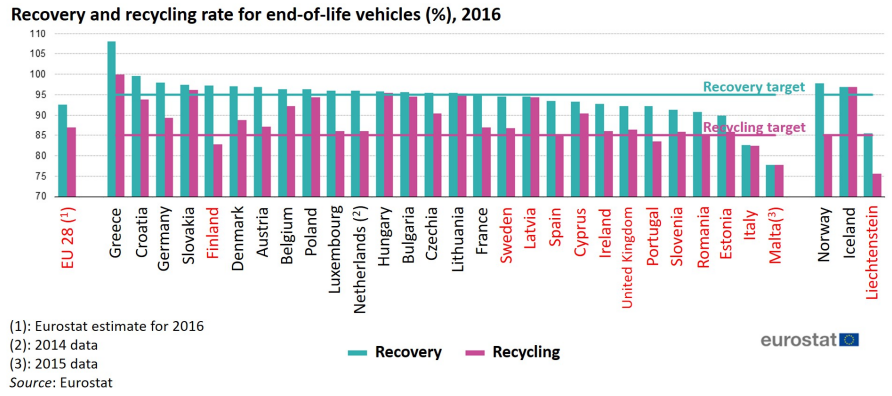

Figure 4: Recovery and recycling rate for end-of-life vehicles, 2016. Countries in red do not fulfil one of the European Targets. [4]

There is a need to efficiently recycle ELV. The amount of wastes from cars has increased due to the number of cars that has grown very rapidly since the beginning of the 19th century [48]. Some 500 million cars joined the global car fleet between 2000 and 2017 [35] and approximately 6% reach their end of life annually. Moreover, we expect a change in the vehicle composition with the use of lighter materials. This change in the automotive sector will increase the need to efficiently recycle ELV [48]. The process of recycling cars will be further examined below.

The amount of ELV has reached more than 40 million units per year [49]. The first step to recycle ELV is the dismantling for direct resale. Over the total of ELV, approximately 80% goes in a dismantling facility. Then, the usable parts are removed and refurbished for direct resale and reuse.

Automotive shredders were introduced in the early 1960s [50]. A shredder is a large hammer mill that tears up the car hulk into chunks of materials. Then, air classification sorts light fractions which is followed by the recovering of ferrous metals with magnets. Subsequently, trommels are used to remove small particles and non-ferrous metals are recovered with eddy-current separators. The ferrous fraction represents around 70-75% of the total shredded output and non ferrous metals represent about 5%. The remaining is the so called automotive shredder residues (ASR). This fraction is expected to increase in the future due to the increasing amount of polymers to decrease the vehicle weight and consumption.

About 15 million tons of shredder residues are produced each year [48]. Shredder residues are composed of a lot of various materials. Among others, it is composed of metals, plastics, foam and rubber, fabrics, glass, automotive fluids, wood, sand, moisture. The composition strongly depends on the raw matter to produce the residues, which ultimately makes the final residues different from one another.

However, shredder residues are composed of approximately 40-50% of material based on hydrocarbons. Plastics and rubber can be recovered via an appropriate separation technique. The separation technique exploits the differences in the properties of the materials (size, shape, color, porosity, density, brittleness, magnetic property, solubility, reactivity, resistivity ...). At least five operations are required to recover the materials: separation of (1) the polymers from the residues, (2) plastics and rubber from the polymers, (3) wood and rubber from the plastics, (4) differentiation of the plastics, (5) removal of the substance of concerns (SOCs). After separation, the materials can be recycled into primary products or secondary products.

If the materials are not recycled, incineration is often used. The combustion of shredder residues for energy recovery, such as incineration, is cost-effective because of the high heating value of the residues (9000-14000 kJ/kg [48]). To produce electricity, the residues can also be converted into liquid and gaseous fuels via pyrolysis, gasification, hydrolysis, selective dissolution, hydrogenation, and de-polymerization. This is also called chemical recycling. The current thesis especially focuses on this type of recycling.

Several methods exist to produce fuel from shredder residues. The main two processes are discussed below: gasification and pyrolysis. Gasification is a process where organic content is converted into CO, H_2, CO_2 and light hydrocarbons. Air and water are supplied to the reactor in conditions that allows partial oxidation. The fuel studied in the current thesis is produced by pyrolysis. Pyrolysis is the decomposition of organic content in an inert atmosphere via the action of high temperatures. It allows the production of fuel from organic feedstock. In practice, the pyrolysis of

shredder residues produces oil, gas and a solid residue. The analysis of the pyrolysis of each product considered separately allows us to estimate the final product of the pyrolysis. Shredder residues are composed of polymer such as polyethylene (PE), polyvinyl chloride (PVC), and polystyrene (PS). The pyrolysis of PE gives hydrogen, benzene, methane, ethylene, propane; PVC gives benzene, acetylene, styrene and hydrogen chloride; PS gives styrene, benzene, toluene and methyl-styrene. Several pyrolysis processes exist [50] such as the Siemens-KWU process where the pyrolysis is followed by combustion of the products for steam generation. The Batrec Process combines pyrolysis with a mechanical separation of the metals. The Takuma process where the pyrolysis is followed by the sorting of the solids. The citron oxyreducer process consists of a large-scale plant where gases are produced and the metals are reduced to their elemental state.

1.2 FUELS PRODUCED FROM AUTOMOTIVE SHREDDER RESIDUES

The recycling and the recovery of ELV are the result of a complex process. In Belgium, the company Comet Traitements and their partners use a chemical process to increase the recovery rate of ELV (Figure 5). With this innovative process, Comet Traitements converts ASR from the processing of ELV into a crude oil-like fuel. After the shredding of ELV, approximately 70-75% of the matter is recovered as ferrous and 5% as non-ferrous metals [5, 49]. ASR can reach up to 25% of the ELV with only 15% recovered with the more advanced processes [49]. As illustrated in Figure 5, some techniques can reach levels as low as 4.5% [5]. ASR are composed of rubbers and foams (ethylene propylene diene-monomer EPDM, polyurethane PUR), polyolefins plastics (polypropylene PP, polyethylene PE), styrenic plastics (acrylonitrile butadiene styrene ABS, polystyrene PS) and other thermoplastics (polyvinylchloride PVC, polycarbonate PC) [50], which make them good candidates to be converted into liquid fuels thanks to pyrolysis. More information on pyrolysis is available in section 2.4.

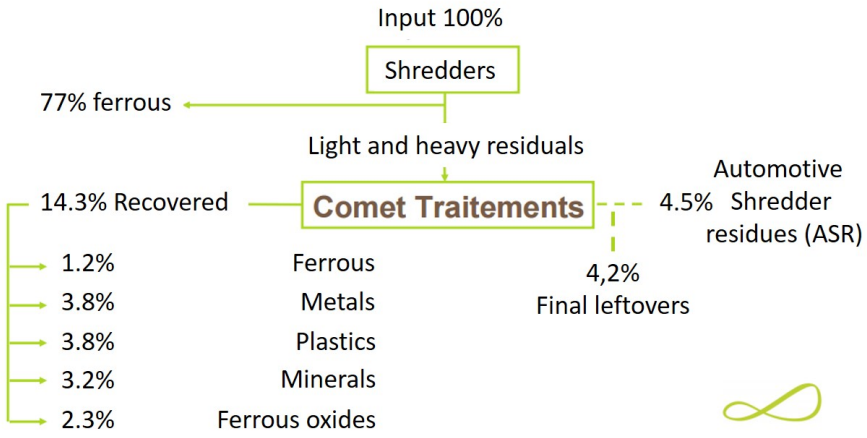

Figure 5: Recovery process by the Belgian company Comet Traitements [5].

The process to convert the ASR into liquid fuels will now be described (Figure 6). First, the ASR are dried (in a drier as the one on Figure 7) and the dust is removed. After a pyrolysis, the crude-oil like fuel is mixed with 6% of NaOH. This blend is heated in order to remove the inorganic compounds which are composed of silica. This first step is of crucial importance as

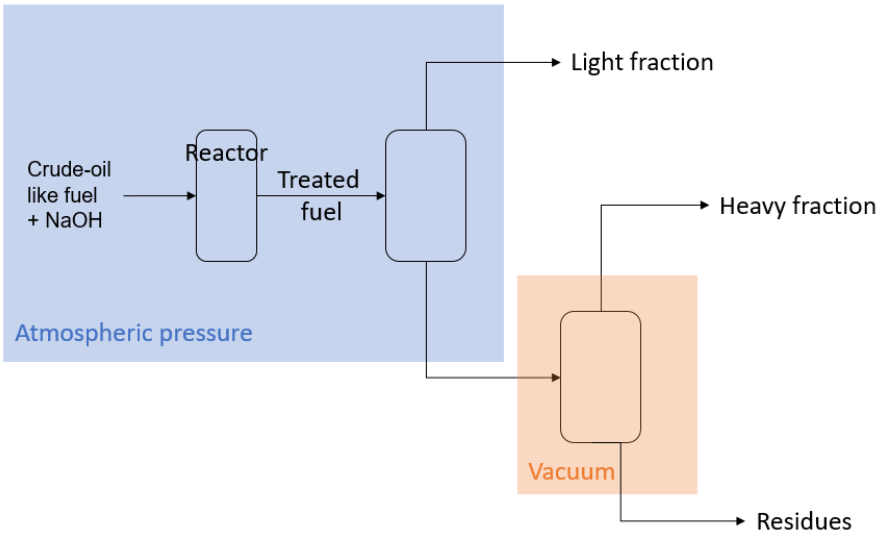

Figure 6: Process of purification and distillation

will be shown in the current thesis. Then, a first distillation occurs under atmospheric pressure in order to extract the light fraction of the crude-oil. Finally, a second distillation under vacuum pressure results in the extraction of the heavy fraction. The mass balance is 50kg/h of feedstock resulting in 15kg/h of light hydrocarbon fraction mixed with water, 25kg/h of heavy hydrocarbon fraction and 10kg/h of heavy residuals.

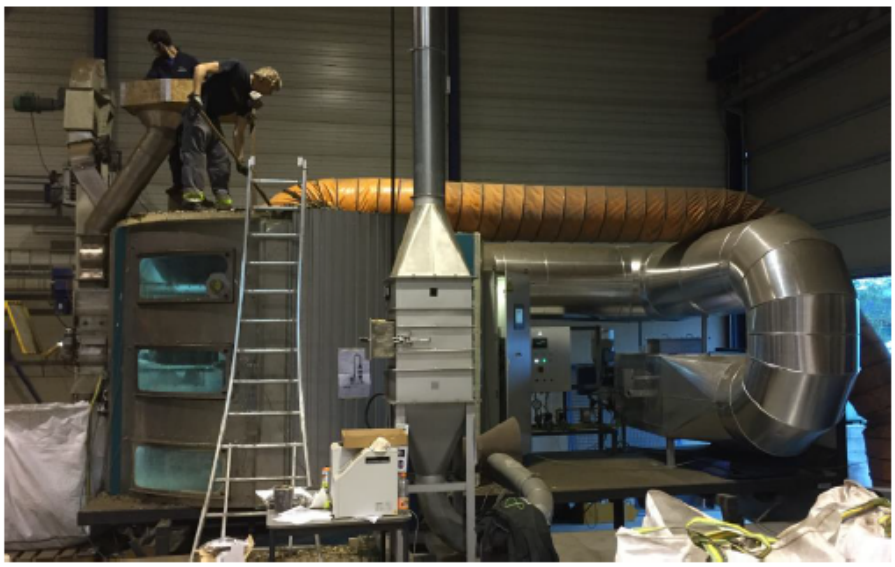

Figure 7: Drier of the company Technic One (Thimister). The matter is dried at a low temperature on two rotating disks.

The different types of raw matter and the pyrolysis and distillation parameters give fuels with a variable set of properties. These differences are discussed on Table 1 for the light fraction and Table 2 for the heavy fraction.

First, we can observe a big difference in the silica and chlorine concentrations between the different feedstocks. For instance, the samples 801LJ02 (light fraction) and 801LJ03 (heavy fraction) show very low concentration in contrast with the other fuels. This can be explained by a modification of

the process which embeds a preprocessing of the fuel with NaOH especially developed to remove the silica. Secondly, we observe major differences in the kinematic viscosity between the fuel, especially for the heavy fractions. As a comparison, the viscosity can be compared with the viscosity of the regulation NF EN 590 where it should be between 2.00 and 4.50 mm^2/s at 40°C. The process should be further understood in order to avoid such a variation of the viscosity. The lower heating value is particularly high which is interesting from an energetic point of view. The composition of the fuel is expected to change as showed by the carbon, hydrogen and oxygen fluctuations. Additionally, the calculated cetane index validates high changes in the fuel composition as it fluctuates from 23 to 37 whereas the diesel standard requires a calculated cetane index of 46. This shows that the fuel has a lower reactivity due to a higher share of aromatic components and substituted molecules. The density is also a good indicator which testifies that the composition is composed of higher fractions of aromatics for the fuels with the higher density. This density fluctuates a lot, especially for the heavy fraction with a minimum of 823.2 kg/m^3 and a maximum of 925.6 kg/m^3. The density according to the diesel standard has to be between 820 and 845 kg/m^3. The density of all the heavy fractions are higher than these limits, which show the peculiar composition of the fuel with a high fraction of heavy compounds. The fluctuation of the refractive index is the last property that characterizes the composition. Indeed, aromatic compounds have higher refractive index than aliphatic molecules. Nevertheless, the refractive index was only measured for two light fractions and two heavy fractions, so the complete span over all the fuels cannot be observed.

Ref.	504LJ03a	612LJ01	801LJ02
Si (ppm)	788		77
Na (ppm)	28		0
Cl (ppm)	1011		162
Br (ppm)	<20		<20
F (ppm)	20.4		<10
S (ppm)	321		900
Kinematic viscosity at 40°C (mm^2/s)	0.8477	0.662	0.889
Lower heating value (MJ/kg)	41.110		
C %w	82.9	84.7	
H %w	11.74	12.37	
O %w		1.91	
Density at 15°C (kg/m^3)		796.1	810.2
Refractive index at 20°C		1.4419	1.4510

Table 1: Properties of three light fractions produced from automotive shredder residues by the Belgian company Comet Traitements.

The last property discussed in this section is the distillation curve (Figure 8 and Figure 9). We observe wide a span of the points over the distillation. More particularly, the light fraction exhibit an abrupt raise with very high temperatures to evaporate the last fractions.

To sum up, the fuel has a kinematic viscosity, a density and a calculated cetane index that are not in accordance with the regulation of conventional diesel. In terms of final application, the viscosity and the density are related to the whole injection system where a particular attention has to be paid for the high pressure pump and for the common rail. A too high viscosity may lead to fuel pump damage due to a too high pressure while a too low

Ref.	504LJ04a sup	604LJ07	801LJ03	805LJ05	C24
Si (ppm)	373	438	1	1742	
Na (ppm)	25	<30	0	0	
Cl (ppm)	923	841	34	683	
Br (ppm)	63.8	186	<20	33	
F (ppm)	11.9	5.2	<10	135	
S (ppm)	427	486	90	757	
Kinematic viscosity at 0°C (mm^2/s)	201.4				
Kinematic viscosity at 40°C (mm^2/s)	4.446	3.407	1.270	1.619	2.287
Kinematic viscosity at 100°C (mm^2/s)	1.783	1.16			
Lower heating value (MJ/kg)	40.195				
C %w	82.5	83.9			
H %w	11.89	10.16			
O %w	3.94	3.37			
Calculated cetane index	36.6	24.6	37.0	33	23
Density at 15°C (kg/m^3)	878.9	925.6	823.2	859.4	890.2
Refractive index at 20°C			1.4575	1.4736	

Table 2: Properties of five heavy fractions produced from automotive shredder residues by the Belgian company Comet Traitements.

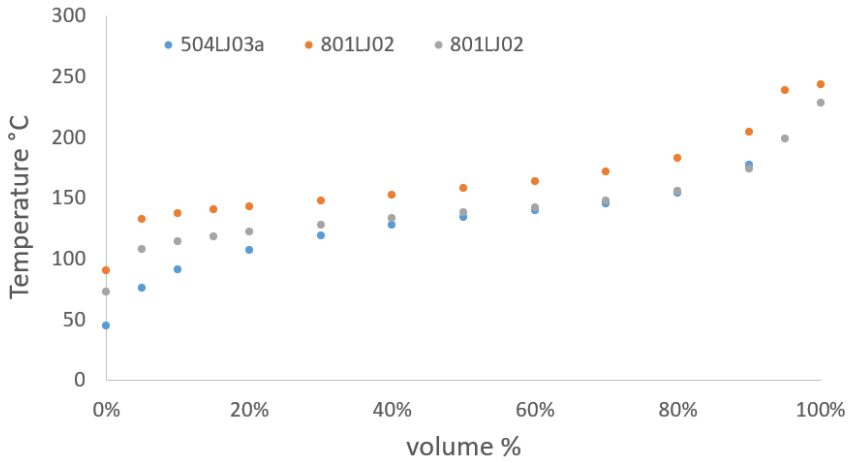

Figure 8: Distillation curve of three light fractions.

viscosity may lead to a lack of lubrication. Additionally, the viscosity is related to the fuel injection and to the atomization in the cylinder, so it is directly linked with the combustion process. Concerning the evaporation curve, its high value could be problematic, especially to evaporate the light fraction as being injected via a port fuel injector in the air during the reactivity controlled compression ignition (RCCI) process. The cetane index is a critical property which is linked with the auto-ignition delay of the fuel. The higher is cetane number, the lower is the ignition delay. Here, the calculated cetane index is too low comparing with conventional diesel. Therefore, relying on a programmable electronic control unit (ECU) would be needed to adapt the injection timing by injecting the fuel earlier so that it has enough time to react. Other important properties could be further studied such as the enthalpy of vaporization that could have an impact on the ignition delay due to a different in-cylinder temperature. This is could also lead to cold start

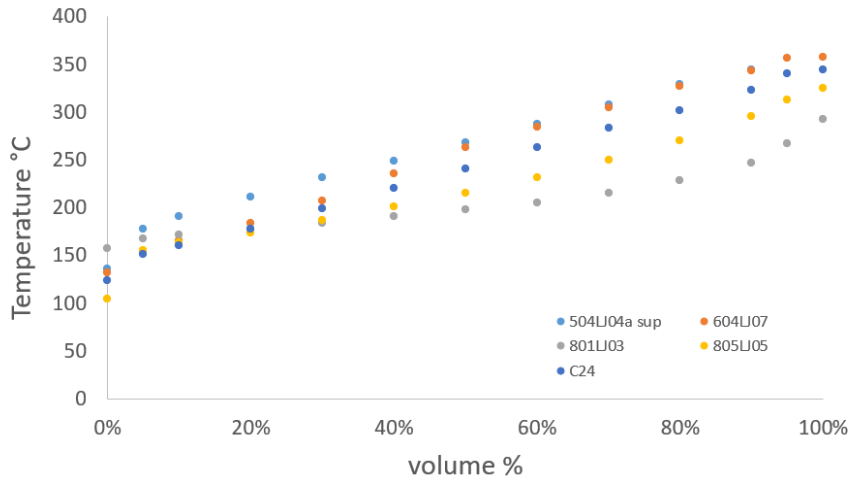

Figure 9: Distillation curve of five heavy fractions.

problems, which could be solved by starting the engine with a conventional fuel.

1.3 COMBUSTION CONSIDERATIONS

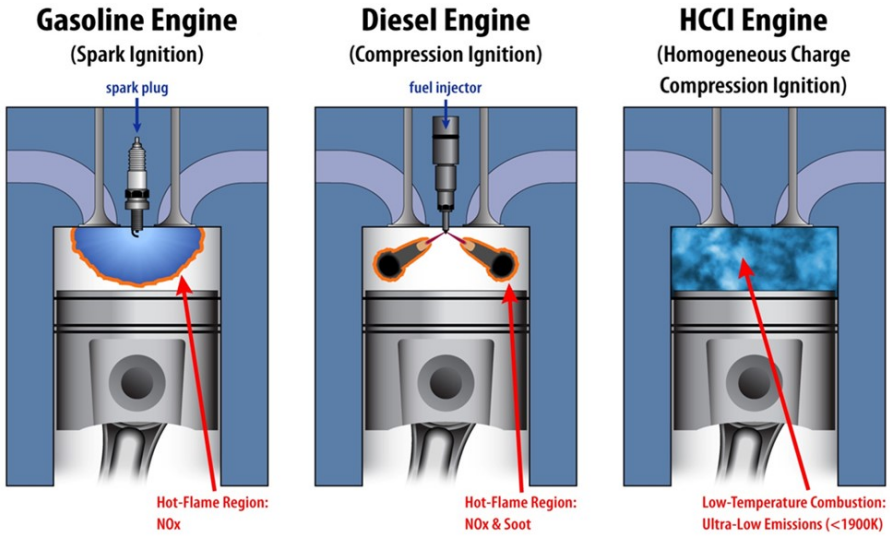

Figure 10: The Homogeneous Charge Compression Ignition (HCCI) combustion mode emits lower levels of pollutant than conventional gasoline and diesel engines. [6]

As far as ASR are concerned, the fuel production plant is owned by a recycling company, so small-scale production plants play a role in the production process. To achieve profitability, small-scale production plants could require a high energy yield. When the heat demand is low, combining heat recovery with electric generation, i.e. combined heat and power (CHP), is the best configuration for ensuring a high energy yield. The production of electricity often goes with piston engines or turbines. We have studied engine conditions for the following reasons. First, the current market offers a wide variety of piston engines, from low (kW) to high (several MW) powers. On

the other side, the power of turbines is most often higher than piston engine. Research on micro-turbine is currently increasing [51], but, piston engines have better efficiency. Second, the properties of the ASR fuels fluctuate over time when the raw matter is modified. The properties are driven by the content of the raw materials, by the cracking conditions and by the distillation parameters which depend on technical and financial constraints [52]. Some of these properties impact turbines more than engines. For instance, the viscosity and the evaporation quality affect the fuel atomization [53], which is more critical for a turbine than an engine. For an engine, this is also important for fine tuning. Third, the produced quantity of fuel also fluctuates over time. The input power affects the operating condition more with a turbine than an engine because the efficiency loss is higher at part load. Similarly, starts and stops are easier with piston engines, which permits extreme fluctuations if the production stops. Fourth, engine cylinders are more robust than turbine blades regarding coating, layer deposits and heteroatom attacks [54]. Last, advanced combustion engines, such as homogeneous charge compression ignition (HCCI) or RCCI engines, offer an increased efficiency and reduced level of pollutants.

1.4 COMPRESSION IGNITION AND SPARK IGNITION

As a light fraction and a heavy fraction are produced after the distillation process, the two fuels could be burnt separately in a spark ignition (SI) and in a compression ignition (CI) engine, respectively.

The performance of SI engines will be discussed before moving onto CI. The first gasoline engine was built in 1876 by Nicolaus Otto. Today, passenger cars are mostly (>80%) powered by SI engines worldwide, except in the European Union, India and South Korea where CI engines have a significant share (39%–52%) [55].

Recent research on spark ignition engines focus on modern fuels and technologies such as different injection modes, turbocharging and engine downsizing.

SI engines rely on gasoline although they can also burn other fuel types such as compressed natural gas (CNG) [56], methanol [57], ethanol, 2,5-dimethylfuran [58]. For instance, it was shown that brass coated piston engine allows us to reach higher performance and lower emissions with methanol blends than conventional engines. Moreover, the optimal methanol blend was determined to be equal to 20% in volume to increase the efficiency and decrease the emissions. Lignocellulosic biomass feedstock can also play a role by substituting gasoline by 2,5-dimethylfuran. It was shown that the performance and emissions of SI fueld with 2,5-dimethylfuran lay between gasoline and ethanol, with different types of injection systems [58].

SI engines are most often fuelled with a port-fuel injector. Nevertheless, recent research concluded that highest combustion heat release rate was achieved with a direct injection (DI) system. Moreover, DI provides an increased turbulence in the cylinder, which increases the combustion rate and has a positive influence on the exhaust emissions [56]. Additionally, DI can increase the combustion stability at various engine speeds and loads [56] and DI has a positive impact on exhaust gas emission at low and part load condition [56]. Finally, various studies in gasoline turbocharged DI engines found that fuels of higher RON and lower MON (i.e. higher S) showed higher knock resistance and therefore allowed modern engines to operate with higher efficiency at high-load conditions [59].

Interestingly, these recent research show that advanced technologies applied to SI engines could be adapted to burn unconventional fuels such as the light fraction produced from automotive shredder residues.

Now moving on to the CI engine, which was invented in 1892 by Rudolf Diesel. In CI engines a fuel is direclty injected into a combustion chamber after the compression of air in this chamber [60]. This invention is still one of the major solutions in automotive, marine and power generation industries. Diesel has been seen for a long time as a good solution as the fuel is burnt more efficiently than in gasoline engines.

Diesel engines have high efficiencies because of their high compression ratios and lack of throttling losses [61] which makes them a good solution for the energy and the marine industries. Moreover, the NOx emissions is of lower concern for power generation application where the implementation of advanced aftertreatment systems is a possibility. This interest in CI engines caused the development of scientific studies to investigate the combustion of unconventional or alternative fuels in CI engines. For instance, a recent study assesses the benefits and limitation of ammonia as an alternative fuel for compression ignition engines [60]. The paper focuses on the combustion of ammonia in dual-fuel operation with diesel and other alternative fuels. The alternative fuels are amyl nitrate, dimethylhydrazine, soy-based biodiesel, dimethyl ether [60] and 2,5-dimethylfuran [62].

Nevertheless, the future of diesel engines is now questioned. Indeed, these engines couple high combustion temperature with high air excess, leading to the production of nitrogen oxides (NOx) compared to SI engines. This changed the public opinion over the use of diesel engines, supported by scientific studies [60]. This even resulted in the ban of diesel vehicles in major cities. The usage of diesel engines became even more questioned in 2015 with the Dieselgate scandal. Automotive manufactures had to provide falsified tests to meet the emission regulations even if expensive and complicated exhaust-gas after-treatment devices are used [61]. This consequently impacted the diesel engine market. [60].

That being said, the research on CI engines is still promising, with the emergence of low temperature chemistry (LTC) modes such as HCCI or RCCI. With LTC strategies, the combustion temperatures are reduced and are homogeneous by running the engine with excess air ratio much greater than one, or by using high amounts of exhaust gas recirculation (EGR). With these reduced in-cylinder temperatures, very low NOx emissions can be achieved. Soot formation can also be minimized from the homogeneity of the air–fuel charge by using multiple injections or EGR to prolong the air–fuel mixing time. To conclude, LTC combustion modes have the potential to decrease NOx and soot level while increasing the thermal efficiency.

1.5 HOMOGENOUS CHARGE COMPRESSION IGNITION

Researchers have already studied waste derived fuel (WDF) in conventional CI engine and all came to the same conclusion: waste-derived fuels emit high levels of pollutants (nitrogen oxides, partially oxidized products and soot particle emissions). Mani et al. [63] explained these high concentrations by the high flame temperature of substituted and cyclic molecules, and by poor mixing capabilities with the formation of local rich areas in the cylinder. Kumar et al. [64] observed similar trends and drew the same conclusions. As previously discussed, RCCI is a low temperature combustion mode that allows high efficiency and low levels of pollutants (Figure 11) as long as it is

correctly operated. Therefore, clean combustion modes, such as HCCI and RCCI have emerged as being the keystone to make lower grade fuels, such as those derived from ASR, acceptable for society.

The specificities of HCCI combine aspects from conventional SI and CI engines (Figure 10). In a conventional SI engine, the air and the fuel are premixed before being ignited by a spark plug. In a conventional CI engine, the air is compressed and the fuel is injected a few crank angle degrees before the end of the compression. The compressed air forms a hot environment where the fuel ignites spontaneously after an ignition delay time (IDT). With both CI and SI, the combustion zone forms a hot spot with high peak temperatures. Under HCCI conditions, the fuel is injected with the air during the admission stroke. Thus, the fuel droplets atomize in the air, and benefit from a sufficient time to lead to an homogeneous fuel and air mixture. This mixture preparation is similar to what happen in a conventional SI gasoline engine. However, no spark ignites the mixture. Moreover, the ignition is governed by compression, as in a conventional CI diesel engine. Nevertheless, unlike the diesel CI engine, the air and the fuel are already premixed in SI gasoline engine when the ignition occurs. This homogeneous mixing leads to a multipoint simultaneous ignition in the cylinder.

The homogeneous mixture combined with an ignition by compression explains the pros of the HCCI mode. HCCI leads to low levels of soot particles and NOx. Moreover, the thermodynamic efficiency is high. First, the low level of NOx is a consequence of a combustion governed by low temperatures. In contrary, high temperature combustion governs the production of NOx in a conventional diesel CI engine. A hot flame burns locally, leading to the production of thermal NOx. In HCCI, the ignition is simultaneous in the whole cylinder and the reaction is governed by the low temperature chemistry. Thus, the level of NOx is very low. Second, the level of soot is low because no fuel rich area exists and the lean mixture is homogeneous. Third, the thermodynamic efficiency is higher than with a SI engine because the compression ratio can be increased. Precisely, the compression ratio of a SI engine is limited by an undesirable and uncontrolled auto-ignition, called knock, that could occur if the compression ratio is too high. HCCI is a combustion mode that was tested with alternative fuels, including low-octane gasolines [65], valeric biofuels [66], syngas [67] and ammonia [68–70].

The pros of HCCI engine are numerous but cons must also be considered. First, the ignition is simultaneous in the cylinder, so, the combustion is fast. This leads to high pressure peaks, which are hazardous for the engine and create a high level of noise [71]. Second, the control of the ignition is more complex. Specifically, there is no spark plug nor direct injection to trigger the ignition. Rather, the ignition is governed by the compression whereas the mixture is created upstream. Thus, the inlet temperature, the compression ratio, the EGR ratio and the equivalence ratio are the main parameters to control the ignition. Third, the indicated mean effective pressure (IMEP) in HCCI engine is limited. The IMEP, i.e. the averaged pressure produced during a cycle, increases with the equivalence ratio of the mixture. In HCCI, increasing the fuel content cause pressure oscillation, called ringing, and an unstable combustion. Specifically, under these conditions, the fuel quantity is high and inhomogeneities can appear in the cylinder. These inhomogeneities counterbalance the simultaneity of the combustion and lead to ringing. Therefore, in HCCI, the equivalence ratio is typically between 0.3 and 0.5. Fourth, with a high fuel concentration, and if the cylinder walls are too cool, the HCCI combustion mode tend to create high levels of

unburned hydrocarbons and carbon monoxide (CO) because the combustion is incomplete near the cylinder walls.

The HCCI combustion mode is attractive due to its high thermal efficiency and its capacity to reduce NOx and soot. Nevertheless, the controllability of this combustion mode is challenging, which has prompted researchers to develop alternative concepts.

1.6 REACTIVITY CONTROLLED COMPRESSION IGNITION

The RCCI combustion mode is appealing as it offers a control of the combustion thanks to a direct injection system. With this technique, two fuels are used. The first is a low reactivity fuel and the second has a high reactivity. The low reactivity fuel is injected early in the engine cycle via an intake port, allowing a good homogeneity with the air and the recirculated gas. The high reactivity fuel is then injected directly in the combustion chamber before the ignition of the premixed fuel to control the ignition timing. The low-reactivity fuel represent 70-90% of the total mass of fuel. The RCCI combustion mode has been shown to provide better control than other concepts such as HCCI. The key feature of this dual fuel approach is the ability to control the combustion process by optimizing the reactivity of the blended fuels. A relationship between the fraction of premixed fuel and ignition timing can be settled in RCCI engines, so that the combustion phasing can be controlled [72]. This led to the terminology "reactivity controlled compression ignition" [73].

The RCCI combustion mode is compared with HCCI below. The combustion duration is higher with RCCI and the peak pressure rise rates are lower, compared to HCCI. This moderate combustion rate in RCCI combustion can be explained by staged combustion and reactivity gradient which was observed in optical engines [72]. As with a HCCI, the RCCI combustion mode offers high thermal efficiency, approaching 60% [73]. The improved efficiency is largely due to reduced heat transfer losses with lower gas temperatures compared to conventional diesel combustion. Moreover, low ringing intensity (RI), low NOx and low soot emissions can be achieved over a wide range of loads [72].

Another advantage of RCCI is its ability to be fuel flexible as long as two fuels with a different reactivity are used [74]. The use of these different fuels show that it is possible to rely on RCCI combustion mode with a wide range of fuels, which makes it particularly interesting for the unconventional fuels that are studied in the current thesis. We discuss the flexibility offered by this combustion mode for the light and the heavy fraction in the next paragraphs.

RCCI allows the usage of a variety of low reactivity fuels, including isooctane, gasoline, natural gas but also renewable fuels such as E20, E85, [73], methanol or dimethyl ether (DME) [72]. Additionally, cetane improvers [72, 73] can also be used to rely on one fuel only. Nevertheless, this type of approach is not considered in the current thesis as a light fraction and a heavy fraction are available. Depending on the type of fuel used, we observe a modification of the combustion properties. For instance, an increase of the in-cylinder maximum pressure and temperature with more DME, leading to the improvement of fuel efficiency. Additionally, with E85, it was observed that the ignition was delayed and the combustion duration was shortened. Moreover, relying on alcohols rather than gasoline increases the maximum achievable load during transient operation. A specific behaviour was also observed with methanol/diesel. The combustion rate of methanol/diesel is faster than that of gasoline/diesel due to longer ignition delays, leading

to higher RI. Finally, the introduction of more premixed ethanol resulted in the reduction of the combustion duration but increased the unburned hydrocarbon and CO emissions.

Other types of high-reactivity fuels than diesel were also studied, more particularly n-heptane or biodiesel [72]. It was shown that high fuel efficiency, low exhaust emissions and moderate combustion rates can be achieved. The study spotlights the importance of the fuel properties which impact the combustion behaviour.

The RCCI combustion mode has proven its potential in being fuel flexible. Indeed, it is possible to handle different types of fuel thanks to several parameters. The same parameters than with HCCI govern the ignition timing (initial temperature, EGR ratio). More precisely, it is important to ensure that knock does not occur with the low-reactivity fuel for a given set of initial parameters. To reach this objective, we developed predicting models to estimate the properties of this fuel. In RCCI, other parameters exist due to the presence of a direct injection. As already discussed, the proportion of low and high reactivity fuels plays a role and the injection timing must also be considered. For instance, the injection strategies can be improved with the use of multiple injections. Relying on this strategy is a way to reduce the presence of rich-fuel regions in the cylinder, thus decreasing the NOx and the soot emissions.

Different strategies can be adopted by modifying some key parameters. To know and understand how to adapt these parameters, the physical and chemical properties of the fuel can be observed. More precisely, the intermediate species such as the hydroxyl radical (OH) give relevant information to understand the combustion behaviour. For instance, the consumption rate of OH was slower with E85/diesel than gasoline/diesel. Therefore, being able to isolate the chemical aspect of the combustion and to study the intermediate species is a way to understand and optimize the combustion process. In the current thesis, the reactivity of the light fraction is studied in a rapid compression machine to understand its behaviour depending on its composition.

RCCI is a promising technique, but it has several drawbacks. RCCI engines can be run at medium load but it suffers from high carbon monoxide and unburned hydrocarbons emissions at low load, and high pressure rise rates at high loads [74]. Moreover, combustion control of RCCI engines is challenging during transient operations due to the sensitivity of reaction to thermal and chemical composition of air-fuel mixtures [74]. Finally, RCCI is a concept suited for stationary applications but it requires additional research to adapt it to transient conditions. The lower exhaust temperatures with RCCI is also challenging for after treatment systems. Developments in oxidation catalyst after-treatment systems are required to treat HC and CO emissions at the available exhaust temperature. More research is required for low temperature catalysts [73].

RCCI combustion is more promising than HCCI to achieve high fuel efficiency, low RI, low exhaust emissions, and stable operation simultaneously over a large range of engine loads and speeds [72]. Moreover, this combustion mode is particularly well fitted for the current study as it relies on two fuels with different reactivity simultaneously.

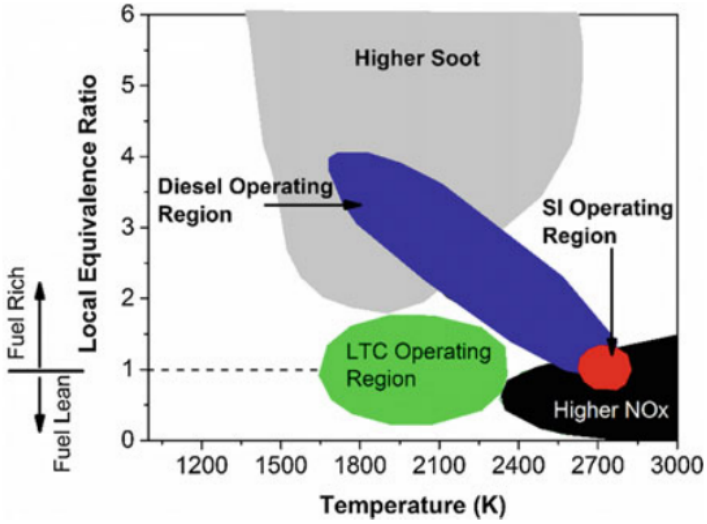

Figure 11: Emission level according to the operating condition with conventional SI, conventional CI engine and LTC engines. Adapted from [7]

1.7 OBJECTIVES

It was shown in the previous section that the RCCI combustion mode is suited for unconventional fuels to reduce the pollutant emissions and enhance the thermal efficiency. In this combustion mode, two fuels are injected at different timings. First, the low reactivity fuel is premixed with the air. Then, the high reactivity fuel is injected to ignite the air-fuel mixture. As a first objective, we focus on the high reactivity (heavy fraction) fuel to investigate its ignition characteristics. This study is done in a conventional CI engine and the fuel is compared with conventional diesel fuel. Moreover, several high reactivity fuels are compared in order to evaluate the fluctuation of the fuel.

In RCCI, the ignition delay of the fuel with the highest reactivity controls the overall ignition of the two fuels. Nevertheless, the injection timing can be adapted to adjust the ignition according to the autoignition delay of the fuel. The fuel with the lowest reactivity is injected before the compression stroke. Thus, its reactivity has to be low enough so that knocking does not occur in the cylinder, whatever are the fuel properties.

The reactivity of the two fuel are important parameters to control the combustion. The first fuel must resist to knock while the injection timing of the second fuel must be in phase with the autoignition delay. As it is possible to adapt the injection timing according to the reactivity of the heavy fraction, we focus in the next chapters on the light fraction.

Among all the properties of the light fraction, the composition of waste-derived fuels have to be controlled for several purposes.

First, the composition is a way to understand the properties. For instance, paraffins have shorter ignition delays than aromatics.

Additionally, knowing the composition is a way to do simulations. In fact, it is possible to understand the peculiar behaviour of the fuel towards combustion and to select appropriate molecules to compose a surrogate fuel.

Secondly, the composition has to be determined for health prevention. Gasoline is traditionally mainly composed of paraffins (30 – 70%) and aromatics (20 – 45%), the remaining molecules being alkenes (5 – 20%) [75, 76]. These concentrations respect the European Directive 2009/30/EC [77]. As

an example, in this directive, the limit for the olefin fraction is due to the formation of aromatic rings soot particle emissions and butadiene, which is registered as a toxic substance [78].

Finally, the composition needs to be known to control the pollutants. A regulation exists to control the pollutants emitted by conventional fuels. ASR fuels are expected to show high levels of olefins, oxygenate molecules and aromatic molecules. This unusual composition is due to the peculiar way the fuel was produced. Conversely to conventional fossil fuels, the double bonds of the olefins in the ASR-derived fuels did not benefit from a long decomposition of matter to react and become saturated [8]. Moreover, these fuels are derived from plastics. Thus, a high amount of olefin could be due to the straight polymers, such as polyethylene or polypropylene [79, 80]. Then, the oxygenated molecules come from the polymers themselves, like polyurethane (PUR) and polyamide (PA) [48]. The fuel treatment process, where the nucleofugic heteroatoms composing the raw matter are substituted by a nucleophile hydroxyl group, is also responsible for unusual composition. Last, plastics used in the automotive industry are composed of monomers with cyclic shapes as in the PS polymer, increasing the aromatic content [48].

Knowing the fuel composition is a first step to understand and monitor ASR derived fuels. It was shown in the section 1.2 that the fuel properties can change depending on the production parameters. These differences can be explained by the fluctuation of the fuel composition. Thus, it is even more important to determine the fuel composition.

However, unconventional fuels can have an unknown and complex chemical composition which makes it impossible to identify the whole chemical group repartition with a one-dimensional gas chromatography (GC) analysis. More advanced experimental techniques such as comprehensive two dimensional gas chromatography (GC $\times$ GC) are time consuming and not always easily available. As a solution, methods exist to estimate the fuel composition if it cannot be measured experimentally, but those have many limits and have never been studied with ASR fuels. As a second objective, the thesis extends the limits of the existing methods to estimate the composition of ASR fuels. Knowing the composition is a way to understand the fuel behaviour and to adapt the composition to get some given properties. Additionally, the composition can be compared with thresholds to monitor the exhaust gas composition.

Although the composition of a fuel gives a good overall view of its behaviour, going a step further is required to fully predict its behaviour. The octane numbers (ONs), namely the research octane number (RON) and the motor octane number (MON), are two important properties that characterize light petroleum fractions. We focus on the reactivity of the light fraction more than the one of the heavy fraction because the injection timing can be adapted according to the reactivity of the heavy fraction. For what concern the light fraction, we must ensure that it will not react too early to avoid knock. The RON and the MON are two properties that express reactivity through the characterization of the resistance of a fuel towards knock in piston engines. In RCCI, the light fraction has to resist to autoignition as long as the heavy fraction is not injected, so characterizing the octane numbers is adequate. More information on the RON and the MON are reported in section 2.5.2.

As exposed in section 1.5, ASR fuels are produced locally in small-scale production plants. Nevertheless, the RON and the MON test methods are not suited for a delocalized production plant nor for a project in the design

phase. The unknown nature of the fuel creates a high failure risk for the cooperative fuel research (CFR) engine in which the fuel is tested according to the standard test methods ASTM D2699 [81] and D2700 [82]. This risk is mainly due to the presence of heteroatoms that could lead to a premature failure (saturation of the filters, obstruction of the fuel line due to deposits, corrosion by sulphur, abrasive wear due to metals or silicon oxides resulting of the combustion). Moreover, the RON and the MON tests require costly reagents and a high level of qualification.

As an alternative to RON and MON measurement, estimating methods exist. Nevertheless, these methods were developed with a reduced training set, so they are fuel-specific methods. As a second objective, this thesis extend the existing methods to estimate the octane numbers of ASR fuels.

Methods to predict the composition and the octane numbers of ASR fuels provide relevant information on the fuel, but, they do not precisely inform us about the real RCCI operating conditions.

Low-temperature combustion modes have already proven their potential in reducing the nitrogen oxides and the soot particle emissions in the exhaust gases thanks to a better mixing between the air and the fuel, thus reducing the in-cylinder peak temperatures and locally rich areas [72, 73]. It has already been tested with alternative fuels such as E20, E85, [73], methanol, DME [72] and biodiesel, so it is fuel flexible. Nonetheless, the low-temperature combustion of fuels derived from ASR is still uncharted. The third objective of the current thesis aims at providing experimental data under low-temperature conditions. These data were acquired in a rapid compression machine (RCM) to investigate the auto-ignition delay time of the low reactivity fuel.

In RCCI, the low-reactivity fuel has to resist auto-ignition as long as the heavy fraction is not injected. The ignition delay of this low-reactivity fuel is extremely sensitive to the initial and compressed conditions (the chemical composition, and the temperature and pressure at top dead center (TDC)) as it is controlled by the kinetics whereas the mixing is homogeneous. It is possible with a RCM to study the effect of the initial condition on the IDT for an homogeneous mixture. Thus, studying the low-reactivity fuel in a RCM is adequate. Additionally, this ignition delay depends on the fuel composition which fluctuates over time. This fluctuation could be problematic if the fuel ignites too soon, leading to knock. As a solution, controlling if the fuel is prompt to auto-ignite for a specific operating condition could be studied numerically. Performing simulations of a fuel made up of hundreds of molecules is unfortunately unrealistic in terms of computational complexity. Instead, a surrogate fuel – mixture of about 2 to 10 molecules traditionally generated and validated based on experiments [20, 21, 30–32, 83–86] – could substitute the real one. The last objective of the current thesis aims at formulating an ASR surrogate fuel.

1.8 THESIS OUTLINE

- The current chapter 1 is a brief statement of the motivations and objectives, aiming at developing the thesis outline while the chapter 2 will explain the background in depth with a review of literature. chapter 3 is an overview of the statistical tools used in the current thesis.

  chapter 2 gives a historical overview of petroleum products and their related environmental challenges to better understand the current stakes for liquid and alternative fuels. This background, coupled with the European recycling rates targets, enabled us to introduce fuels

derived from ASR. These unconventional fuels will be discussed with regards to advanced combustion modes, such as RCCI. This is a promising engine technology, in terms of pollutant reduction, efficiency enhancement and fuel flexibility.

Then, chapter 2 recalls the main experimental and numerical fuel characterization techniques. Three different aspects, namely the chemical composition, the physical properties and the numerical simulation of the reactivity, are addressed. This chapter will introduce the principal issues of the current state of the art, introducing the main objective, which is the adjustment of the current prediction methodologies to fuels derived from ASR.

chapter 3 explains the tools used in the current thesis. Among others, latin hypercube sampling (LHS), principal component analysis (PCA), artificial neural network (ANN) and Bayesian inference are discussed.

- After the introduction, we study separately the light and the heavy fraction.

  In chapter 4, the heavy fraction is studied in a CI engine to investigate its ignition delay, compared with conventional diesel. As we can adapt the injection timing of the heavy fraction depending on its auto-ignition delay, we aim at modifying the current predictive methods to fit with the light fraction derived from automotive shredder residues.

  chapter 5 focuses on the prediction of the major hydrocarbon group fractions. This chapter contains the results published in the following proceeding:
  Steven Tipler, Alessandro Parente, Steffen H. Symoens, Marko R. Djokic, Kevin M. Van Geem, Francesco Contino, and Axel Coussement. Prediction of the piona and oxygenate composition of unconventional fuels with the pseudo-component property estimation (pcpe) method. application to an automotive shredder residues-derived gasoline. In *WCX World Congress Experience*. SAE International, apr 2018

  chapter 6 and chapter 7 investigate the prediction of octane numbers, with gasoline blendstock for oxygenate blending as a case study. The study embed uncertainty quantification to characterize the precision of the model. The main results of this chapter were published in:
  S. Tipler, M. Fürst, Q. Van Haute, F. Contino, and A. Coussement. Prediction of the octane number: A bayesian pseudo-component method. *Energy & Fuels*, 34(10):12598–12605, 2020

  chapter 8 focuses on the prediction of the IDT. Specifically, it describes the experiments carried out in the ULille RCM, with particular attention dedicated to exploring the reactivity under RCCI conditions and explaining the ignition delay times based on the major molecules in the fuel. As a result, a surrogate fuel with similar IDT as the real fuel was formulated. RCM is particularly interesting to represent the low-reactivity fuel under the RCCI combustion mode. Indeed, the fuel is premixed as in RCCI. Nevertheless they are some differences such as the evaporation or the fluid dynamics aspects. Part of this chapter has been published in the following scientific article:
  S. Tipler, C. S. Mergulhaõ, G. Vanhove, Q. Van Haute, F. Contino, and A. Coussement. Ignition study of an oxygenated and high-alkene light petroleum fraction produced from automotive shredder residues. *Energy and Fuels*, 33(6):5664–5672, 2019

- Finally, the thesis conclusions (chapter 9) are put into perspectives by comparison with final applications, followed by discussions about the barriers and limits of the current engine technologies and the level of understanding of reaction kinetics, bringing us to further perspectives (chapter 10).

1.9 PUBLICATION

Steven Tipler, Alessandro Parente, Steffen H. Symoens, Marko R. Djokic, Kevin M. Van Geem, Francesco Contino, and Axel Coussement. Prediction of the piona and oxygenate composition of unconventional fuels with the pseudo-component property estimation (pcpe) method. application to an automotive shredder residues-derived gasoline. In *WCX World Congress Experience*. SAE International, apr 2018

S. Tipler, C. S. Mergulhaõ, G. Vanhove, Q. Van Haute, F. Contino, and A. Coussement. Ignition study of an oxygenated and high-alkene light petroleum fraction produced from automotive shredder residues. *Energy and Fuels*, 33(6):5664–5672, 2019

S. Tipler, M. Fürst, Q. Van Haute, F. Contino, and A. Coussement. Prediction of the octane number: A bayesian pseudo-component method. *Energy & Fuels*, 34(10):12598–12605, 2020

Steven Tipler, Giuseppe D'Alessio, Quentin Van Haute, Francesco Contino, and Axel Coussement. Predicting octane numbers with inexpensive properties relying on principal component analysis and artificial neural network. *To be submitted*

2 FROM CONVENTIONAL FUELS TO ASR FUELS

2.1 CRUDE OIL AND PETROLEUM PRODUCTS

The history of petroleum dates from long time ago. The word petroleum is derived from the Latin *petra* and *oleum*, meaning literally rock oil. The role of petroleum products has evolved, starting from 3000 before Christ (BC) when Sumerians used asphalt as an adhesive for making mosaics. Mesopotamians used bitumen to seal boats and build roads. Egyptians greased chariot wheels and used asphalt to embalm mummies. Petroleum became more and more important from 1859. Now, petroleum is the most consumed product. It is used to produce energy, plastics and other chemicals. The fuels derived from petroleum supply more than half of the world's total supply of energy [91]. Gasoline, kerosene and diesel oil provide fuel for automobiles, trucks, aircraft and ships. Fuel oil is used to heat homes and commercial buildings, and to generate electricity. Petroleum products are the basic materials used for the manufacture of synthetic fibers for clothing and in plastics, paints, fertilizers, insecticides, soaps, and synthetic rubber.

The main theory behind the formation of petroleum is as follow. Oil is developed after millions of years from organic materials such as dead plants and animals. The dead organisms sank to the bottom of water areas, where the environment tends to be anaerobic. They accumulate, compressing the organic matter under its weight. There is an increase in temperature (100-140°C) and pressure due to the continued sediment deposition. With time, the conditions broke down the organic compounds into shorter hydrocarbon chains. Oil and natural gas accumulates in a reservoir rock which is a thick and porous rock. Earth movements trapped the oil and natural gas in the reservoir rock between layers of impermeable rock, also called oil trap.

The reaction behind the formation of petroleum are described thereafter. Aquatic plants and animals converts inorganic compounds dissolved in water to organic compounds with the energy provided by the sun. For instance the following reaction can occur:

$$6CO_2 + 6H_2O + \text{energy} \rightarrow 6O_2 + C_6H_{12}O_6, \tag{1}$$

when organic compounds exist in an aquatic environment, they can be decomposed into hydrocarbons:

$$(CH_2O)_n \rightarrow xCO_2 + yCH_4. \quad (2)$$

The conditions to produce hydrocarbon are: geologic time of about one million years, a maximum pressure of about 17 MPa and temperature of about 100-140 °C.

Due to its formation, crude oil is a complex mixture composed of hundreds of different hydrocarbons [92], which are discussed in the current thesis. With enough time, the different types of hydrocarbons can be converted in the others according to the geological conditions. This is also called in-situ alteration. Two oils from different location around the world can be distinguishes with their composition of hydrocarbon compounds. They are called hydrocarbon because they are mainly composed of carbon (84-86%) and hydrogen (11-14%). They are also composed of sulfur, nitrogen, oxygen, metals and salts. The salts can be removed easily but not the other atoms as they are linked to the molecules with chemical bonds.

Two-thirds of the world oil reserves are in the Middle East. The quantity of oil is expected to last 40 years. Nevertheless, undiscovered oil reservoirs exist offshore and due to the development of other energy sources, the oil production is expected to continue till the end of the century.

2.2 HYDROCARBON COMPOUNDS

Hydrocarbon are divided into 4 groups: paraffins, olefins, naphthenes and aromatics. Paraffins and naphthenes are also called saturates, saturates and olefins can sometimes be called aliphatic. Other hydrocarbon types exist but are rare in conventional hydrocarbons such as oxygenated compounds. The composition of hydrocarbon fractions is complex and depends on its distillation cut points as showed on Figure 12.

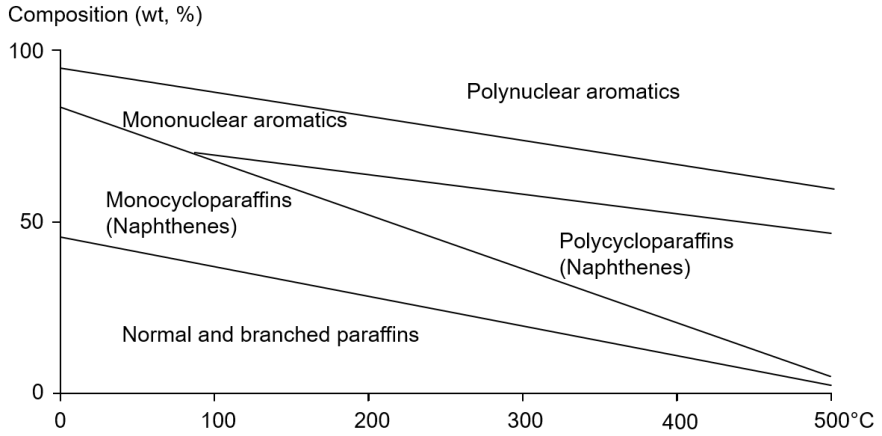

Figure 12: Variation of composition of petroleum fractions with boiling point. Adapted from [8]

2.2.1 *Paraffins*

Paraffins, or alkanes, have as a raw formula C_xH_{2x+2}. The paraffins are divided into normal paraffins, or n-paraffins, and iso-paraffins. n-paraffins

and iso-paraffins have the same raw formula but the location of the methyl groups is different. n-paraffins are straight, while iso-paraffins are branched. The smallest n-paraffin is methane, while the smallest iso-paraffin is isobutane. Methane is the major constituent of natural gas. Compounds with different structure but the same formula, such as isobutane and n-butane, are called isomers (Figure 13). Although isomers have the same formula, they can have very different properties. The number of isomers increases with the number of carbon atoms. For instance, octane, with 8 carbon atoms has 18 isomers, while dodecane, with 12 carbon atoms, has 355 isomers. Large hydrocarbons compose heavy fuels, such as diesel, while small hydrocarbons compose gasoline. Moreover, the properties of the fuel depends on the types of isomers. This is why studying diesel is more complex than studying gasoline. Paraffins from C_1 to C_{40} composes crude oils. Paraffins have no double bonds (also said saturated) so they are stable in time. Paraffins can reach up to 20% of a conventional crude-oil.

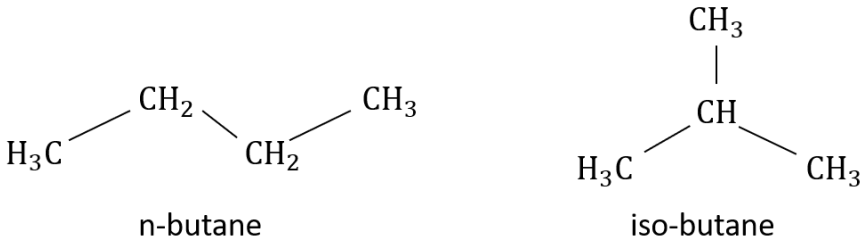

Figure 13: Comparison of n-butane and iso-butane, two representatives of the n-paraffins and iso-paraffin groups, respectively.

2.2.2 *Olefins*

Conversely to paraffins, olefins are composed of one or several double bond (they are unsaturated). Therefore, they are less stable in time due to their reactivity and are found in small quantities in conventional hydrocarbon mixtures. Compounds with one double bond are called monoolefins, or alkenes. The general formula of alkenes is C_xH_{2x}.

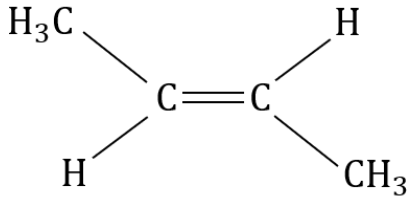

Figure 14: (E)-2-butene.

2.2.3 *Naphthenes*

Naphthenes, also called cycloalkanes, are ring or cyclic saturated hydrocarbons. They have the same general formula as the olefins, i.e. C_xH_{2x}. As for the n-paraffins, they compose crude oils. If there is one alkyl group from a n-paraffin attached to a cyclopentane, they are called n-alkylpentanes. In heavy oils, multirings attached to each other can be present. Up to 60% of cycloparaffins can compose a petroleum product.

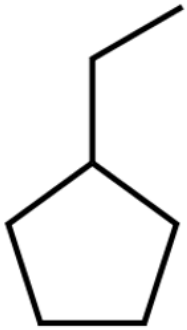

Figure 15: Ethylcyclopentane.

2.2.4 *Aromatics*

Aromatics are unsaturated cyclic molecules composed of double bonds. Benzene, the simplest aromatic molecule with six carbon atoms is known for inducing cancer. Therefore, its amount is restricted in petroleum products. Benzene with an alkyl group attached are called alkylbenzenes and have as a formula C_xH_{2x-6}. Aromatics with one benzene ring are called monoaromatics while those with two rings are called diaromatics. For aromatics with a higher number of rings, the term polyaromatic is used. Polyaromatic molecules can be composed of heteroatoms, such as sulfur. Nevertheless, the presence of sulfur must be limited as it can damage engine parts.

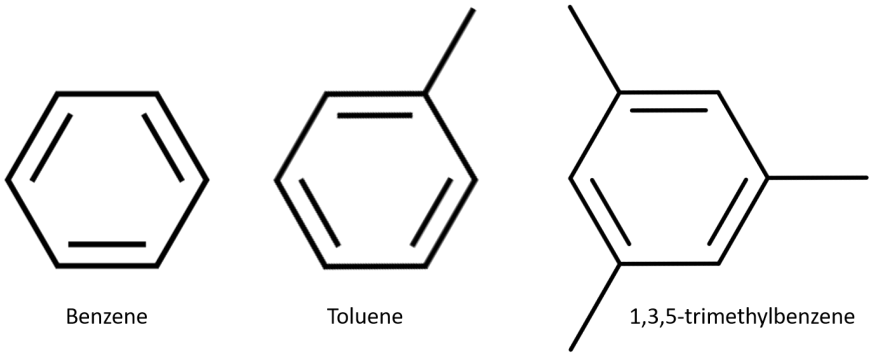

Figure 16: Comparison of several aromatic compounds.

A crude oil is separated into different petroleum fractions thanks to the process of distillation. During this process, the compounds are separated depending on their boiling points. Several types of distillation conditions exist depending on the final product that is to be separated from the crude oil. Under atmospheric conditions, the molecules in the crude oil have boiling point from -160°C (methane) to more than 600°C for heavy compounds. Nevertheless, the carbon-carbon bond starts to break at around 350°C. This undesirable process is also called cracking. To avoid it, the distillation occur under several conditions. First, it occurs under atmospheric conditions, then, the residuals of this first distillation are removed and sent to a vaccum distillation column. Thanks to this process, the hydrocarbon can be separated

under much lower temperatures. A petroleum fraction is constituted of several molecules that where evaporated under specific conditions. As an example, the products and composition of Alaska crude oil is given on Figure 17.

2.3 PETROLEUM FRACTIONS

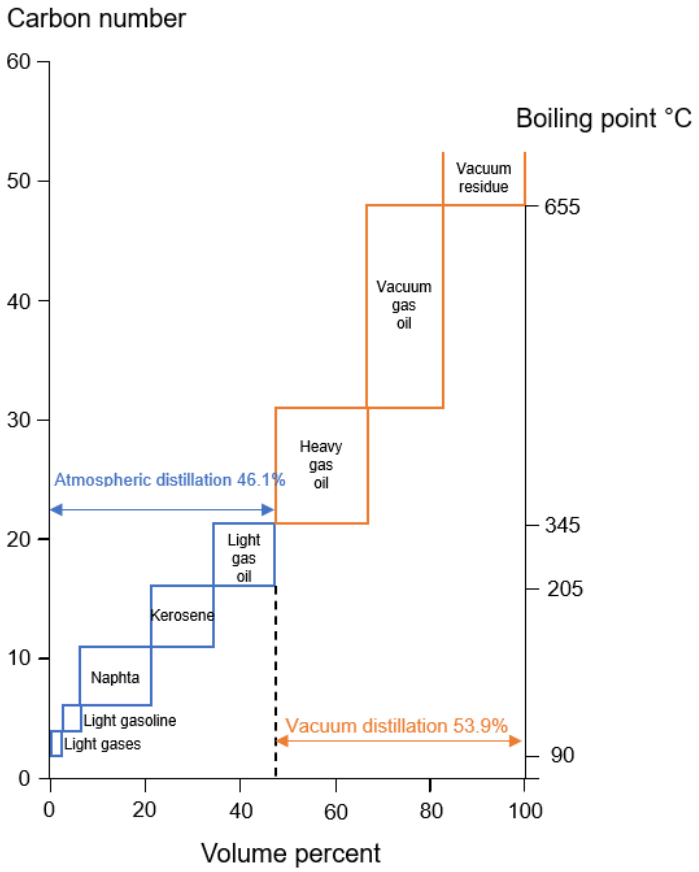

Figure 17: Petroleum fractions of Alaska crude oil. Adapted from [8].

The major fuel petroleum products are summarized thereafter.

Liquefied petroleum gases (LPG) is a mixture of propane and butane. It is used for domestic heating and cooking (50%), industrial fuel (15%), steam cracking feed stock (25%) and in spark ignition engine (10%).

Gasoline is used as a fuel for cars. It contains hydrocarbons from C_4 to C_{11}. The octane numbers are important properties of gasoline fuels. They qualify the antiknock characteristic, where knock is an undesirable early end-gas autoignition. The volatility is another important property as the fuel has to evaporate correctly before its ignition. A good evaporation ensures a good efficiency and avoids cylinder wall covering, which creates unburned hydrocarbons and CO. The density is also an important property as it is related to its composition, thus it provides a useful information. The properties of gasoline are given by the regulation EN 228.

Kerosene and jet fuel are used for lighting and jet engines, respectively. They are characterized mainly by their density and their ignition quality.

Diesel and heating oil are respectively used for motor compression ignition (CI) engine and domestic heating. Diesel is characterized by its cetane number, which characterizes its autoignition. Its volatility and viscosity are also important. The sulfur content must be monitored to avoid corrosion. The properties of diesel are given by the regulation EN590.

Residual fuel oil is used for the production of electricity or as a motor fuel for low speed engines.

Other non-fuel petroleum products exist, such as solvents, lubricants, waxes, asphalt.

2.4 PYROLYSIS

Pyrolysis is used to convert wastes into carbonate matter. This is an attractive thermochemical process to tackle the waste disposal problem with energy recovery. Pyrolysis is a thermochemical process to break chemical bonds through the thermal decomposition under non-oxidative conditions. The feedstock needs to be elevated at higher temperatures than 400°C in the absence of oxygen, leading to the decomposition of the structures that composes the feedstock. It has been used to produce charcoal from biomass for thousands of years. Pyrolysis of coal and biomass was used commercially from the 1700s [9]. Semantically the term thermolysis would be more appropriate than pyrolysis since pyro, the Latin word for fire, implies the presence of oxygen [9].

There are many types of pyrolysis depending on the operating condition. In general, a simple classification is done to distinguish slow, fast (also called flash) and catalytic pyrolysis. The slow pyrolysis considers a slow pyrolytic decomposition at low temperatures. Under slow pyrolysis, the heating rate is low, yielding mainly in char production. With fast pyrolysis, the decomposition is rapid with higher heating rates. These high heating rates coupled with short residence times and rapid quenching favour the formation of liquid products. The reaction time is of order of milliseconds to seconds. Longer residence times result in secondary reactions as thermal cracking. Catalytic pyrolysis is the name given to any pyrolytic process with a catalytic material in order to favour or upgrade some yield or some properties of the products. Several catalysts were studied such as zeolite catalysts, perlite, NaOH, Ru/MCM-41, Ni–Mg–Al (1:1:1) [9].

Additionally to the type of catalyst, the main process parameters influence the chemical composition and the properties of the resulting products. The main parameters are the heating rate, the temperature, the pressure, the residence time, the catalyst type and the resulting products are composed of gas, liquid and a solid fraction. Additionally to the process parameters, the composition of the feedstock plays a major role. Although all of these parameters were not studied with automotive shredder residues (ASR)-derived fuels, a review of these parameters for other feed types would give a first overview and a first understanding of the pyrolysis process. The effects of temperature, pressure, heating rate, carrier gas flow rate and type and residence time on the liquid, gas and solid yields are discussed below.

- The main variable affecting pyrolysis is temperature. From the conversion point of view, 500°C appears to be the optimum temperature at atmospheric pressure for pyrolysis as total conversion is achieved. An increase of the temperature promotes an increase in the gas fraction. A thermal cracking effect of the liquid fraction can occur when the process temperature is increased. Moreover, the solid fraction can also increase

in fluidised bad at very high temperature (900°C) where tar and char formation are favoured. Figure 18 shows the impact of the temperature on the pyrolysis yield for different scenario. The properties of the obtained liquid fraction is also impacted by the temperature. It usually contains larger quantities of aliphatic compounds at lower temperature than at higher temperature where aromatic production is promoted. In contrast, lower temperatures leads to olefinic hydrocarbons which are undesirable due to their oxidation and polymerisation tendencies, leading to the formation of gums that could damage the engine fuel delivery systems. To summarize the effect of temperature on the liquid fraction, higher temperatures than 450-500°C reduces the liquid yield in favour of the gas fraction while the aromatic fraction increases in the liquid part. The modification of the composition will have a direct impact on the fuel properties such as the calorific value, the H/C ratio, the boiling point and the octane number [9]. This shows why estimating the composition of the fuel is important, as it has a direct control on the fuel properties. The composition (chain length with the number of carbon atoms, cyclisation) and the properties (calorific value, H/C fraction, gas volume) of the gas fraction are also impacted by the pyrolysis temperature. In contrast, no major changes on the solid fraction are observed when the pyrolysis temperature increases. Nevertheless, the properties of the solid fraction depend on other variables linked with the occurrence of secondary reactions. The properties of the solid and gas fractions are not discussed in the current thesis as it deals with liquid fuels from ASR.

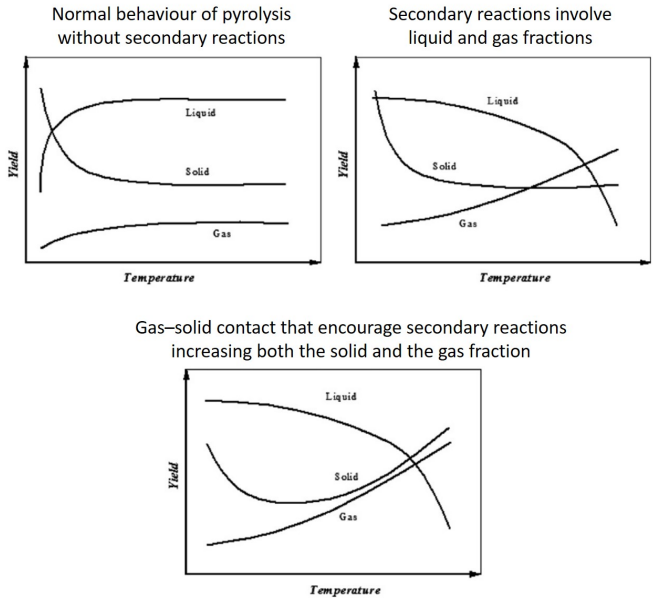

Figure 18: Impact of the temperature on the pyrolysis yield for different scenario. Adapted from [9].

- The heating rate is a key variable on pyrolysis since it has a role on the reaction rate and on the temperature profile [9]. The heating rate is one of the most studied parameter since it affects product yields and infuences the energy required for the process. The degradation rates increases with an increase in the heating rate. Moreover, the start and

the end of the devolatilisation are affected by the heating rate. This delayed decomposition is attributed to the combined effects of the heat transfer and the kinetics. Higher heating rates in fast pyrolysis promote an increase of the volatiles. Additionally, it leads to an increase in the temperature in comparison with slow pyrolysis. This encourages secondary reactions and could increase the gas yield. Therefore, the residence time in fast pyrolysis must be lowered to minimise secondary reactions and maximise the liquid fraction. There is a high sensitivity in the appearance of secondary reactions by varying the heating rate. In order to increase the liquid fraction, the heating rates have to be increased [9]. The heating rate also impact the composition and the properties of the obtained products. For instance, the liquid fraction shows more aliphatic and less aromatic molecules for higher heating rates. In terms of energy consumption, it has been showed that lower heating rates require less energy to complete the process even if the pyrolysis time increases. To conclude, the heating rate have several effect on the produced fractions and depends on the occurrence of secondary reactions.

- After having discussed the effect of temperature and heating rate, the role of pressure is detailed. An increase of the pressure on plastics feedstock leads to more viscous liquid produce while a vacuum pyrolysis reduces the influence of secondary reactions in the vapour phase [9]. Moreover, the liquid fraction increases under vacuum while the yields of char and gas decrease. Some advantages of vacuum pyrolysis is the reduction of the temperature, and the decrease of the mass flow rate. Studies showed that pressure does not have a high influence on the yields of gas, liquid and solid. It is noteworthy that under lower pressures, the occurrence of secondary reactions decrease but are still present, leading to deposits or to a higher gas yield.

- The carrier gas also influence the produced fraction. The presence of an inert gas controls the occurrence of secondary reactions such as thermal cracking, repolymerisation, recondensation and char formation [9]. The flow rate of the carrier gas impact the superficial velocity and the residence time of the produced fractions. Increasing the flow rate increases the superficial gas velocity, so, it decreases the residence time of the vapours. As a consequence, the vapours spend lower times in the reaction zone which minimise secondary reactions. Relying on low carrier gas flow increases the volatile residence time which decrease the liquid and char yields. The type of carrier gas is now discussed. If a non-inert gas is used, the properties of the products are affected as reactions can take place [9]. It was also showed that H_2 and N_2 result in similar products over the conversion although the H_2 pressure influences the composition of the liquid fraction with more saturates and less aromatics. Moreover, it increases the liquid yields. Finally, the carrier gas is a variable to control the appearance of secondary reactions: higher flow rates prevent secondary reactions and the pressure of the carrier gas impacts the properties of the pyrolysis products.

- The residence time of the vapours has also to be discussed. It is related to the carrier gas flow and to the type of reactor. Higher residences times favour secondary reactions which impact the composition and the properties of the resulting products. An increase in the gaseous

products and a decrease of the liquid and char products were observed with higher residence time of the vapours. A longer contact time between the volatiles and the chars could favour the Boudouard reaction, leading to a reduction in the char yield [9]. The type of reactor has also a role. For instance, a higher liquid fraction and a lower gas fraction were obtained in a fixed bed reactor than in a auger reactor [9].

- The pyrolysis time, also called residence time or reaction time is the last parameter discussed. It has a role to scale the industrial system. The cost of the system decreases with lower reactor volumes allowed by lower reaction times. Additionally, the particle size has to be considered to determine the pyrolysis time. Bigger particles need longer reaction times than small particles. The type of reactor impacts also the pyrolysis time. For instance, a longer pyrolysis time of a factor 10 was observed with a fixed bed reactor than in a auger reactor [9]. It was also shown that the temperature and the pyrolysis time are linked. A high temperature results in a lower pyrolysis time. It is noteworthy that longer pyrolysis time and higher temperature increases the quantity of heat required for the pyrolysis and increases the process efficiency. To conclude, longer reaction times are required for large waste particles although an increase in the temperature could lead to shorter pyrolysis times. Nevertheless, this could have an impact on the final products with the appearance of secondary reactions.

- The type of raw matter on the produced molecules is discussed below where additional information on the source of polymer is reported. polyethylene (PE) (present in car bodies, electrical insulation [93]) and polypropylene (PP) (automotive bumpers, chemical tanks, cable insulation, battery boxes, bottles, petrol cans, indoor and outdoor carpets, carpet fibers [93]) are polyolefin plastics which tend to produce olefins, polyurethane (PUR) (flexible foam seating, foam insulation panels, elastomeric wheels and tires, automotive suspension bushings, cushions, electrical potting compounds, hard plastic parts [93]) and polyamide (PA) (gears, bushes, cams, bearings, weather proof coatings [93]) are composed of oxygen atoms so they tend to produce oxygenated compounds. PUR induces also high amounts of alkylbenzenes. polystyrene (PS) (equipment housings, buttons, car fittings, display bases [93]) and acrylonitrile butadiene styrene (ABS) (automotive body parts, dashboards, wheel covers manufacture of housings, covers and linings [93]) are styrenics plastics that will produce aromatics such as styrene, α-methylstyrene and iso-propylbenzene [94]. ABS decomposition gives also different types of naphthenes such as alkylcyclohexane and cyclohexanes substituted by several methyl groups (for instance 1,1-dimethylcyclohexane) [80].

These different parameters could be adjusted with a feedback loop to obtain different types of liquid hydrocarbons. For instance, the composition of the row matter could be adjusted in order to decrease the reactivity of the fuel (higher octane numbers and lower cetane number) by promoting the presence of plastics giving oxygenates and aromatics. Nevertheless, the producer of the fuel, the Belgian company Comet Traitements, is not setting the proportions of the different wastes. Thus, another way to adjust the production properties could be interesting. For instance, the reactivity could also be decreased with the following adjustments: higher pyrolysis temperature, lower heating rate and lower carrier gas pressure. In fact these

adjustment would increase the aromatic fraction and decrease the aliphatic content.

As a conclusion, the type of molecules obtained from two different types of shredder residues coming from two different feedstocks are discussed to assess the variability of the obtained composition. These data are obtained from the study done by Jody et al. [48]. The types of plastics which are nearly constant between the two types of ASR are PUR (3.6 VS 2.1 %), PE (7.6 VS 8.7 %), PS (1.6 VS 2.7 %), polycarbonate (PC) (3.0 VS 2.9 %), polyvinyl chloride (PVC) (1.9% VS 3.4%). In contrast, the fractions of PP is much higher for the second type of shredder residues (8.8% VS 21.2%) and the ABS fraction is also higher for the second fraction (4.5% VS 7.8%). The remaining fractions are metals and unknown polymers, which are higher in the first ASR. Due to the higher difference in the PP than in the ABS fraction, the second type of ASR is expected to produce a fuel with more aliphatic compounds than the first type of ASR. Nevertheless, it is noteworthy that the types of polymers are similar, which will result in the same final molecules for a given pyrolysis and distillation parameter set.

2.5 EXPERIMENTAL CHARACTERIZATION TECHNIQUES

The previous section showed that fuels obtained from pyrolysis are complex blends composed of a lot of molecules. This complexity is even more challenging for fuels derived from ASR because they are new and uncharted fuels. Moreover, if the properties of the fuel are not suited for their final application, they can damage the appliance in which they are burnt. It shows that the properties of unconventional fuels must be characterized and monitored if their production process or their feed is variable. Knowing the composition is also important as the composition explains the fuel behaviour.

Several characterization methods exist. After having described the experimental methods to estimate the composition of a fuel, the methods to characterize their properties are discussed.

2.5.1 *Characterization of the composition*

Three characterization techniques are studied within the thesis, namely gas chromatography (GC)-mass spectrometry (MS), nuclear magnetic resonance (NMR) and comprehensive two dimensional gas chromatography (GC $\times$ GC).

With GC-MS, the components of a complex mixture are separated based on their volatility. The components of the complex mixture move in a capillary column due to a carrier gas. The separation of the components depends on their affinity with the carrier gas and a stationary phase. The components are called effluents and their concentrations are given by a detector, the mass spectrometer. In this detector, the molecules are ionized by collision with electrons.

However, it is difficult to get a lot of information on the fuel composition with traditional chromatography techniques due to the complexity of the fuel composition. Only part of the fuel molecules could be identified with this method. GC $\times$ GC is an advanced analytical method relying on two columns with two different selectivities. Relying on two columns enables a better separation of the molecules. GC $\times$ GC can be coupled with flame ionization detector (FID), time of flight (TOF)/MS, nitrogen chemiluminescence detector (NCD), sulfur chemiluminescence detector (SCD) to determine the chemical

fractions, to identify the molecules, and to measure the nitrogen and sulphur content, respectively. A scheme of GC × GC is showed on Figure 19. The gas passes through a first rtx-1 PONA apolar column, then liquid CO_2 is injected, playing the role of a cryogenic modulator, allowing to stop the effluent until its relaxation toward the second column. Then, the components can either go in one of the two polar BPX-50 column. The first, being coupled with FID to measure the chemical fractions and the second with TOF-MS to identify them. In practice, the fuel will be injected twice in the system to pass through the two columns. As an example, a GC × GC chromatogram is reported on Figure 20. We can see a good distinction of the different hydrocarbons.

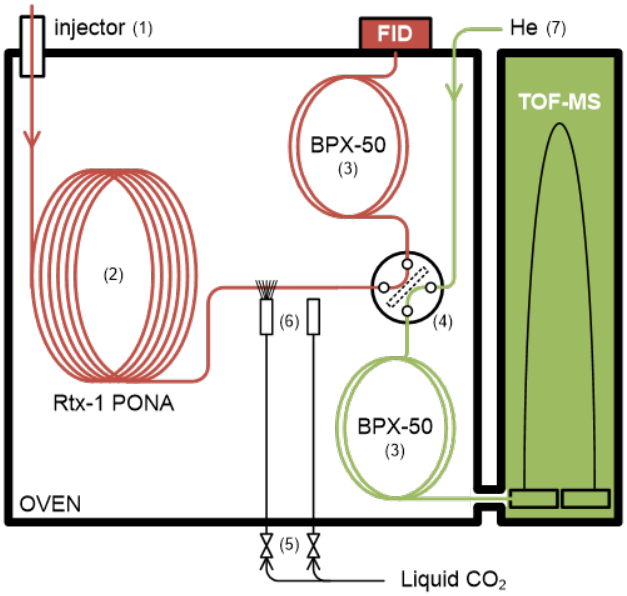

Figure 19: Analysis of a fuel by GC × GC. FID gives quantitative results while the molecules are identified via TOF-MS [10]. The fuel is injected (1) into a first dimension column (2). CO_2 is injected through solenoid valves (5) towards the two-jet cryogenic CO_2 modulator (6). The fuel goes into the second dimension column (3) to be analysed by FID or TOF-MS depending on the position of the 4-port 2-way valve (4). (7) is a protective helium flow.

NMR spectroscopy is a method based on the identification of atoms. The most common identifiers are carbon 13 and proton 1H. Specifically, a 1HNMR spectra was obtained and analysed. Each proton H^+ emits a signal that depends on the neighbour protons. Thus, each signal is a consequence of a specific bound. On a 1HNMR spectra, the peaks intensity corresponds to its concentration, and the number of peaks in the same region corresponds to the presence of hydrogen atoms in the same neighbourhood. NMR is powerful as it has a good selectivity, but identifying components that are similar is challenging. For instance, a high overlapping occurs in the region from 0.5 ppm to 1.5 ppm, which makes the identification of paraffinic molecules difficult (Figure 21). The auto-ignition depends on the structure of the fuel, thus, it is theoretically possible to formulate a surrogate fuel if the NMR spectra corresponds to the one of the real fuel. To reach this goal, the chemical signals must be decorrelated to identify the chemical functions. Nevertheless, the region 0.5 ppm to 1.5 ppm is particularly problematic as n-paraffins, iso-paraffins, naphthenes and olefins overlap.

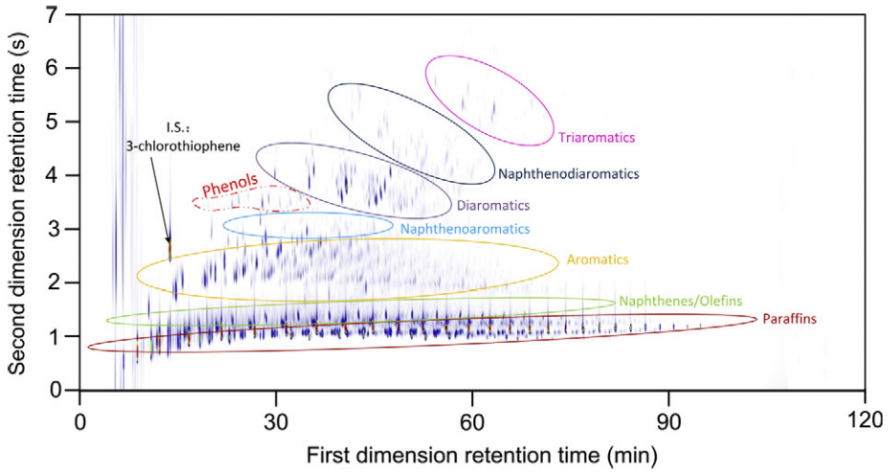

Figure 20: GC × GC – FID chromatogram of a shale oil sample with different hydrocarbon group types, adapted from [11]

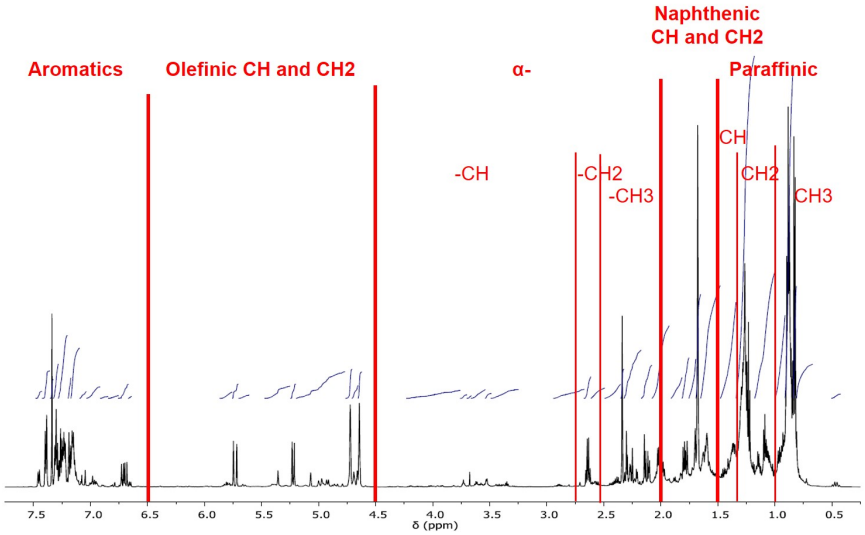

Figure 21: NMR spectrum of a ASR fuel.

2.5.2 *Characterization of the octane number*

Characterizing properties is important to ensure the safe operation of the engine in which a fuel is burnt. In the current thesis we specifically study the ignition delay time (IDT) and its similar properties. For instance, the octane number (ON), namely the research octane number (RON) and the motor octane number (MON) are properties that characterize the resistance to an end-gas autoignition of a light fuel under specific conditions. These conditions can be linked with the resistance to autoignition of the light fraction before injecting the heavy fraction in reactivity controlled compression ignition (RCCI). A too early ignition creates knock which is destructive for the engine. Knocking is characterized by an early ignition which causes a ringing sound. More importantly, this early ignition damages the engine. A gasoline with a high octane number provides the following advantages [76]: it can be used in an engine with a high compression ratio, it enables the

Table 3: Functional groups in the ^{1}H NMR spectrum.

.

Label	Functional group	Shift (ppm)
A	Aromatics	8 - 6.7
a_1	Naphthalene	8 - 7.4
a_2	Benzene	7.4 - 7.3
a_3	Substituted A	7.3 - 6.7
O	Olefin	4.5 - 6.6
Ox	Alcohol	3.5 - 3
ox_1	Methanol	3.5 - 3
ox_2	MTBE	3.2 - 3
α_A	α-C α_{a1}+α_{a2}+α_{a1}	3 - 2.1
α_{a1}	α-CH	3 - 2.7
α_{a2}	α-CH_2	2.7 - 2.5
α_{a3}	α-CH_3	2.5 - 2.1
Ov1	Overlapping 1 N+γ_{o2}+γ_{o3}+i	2.2 - 1.4
Ov2	Overlapping 2 CH_2 Napht+γ_{o3}+i	1.85 - 1.4
γ_{o1}	γ-CH	2.5 - 2.1
γ_{o2}	γ-CH_2	2.1 - 1.85
γ_{o3}	γ-CH_3	1.85 - 1.4
N	-CH/CH_2 Naphthene	2.2 - 1.4
i	-CH iso	1.6 - 1.4
Ov3	Overlapping 3 p1 +C=C-C-CH_2- +Ph-C-CH_3	1.4 - 1
p1	-CH_2 paraffin	1.4 - 1
p2	-CH_3 paraffin	1.1 - 0.6

ignition timing to be advanced, resulting in a greater power output, and the engine efficiency is improved, reducing the fuel consumption.

Conversely, if the octane number is too low comparing with the compression ratio of the engine, the following disadvantages occur: knocking, power loss, overheating of the engine.

The ONs are measured in a cooperative fuel research (CFR) engine - an engine whose compression ratio can be adjusted - according to the regulations ASTM D2699[81] and ASTM D2700[82] respectively. In these regulations, the resistance of a fuel towards an end-gas autoignition is compared with a mixture of iso-octane and n-heptane, also called primary reference fuel (PRF). For instance, a fuel that behaves similarly than a mixture of 90% of iso-octane and 10% of n-heptane, called PRF90, has an octane number of 90.

Different operating conditions distinguish the RON and the MON. The research (RON) method traduces city conditions while the motor (MON) one characterizes road conditions [8]. The RON (resp. the MON) test conditions are an intake temperature of 52°C (resp. 149°C), an engine speed of 600 rpm (resp. 900 rpm) and a spark ignition advance of 13° (resp. 14 to 26°). These differences in the operating condition explains why the RON is higher than the MON. The MON operating conditions are more severe than the RON [95]. RON tends to be higher than the MON by 6-12 points in practical fuels [8].

Generally speaking, n-paraffins are characterized by a lower ON than iso-paraffins. Naphthenes tend to have even higher RONs, while aromatics and oxygenates have very high RONs. Therefore, the octane number of a gasoline is strongly correlated with its molecular composition.

The ON of a mixture is often calculated with a linear blending law. Nevertheless, the octane number is non linear regarding to blending, especially when paraffins are mixed with another hydrocarbon class [96]. For this reason, the concepts of blending RON (BRON) and blending MON (BMON) were introduced. These blending ON (BON) are calculated by measuring the ON of 20% of the studied molecule mixed with 48% of iso-octane and 32% of n-heptane. This blend is equivalent to a mixture of 20% of the studied molecule with PRF60. The measured ON is thereafter rescaled as if the molecule was pure, which is given by the following equation:

$$\mathrm{BON} = 60 + \frac{20}{100}(\mathrm{ON}_{\mathrm{measured}} - 60) \tag{3}$$

Due to the definition of BON, it is recognized that measuring BON leads to high experimental errors due to the dilution per a factor five [96].

The BRON and the BMON of more than 340 molecules are gathered in the report of the API project 45 [26]. As an example, the blending ON of major molecules in hydrocarbons are reported in Table 4.

Table 4: Octane numbers and blending octane number of major molecules in hydrocarbon fuels

	Molecule	RON	BRON	MON	BMON
Paraffin	n–Heptane	0	57.6	0	57.6
	2–Methyl–hexane	42.4	40	46.4	42
	2,2,4-Trimethylpentane	100	61.6	100	61.6
Olefin	2–Methyl–1–hexene	90.7	118	78.8	108
Naphthene	Methylcyclohexane	74.8	104	71.1	84
Aromatic	Toluene	120.1	124	103.5	112

The molecules in Table 4 are all similar in shape and size so they can be compared. N–heptane and 2,2,4-Trimethylpentane, i.e. iso-octane, are the two reference. They frame the octane scale from 0 to 100. For molecules with a high ON, such as toluene, tetraethyllead (TEL) is added to obtain the ON. TEL is an antiknock compound, so, it increases the ON, which can be calculated with the following equation:

$$\mathrm{ON} = 100 + \frac{28.28\mathrm{T}}{1 + 0.736\mathrm{T} + (1 + 1.472\mathrm{T} - 0.035216\mathrm{T}^2)^{0.5}}, \tag{4}$$

where T is the quantity of TEL in mL per U.S. gal in iso-octane.

In Table 4, 2–methyl–hexane has an intermediate ON, comparing with n–heptane and iso–octane. First, the number of substitutive –CH_3 is higher than pure n–heptane. Second, iso–octane is hindered whereas 2–methyl–hexane shows four molecules that can be attacked easily during a chemical reaction. As showed by the other molecules, cyclic shapes and double bounds tend to increase the chemical bonding, thus the octane number of naphthene, olefins and aromatics increases. Moreover, this type of configuration leads to the formation of stable intermediates, which also contributes to increase the

ON. For most of the molecules, the MON is lower than the RON because the condition of the MON test are more sever [81, 82]. Finally, the BON are higher than ON, except for the paraffins. The chemical origin of this non-linear blending was studied by Leppard in 1992 [96]. The octane quality of a molecule is governed by the dynamics of the radical pool, and not only by the initial shape of the molecule. The high blending octane qualities are a consequence of the presence of a molecule that act as radical scavengers, retarding the reactivity of the paraffin. For instance, in a mixture of olefin and n-heptane, radicals are placed in the olefin non-branching chain that reacts slower than the paraffin chain [96].

Three additional properties are calculated based on the RON and the MON. The first is the octane sensitivity (OS), the second is the antiknock index (AKI) and the third is the octane index (OI).

As previously stated, the RON tends to be higher than the MON. The difference is known as the OS:

$$OS = RON - MON. \tag{5}$$

The sensitivity of PRF is zero, which is the reason why adding another molecule, such as toluene, is important to represent correctly a real gasoline fuel. Such a mixture is called toluene reference fuel (TRF).

The AKI is the average between the RON and the MON:

$$AKI = \frac{RON + MON}{2}. \tag{6}$$

The OI is defined as:

$$OI = (1 - k)RON + kMON. \tag{7}$$

This number takes into account the engine's operating condition via the introduction of a linear weighting factor k. Thanks to this factor, the OI indicates if the actual operating conditions are similar to the RON or to the MON conditions. The values of k evolve from 0 or 1. It has also been showed that k can reach negative values due to the technologies of modern engines [97]. As the RON tends to be higher than the MON, a negative k results in fuels that have an OI higher than the RON and the MON. This means that the fuel has a better resistance to autoignition.

The method to calculate k follows.

$$k = \frac{b}{a + b} \tag{8}$$

with a and b the linear coefficients between the RON and the MON. These parameters are calculated based on the knock limited spark advance (KLSA):

$$KLSA = c + aRON + bMON \tag{9}$$

KLSA is the ignition timing at which the average knock intensity is 0.5V in the engine to be tested under specific operating conditions [98, 99]. With this definition, the knock intensity was measured with a knock detector hardware developed in-house. The knock intensity was reported in terms of the average knock amplitude in volts. KLSA, RON and MON are measured with different fuels. In their study, Kalghatgi et al.[98] typically measured the properties of 6 to 13 fuels. To compute k, a simple linear regression is processed to obtain a, b, c, and k.

2.5.3 *Characterization of the cetane number*

To quantify the ignition quality of a diesel fuel, the cetane number (CN) can be measured according to the standard test method American Society for Testing and Materials (ASTM) D613 [100]. The CN scale is based on two PRF. Historically, a CN of 100 was attributed to cetene (1-hexadecene). This molecule was substituted by cetane (n-hexadecane) due to the change in reactivity of cetene depending on the location of the double bound. On the opposite, a CN of 0 was attributed to mesitylene (1,3,5-trimethylbenzene). Mesitylene was substituted by α-methylnaphthalene which was itself replaced by iso-cetane (2,2,4,4,6,8,8-heptamethylnonane) [97]. The fuel to be tested is burned in a CFR engine and compared with a mixture composed of the two PRF. A diesel fuel has a cetane of 60 if it behaves like a mixture of 60% cetane and 40% of $\alpha-$methylnaphthalene.

The shorter the ignition delay, the higher the CN. Fuels with a high CN ignites shortly after their injection, so, they have enough time to burn. A high CN promotes an easy cold start-up, increases the fuel economy and reduce the emissions. In contrast, a low CN leads to a late ignition. Due to this late ignition, the fuel reacts in a short amount of time, leading to diesel knock. Moreover, low cetane numbers result in high emissions of smoke and particulate matter [101]. The minimum rating depends on the final usage as shown for several standards in Table 5. The product distributed in France and Europe have CN in the range of 48-55.

Table 5: Cetane number of several specifications

Standard	CN
NF EN 590 (road usage)	>51
Distillate Marine X (DMX)	>45
Distillate Marine A (DMA)	>40
Distillate FAME A (DFA)	>40
Distillate Marine Z (DMZ)	>40
Distillate FAME Z (DFZ)	>35
Distillate Marine B (DMB)	>35
Distillate FAME B (DFB)	>40

The measurement of the RON, MON and CN suffers of a lot of disadvantages. It requires the usage of an expensive CFR engine and a high amount of fuel.

More recently, the CN was substituted by the derived cetane number (DCN) as an alternative. This property is measured in an ignition quality tester (IQT) according to the ASTM standard D6890 [102] rather than in an engine. An IQT is a constant volume chamber. The uncertainty is equal to 0.7 for a DCN between 33 and 60 [101].

2.5.4 *Other properties*

The most important properties are listed in this section.

The specific gravity (SG) and the density are reported respectively at 15.5°C and 20°C at 1atm. SG is defined as the ratio of density of a liquid to the one of water. This property is important to characterize the petroleum product. For instance, aromatic molecules are denser than paraffinic ones. Moreover,

the SG can be used to estimate other properties, such as the composition, the sulfur content, critical constants, viscosity or thermal conductivity. The SG and the density can be measured according to ASTM D4052. Another method exist, simpler, but less accurate: ASTM D1298.

The boiling point and the distillation curve characterizes the volatility of the fuel. Unlike pure molecule that are characterized by a single boiling point, fuels are characterized by a range of evaporation. This range is as wide as the difference in evaporation temperature between the most and the least volatile molecules. The distillation curve is presented as the temperature of distillation versus the volume fraction of evaporated mixture. The initial and the final boiling points are important parameters as they define the boiling range. The wider the boiling range, the more the number of compounds. In some cases, the final boiling point will not be achieved, which means that the heaviest molecules does not evaporate in the studied range of temperatures. The distillation curve is also used to determine if the petroleum product has a narrow or a wide boiling range. It is used to estimate other properties such as the molecular weight, the composition, the vapor pressure, thermal properties and others. Several methods exist to measure the boiling points of petroleum fractions. In the current thesis, the method proposed in the ASTM D86 is used as it is simple and old. Moreover, majority of the distillation curves reported in the literature was measured with this method.

With this method, a sample of 100mL is evaporated under atmospheric pressure and the distillation curve is reported at 0, 5, 10, 20, 30, 40, 50, 60, 70, 80, 90, 95 and 100% of the evaporated volume. When the fuel is composed of heavy molecules, the highest fraction evaporated may not be 100% due to the risk of cracking the molecules when the temperature is too high. Similarly, the result may be distorted at high temperatures. The measure of the distillation curve gives several temperatures.

However, it is of interest to characterize the distillation by a single temperature. For this reason, the distillation profile is averaged. Several average values exist, the volume average boiling point (VABP), the weight average boiling point (WABP), the molal average boiling point (MABP) depending on the type of fraction used to calculate the average (volume, mole, weight). Correlations reported in [8] can be used to convert the VABP, given by ASTM D86, to another type of average boiling point. Another important parameter is the mean average boiling point (MeABP) which is used in the pseudo-component (PC) method to characterize a petroleum fraction. We relied on the PC method to develop methods to predict the composition of the studied unconventional fuel and to predict the ON. In the current thesis, the MeABP was calculated from the VABP [8] obtained by the volumetric distillation curve measured experimentally according to the standard test method ASTM D86 [103]:

$$\mathrm{VABP} = \frac{T_{10} + T_{30} + T_{50} + T_{70} + T_{90}}{5}, \tag{10}$$

where T_p (expressed in Kelvin) is the temperature at which p% of the fuel is evaporated. The VABP was converted into MeABP [8]:

$$\mathrm{MeABP} = \mathrm{VABP} + \Delta_{\mathrm{Me}}, \tag{11}$$

where the shifting coefficient Δ_{Me} is defined as [8]:

$$\ln(\Delta_{\mathrm{Me}}) = -1.53181 - 0.0128(VAPB - 273.15)^{0.6667} + 3.646064SL^{0.333} \tag{12}$$

and SL is the 10-90 slope defined by [8]:

$$SL = \frac{T_{90} - T_{10}}{80}. \tag{13}$$

A third important property is the molecular weight which is useful for calculations. For instance, the combustion equations involve molar quantities while manipulations involves a weight (or a volume). The molecular weight is also used to characterize the fuel and to predict other properties. It gives an overview of the size of the molecules. For petroleum fractions, the molecular weight corresponds to an average over the molecules in the fuel. Nevertheless, as identifying all the molecules in a petroleum product is impossible, such a calculation cannot be realized. As an alternative, three methods exist: cryoscopy, the vapor pressure method, and the size exclusion chromatography [8]. The most used is the cryoscopy method. The freezing point of the petroleum product is measured and a relation exist to relate this property with the molecular weight.

The refractive index at 20°C is another property useful to estimate the composition of petroleum fractions and additional properties such as the molecular weight, or transport properties. It is defined as the velocity of light in vacuum to the velocity of light in the substance. The speed of light depends on the temperature, so, the refractive index is reported at a given temperature. What makes it very popular is its relationship with the molecule type. The refractive index increases from paraffins to naphthenes, and the maximal values are hold by aromatics. Refractive index up to 1.5 can be measured with refractometers according to ASTM D1218. For values up to 1.6, ASTM D1747 is used.

Some properties can be combined to create a new property such as the Watson factor K_w (combination of density and boiling point), m parameter (combination of refractive index and molecular weight), the carbon-to-hydrogen ratio (combination of carbon and hydrogen weight ratios), the viscosity gravity constant (VGC) and the viscosity gravity function (VGF) (combination of the SG and the viscosity). These properties are useful to characterize the fuel as well as to predict the composition of a petroleum fraction. Aromatics have a low K_w while paraffins have high values.

$$K_w = \frac{(1.8T_b)^{1/3}}{SG}, \tag{14}$$

with T_b the normal boiling point in K and SG the specific gravity. The factor 1.8 is a conversion factor applied because the boiling temperature was initially defined in degrees Rankine [8]. This factor classifies the hydrocarbons in the mixture. Aromatics have low values and paraffins have high values.

The m parameter identifies the hydrocarbon type. This parameter m was defined with the following formula based on the observation that the refractive index varies linearly with 1/M [104]. Paraffins have low m values while aromatics have high m values. Paraffinic and naphthenic oils have negative m values. Moreover, m increases as the number of rings increases in an aromatic. This parameter is defined by:

$$m = M(n - 1.475), \tag{15}$$

with n the refractive index at 20°C and M the molecular weight.

The VGC and the VGF are other empirical properties which separates well the hydrocarbon classes. The VGC is defined with the Saybolt viscosity at two temperatures:

$$VGC = \frac{10SG - 1.0752\log_{10}(V_{38} - 38)}{10 - \log_{10}(V_{38} - 38)}, \tag{16}$$

$$VGC = \frac{SG - 0.24 - 0.022\log_{10}(V_{99} - 35.5)}{0.755}, \tag{17}$$

with V_{38} and V_{99} the Saybolt viscosities at 38°C and 99°C.

These two equations give similar results and equation 16 is preferred when the viscosity at 38°C is known. When the viscosity at 40°C is known, another equation is recommended, given by ASTM D2501:

$$VGC = \frac{SG - 0.0664 - 0.1154\log_{10}(\nu_{40} - 5.5)}{0.94 - 0.109\log_{10}(\nu_{40} - 5.5)} \tag{18}$$

Another equation was reported relying on the kinematic viscosity and the density at 20°C:

$$VGC = \frac{d - 0.1384\log_{10}(\nu_{20} - 20)}{0.1526\left(7.14 - \log_{10}(\nu_{20} - 20)\right)} \tag{19}$$

with d the density at 20°C and 1 atm in g/cm^3 and ν_{20} the kinematic viscosity at 20°C in cSt.

When the viscosity is too low, these equation cannot be applied due to the $\log_{10}$. Thus, the VGF is defined for fuels with a low viscosity:

$$VGF = -1.816 + 3.484SG - 0.1156\ln(\nu_{38}) \tag{20}$$

$$VGF = -1.948 + 3.535SG - 0.1613\ln(\nu_{99}) \tag{21}$$

where ν_{38} and ν_{99} are the kinematic viscosities in cSt at 38°C and 99°C. These two equations give similar results, nevertheless relying on ν_{38} is to be favoured when possible. The parameter VGF is defined for light fuels with a molecular weight lower than 200 g/mol.

These equations are a consequence of the fact that SG versus $\ln(\nu_{38})$ is linear for each hydrocarbon group. The kinematic viscosity is useful for heavy petroleum products. In fact, for these products the boiling point is not available due to thermal decomposition during distillation. The viscosity depends on the temperature. It is generally reported at 37.8°C (100°F) and 98.9°C (210°F). When the viscosity is known at two temperatures, it can be calculated for other temperatures. The viscosity is measured in a viscometer and the test method is reported in ASTM D445.

The air-to-fuel ratio under stoichiometric conditions (AF_s) is also a good indicator of the hydrocarbon class fraction. It is defined by the global equation of complete combustion:

$$C_xH_yO_zN_\alpha + \omega(O_2 + 3.76N_2) \rightarrow xCO_2 + \frac{y}{2}H_2O + (3.76\omega + \frac{\alpha}{2})N_2, \tag{22}$$

where ω is the needed number of moles of oxygen to burn the fuel under stoichiometric condition and is defined as:

$$\omega = x + \frac{y - 2z}{4}. \tag{23}$$

The stoichiometric air to fuel ratio is defined by:

$$AF_s = \frac{1}{M_c} \frac{1 + \frac{HC_W \frac{M_C}{M_H} - 2OC_w \frac{M_C}{M_O}}{4} (M_{O_2} + 3.76 M_{N_2})}{1 + HC_w + OC_w + NC_w}, \tag{24}$$

where the weight ratio between atom A and carbon, AC_w, is deduced from the atomic mass fractions:

$$AC_w = \frac{y_A}{y_c}, \tag{25}$$

where y_A refers to atom A and y_C refers to carbon.

For what concerns the carbon-to-hydrogen ratio, the formula of paraffins, naphthenes and aromatics shows that it increases from paraffins to aromatics. Moreover, the CH changes from low to high carbon number. The CH value tends towards 5.96 for extremely large molecules. The CH ratio can be measured via elemental analysis, which also gives the atom fraction of sulphur, nitrogen and oxygen. Methods exist to analyze each element individually. Elemental analyzers also exist to measure these elements all together. For instance, in CHN analyzers a combustion occurs. Carbon is oxidized into CO_2, hydrogen to H_2O, and N to nitrogen oxides. The last are reduced over copper to nitrogen by eliminating oxygen. The mixture of CO_2, H_2O and N_2 is separated by gas chromatography. Similarly, sulfur is oxidized to SO_2. Oxygen is determined after its conversion to CO.

Metallic compounds can also be found. In conventional petroleum fractions, they can reach a thousand ppm. A small number can have a negative effect and result in coke formation. Several methods exist to determine the composition of these metals. For instance ASTM D1026, D1262, D1318 and D1548.

Many other properties are important design parameters, or are useful to characterize a petroleum fraction. Nevertheless, they were not used in the current thesis so they are not described.

A high number of estimation method exist so that different set of properties can be used to estimate other properties. Thus, measuring the right properties is important to access to the full property set. A useful method is the pseudo-component method which requires the distillation curve and the hydrocarbon class composition to access to other properties. This method is described in the next section to predict the ON.

2.6 PREDICTION METHODS APPLIED TO LIQUID FUELS

2.6.1 *Prediction of the octane numbers*

As an alternative to RON and MON measurement, estimating methods exist. They differ one another by the principles behind the model. Statistical methods rely on different input quantities. They can either be the chemical properties [105–110], physical properties [111], or the ignition delay [95, 97, 112, 113]. Composition-based models rely on several methods such as partial least square (PLS) regression [107, 108], neural networks [106, 109] and multivariate calibration [105, 110]. Other models rely on physical properties. Among others, Mendes et al. developed models based on distillation curves and partial least squares regression [111].

The prediction of the octane number of a fuel can be obtained with a simple linear blending law. Traditionally, the mixing law is based on a linear

average weighted by the volume fractions. Nevertheless, Pera et al. [85] showed that a linear averaging weighted by compound molar fractions is more precise than a average weighted by volume fractions.

$$ON = \sum_{i=1}^{N} x_i ON_i \tag{26}$$

where x is the molar fraction of the component i.

Similarly, when an oxygenated molecules is added into the fuel, the following relation can be applied [8]:

$$ON = x_{ox} ON_{ox} + (1 - x_{ox}) ON_{clear}, \tag{27}$$

with ON_{clear}, the octane number measured or calculated without the oxygenated component.

Nevertheless, this simple formulation does not take the interactions between the components, also called antagonist and synergistic blending effects, into account. Nikolaou et al.[22] proposed a non linear blending law with blending coefficients that depend on the BON, a concept introduced in the API project 45 [26] and described in Section 2.5.2.

$$RON = \sum_{i=1}^{N} K_i RON_i y_i \tag{28}$$

where y_i are the volume fractions of the components in the studied blend, RON_i is the measured pure RON and K_i is the following factor:

$$K_i = \frac{RON_i}{BRON_i} \frac{\sum_{i=1}^{N} BRON_i y_i}{\sum_{i=1}^{N} RON_i y_i} \tag{29}$$

with $BRON_i$ the blending octane number of the component i in the blend.

An example applied to a gasoline fuel is given in Table 6. For this sample fuel, the sum of the octane numbers weighted by the volume fractions gives 85.1 while 86.9 is obtained with Equation 28.

The previous formula gives an accurate estimation of the octane number, but is hardly applicable with a real fuel made of hundred of molecules. Identifying all the molecules and knowing all of their ON is impossible.

The ON of complex fuels can be calculated with the PC method. With this method, the fuel is divided into PCs. A PC is a virtual molecule that represents a hydrocarbon class and its properties depending on the boiling point (the MeABP) of the fuel. Thus, all the molecules in a hydrocarbon class are substituted by a single molecule as long as the fuel boiling point is known.

$$ON = \sum_{i=1}^{N} y_i ON_i^{pc} \tag{30}$$

where ON_i^{pc} is the octane number of the PC i. This octane number depends on the fuel boiling point. The dependency law between the PC octane number and the boiling points are calculated with a regression. This regression is obtained seeking the best law between the boiling points and the octane number of pure molecules in the hydrocarbon class. An example of is given on Figure 22 where the regressions are calculated with Equation 31 and Table 7. The octane number of the pseudocomponent for the iso-paraffins group

Table 6: Example of calculated weighting factor and effective research octane numbers [22]

Molecule	Volume fraction	K_i	Pure RON	Measured BRON	Calculated BRON
2-methyl-butane	0.4507	0.974	92.3	100	89.9
2,2-dimethyl-butane	0.2342	1.088	91.8	89	99.9
n-pentane	0.1335	1.05	61.7	62	64.8
2-methyl-pentane	0.049	0.944	73.4	82	69.3
2,3-dimethyl-butane	0.027	1.137	103.5	96	117.7
n-hexane	0.026	1.377	24.8	19	34.1
cyclohexane	0.0249	0.796	83	110	66.4
3-methyl-pentane	0.02	0.914	74.5	86	68.1
cyclopentane	0.0116	0.758	101.3	141	76.8
methylcyclopentane	0.0113	0.9	91.3	107	82.2
n-butane	0.0043	0.876	93.8	113	82.1
methyl-cyclo-hexane	0.0039	0.759	74.8	104	56.7
2-methyl-hexane	0.0006	1.118	42.4	40	47.4
3-methyl-hexane	0.0005	0.979	52	56	50.9
2,2-dimethyl-pentane	0.0004	1.1	92.8	89	102.1
2,2-dimethyl-propane	0.0003	0.902	85.5	100	77.1
2,4-dimethylpentane	0.0003	1.153	83.1	76	95.8
2,3-dimethyl-pentane	0.0003	1.102	91.9	88	101.2
3,3-dimethyl-pentane	0.0002	1.015	80.8	84	82
1,1-dimethyl-cyclo-pentane	0.0002	1.014	92.3	96	93.6
1,3-dimethyl-cis-cyclo-pentane	0.0002	0.852	79.2	98	67.5
1,3-dimethyl-trans-cyclo-pentane	0.0002	0.945	80.6	90	76.1
3-E-pentane	0.0002	1.071	65	64	69.6
n-heptane	0.0002		0	0	0
2,2,3-trimethyl-butane	0.0001	1.056	112.1	112	118.4
E-cyclo-pentane	0.0001	1.158	67.2	61.2	77.8

is the average between the 2-methyl-alkane, 3-methyl-alkane, 2,2-dimethyl-alkane and 2,2-dimethyl-alkane.

$$RON = a + bT + cT^2 + dT^3 + eT^4 \tag{31}$$

where $T = (T_b - 273.15)/100$ where T_b is the boiling temperature in kelvin.

When the RON is known, the MON can be calculated with the following formula:

$$MON = 22.5 + 0.83RON - 20.0SG - 0.12\%O + 0.5TML + 0.2TEL, \tag{32}$$

with SG the specific gravity, %O the volume fraction of olefins, TML the concentration of tetra methyl lead and TEL the concentration of tetra ethyl lead. The TEL and TML are octane boosters. Moreover, this equation shows that olefins tend to decrease the MON.

Other predicting laws were proposed for other mixtures. For instance, Morgan et al. [114] mapped the octane numbers of TRF. Morgan et al.

Table 7: Coefficients to calculate the octane numbers of pseudocomponents in Equation 31 according to Riazi [8]

Hydrocarbon family	a	b	c	d	e
n-paraffins	92.809	-70.97	-53	20	10
isoparaffins					
2-methyl-alkane	95.927	-157.53	561	-600	200
3-methyl-alkane	92.069	57.63	-65	0	0
2,2-dimethyl-alkane	109.3	-38.83	-26	0	0
2,3-dimethyl-alkane	97.652	-20.8	58	-200	100
Naphthenes	-77.536	471.59	-418	100	0
Aromatics	145.668	-54.336	16.276	0	0

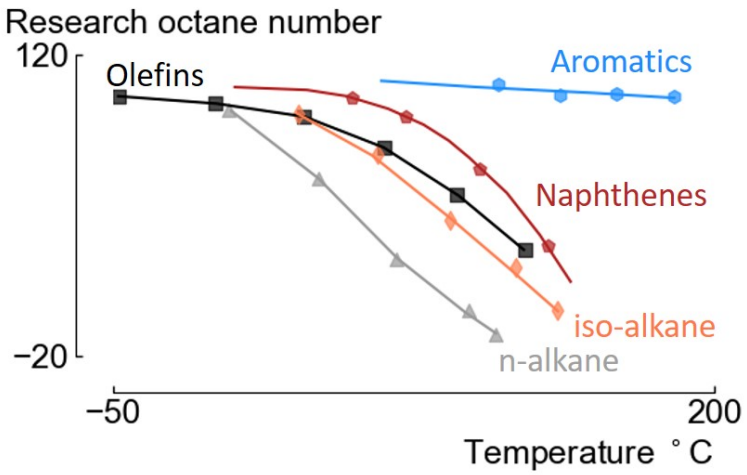

Figure 22: RON of pseudocomponents of several hydrocarbon classes [8]. The dots refer to the experimental octane numbers of pure molecules.

fitted several forms of response surface to evaluate the RON and the MON. Specifically, Morgan et al. tried a linear-by-volume model, defined by:

$$\mathrm{RON} = 120x_{\mathrm{tol}} + 100x_{\mathrm{iO}} + 0x_{\mathrm{nH}} \tag{33}$$

and

$$\mathrm{MON} = 109x_{\mathrm{tol}} + 100x_{\mathrm{iO}} + 0x_{\mathrm{nH}} \tag{34}$$

Nevertheless, such a simple law cannot correctly predict the octane numbers. In fact, synergistic and antagonistic effects exist between the molecules. For this reason, Morgan et al. proposed second order models with interaction coefficients [114]. Thanks to these equations, the authors showed that the interactions are especially present when toluene and iso–octane are mixed. The different equations were also inverted, allowing to calculate the composition of a TRF to get a predefined octane number.

The interest in ethanol blending has recently increased due to the presence of bioethanol in fuels. Thus, Aronsson et al. proposed law to correlate the

octane number of TRF mixed with ethanol with their composition [115]. To do so, they rely on second order models.

The octane number can also be estimated by the mean of an IQT, a system traditionally developed to determine the DCN of diesel fuels based on ASTM D6890 [102]. Recent findings regarding the link between the ignition delay time and the octane number have led to the estimation of the octane number with an IQT. In 2015, Badra et al. achieved a good prediction of the TRF research octane numbers with constant volume ignition delay times calculated at 850 K and 50 atm [113]. Two years later, Naser et al. defined the optimal temperature to predict the octane number of TRF and real fuels [95]. This concept had later been extended in 2018 to introduce the ignition delay time sensitivity, an equivalent of the octane sensitivity but determined with ignition quality testers [97].

Other method exist to predict the octane number such as the group contribution method. Albahri proposed the following formula to calculate the octane number of a pure components [116]:

$$\begin{aligned} RON = a + b\Big(\sum_i ON_i\Big) + c\Big(\sum_i ON_i\Big)^2 \\ + d\Big(\sum_i ON_i\Big)^3 + e\Big(\sum_i ON_i\Big)^4 + f/\Big(\sum_i ON_i\Big) \end{aligned} \quad (35)$$

with $\sum_i ON_i$ is the sum of the group contributions listed in Table 8 and 9. The coefficients a, b, c, d, e and f are constants from Table 10. This formula is valid for octane numbers from -20 to 120. However, these method lack generality. They are not capable of predicting non linear interaction between the functional groups.

A similar method was proposed by Meusinger et al.[117] where the integral regions obtained with a NMR analysis are used to calculate the ON. The regions are sorted according to Table 11. The octane numbers can be calculated with the integrals according to the following equations:

$$\begin{aligned} RON_{cal} = 0.0759I_A + 0.0747I_B + 0.1276(I_C + I_H) + 0.1307(I_D + I_I) + 0.1239I_E \\ + 0.188I_F + 0.0204I_G + 0.0933I_K + 0.0437(I_L - 3I_F) + 0.1006I_M, \end{aligned} \quad (36)$$

$$\begin{aligned} MON_{cal} = 0.064I_A + 0.034I_B + 0.1058(I_C + I_H) + 0.0759(I_D + I_I) + 0.1019I_E \\ + 0.1456I_F + 0.0671I_G + 0.0743I_K + 0.0514(I_L - 3I_F) + 0.095I_M. \end{aligned} \quad (37)$$

The factors that multiply the integrals give an information on the role of each functional group on the octane number. MTBE (F), methanol (E), the aromatic rings and methyl substituents (C+H) have the largest influences. The difference between the RON and the MON informs about the sensitivity. For instance, the alkyl substituent in the α position (G) have a strong influence on the sensitivity. NMR methods are appropriate to estimate the octane number as long as extrapolation is not requested, and as long as there is no strong interaction coefficient. The methods relying on NMR requires only 30 minutes and 100 µl. Nevertheless, the separation of the olefin, n-paraffins and iso-paraffins with NMR is a challenge. Therefore, this method may not be accurate for fuels with a high concentration of olefins and paraffins.

Table 8: Group Contribution for Estimation of the Octane Number

HC type	Group	RON_i	MON_i
Paraffins	$-CH_3$	-2.315	-0.202
	$>CH_2$	-8.448	-9.082
	>CH-	-0.176	-1.821
	>C<	11.94	11.90
Olefins	=CH-	0.392	-2.293
	>C=	8.697	2.703
	$=CH_2$	3.623	-0.254
	=C=	-37.37	-42.43
	=CH- (cis)	6.269	2.725
	=CH-(trans)	6.449	4.743
	≡CH	18.36	21.36
	≡C-	-7.201	-12.96
Cyclic	$>CH_2$	-4.421	-5.377
	>CH-	-2.177	-3.631
	>C<	8.916	10.52
	=CH-	2.879	-4.765
	>C=	5.409	5.065
Aromatics	=CH-	3.591	9.725
	>C=	2.382	-5.650
	>C=(o)	-1.768	1.712
	>C=(m)	10.24	14.16
	>C=(p)	11.51	10.09

2.6.2 *Prediction of the cetane number*

The cetane number evaluates the propensity for a fuel to autoignite under the diesel condition. The determination of cetane number is costly because it requires expensive products and an expensive engine, so, alternative methods exist. Calculated cetane index (CCI) can be determined with the distillation curve and the specific gravity:

$$CCI = 454.74 - 1641.41SG + 774.74SG^2 - 0.554T_{50} + 97.083(\log_{10}T_{50})^2, \quad (38)$$

with T_{50} the ASTM D86 temperature at 50%v in °C. This equation may give bad results if additives are present in the fuel.

The diesel index (DI) is another characteristic parameter of diesel fuels. It is related to the API gravity and the Aniline point (AP) (in °C) by the following relation:

$$DI = \frac{API(1.8AP + 32)}{100}, \quad (39)$$

CCI, DI and AP are empirically correlated as:

$$CCI = 0.72DI + 10, \quad (40)$$

and

$$CCI = AP - 15.5. \quad (41)$$

The n-paraffin content is also well correlated with CCI:

$$x_P = 1.34CCI - 57.5. \quad (42)$$

Table 9: Group Contribution for Estimation of the Octane Number

HC type	Group	RON_i	MON_i
Paraffins	$-CH_3$	0.459	0.491
	$>C_2H_5$	0.948	0.517
	$>CH_2-$	0.680	0.722
	>α->CH-	-0.139	-0.430
	>β->CH-	-0.362	-0.186
	>δ->CH-	-0.358	-0.768
	α>C<	-1.357	-1.983
	β>C<	-1.828	-12.88
Olefins	=CH-	-0.078	0.454
	=CH- (C#⩾5)	-0.660	-4.438
	$\alpha- > C \equiv$	-0.811	-1.542
	$\beta- > C \equiv$	-0.6441	-1.529
	$=CH_2$	0.119	-1.603
	=C=	2.693	4.691
	=CH- (cis)	-0.409	-2.414
	=CH-(trans)	-0.387	-2.378
	≡CH	-1.267	-8.110
	≡C-	0.603	-6.501
Cyclic	$>CH_2$	0.400	-0.105
	>CH-	0.122	1.301
	>CH-(o)	-0.330	1.199
	>C<	-0.800	-3.878
	=CH-	-0.064	0.206
	>C=	-0.356	-9.033
	Correction for C_3 ring	-1.217	-2.521
	Correction for C_4 ring	1.117	-1.057
	Correction for C_7 ring	0.75	2.481
	Correction for C_8 ring	-0.468	0.562
Aromatics	=CH-	-0.202	-1.859
	>C=	0.193	-1.912
	>C=(o)	-0.337	-3.151
	>C=(m)	-0.959	-3.141
	>C=(p)	-0.498	-1.449

Table 10: Group Contribution for Estimation of the Octane Number

ON	use with Table	a	b	c	d	e	f
RON	1	103.6	0.231	-0.0226	0.001	1.42E-05	1.58
RON	2	104.8	-5.395	6.532	-5.165	0.6189	-0.0037
MON	1	88.87	0.212	-0.0093	0.00104	9.59E-6	0.339
MON	2	84.04	1.840	-1.452	-0.357	-0.0179	0

The cetane index is another estimation of the CN, given by the four variable Equation. The four variable equation is known as:

$$CI = 45.2 + 0.0892T_{10N} + (0.131 + 0.901B)T_{50N} + (0.0523 - 0.42B)T_{90N} + 0.00049({T_{10N}}^2 - {T_{90N}}^2) + 107B + 60B^2, \quad (43)$$

Table 11: Chemical shift regions and corresponding structural groups

^{1}H chemical shift (ppm)	Class	Structural group	Integral regions
8.0-7.4	Aromatics	Naphthalene	A
7.4-7.3		Benzene	B
7.3-6.7		Substituted aromatics	C
6.0-5.5	Olefins	HHC=C**H**R	D_1
5.5-5.25		RC**H**=C**H**R	D_2
5.25-5.05		RRC=C**H**R	D_3
5.05-4.8		**HH**C=CHR	D_4
4.8-4.6		**HH**C=CRR	D_5
3.5-3.3	Oxygenates	C**H$_3$**-OH	E
3.2-3.0		C**H$_3$**-OC(CH$_3$)$_3$	F
3.0-2.7	Aromatics	Ph-C**H**<	G_1
2.7-2.5		Ph-C**H$_2$**-	G_2
2.5-2.1		Ph-C**H$_3$** and C=C-C**H**<	H
2.1-1.85	Olefins	C=C-C**H$_2$**-	I
1.85-1.4	Saturates and olefins	-C**H**< -C**H$_2$**-(cycl.) C=C-C**H$_3$**	K
1.4-1.1		-C**H$_2$**- C=C-C-C**H2**- Ph-C-C**H$_3$**	L
1.1-0.5		-C**H$_3$**	M

where:

$$\begin{aligned} T_{10N} &= T_{10} - 215, \\ T_{50N} &= T_{50} - 260, \\ T_{90N} &= T_{90} - 310, \end{aligned} \tag{44}$$

T_X is the X% distillation recovery temperature, in degrees Celsius,

$$B = \exp(-0.0035 D_N) - 1, \tag{45}$$

with $D_N = D - 850$, where D is the density at 15 °C, in kg/m^3.

Group contribution methods were developed to estimate the CN. With this method, De Fries et al. proposed the following equation [118]:

$$CN = \sum_i f_i cn_i, \tag{46}$$

with f_i the fraction of group i in the molecule and cn_i the group contribution for group i. The groups could for instance be measured by NMR. This method does no include ringed compounds and carbon-carbon double bonds. As for the ON, the main issues with group contribution methods is the error when another molecule than the ones of the training set is tested. In fact, the predicting laws are especially fitted for the training set. The results are good when the tested molecule is similar in size and shape to the molecules of the training set, but the prediction are poor when the model is extrapolated.

One issue with existing group contribution methods is the lack of capacity in predicting non linear interactions between the functional groups. This is true for all the group but especially with oxygenated molecules. This is due to the complexity of such properties that depend on a complex chemical kinetic mechanism.

Additionally, attempts to create a single model to predict the RON, the MON and the CN failed [119]. This is due to the difference between these methods. Even if they all aim at characterising the autoignition, they do so in largely different conditions.

2.6.3 *Prediction of the composition*

The composition of a fuel must be monitored because it controls the level of pollutant thanks to a comparison with predefined threshold, and it gives a first insight on the combustion behaviour. Models to predict the composition of olefin-free and oxygenated-free petroleum fractions are reported by Riazi [8]. Three equations are required to obtain the three unknowns: the fractions of paraffin, naphthenes and aromatics. A first equation is given by:

$$x_P + x_N + x_A = 1. \tag{47}$$

For the two other parameters, two mixing laws can be applied:

$$\theta = x_P\theta_P + x_N\theta_N + x_A, \tag{48}$$

where θ is a physical property and θ_P, θ_N and θ_A are the values of θ for the model pseudocomponents from the three groups.

The comparison of four properties on Figure 23 shows that R_i and VGC are appropriate properties. Average values of these parameters were determined for each hydrocarbon class. They are listed in Table 12. Applying these values with Equation 48 gives:

$$R_i = 1.0482x_P + 1.038x_N + 1.081x_A, \tag{49}$$

and

$$VGC = 0.744x_P + 0.915x_N + 1.04x_A. \tag{50}$$

Table 12: Average values of several properties for the considered hydrocarbon class.

Hydrocarbon class	R_i	VGC
Paraffin	1.0482	0.744
Naphthene	1.0138	0.915
Aromatics	1.081	1.04

These equations were modified based on a regression of 33 hydrocarbon mixtures, which gives new constants modified by less than 2% [120, 121]:

$$R_i = 1.0486x_P + 1.022x_N + 1.11x_A, \tag{51}$$

and

$$VGC = 0.742x_P + 0.9x_N + 1.112x_A. \tag{52}$$

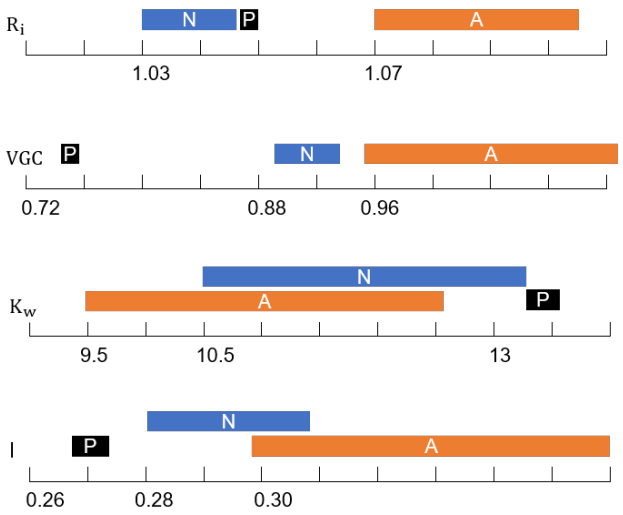

Figure 23: Comparison of several properties (refractivity intercept, viscosity gravity function, Watson factor, refractive index parameter) to distinguish the hydrocarbon class fractions (n-paraffin, napthene and aromatic (PNA)) adapted from [8].

The resolution of Equations 47, 51 and 52 gives for fractions with molecular weight between 200 and 600:

$$x_P = -9.0 + 12.53R_i - 4.228VGC, \tag{53}$$

$$x_N = 18.66 - 19.9R_i + 2.973VGC, \tag{54}$$

$$x_A = -8.66 + 7.37R_i + 1.255VGC. \tag{55}$$

Similar equations were developed for fuels with a kinematic viscosity less than 38 SUS with the VGF. Moreover, additional data were added to modify the Equations 53 to 61 [122]. Finally, the following equation can be used to estimate the paraffin, naphthene and aromatic fractions in heavy and light petroleum fractions.

For light fractions with M$\leqslant$200:

$$x_P = -13.359 + 14.4591R_i - 1.413344VGF, \tag{56}$$

$$x_N = 23.9825 - 23.33304R_i + 0.81517VGF, \tag{57}$$

$$x_A = 1 - x_P - x_N. \tag{58}$$

For light fractions with M>200:

$$x_P = 2.5737 + 1.0133R_i - 3.573VGC, \tag{59}$$

$$x_N = 2.464 - 3.6701R_i + 1.96312VGC, \tag{60}$$

$$x_A = 1 - x_P - x_N. \tag{61}$$

These equations can give a negative value for the one of the fractions. In that case, it should be set to zero. This shows a first limit of this methodology.

If the kinematic viscosity if not available, other correlations were developed based on other parameters. They are SG, m and CH and the equations are given thereafter.

For light fractions with M⩽200:

$$x_P = 2.57 - 2.877SG + 0.02876CH, \tag{62}$$

$$x_N = 0.52641 - 0.7494x_P - 0.021811m, \tag{63}$$

or:

$$x_P = 3.7387 - 4.0829SG + 0.014772m, \tag{64}$$

$$x_N = -1.5027 + 2.10152SG - 0.02388m. \tag{65}$$

Then, the aromatic fraction can be calculated with Equation 61. These equations were evaluated with the PNA composition of 85 fractions in the molecular weight range of 78 to 214 and give average deviation of 0.05, 0.08 and 0.07 for x_P, x_N and x_A, respectively with Equations 62 and 63. For Equations 64 and 65 the average deviations were 0.05, 0.086 and 0.055.

For fractions with M>200:

$$x_P = 1.9842 - 0.27722R_i - 0.15643CH, \tag{66}$$

$$x_N = 0.5977 - 0.761745R_i + 0.068048CH, \tag{67}$$

or:

$$x_P = 1.9382 + 0.074855m - 0.1966CH, \tag{68}$$

$$x_N = -0.4226 - 0.00777m + 0.107625CH. \tag{69}$$

These equation were evaluated with the PNA composition of 72 fractions in the molecular weight range of 230 to 570 and give average deviations of 0.06, 0.06 and 0.02 for x_P, x_N and x_A, respectively.

Equations 64 and 65 were expanded for heavier fractions (between 70 and 250) [123]:

$$x_P = 3.2574 - 3.48148SG + 0.011666m, \tag{70}$$

$$x_N = -1.9571 + 2.63853SG - 0.03992m. \tag{71}$$

The aromatic content can also be calculated in another way. When the aromatic content is high (up to 96%), it may be divided into monoaromatics and polyaromatics, and relying on the following equations results in the calculation of the total amount of aromatics [122].

$$x_{MA} = -62.8245 + 59.90816R_i - 0.0248335m, \tag{72}$$

$$x_{PA} = 11.88175 - 11.2213R_i + 0.023745m, \tag{73}$$

$$x_A = x_{MA} + x_{PA}. \tag{74}$$

These formula are valid for a molecular weight range from 80 to 250. These equations give an average deviation of 0.055, 0.065 and 0.063 for x_{MA}, x_{PA} and x_A, respectively.

The formula exposed in the current section give good result but they can only be applied to fuels with no olefins and no oxygenates. However, it will be showed in chapter 5 that fuels produced from ASR have high fractions of these types of molecules.

2.6.4 *Definition of surrogate fuels*

The RON, the MON and the CN are measurement of ignition delay times in a specific engine (CFR engine) under predefined conditions. They are good indicators of the behaviour of a fuel. Thus, simulations are sometimes required to get a more precise prediction. Nevertheless, doing these simulations with real fuels is impossible because they are too complex, composed of hundred of molecules. Thus, the complex fuel is usually substituted by a surrogate fuel, i.e. a blend of a small number of molecules with similar properties than the complex fuel. Combustion scientists rely on surrogate fuels to have an a priori insight on a diesel [83, 124], jet fuel [124], naphta [125] or gasoline [126–128] behaviour through simulations or experiments.

Examples are first given for simulations. Autoignition was studied with a gasoline surrogate fuel by Andrae et al. thanks to parametric simulations as the phenomenon depends on the operating conditions [128]. Moreover, Agbro et al. studied the influence of n-butanol blended with TRF (n-heptane + iso-octane + toluene) in a modelled spark-ignition engine with a particular attention on knock [127].

Surrogate fuels can also be tested experimentally during a pre-design phase to improve the engine settings. For instance, Andrae et al. discussed the autoignition of four gasoline surrogate fuel blends depending on intake temperature and pressure in a homogeneous charge compression ignition (HCCI) engine [129]. Additionally, the surrogate fuel can be studied in simple reactors such as jet stirred reactor and shock tube to investigate the ignition delay [130]. Other properties than the ignition delay can be studied experimentally. Perez et al. investigated the thermal efficiency, the combustion phasing and the maximum pressure rise rate of gasoline surrogate fuels in a Ricardo Hydra single-cylinder engine under HCCI [126]. Similarly, Vallinayagam et al. tested experimentally a surrogate light naphtha and analysed the ignition delay, the pressure curve, the stratification and the emission levels [125].

Preliminary conclusions on a surrogate fuel can be applied to the real fuel as long as the two fuels behave similarly in the final installation. This

behaviour is a consequence of physical laws applied to the fuel properties. Thus, the properties of the surrogate fuels are selected and designed accordingly. Specifically, the selection depends on the application. Moreover, their value matches with the properties of the real fuel. To sum up, the designed properties are the central point from which the surrogate formulation flows towards the final usage. For instance, extinction and autoignition in laminar non premixed flows reproduced some ignition characteristics of JP-8 and Jet-A [131]. Similarly, Knop et al. validated octane number-based surrogate fuels in controlled auto-ignition (CAI) combustion engines [85, 132]. To go further, applications with a direct injection requires the fuel evaporation characteristics to be matched. As exposed by Pitz et al. and Sarathy et al., a wide range of properties exist for gasoline [133] and diesel [83] fuels, which offer different angles of attack to formulate a surrogate fuel, depending on the final application.

As previously depicted, the properties of a surrogate fuel are designed to match with the properties of a real fuel, such as the RON and the MON. This very basic concept raises an issue if the properties cannot be measured for technical reasons. During their design phase, unconventional fuels are expensive and scarce. Under these conditions, the RON and the MON cannot be measured. As an answer, pivot properties substitute the usual properties. In this recent concept of indirect design, the molecular scale often substitutes the macroscopic scale. For instance, the functional groups [134], or the carbon types [86], are pivot properties that have a direct consequence on underlying properties, for instance the RON and the MON. However, the surrogate fuel must be validated after its formulation, so, additional tests are required. Abdul Jameel et al. [134] relied on rapid compression machine (RCM) tests. We propose an alternative to the ON as target properties in chapter 8. The results of tests in a RCM are used instead of the RON and the MON.

3 METHODOLOGY

The current chapter summarizes the methodologies used to formulate the models. Samples were generated following latin hypercube sampling (LHS). Set of variables were selected relying on a principal component analysis (PCA) and regression were based on artificial neural network (ANN). Finally, the parameters of a model were determined relying on Bayesian inference.

3.1 LATIN HYPERCUBE SAMPLING

In the current thesis, LHS was used as space filling design. Designs of experiments were detailed by Iavarone in its introduction of LHS [135]. Designs of experiments can be seen as the design of computer experiments where a computer experiment can be seen as a blackbox with inputs and observed outputs (targets). The objective of design of experiments is to perform the smaller number of experiments with the larger number of information on the output. LHS is a modern design of experiments statistical method for generating sample of a parameter and which optimizes the space covering. LHS can easily be represented into two dimensions but can be realized in a space of dimension n. A square grid is plotted with hypothetical sampling positions. Let the studied ranges be [0,1]. They can be divided into M intervals I_k such as:

$$I_k = [\frac{k-1}{M}, \frac{k}{M}], \text{ for } k = 1...M. \tag{75}$$

Then, each line and column must be occupied by a sample point as showed on Figure 24. This figures show that the space filling may not be optimal as the first figure is almost diagonal and the middle of the second is almost empty. As a solution to this, a convergence study was performed with each carried out LHS and several iterations were performed to ensure the space to be correctly filled.

A Latin hypercube is the generalization of a Latin square with a number of dimensions n with $n \geqslant 3$. To perform LHS, let's consider M samples with N components each. N permutations of the samples are realized randomly and uniformly among the N! possible permutations. π_i being a single permutation, the i-th component of the j-th sample is obtained by randomly

picking a value in the interval $I_{\pi_i(j)}$ where $\pi_i(j)$ is the j-th element of the i-th permutation. An advantage is that random samples can be chosen one at a time, remembering which samples were used.

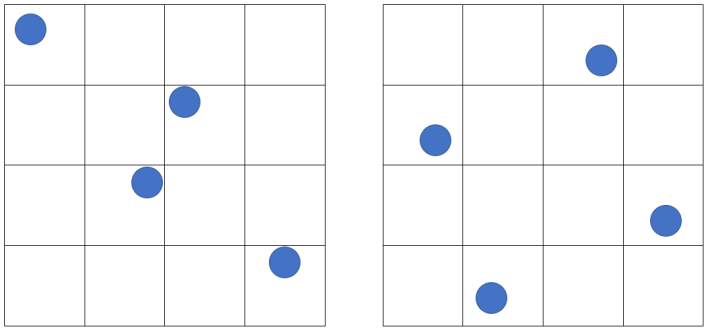

Figure 24: Examples of latin hypercube sampling with 4 samples. Each line and each column are occupied by one sample, which optimizes the space covering.

3.2 PRINCIPAL COMPONENT ANALYSIS

The origin of PCA is associated with the work of Pearson (1901) and Hotelling (1933). Behind the concept of PCA, we aim at reducing the dimensionality of a dataset composed of a large number of variables which depends on each others. The relationship of these variables is sought in order to transform the initial data into a new set of variables, the principal components, which are uncorrelated. This way of proceeding reduces the dimensionality but keep as much as information as possible.

Suppose that $\mathbf{X}$ is a matrix of n random variables, each of these variables being defined by p observations. A way of proceeding these data would be to look at the variances and covariances. As an alternative, relying on linear algebra is a way to consider the original data into a new coordinate system. In this new coordinate system, the original information will be conserved but the dimensionality of the data will be reduced.

In the original coordinate system, each observed variable $\mathbf{x}$ can be written as

$$\boldsymbol{\alpha}_1^T \mathbf{x} = \sum_{j=1}^{n} \alpha_{1,j} x_j \tag{76}$$

In a new coordinate system, we can consider a linear function $\boldsymbol{\alpha}_2^T \mathbf{x}$, uncorrelated with $\boldsymbol{\alpha}_1^T \mathbf{x}$ and having maximum variance. This process can be conducted k times so that $\boldsymbol{\alpha}_k^T \mathbf{x}$ has maximum variance and is uncorrelated with $\boldsymbol{\alpha}_1^T \mathbf{x}$, $\boldsymbol{\alpha}_2^T \mathbf{x}$, ..., $\boldsymbol{\alpha}_{k-1}^T \mathbf{x}$. The k-th derived variable is the k-th principal component. We assume that the number of principal components is lower than the original number of variables n as the variance is limited around certain dimensions.

To illustrate, let us consider the simple case where n=2. Figure 25 shows 20 observations on two highly correlated variables x_1 and x_2. If we change the coordinate system to the principal components, we obtain the plot in Figure 26. In this new coordinate system, most of the variation is captured by the first direction z_1 while the second z_2 contains few information.

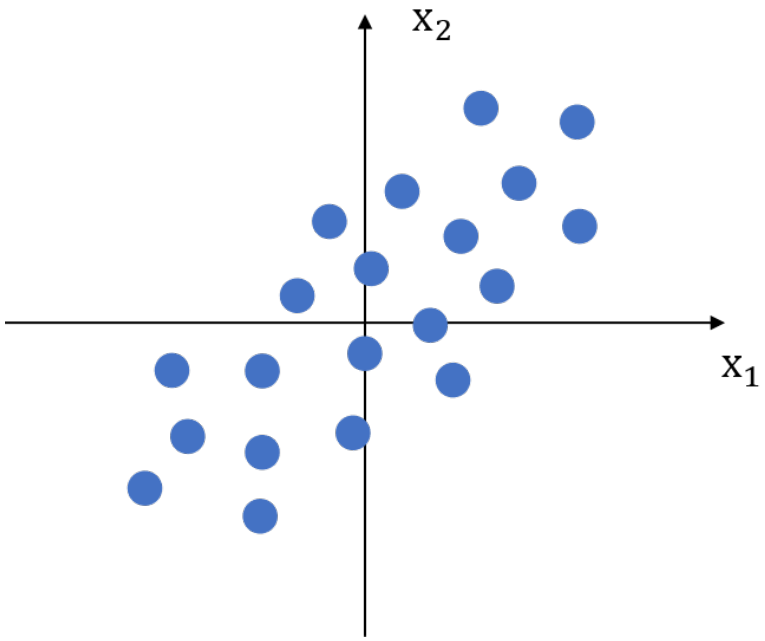

Figure 25: Plot of 20 observation on two variables x_1 and x_2.

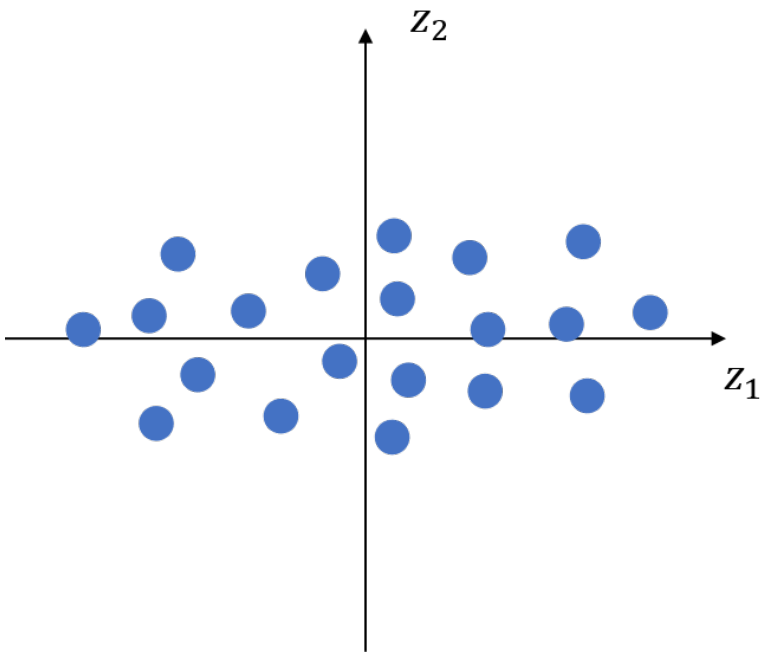

Figure 26: Plot of the 20 observation projected onto their principal components z_1 and z_2. The variance is almost entirely captured by the first direction.

If we consider a system with p dimensions, where p is large, the projection of the original data onto the principal components, will concentrate the information on the firsts principal components while for the lasts principal components, only a small amount of the variance will be represented.

The data considered until this point must be centered and scaled. This is particularly important for multivariate data, for instance for data expressed under different units or scales. This is illustrated by Figure 27. To center the

data, each observation is subtracted by the mean of each variable so that we are considering a variations comparing to a mean. Then, the scaling is the division of the remaining quantity by a scaling factor.

$$\tilde{\mathbf{x}} = \frac{\mathbf{x} - \bar{\mathbf{x}}}{d} \tag{77}$$

The scaling factor, d, depends on the method used. In the current thesis, we consider several scaling methods: Auto, Range, Vast. The scaling factor for each of these method is respectively the standard deviation, the difference between the maximum and the minimum of each variable and the product between the standard deviation and the so-called coefficient of variation, defined as the standard deviation divided by the mean value.

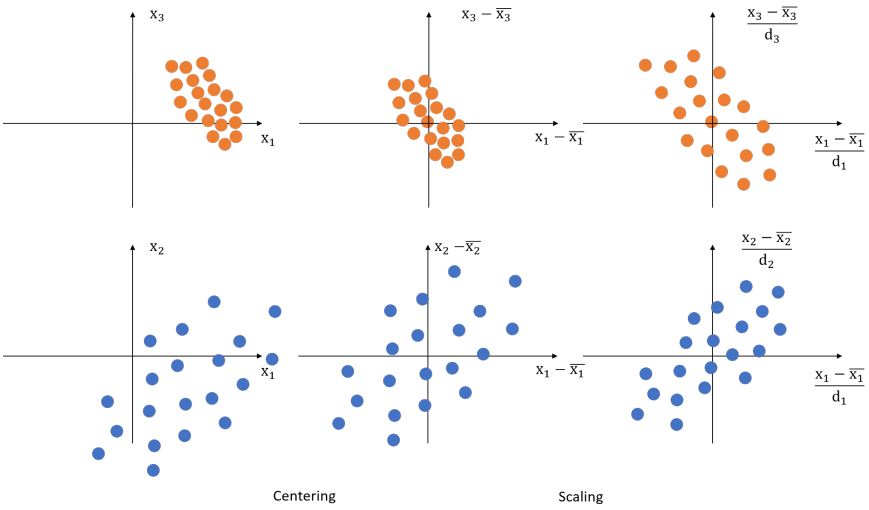

Figure 27: Illustration of the importance of centering and scaling. Thanks to these procedures, the data can be compared between each others.

The principal components have been defined, now we detail how to find them. This is based on the covariance matrix of the data $\mathbf{x}$. This covariance matrix is composed of (i, j)th elements which are the covariances between the ith and the jth elements of $\mathbf{x}$ and the variance of the ith element of x when i=j. The kth principal variable is given by $z_k = \boldsymbol{\alpha}^T \mathbf{x}$ where $\boldsymbol{\alpha}_k$ is an eigenvector of the covariance matrix corresponding to the kth largest eigenvalue λ_k. Moreover, if the eigen vector is chosen to have unit length, then $\text{var}(z_k) = \lambda_k$.

The advantage of working with principal components is the possibility to reduce the dimensionality by selecting a subset of variables. In fact, when the number of observed variable n is large, there is often a subset m of variables such as m<<n which contains all the information available in all n variables. Then, the problem is to define what is the optimal number m and how to retain the m variables.

In the current thesis, the number of selected variables is defined by analysing the percentage of the observed variance, defined by:

$$p = \frac{\sum_{i=1}^{m} \lambda_i}{\sum_{j=1}^{n} \lambda_j} \tag{78}$$

where λ are the eigen values. When this percentage reaches 99%, the number of eigen vectors was considered to be enough [136].

Then, to select the principal variables, several methods were considered, the B2 and the Procrustes methods. First, with the B2 method, let us consider that m variables must be deleted. The last m principal components are a combination of all the original variables. Each variable has a certain weight, indicating how much that variable is represented by the principal component (PC). Then, the variable with the highest weight for the last PC is deleted. This process is repeated until m variables are deleted.

For the Procrustes method, let us consider $\mathbf{X}$ that is to be reduced to a smaller size. Each variable is deleted from this matrix, which gives p matrices $\tilde{\mathbf{X}}$. PCA is applied to obtain the corresponding $\mathbf{Z}$ and $\tilde{\mathbf{Z}}$ matrices. A Procrustes analysis is applied to each of these matrices. This means that p coefficients M^2 are calculated to evaluate the differences between Z and $\tilde{\mathbf{Z}}$. These coefficients are given by:

$$M^2 = \mathrm{Tr}(\mathbf{Z}\mathbf{Z}' + \tilde{\mathbf{Z}}\tilde{\mathbf{Z}}' - 2\boldsymbol{\sigma}) \tag{79}$$

where $\boldsymbol{\sigma}$ is the matrix of the values obtained from the decomposition of the square matrix $\tilde{\mathbf{Z}}'\mathbf{Z}$.

3.3 ARTIFICIAL NEURAL NETWORK

ANN is a non linear, multivariate regression model [12]. It is a machine learning tool based on statistic which can learn complex relationships between inputs and outputs. They are specifically powerful to capture non-linear and complex relationships. ANN are computational models consisting of interconnected nodes that represent features or attributes of the analyzed dataset, which form a network. An ANN is a directed graph consisting of multiple layers of interconnected nodes. The nodes are structured in layers. Each ANN has a single input layer, one or several hidden layers and a single output layer.

We detail the basic ANN model, which can be described by a series of functional transformations [12]. Let us consider the input variables $x_1, ..., x_n$. The first transformations are M linear combination of the input variables:

$$a_j = \sum_{i=1}^{n} w_{ji}^{(1)} x_i + w_{jo}^{(1)}. \tag{80}$$

The superscript $^{(1)}$ indicates that the corresponding parameters are the first layer of the network. The parameters w_{ij} are the weights and the parameters w_{jo} are the biases. The variables a_j are called activations. Each of them is then transformed with a non linear activation function h:

$$z_j = h(a_j). \tag{81}$$

The values z_j are called hidden units. The nonlinear functions h are generally chosen to be sigmoidal functions such as the logistic sigmoid function or the tanh function. These quantities are again linearly combined to obtain the output unit activations:

$$a_k = \sum_{j=1}^{m} w_{kj}^2 z_j + w_{ko}^{(2)} \tag{82}$$

with k=1...K, and K is the total number of outputs. This transformation corresponds to the second layer of the network and the w_{ko} are the bias

parameters. Finally, the output unit activations are transformed with an appropriate activation function to give a set of network outputs y_k. The activation function is set depending on the nature of the data and the assumed distribution of target variables. For standard regression problems, the activation function is the identity so that $y_k = a_k$. For multiple binary classification problems, each output unit activation is transformed using a logistic sigmoid function so that

$$y_k = \sigma(a_k), \tag{83}$$

where

$$\sigma(a) = \frac{1}{1+\exp(-a)}. \tag{84}$$

Combining these various stages gives the overall network function:

$$y_k(x, w) = \sigma\left(\sum_{j=1}^{M} w_{kj}^{(2)} h\left(\sum_{i=1}^{D} w_{ji}^{(1)} x_i + w_{jo}^{(1)}\right) + w_{ko}^{(2)}\right) \tag{85}$$

where w is the vector composed of all the weights and biases. Figure 28 shows a graphical representation of Equation 85.

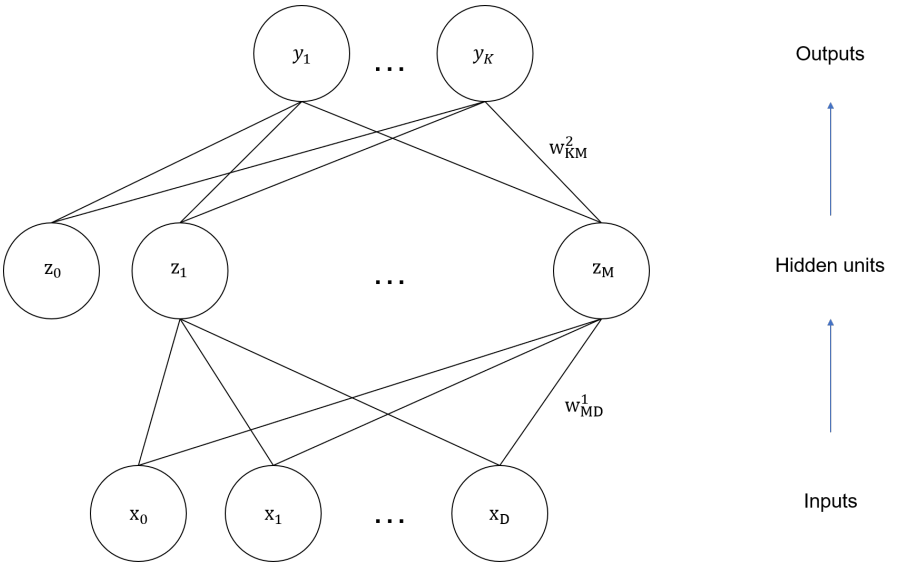

Figure 28: Network diagram for the neural network corresponding to Equation 85. [12]

3.4 BAYESIAN INFERENCE

The last section of the chapter on methodology deals with Bayesian inference. The methodology described in the present thesis is inspired from the work of Josephson et al. [137] et al. who themselves refer to Gelman [138].

The objective of applying Bayes' law is to set the correct values for model parameters knowing some experimental values.

Bayes' law is given by

$$f_{X|Y}(\mathbf{x}|\mathbf{y}) \propto f_{Y|X}(\mathbf{y}|\mathbf{x}) f_X(\mathbf{x}) \tag{86}$$

where $\mathbf{x}$ is a vector of the parameters to be determined of a given model and $\mathbf{y}$ is a vector of experimental data values, f refers to a probability density

function (PDF). This equation means that the probability of getting a set of parameters given the experimental data is proportional to the probability of getting the data given a set of parameters times the probability of getting the parameters. We aim at calculating the term of the left, also called posterior. On the right, we have the likelihood $f_{Y|X}(\mathbf{y}|\mathbf{x})$ and the prior $f_X(\mathbf{x})$.

The likelihood $f_{Y|X}(\mathbf{y}|\mathbf{x})$ represents the probability of the experimental data $\mathbf{y}$ with a set of parameters $\mathbf{x}$. Each data is a matrix of n experiments, each being separated in p observations. Then, each data point is $y_{z,i}$ with z the experiment and i the observation. Each data point is compared with the model value $\mu_{z,i}$ calculated with a set of parameters $\mathbf{x}$. We compare the difference between the experiment and the model which give the following form for the likelihood:

$$f_{Y|X}(\mathbf{y}|\mathbf{x}) = \prod_{z=1}^{n_e} \prod_{i=1}^{n_{z,i}} p(y_{z,i}|\mu_{z,i}(\mathbf{x})) \tag{87}$$

where n_e is the number of experiments and $n_{z,i}$ the number of observations in the experiment z. $p(y_{z,i} \mid \mu_{z,i}(\mathbf{x}))$ is the probability to get an observation compared to the evaluated point with a set of parameters $\mathbf{x}$.

$$\begin{aligned} &p\left(y_{z,i}|\mu_{z,i}(\mathbf{x})\right) = \\ &\frac{1}{\sqrt{2\pi\sigma^2}} \exp\left(-\frac{\left(y_{z,i} - \mu_{z,i}(\mathbf{x})\right)^2}{2\,\sigma}\right) \end{aligned} \tag{88}$$

When the uncertainty has been quantified, σ can be calculated in terms of quantified uncertainty.

The prior $f_X(\mathbf{x})$ represents an initial knowledge for the parameter $\mathbf{x}$. This function can be a result of a first study. If no information is available, the distribution would be rectangular.

4

FIRST INSIGHT OF ASR-DERIVED FUELS IN A COMPRESSION IGNITION ENGINE

4.1 INTRODUCTION

The fuel considered in the current thesis is a new and uncharted fuel. Therefore, it is important to test it in a simple engine before any further study. This will provide us a first insight on the fuel behaviour to answer basic questions such as: does the fuel is able to burn? Does the fuel burn similarly than a conventional diesel? Is the fuel hazardous for the engine? The current section answers these questions. A particular attention is devoted in characterizing the ignition delay time (IDT). In fact, in reactivity controlled compression ignition (RCCI), the high reactivity fuel (the heavy fraction) is injected directly in the combustion chamber, which trigger the combustion after a given IDT. Thus, being able to compare this IDT to a conventional diesel fuel is important to adapt the injection timing accordingly.

4.2 POST-PROCESSING OF EXPERIMENTAL DATA

Before digging further, let us develop the theoretical laws to post-process the data. For instance, calculations gives the heat release rate (HRR).

The first law of thermodynamics applied to a closed system gives:

$$dU = \delta W + \delta Q, \tag{89}$$

with $\delta W = -pdV$

$$dU = -pdV + \delta Q. \tag{90}$$

We introduce the fraction of burned gas, x_b defined by

$$x_b = \frac{m_b}{m_u + m_b}, \tag{91}$$

where m_u and m_b are respectively the masses of the unburned and burned gases.

Then, equation 90 can be written as

$$mc_V dT + m(u_b - u_u)dx_b = -PdV + \delta Q. \tag{92}$$

$m(u_u - u_b)dx_b$ is the change of energy due to the combustion. Therefore, the previous equation can be written as:

$$mc_V dT = -pdV + \delta Q + \delta Q_{combustion}. \tag{93}$$

With the ideal gas law, this equation becomes:

$$\frac{c_V}{R}(pdV + VdP) = -pdV + \delta Q + \delta Q_{combustion}. \quad (94)$$

Or, written differently, and introducing $\delta Q_{walls} = \delta Q$:

$$\frac{dQ_{combustion}}{d\theta} = -\frac{dQ_{walls}}{d\theta} + (1 + \frac{c_V}{R})p\frac{dV}{d\theta} + \frac{c_V}{R}V\frac{dp}{d\theta}. \quad (95)$$

In this equation, $\frac{dp}{d\theta}$ is obtained thanks to the measured pressure and crank angle. The heat transfer to the walls, $\frac{dQ_{walls}}{d\theta}$ is calculated with the Woschni empirical model for convection and $\frac{dV}{d\theta}$ is calculated with a rod/crank kinematic model obtained with trigonometry [139–141].

4.3 COMPARISON WITH CONVENTIONAL DIESEL

After its production, the crude-oil like fuel is distilled, giving a heavy (diesel-like fuel) and a light fraction (gasoline-like fuel). In RCCI, the two fuels are injected in the engine. The light fraction is injected via a port-fuel injector and the heavy fraction is injected directly in the cylinder. In the current chapter, we focus on the reactivity of the heavy fraction while the light fraction will be discussed in the other chapters. In order to get a first insight of ASR-derived fuels, the heavy fraction was burnt in a compression ignition (CI) engine. In this section, we compare the combustion of a conventional diesel with the heavy fuel produced from automotive shredder residues (ASR).

The test bench is presented on Figure 29. The engine is a one cylinder 555cc Petter AVB Lab engine. This type of engine is a modification of the standard AV series for research. The AV series equip agricultural machineries, which makes it very robust. For instance, the injection is provided by a simple mechanical pump, controlled by a cam. Therefore, no electronic or sensitive parts could be damaged by the unconventional fuel. A Bosch HFM 5 returns the air flow and its temperature. The fuel mass flow is measured with a weighting scale Kern PKS. DHT22 sensors monitor the temperature of the fuel, the oil and the cooling water. The cylinder head was bored to fit in a Kistler dynamic pressure sensor 7061C whose signal is amplified by the amplifier Kistler 5015A. The crank angle is also monitored with an encoder WDG 58B 4096, which allowed us to obtain the pressure trace in the cylinder according to the crank angle. The crank angle gives also the engine speed in revolution per minutes. The sensors are coupled to an acquisition card National Instrument 6351 which is connected to the computer via USB. The engine is coupled to a Eddy current brake Zöllner A160. This brake applies an adjustable load and returns the torque measured on the engine shaft.

The test procedure is the following. The engine is started with conventional diesel from the fuel station. 200mL of the unconventional fuel from ASR to be tested fills a beaker. The fuel is heated up to 60°C to avoid any obturation and overpressurization in the fuel line and in the pump. A manual shift allows the user to commute from the tank filled with conventional diesel to the beaker filled with the sample that is to be tested. This sample is injected when a stationary operation is achieved. After 50 engine cycles (100 crankshaft rotations), the data are saved.

Two different unconventional heavy fuel fractions from ASR are compared according to this test procedure. Before discussing the results of the tests, let us compare their properties, specifically their cetane index which are reported in Table 14. In the same table, the regulations for road diesel,

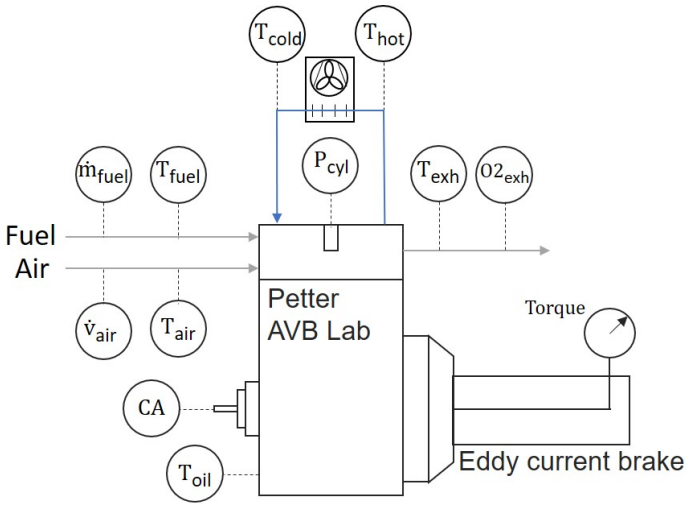

Figure 29: Schematic representation of the test bench.

Table 13: Specifications of the Petter AVB Lab engine.

Engine type	Diesel, 4 strokes, 1 cylinder
Displacement	555 cm^3
Compression ratio	15.3
Fuel injection timing	24° before TDC
Inlet valve opening	4.5 before TDC
Inlet valve closing	35.5 after BDC
Exhaust valve opening	35.5 before BDC
Exhaust valve closing	4.5 after TDC
Bore	80 mm
Stroke	110 mm

distillate marine fuels and distillate fatty acid methyl esters (FAME) fuels are given. The cetane index are calculated according to ISO 4264 with the so-called four variable equation (Equation 43). The cetane index is an equivalent to the cetane number (CN). The CN indicates if a fuel is likely to auto-ignite. More information on the CN and on the cetane index is reported in sections 2.5.3 and 2.6.2, respectively.

As showed by Tables 14 and 15, the calculated cetane index of the two ASR fuels are low. This corroborate the ignition delay of Figure 30 which is higher for the first ASR fuel than for the conventional diesel. The HRR shows that the combustion of the ASR fuel 1 is faster and more abrupt than the combustion of the conventional diesel. The peak pressure rise rate (PPRR) is equal to 3.09 bar/CA° with the conventional diesel against 6.27 bar/CA° with the ASR fuel. Moreover, the exhaust temperature is 240°C higher with the ASR fuel. The cetane index of the second ASR fuel is too low, which makes the ignition delay too high for the fuel to ignite, as shows Figure 31.

4.4 ENDURANCE TEST WITH SILICON OXYDES

In Section 1.2, the process to produce the fuel was discussed. It includes a mixing of the crude oil-like fuel with NaOH to remove inorganic compounds

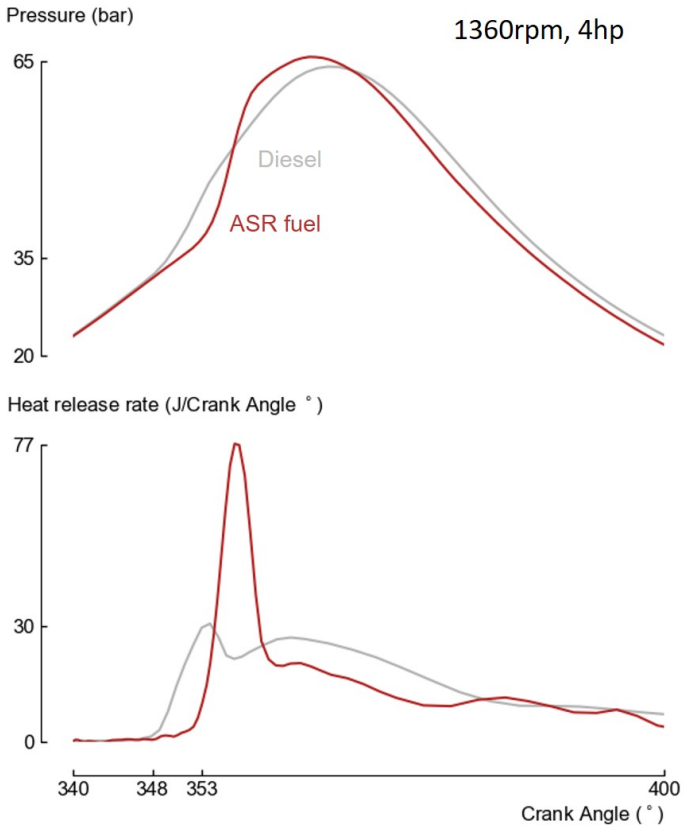

Figure 30: The pressure curve and the heat release rate of conventional diesel and the fuel 1 from ASR present different shapes. The combustion duration is longer with conventional diesel and more intense with the fuel 1 derived from ASR. The IDT is also higher with the fuel derived from ASR.

Table 14: Calculated cetane index of two heavy fuel fractions derived from ASR.

	Cetane index
ASR fuel 1	36.6
ASR fuel 2	24.6

Table 15: CN of reference fuels.

	Lower limit (CN)
NF EN 590(road diesel)	51
Distillate Marine X	45
Distillate Marine A	40
Distillate FAME A	40
Distillate Marine Z	40
Distillate FAME Z	40
Distillate Marine B	35
Distillate FAME B	35

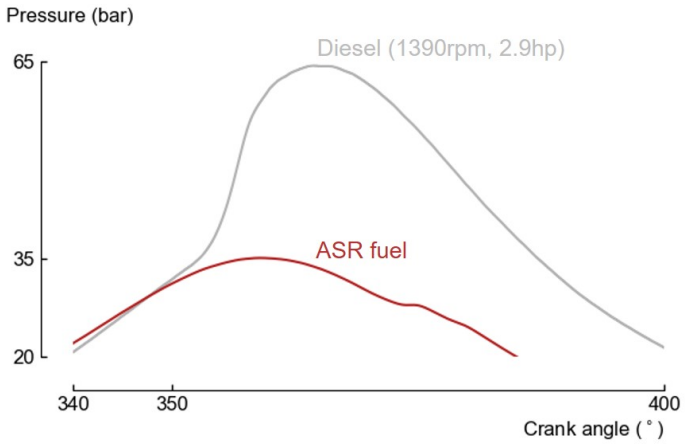

Figure 31: The fuel 2 from ASR does no ignite because the IDT is too long.

such as silica. This step was not always followed up during the process. The current section shows why such a step is crucial.

Among the two fuels studied in the previous section, only the first fuel reacts. This is due to the properties of the fuels measured via the calculated cetane number. On the opposite, fuel 2 has a too low calculated cetane number (Table 14). The current section present the results of an endurance test with the fuel 1. We were previously talking about the importance of removing the silica. The tested fuel did not receive such a treatment, which cause the failure of the engine. More information on this failure is given thereafter.

Before the test, the engine was refurbished with a new piston, a new cylinder, new liners, a new pump and a new conrod (Figure 32). Moreover, a complete metrology was accomplished. The metrology was in accordance with the engine specifications. It shows that the engine was in good state before the test.

The performance of the engine as represented on Figure 33. This Figure shows the pressure profiles compared with a reference time when the engine performed well. After twenty minutes, the engine showed an erratic behaviour. Then, the engine performances declined. To maintain a constant engine speed and torque, the gas potentiometer had been increased. Moreover, the in-cylinder pressure declined.

We dissembled the engine to diagnose the cause of the failure. The piston showed a black trace on its side and the cylinder shows vertical scratches which testify a leak. The cylinder was not tight anymore, which explains the pressure losses. Moreover, the piston shows black and green particle deposits.

Particles from the piston were gathered and analysed by thermogravimetric analysis. With this method, the mass of a substance is monitored as a function of temperature. The sample showed 85% of organic matter and 15 % of ashes (Figure 35).

The 15% of ashes were analyzed with Scanning Electron Microscopy (SEM) with Energy Dispersive X-Ray Analysis (EDX). This is a technique to determine the elemental composition of a sample. The results of this analysis shows the high content of oxygen and silica (Figure 36). Thus, silicon oxide is the solid which damaged the engine during the endurance test.

Figure 32: New parts of the Petter AVB Lab. The piston was also refurbished.

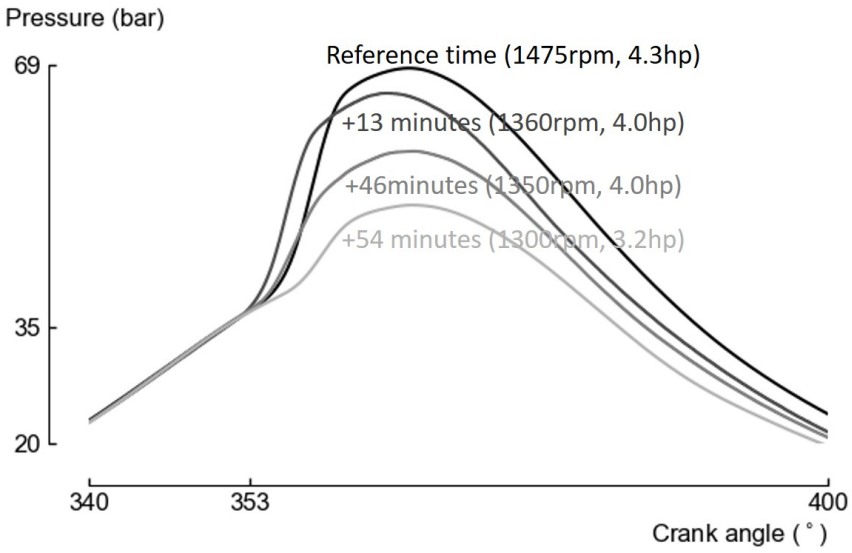

Figure 33: Decline of the engine behaviour during the endurance test.

4.5 ENDURANCE TEST WITHOUT SILICON OXYDES

Combustion tests were carried out in the same engine with four additional fuels derived from ASR. Conversely to the fuel of the previous section, the silica was removed from the fuel thanks to the addition of NaOH. A comparison of the four fuels with conventional diesel is first done. Then, the results of the endurance test are reported.

Figure 34: Left: Black trace on the side of the piston. Middle: Vertical scratches in the cylinder. Right: Cylinder head with black and green deposits.

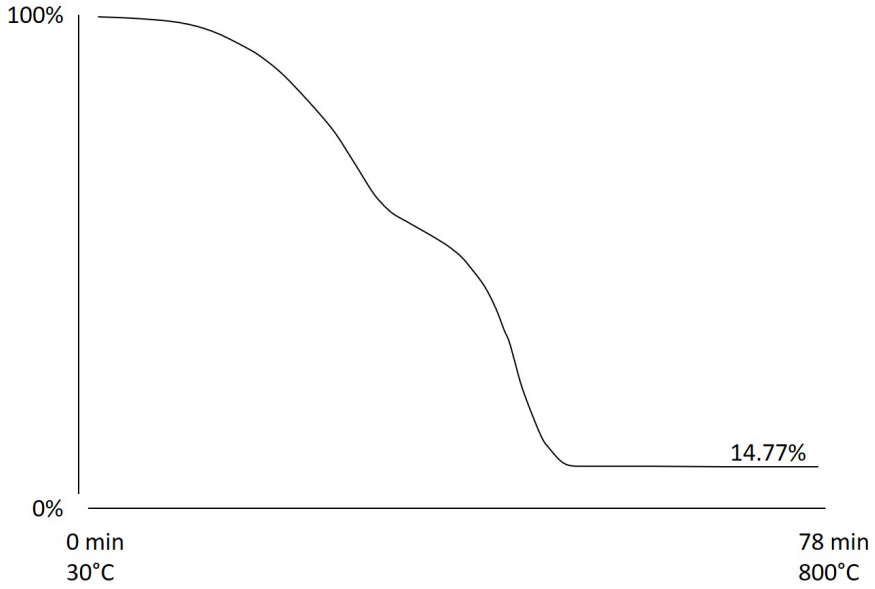

Figure 35: Thermogravimetric analysis of combustion deposits. Evolution of the mass depending on the calcination temperature.

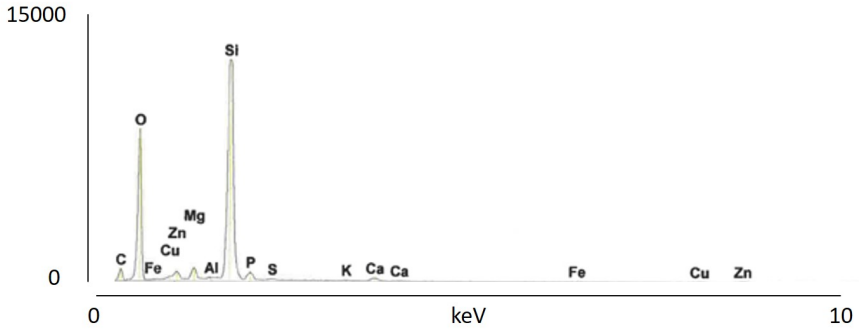

Figure 36: SEM-EXD spectrum shows the presence of silica.

4.5.1 *Comparison of four fuels derived from ASR*

Four fuels produced from ASR were tested in the same piston engine. The fuels were tested under similar conditions (near 3kW and near 1360rpm),

except for the fuel 1 for which the rotational speed was slightly low (Figure 37). Keeping the exact same operating conditions was hard due to a manual setting of a mechanical shaft.

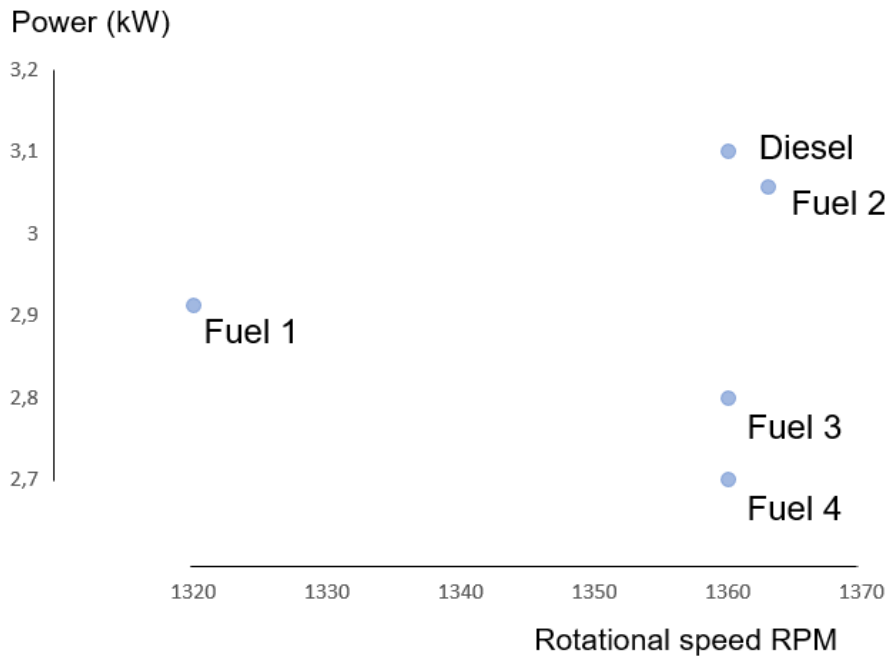

Figure 37: The test conditions for all the fuels were around 3kW at 1360rpm.

The pressure profile and the HRR for all the fuels are compared with the pressure profile and the HRR obtained with conventional diesel. With the fuels derived from ASR, the IDT is longer and the combustion is more abrupt (Figures 38 and 39). The HRR shows that the IDT of the four fuels are similar. Nevertheless, fuels 2 and fuel 4 have lower HRR than fuels 1 and 3.

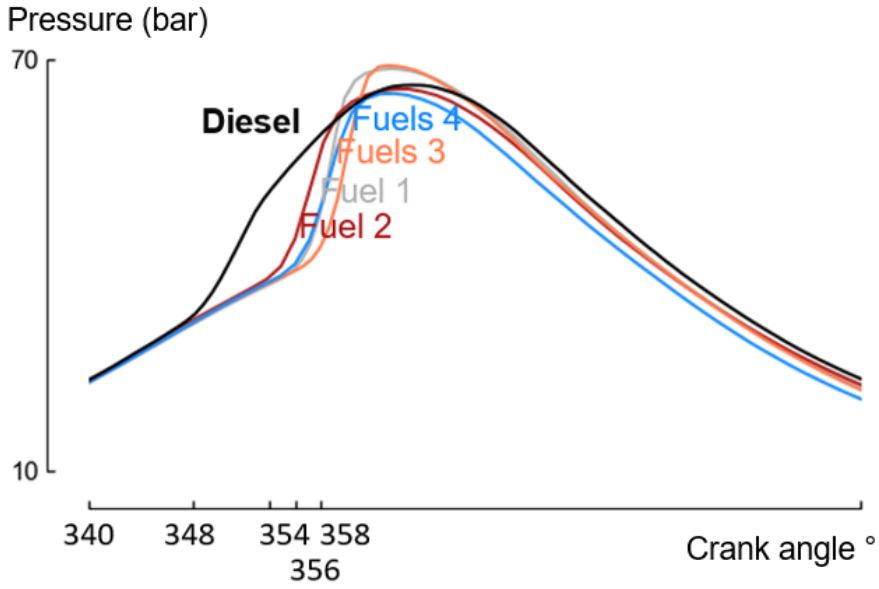

Figure 38: Pressure profiles obtained with the four fuels derived from ASR compared with conventional diesel.

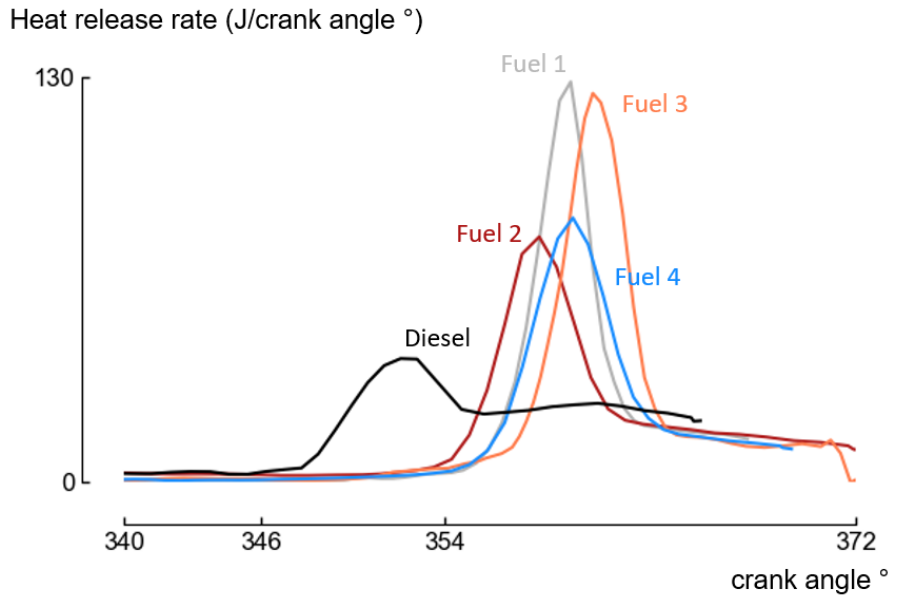

Figure 39: Heat release rates obtained with the four fuels derived from ASR compared with conventional diesel.

The production of CO and NO of the four fuels are also compared with the conventional diesel. The CO tends to decrease while the NO tends to increase. The increase of NO could be due to an increase of the HRR.

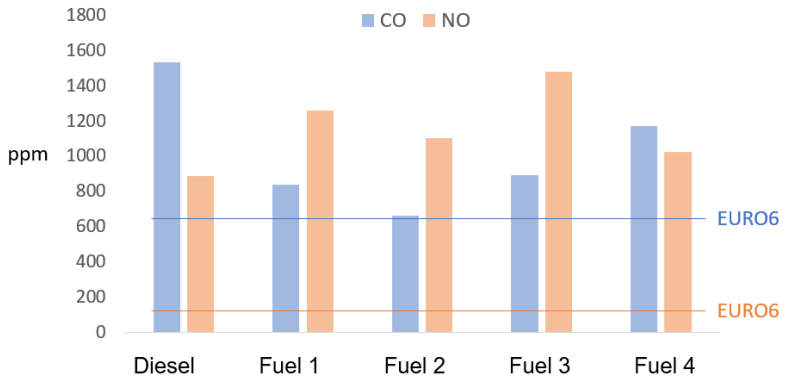

Figure 40: The fuels produced from ASR tend to produce less CO and more NO than conventional diesel. The uncertainty is 5% for the two molecules.

The pressure profiles and the HRR of these four fuels (obtained in 2020) are quite similar compared with those of the diesel. Nevertheless, they can be sorted by pairs as shown by the HRR. They are compared with the pressure profile and the HRR of the fuel that produced silicon oxides (obtained in 2014) of the previous section on Figures 41 and 42. The pressure raise is similar although the fuel from 2014 is slightly more reactive.

4.5.2 *Endurance test*

The four fuels of the previous section were burnt each one after another to accomplish an endurance test without silica. These four fuels compared in the previous section gave similar result in terms of combustion. The pressure

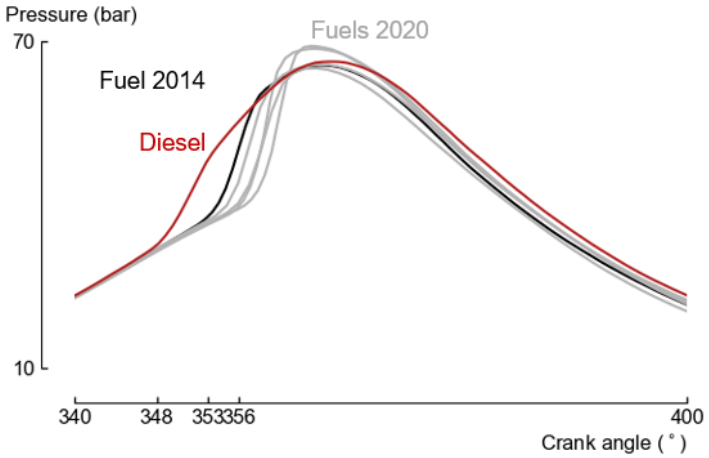

Figure 41: Pressure profile obtained with the four fuels derived from ASR(2020) compared with the fuel that produced silicon oxides (2014).

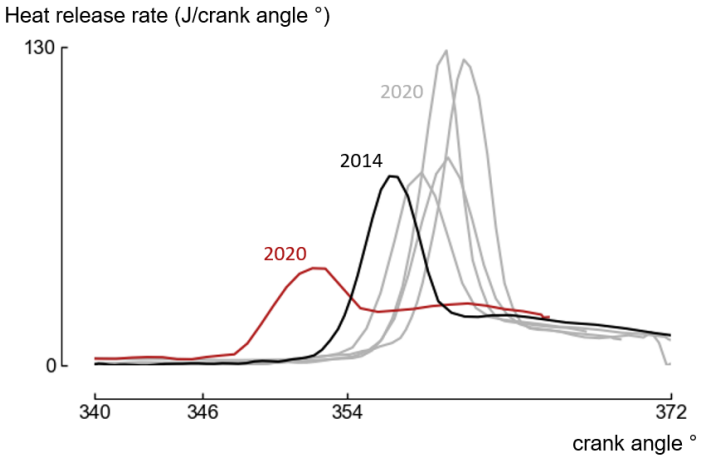

Figure 42: Heat release rates obtained with the four fuels derived from ASR(2020) compared with the fuel that produced silicon oxides (2014).

curves of each fuel were similar. Thus, a change of fuel has a negligible effect on the pressure curve. Therefore, if considerable difference in the pressure curve would be noticeable during the endurance campaign, they must be inferred to a change in the engine behaviour.

The results of the endurance are shown on Figure 43. The HRR was computed and is reported on Figure 44.

The engine was hot and in steady state at 10:00 am. This condition is the reference point. The plots obtained at 10:42 am and 11:02 am correspond to the fuels 1 and 2. The plot is similar to the ones of the previous section. The ignition delay, the pressure derivative and the ignition delay are higher than the reference diesel at 10:00 am. These characteristics were previously observed.

The plots obtained with the fuel 3 at 11:40 and 12:08 are very different than the ones obtained with the previous fuel 1. The ignition delay is higher while the maximal pressure decreased. Moreover, the ignition delay increased. It was showed in the previous section that the fuels 1, 2, 3 and 4 behave similarly. Thus, the difference observed is a consequence of the engine behaviour. As a conclusion, a degradation of the autoignition condition

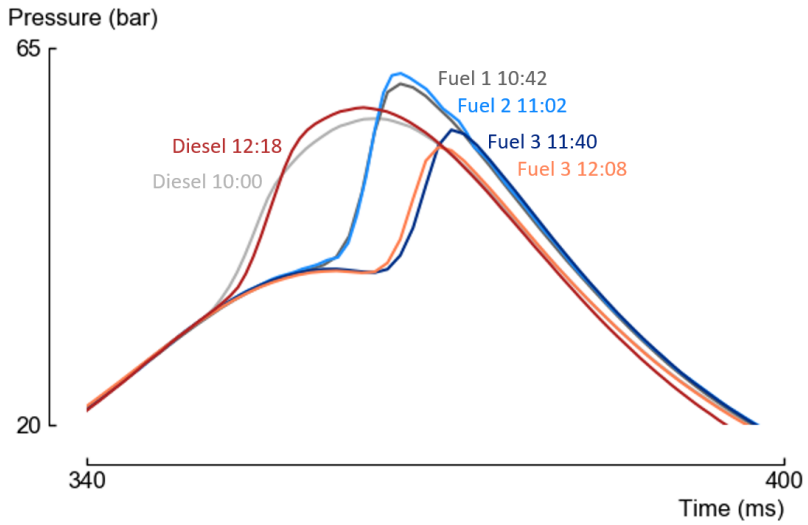

Figure 43: Results of the endurance campaign without Si atom in the fuel.

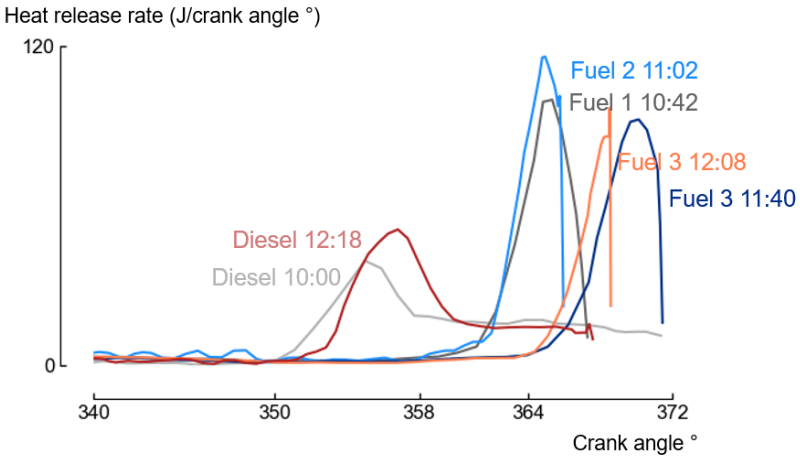

Figure 44: Heat release rates obtained during the endurance campaign without Si atom in the fuel.

occurred between the fuels 1 and 3. This degradation could be caused by the pressure peak which is higher than with conventional diesel. The analysis of the HRR corroborate this hypothesis because the HRR increases abruptly. Additionally, a leakage at the cylinder-head gasket was observed.

At 12:18, conventional diesel was burnt. We observe a pressure trace similar than the reference at 10:00 but the ignition delay is slightly higher. The deterioration of the engine affects more the fuel derived from ASR than the conventional diesel. This can be explained by the higher ignition delay of the fuel derived from ASR. In fact, the pressure loss due to the engine degradation is low, thus it has a negligible effect on the conventional diesel that has a lower auto-ignition delay that the fuel derived from ASR.

The analysis of the data acquired between 11:02 and 11:40, minute after minute, allowed us to determine the exact time where the cylinder head gasket lost its properties. This failure clearly appeared between 11:38 and 11:39 (Figures 45 and 46). The failure is probably due to a combustion too abrupt, with a too high pressure rise rate.

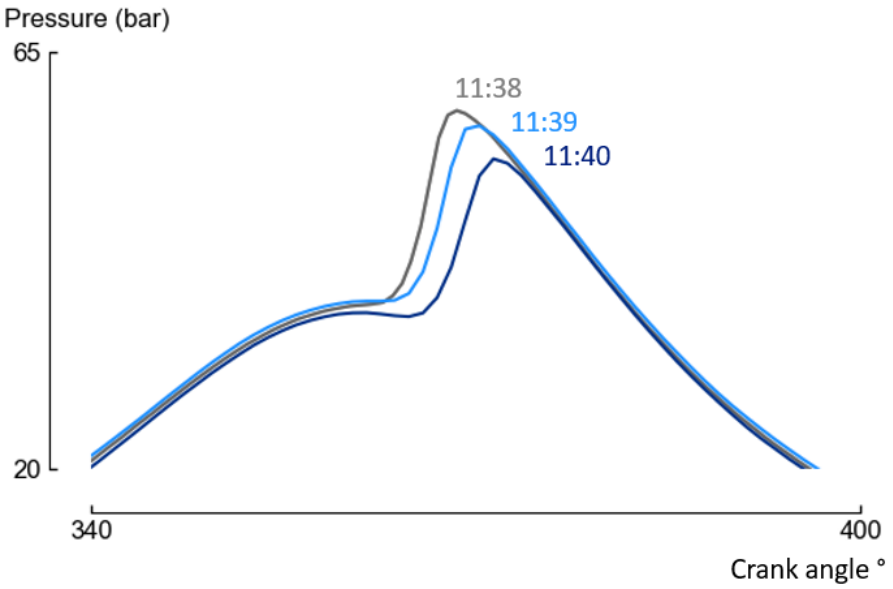

Figure 45: Pressure profile between 11:38 am and 11:40 am. The failure appears between 11:38 am and 11:39 am.

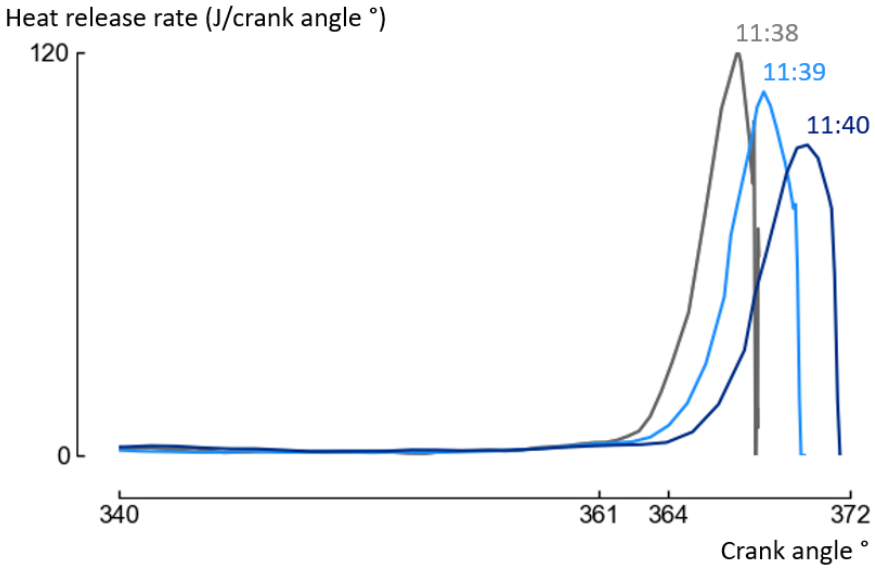

Figure 46: Heat release rates between 11:38 am and 11:40 am. The failure appears between 11:38 am and 11:39 am.

The analysis of the pollutant also shows the degradation of the cylinder-head gasket (Figure 47). The CO increase could be due to the fact that oil was burnt or to a later combustion.

4.6 CONCLUSION

In the current chapter, heavy fuel fractions produced from ASR were studied in a CI engine. From a technical point of view, it has been showed that removing the silica is crucial in order to burn safely the fuel. Else, the formation of silicon oxide may damage the cylinder. Moreover, it was showed that the heavy fraction from ASR tends to have a higher ignition

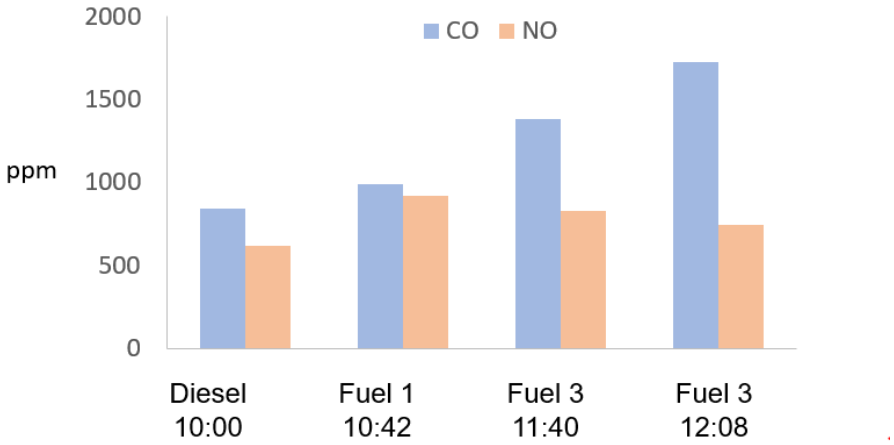

Figure 47: Pollutant emissions during the endurance test without Si atom in the fuel. The CO concentration increases along the test.

delay than conventional diesel fuel. This observation comes with a more abrupt heat release with a higher peak pressure raise rate.

It was showed that the high fraction from ASR has a longer ignition delay than conventional diesel. Relying on a programmable electronic control unit (ECU) is a solution to modify the ignition timing of the high reactivity fuel. This will enables the fuel to have enough time to react with an advanced ignition timing. Moreover, we could cope with the variation of the fuel by changing the injection timing dynamically. Consequently, the remaining part of the thesis aims to characterize the low-reactivity fuel.

The second challenge to tackle is the ignition delay of the low-reactivity fuel. The premixed charge of low-reactivity fuel and air needs to ignite after the end of the compression so that no knock occurs. The auto-ignition of the low-reactivity fuel is governed by its chemical behaviour, govern by its composition and structure. The composition can be used to understand how the fuel reacts. Thus, being able to predict the composition of the low-reactivity fuel is important. Moreover, having some information on the fuel composition enables to set limit in terms of pollutant emissions, as done for conventional fuels. Knowing the composition is important but other properties exist to estimate the fuel reactivity. The research octane number (RON) and the motor octane number (MON) are two interesting properties of light fractions that traduces the resistance towards an end-gas auto-ignition.

5

PREDICTION OF THE COMPOSITION OF ASR-DERIVED FUELS

The content of this chapter has been published in the following scientific article:

Steven Tipler, Alessandro Parente, Steffen H. Symoens, Marko R. Djokic, Kevin M. Van Geem, Francesco Contino, and Axel Coussement. Prediction of the piona and oxygenate composition of unconventional fuels with the pseudo-component property estimation (pcpe) method. application to an automotive shredder residues-derived gasoline. In *WCX World Congress Experience*. SAE International, apr 2018

5.1 INTRODUCTION

Being able to approximate the fuel composition from easy to quantify properties that are measured anyway for technical needs (like the viscosity) enables two targets to be hit with one single set of tests. Knowing the composition enables us to get several information. The other properties (such as the octane numbers) can be estimated with the pseudo-component method as long as the composition is known. Knowing all these properties enable the producer to monitor the fuel and to retrofit the production parameters according to the fuel properties. Knowing the composition of the fuel is a way to understand its reactivity. Additionally, from a more theoretical point of view, the variation of the fuel properties can be explained when a variation of the composition is observed. Moreover, the composition can be compared to predefined thresholds in order to quantify its toxicity and the pollutant emissions, as done in the regulations for conventional fuels.

Methods exist to estimate the fuel composition if it cannot be measured experimentally but those have many limits. Riazi summarized the American Petroleum Institute (API) methods [8] based on the weighted average of the n-paraffin, napthene and aromatic (PNA) group properties. However, because of the unconventional nature of the fuel which could be composed of many olefins and oxygenates, the existing methods cannot be applied directly. This chapter outlines a methodology to build a model for estimating the n-paraffin, iso-paraffin, olefin, napthene, aromatic and oxygenate (PIONAOx) composition of any fuel. As an example, a model suited for an ASR-derived light fraction was established. Using the present method enables the estimation a fuel composition with easy to quantify properties.

The first section explains the methodology, from a general overview to a more precise description of the experimental tests carried out and of the numerical database setting. In the second section, the mathematical formulations behind the pseudo-component properties, and the problem

resolution are defined. The third section explores the accuracy of the model compared to the confidence interval of comprehensive two dimensional gas chromatography (GC × GC) measurements for a fuel composition.

5.2 DESCRIPTION OF THE METHOD

5.2.1 *Basis of the method*

Since the conventional API (Riazi-Daubert) models [8] were developed to predict the PNA composition of usual fuels, the current work elaborates an overall methodology to build a new model especially adapted to predict the PIONAOx composition of any fuel.

The model was built based on a reference fuel whose composition represents well the studied type of fuel. If another fuel is to be studied, two cases have to be considered.

If the studied fuel is an automotive shredder residues (ASR)-derived fuel with a composition close to the fuel used as a reference in the present chapter (with molecules similar than the major molecules identified in Table 16), the proposed model could be applied directly and only the fuel properties characterized by the American Society for Testing and Materials (ASTM) standard test methods are mandatory to estimate the PIONAOx composition. Further work is required to study the achieved accuracy with a deviation of the reference fuel composition.

For another type of fuel (i.e. a fuel with molecules dissimilar to the major molecules identified in Table 16), the molecular information of a reference fuel has to be defined so the experimental PIONAOx composition and the major components analysed by GC × GC and gas chromatography (GC)-mass spectrometry (MS) respectively are also mandatory to run the whole methodology and create a new model. Then, the model estimates the PIONAOx composition of a fuel similar to the reference with its properties only. Once again, the achieved precision with a deviation of the reference fuel composition needs to be evaluated in a separate study.

The next paragraphs report the principle of the model and the last paragraph refers to the whole methodology. The model is separated in three steps: retrieving the database, calculating the properties of each hydrocarbon group and resolving an optimization problem to define the composition (Figure 48). More details on each step are given hereafter.

First, the molecule database was created thanks to the software Aspen Properties® and additional relations are used to calculate the missing properties.

Second, the property values used to characterize each hydrocarbon group were calculated. Then, the properties of the fuel were equated as a weighted average depending on the group fractions and on the properties of each group. As the fuel is composed of many molecules, each group was characterized by a single notional molecule, called pseudo-component, to simplify the calculations and to circumvent the impossible experimental identification of all the molecules. A pseudo-component is characterized by its boiling point and by its hydrocarbon group as the properties of the molecules depend on those two characteristics [8].

Last, an optimization problem was solved to minimize the difference between the properties of the mixture of the pseudo-components and the real fuel properties. This resolution gives the hydrocarbon group fractions. Each property does not have the same impact on the calculated fractions,

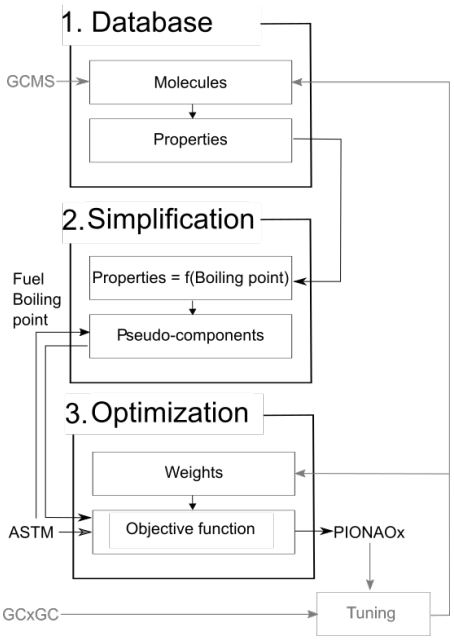

Figure 48: If a model is already set for a studied type of fuel, the fuel properties measured according to ASTM standards are the only inputs needed to calculate the fuel composition. Once the molecule database to represent each hydrocarbon family is set (step 1), the properties of the pseudo-components representing each group can be calculated thanks to the fuel boiling point estimated with ASTM D86 (step 2). Then, the resolution relies of an optimization problem to reduce an objective function based on the difference between the predicted and the real fuel properties pondered with weights to calculate the PIONAOx fractions (step 3). If no model exists for the studied type of fuel, identifying the major molecules present in the fuel (with GC-MS) and knowing a reference composition (with GC $\times$ GC) enables the creation of a new model suited for the studied type of unconventional fuel.

therefore, a weight was allocated to each property in the objective function to change their relative importance. This method offers more flexibility of resolution than the commonly used linear regression [8].

When a new type of fuel is studied, a new model must be set. A fuel is new if its composition is not covered by the range of applicability of the model such as the PIONAOx fractions are badly predicted. To set a new model, the composition and the major molecules of the reference fuel are required to run the whole methodology. The structure of the molecules detected by an analysis method, as GC-MS, defined the database. The database and the weights were modified until reaching a good match between the measured and the predicted composition. The group fractions were analyzed experimentally by GC $\times$ GC. The model was set when the accuracy was considered acceptable.

The first step of the model, i.e. selecting the molecules belonging to the database is described in the next section.

5.3 CHEMICAL CHARACTERIZATION AND CHEMICAL DATABASE

This section first describes the experimental methods and their post-processing to characterize the fuel, then, it explains the procedure to build a coherent molecular database to set a model that properly represent the fuel.

5.3.1 *Chemical characterization*

Experimental tests were carried out to analyze the fuel composition. This fuel is a light fraction obtained from different types of plastics from ASR. Among others, the GC × GC enabled the measurement of the PIONAOx composition of the fuel. However, a post-processing of the results was required to deal with an overlapping of the oxygenate molecules and to estimate the confidence interval. The next part describes the tests and explains their purpose while the second reports the GC × GC post-processing.

5.3.1.1 *Experimental methods*

The fuel composition must be experimentally characterized for three reasons. First, the major molecules identified in the fuel by GC-MS define the basis of the molecule database. The selection of the molecules is only mandatory to set the model for the first time with a new type of fuel. Secondly, the elemental composition measured with an elemental analyzer (EA) was used as an input property of the optimization problem to calculate the PIONAOx fraction so this analysis is required whenever the model is run. Finally, the hydrocarbon group fractions measured using GC × GC coupled with flame ionization detector (FID) must be characterized to enhance the molecule selection and the objective function by defining the best set of weights. This characterization is only required to set the model for the first time.

The results of GC-MS, EA, and GC × GC tests realized at the chemical research center CERTECH and at the Laboratory for Chemical Technology of Ghent University are described in the next paragraphs.

One-dimensional GC analysis as GC-MS is commonly used in the industry (ASTM standard test methods D5134 [142], D6729 [143], D6730[144], D6733 [145], D6839 [146]) as well as in the academic area [84, 147, 148]. The molecules identified by GC-MS were employed to set the molecule database. Around 0.5 µl was directly injected in an apolar column of dimensions 50 m long, 0.25 mm diameter and 0.5 µm of film thickness. The blend showed the following typical features regarding the iso-paraffins and the olefins configuration (Table 16). First, the maximal number of substituting -CH_3 is two. Second, the position of the substituting -CH_3 is often located on the second and on the fourth position of the principal chain. Last, the double bond is frequently situated on the first position.

One-dimensional GC enabled the identification of the molecules in the fuel but suffered of a lack of sensitivity due to co-elution because similar molecules were blended. Then, many constituents were not identified and the molecules cannot be finely sorted into hydrocarbon groups.

GC × GC is an improvement developed in 1991 by Liu and Phillips [149] and relies on the GC technique with two capillary columns using different selectivity [150]. The molecules are disassociated according to two different axis to increase the post-processing selectivity. Although this method is rare compared to one-dimensional chromatography, it is now used in research [11, 151–156] and in industry (standard ASTM UOP990-11 [157]). Jennerwein

Table 16: Major identified molecules with the GC–MS. The origin of these molecules is detailed in subsection 5.3.2.

Decane	Benzene
4–methyl–Heptane	Toluene
2,4–dimethylheptane	p–xylene
2–methyl–1–pentene	Ethylbenzene
1–heptene	1–methylethylBenzene
1–octene	1,3,5–trimethylBenzene
2,4–dimethyl-1-heptene	1,2,3–trimethylBenzene
1,2,3–trimethylcyclohexane	Styrene
1,3,5–trimethylcyclohexane	α–Methylstyrene

et al. showed this test method to be more reliable for modern and complex fuels because of a higher selectivity [155].

The GC $\times$ GC analysis was performed using an apolar column (Rxt-1 PONA, 50 m long, 0.25 mm internal diameter, 0.5 µm film thickness) and a mid-polar column (BPX-50, 2 m long, 0.15 mm internal diameter, 0.15 µm film thickness). Further information as the sample preparation and the method description are detailed below, more information is available in an article by Dijkmans et al. [11].

An internal standard was added to each sample for the FID, sulfur chemiluminescence detector (SCD) and nitrogen chemiluminescence detector (NCD). The internal standards for each of the chromatograms were chosen in such a way that they were properly separated from all other peaks. An additional pre-requisite is that for the NCD and SCD analysis nitrogen or sulfur also needs to be present in the internal standards. Therefore for the FID and the SCD analysis 3-chlorothiophene was chosen, while for the NCD analysis 2-chloropyridine was chosen. The amount of internal standard that is added is chosen in such a way that the internal standard would have a similar peak height as the components quantified by the internal standard [11].

The set-up is equipped with a program temperature vaporizer (PTV) injector. The carrier gas was He. A temperature program was applied to the columns. They were heated from 0°C to 250°C at a heating rate of 3°C/min. Modulation was carried out on the piece of deactivated column. The modulation period was optimized to be as low as possible (maximal resolution in first dimension) without causing wrap-around [11]. A built-in switching system, i.e. a 4-port 2-way valve (VICI AG International, Switzerland), allows to switch between FID and MS without the need to cool down and vent the TOF-MS. With this method, the appliance was used once to obtain qualitative data with the TOF-MS, and a second time to obtain quantitative data with the FID.

The mass fraction of each compound on the FID was be calculated using the mass fraction of the internal standard based on their response factors which has been demonstrated to be approximated by:

$$f_i = \frac{M_i}{M_{CH_4} N_{C,i}} \tag{96}$$

where M_i is the molar mass of compound i, $N_{C,i}$ is the carbon number of compound i, and CH_4 is the molar mass of methane. This approximation removes the need to calibrate each compound present in the mixture. Calibration was however carried out for 3-chlorothiophene, since it is used as an

internal standard and the presence of a halogen atom is expected to influence the response factor significantly.

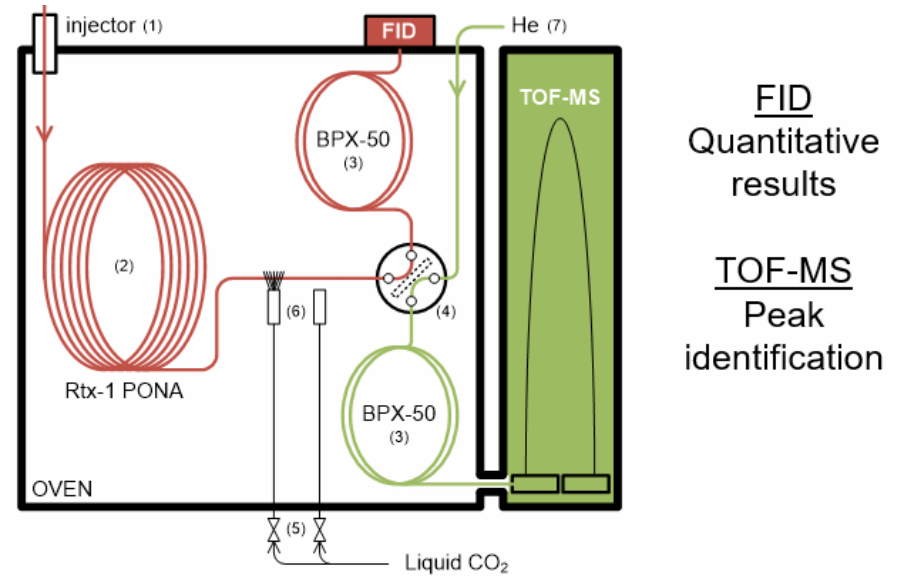

Figure 49: After its injection, the fuel reaches a first rtx-1 PONA apolar column, then liquid CO2 is injected, playing the role of a cryogenic modulator, allowing to stop the effluent until its relaxation toward the second column. Then, the substance can either go in one of the two polar BPX-50 column. The first, being coupled with FID to measure the chemical fractions and the second with TOF-MS to identify them.

The components were quantified by averaging three GC × GC-FID analyses and their identification was performed via GC × GC-time of flight (TOF)/MS analysis (see Table 17). The uncertainty was defined based on the standard deviation obtained with the three measurements. GC × GC analyzes the whole fuel composition, including naphthenoaromatics, diaromatics, nitrogenates and sulfurates whereas the current method only focuses on the PIONAOx fractions. The calculated and the measured fractions must be compared on a same basis. Therefore, the whole fuel composition was simplified into a PIONAOx composition with the following procedure. The measured naphthenoaromatics were equally distributed between the naphthenes and the aromatics, the diaromatics were considered as monoaromatics, and the nitrogenates and the sulfurates were neglected.

Three GC × GC analyses using NCD and SCD, i.e., GC × GC-NCD and GC × GC-SCD, were realized to measure an average nitrogen and sulfur content. An EA was also used to compare and validate the carbon, hydrogen, and oxygen contents (Table 18).

The oxygen content deduced by an EA was compared with the one calculated from the number of oxygen atoms in the molecules identified by GC × GC-FID and GC × GC-TOF/MS. A difference was observed, due to an overlap of the oxygenate molecules. Consequently, a correction, presented in the next paragraph, was applied. The experimental random error is also presented in the following part by the mean of a confidence interval calculation.

Table 17: Hydrocarbon class repartition

Hydrocarbon class	% wt/wt
Olefin	31.09
Monoaromatic	28.39
Mononaphthene	14.18
iso-paraffin	12.38
Oxygenated	6.66
n-paraffin	5.47
Naphthenaromatic	1.11
Nitrogenated	0.66
Diaromatic	0.04
Sulfurate	0.02
Total	100

Table 18: Elemental composition

Atom	% wt/wt	Method
Carbon	84.58	EA
Hydrogen	12.76	EA
Oxygen	2.34	EA
Nitrogen	0.26	GC × GC-NCD
Sulfur	0.06	GC × GC-SCD

5.3.1.2 *GC × GC post-processing*

A difference between the amount of oxygen atoms measured by GC × GC and by the EA was observed. After having explained this difference, a correcting factor was introduced to estimate a corrected oxygenate fraction. Then, the whole fuel composition was known which allowed to estimate the confidence interval.

If a hydrocarbon group is several orders of magnitude more concentrated than another group whereas their similarity regarding to the columns selectivity is too high, the peak signal of the first group will hide the peak of the second group. The identification of oxygenates is still a challenge with GC × GC because oxygenates overlap with monoaromatics, diaromatics, triaromatics, naphthenoaromatics and naphtheneodiaromatics [11, 156]. In the present study, the oxygenates overlapped with the monoaromatics.

A correction was applied to estimate the amount of overlapped oxygenates that cannot be identified with GC × GC. This correction relies on an EA to relate the real amount of oxygen in the fuel with the amount of oxygen in the identified molecules that did not suffer of the overlapping. The hypothesis adopted to perform this correction are described in the next paragraph.

The oxygen content analyzed with the EA and the amount of the overlapped oxygenate molecules are tied together with the composition of two types of molecules (oxygen to carbon ratio (O/C) (%w), the hydrogen to carbon ratio (H/C) (%w) and the molar mass (Mm)). Therefore, the type of molecules, which drives the OC and HC, and the size of the molecules are mandatory.

The types of the molecules is first discussed. Usually, monoaromatics overlap with aliphatic ketones [26] so the overlapped oxygenate molecules were considered as aliphatic ketones. The identified molecules with GC × GC were mainly ketones and alcohols. They have the same O/C and a similar H/C so both ratios of the overlapped oxygenates and the identified oxygenate molecules were considered equal. For instance, pentanone and pentanol have one hydrogen of difference between their respective compositions.

The number of carbon atoms of the overlapped oxygenate is discussed in a second step. As no information were available, the molecules were supposed similar in size with the identified oxygenate fraction.

Then, the O/C, the H/C and the size of the overlapped oxygenate were esteemed similar with those of the identified oxygenates. Therefore, the proportionality between the oxygenate molecules and the oxygen atomic content observed with GC × GC were considered respected with the EA. Then, under this hypothesis, a corrected response volume defined by the following equation was introduced to estimate the overlapped volume of oxygenate molecules:

$$V_{O_c} = \frac{OC_{EA}}{OC_{GC\times GC}} V_O, \tag{97}$$

where OC_{EA} and $OC_{GC\times GC}$ are the O/C measured with the EA and with the GC × GC respectively. The oxygen content calculated from the molecules identified by GC × GC-FID and GC × GC-TOF/MS is 56.4% lower than the oxygen fraction measured with the EA (Table 18). The calculation steps to obtain the calculated volumes of oxygenates and aromatics are summarized on Figure 50.

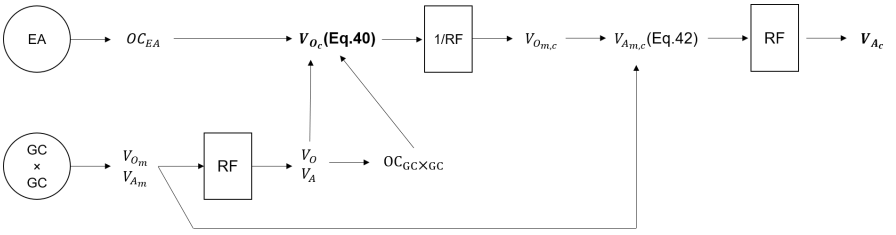

Figure 50: Calculation steps to obtain the corrected volumes.

A corrected volume was also introduced to calculate the overestimated concentration of aromatic compounds due to the overlapping. However, the overlapping concerns the measured volume peaks which are not equal to the real volume peaks reported in equation 97. They were given by a response factor (RF) defined by:

$$RF_g = \frac{V_g}{V_{gm}}, \tag{98}$$

where g refers to the group and m to the measurement. This factor RF is different for each molecule but strongly depends on the group (Table 19). Therefore, an averaged response factor was used for each group. The overlapped oxygenate being considered as aliphatic ketones, the factor range of the overlapped oxygenates is equal to the range of aliphatic ketones.

Table 19: response factor (RF) The RF were obtained in the references [23, 24]. The RF of the individual molecules were applied to estimate the hydrocarbon fractions when the molecules were correctly identified. The average value was only used in order to estimate the fraction of overlapped aliphatic ketones. This was the only available method to correct the measured fractions and take into account the overlapping.

Chemical group	RF range	Averaged RF
Monoaromatics	[0.81;0.85]	0.83
Aliphatic ketones	[1.00; 1.20]	1.10

Then, the overlapped measured volume of oxygenates $V_{O_{m,c}} - V_{O_m}$ was subtracted to the measured aromatic volume peak V_{A_m} , giving the corrected volume $V_{A_{m,c}}$:

$$V_{A_{m,c}} = V_{A_m} - (V_{O_{m,c}} - V_{O_m}). \tag{99}$$

Once the corrected real volume peak of the aromatics V_{A_c} was deduced from $V_{A_{m,c}}$ and the averaged response factor RF_A (Table 4), the corrected fractions and the confidence intervals could be evaluated.

Three experimental test runs were realized to calculate a confidence interval at 95% of the PIONAOx averaged values. The standard deviation of the mean value was given by the standard deviation of the measured values and by the number of runs led with the GC × GC (3 in this study). The average fractions were normalized to be expressed in percentage Y_g (Table 20). This last calculation is equivalent of applying a scale factor which was used to get the standard deviation of the mean value of the normalized fractions. This deviation gave the confidence interval of the mean value at 95% by applying the Student's distribution for an estimated variance and a low number of run (Table 20).

Table 20: Normalized mean value and confidence intervals (CI) of the PIONAOx fractions (%wt/wt).

Chemical group	Y_g	CI
n-paraffin	5.4	[5.1;5.7]
iso-paraffin	12.2	[11.6; 12.9]
Olefin	30.8	[28.9;32.6]
Naphthene	14.6	[14.0;15.2]
Aromatic	24.4	[23.4;25.4]
Oxygenate	12.6	[12.5;12.7]

5.3.2 *Chemical database*

A chemical database was created to calculate the mean properties of each hydrocarbon group. A new database must only be created if a fuel whose most representative molecules and whose composition are very different from the one studied in this chapter. This difference can be observed if the identified major molecules are different from those listed in Table 14.

The following criteria must be respected to select molecules representing correctly each PIONAOx hydrocarbon group in the studied fuel.

1. The ranges of the hydrocarbon group boiling points must contain the fuel mean average boiling point (MeABP). When several isomer sub-groups are selected in a single hydrocarbon group to consider isomers, their boiling point ranges must be similar such as the sub-groups are all equally represented over the whole boiling point range.
2. For each sub-group of each hydrocarbon family, four molecules were selected to rely on a smooth group representation.
3. The selected isomer forms must have a quite similar structure to avoid a too wide distribution of the properties.
4. To rely on a relevant database, the molecules were selected based on the results of the GC-MS analysis and on the predominant molecules produced during the decomposition of the most current polymers used in the automotive industry [48, 94].

The consequences of the four previous rules on the molecules selected to build the model for an ASR-derived fuel are described in the next paragraphs. They refer only to the fuel studied in the present chapter but a similar logic could be applied to any fuel.

5.3.2.1 n-*paraffin (P)*

As no isomers exist for n-paraffin, only one molecule per number of carbon atom was selected. The boiling point rules impose the selection of molecules with a number of carbon atoms from 7 to 11.

5.3.2.2 iso-*paraffin (I)*

iso-paraffins can be substituted with several -CH_3. Primary carbons are more likely to be present in the ASR fuel because usual polymers used in the automotive industry present only one substituting -CH_3 on each carbon atom as in polypropylene (PP) or ethylene propylene diene monomer (EPDM). Based on the GC-MS analysis, molecules with a higher number of substituting -CH_3 than two were not selected. Moreover, the boiling point range is the same for each sub-group such as the lowest number of carbons in the principal branch of the bi-substituted alkanes is five. The position of the substituting -CH_3 was set preferentially at the second and at the fourth position according to the GC-MS analysis. The substitutes of mono-substituted paraffins are only at the second position because the database of Aspen Properties® does not include all the paraffins substituted at the fourth position. Mono and bi-substituted paraffins ranging from C_7 to C_{10} were selected.

5.3.2.3 *Olefin (O)*

Olefins can be straight or branched so both sub-groups were considered. According to the GC-MS analysis, the position of the double bond tends to be located at the first position and, similarly to the iso-paraffins, one to two substituted -CH_3 can be located at the positions 2 and/or 4, i.e. alpha and/or gamma position. If the Aspen Properties® database did not include a requested molecule, another molecule – considered equivalent

– with a different double bond position and with one or two substituting -CH_3 located at the alpha and gamma positions was selected. As for the iso-paraffin case, mono-substituted olefins were only substituted at the second position because the Aspen Properties® database does not include the fourth position substituted 1-olefins or their equivalents. An exception was made with the selection of 2,5-dimethyl-4-octene which is the only available bi-substituted octene-based molecule in Aspen Properties®. No diene olefins were selected because their properties show major differences and they were not analyzed by GC-MS (Table 16).

5.3.2.4 *Naphthene (N)*

According to the results of the GC-MS, naphthenes were selected on a cyclohexane basis with three substituting -CH_3. In order to cover a wider range of boiling points, molecules with a substituting chain containing 1 to 3 carbon atoms were added. The bi-substituted 1,1-dimethylcyclohexane was also included in the model to consider the possibility to face a di-substituted carbon. Those different types of naphthenes were found during the polystyrene (PS) decomposition [80].

5.3.2.5 *Aromatics (A)*

acrylonitrile butadiene styrene (ABS) decomposition produces a high quantity of styrene, α-methylstyrene and iso-propylbenzene [94] while polyurethane (PUR) induces high amounts of alkylbenzenes. The molecules were selected assuming only mono-substituted carbons. Alkylbenzenes with a number of carbon atoms ranging from 6 to 10 were selected.

5.3.2.6 *Oxygenate (Ox)*

The model was based on 1-alcohols and 3-ketones with a number of carbons from 3 to 6 and from 5 to 8 respectively. The hydroxyl group was set at the first position because 1-alcohols are usually used in the pseudo-component technique [8] while 3-ketones are well-described in the software Aspen Properties®.

The proposed database (Table 21) may be suitable for a wide number of ASR-derived like fuel but a deeper study investigating the accuracy of the method with a variation of the reference fuel composition could validate that hypothesis.

5.4 SELECTION AND CHARACTERIZATION OF THE PROPERTIES

After having described how the properties currently used in other methods can be adapted to the new methodology, the experimental tests performed to characterize the properties according to a reproducible ASTM method are reported, followed by the listing of the property database sources.

5.4.1 *Selection of the properties*

This section first fixes the needed number of properties and then describes the properties selected to calculate the PIONAOx fractions. This step is not mandatory to run or create a model.

Although an optimization problem was solved rather than relying on a linear resolution as in conventional methods [8], the number of properties

was determined as if the resolution was depending on a degree of freedom. Six compositional groups must be predicted, so five properties and one additional constraint (sum of the fraction equal to one) were first tested. However, better results were obtained with the same five properties and constraint, and with the O/C as a sixth property.

Table 21: Molecular database

Molecule	Group	Boiling point (C)
n-heptane	n-paraffin	98.43
n-octane	n-paraffin	125.68
n-nonane	n-paraffin	150.82
n-decane	n-paraffin	174.16
2-methylhexane	iso-paraffin	90.05
2-methylheptane	iso-paraffin	117.65
2-methyloctane	iso-paraffin	143.30
2-methylnonane	iso-paraffin	167.00
2,4-dimethylpentane	iso-paraffin	80.49
2,4-dimethylhexane	iso-paraffin	90.43
2,4-dimethylheptane	iso-paraffin	132.50
2,4-dimethyloctane	iso-paraffin	155.90
Methylcyclohexane	Naphthene	100.93
Ethylcyclohexane	Naphthene	131.79
n-propylcyclohexane	Naphthene	156.75
1,1-dimethylcyclohexane	Naphthene	119.55
1,2,3-trimethylcyclohexane	Naphthene	151.08
1,3,5-trimethylcyclohexane	Naphthene	140.55
1-heptene	Olefin	93.64
1-octene	Olefin	121.26
1-nonene	Olefin	146.87
1-decene	Olefin	170.60
2-methyl-1-hexene	Olefin	91.84
2-methyl-1-heptene	Olefin	119.22
2-methyl-1-octene	Olefin	144.65
2-methyl-1-nonene	Olefin	168.40
2,4-dimethyl-1-pentene	Olefin	81.59
2,4-dimethyl-1-hexene	Olefin	110.79
4,6-dimethyl-2-heptene	Olefin	129.87
2,5-dimethyl-4-octene	Olefin	153.48
Benzene	Aromatic	80.09
Toluene	Aromatic	110.63
n-ethylbenzene	Aromatic	136.20
n-propylbenzene	Aromatic	159.24
Styrene	Aromatic	145.16
α-methylstytene	Aromatic	165.50
Propan-1-ol	Oxygenate	97.20
Butan-1-ol	Oxygenate	118.75
Pentan-1-ol	Oxygenate	137.75
Hexan-1-ol	Oxygenate	156.75
3-pentanone	Oxygenate	101.99
3-hexanone	Oxygenate	123.50
3-heptanone	Oxygenate	147.40
3-octanone	Oxygenate	167.50

Two criteria should be met to select the six properties. First, the values of the properties included in the model must be strongly dependent on the hydrocarbon group. Conversely to the existing methods, this criterion was facilitated in the present study thanks to the pseudo-component method that

enabled the dependency of the properties on the boiling point to be put aside. In the existing methods, the measured properties were not always used in the equations but were included in the calculation of another property - which was integrated into the system - especially created in purpose. However, calculations could create error propagations, so the second criterion is the selection of measured properties instead of calculated properties. The first criterion prevails. Properties respecting the first criteria are already known thanks to the existing methods to predict the PNA fractions. The API (Riazi-Daubert) [8] method proposed several systems of equations operating with different properties which depend on the hydrocarbon group and are quite constant over the boiling point range. However, some properties are the results of a calculation between two other measured properties which is opposed to the second criteria. In this case, the measured properties were used as candidates instead of the one resulting of the calculation. A candidate was accepted if the measured property validates the first criteria. The upcoming properties were adopted.

5.4.1.1 *Specific gravity*

The specific gravity (SG) was defined by comparing the fuel and the water densities at 15.5°C:

$$SG = \frac{\rho_{fuel,15.5}}{\rho_{water,15.5}.} \tag{100}$$

The SG is linked with the length of the intra-molecular bonds in the fuel blend. This parameter is clearly dependent on the hydrocarbon group and is a simple property which can be used in this method.

5.4.1.2 *Refractive index*

Conventional methods rely on the refractivity intercept (Ri) or on the m-parameter. The Ri was created because the refractive index against density for each hydrocarbon group is linear [8]:

$$R_i = n_{20} - \frac{\rho_{20}}{2}, \tag{101}$$

where n_{20} and ρ_{20} are the refractive index and the density of the studied molecule at 20 °C.

For each type of chemical group, the refractive index is inversely proportional to the Mm. Then, the m-parameter is also a good hydrocarbon group indicator [5]:

$$m = Mm(n_{20} - 1.475) \tag{102}$$

The refractive index n_{20} is not the result of a calculation so it respects the previous condition 2 whereas R_i and m do not. Moreover, the refractive index allows to separate the group fractions for a given boiling point (condition 1). Therefore, the refractive index at 20°C was selected.

5.4.1.3 *Viscosity gravity function*

The viscosity gravity function (VGF) was proposed for fuels with a kinematic viscosity at 38°C (ν_{38}) lower than 3.6 cSt, which are typically light fractions,

on the observation that the plot of the SG against $\ln(\nu_{38})$ is linear for each hydrocarbon group [8]:

$$VGF = -1.816 + 3.484SG - 0.1156\ln(\nu_{38}). \quad (103)$$

$\ln(\nu_{38})$ and ν_{38} do not respect the previous condition 1, so, the VGF was preferred.

5.4.1.4 *Watson K factor*

The Watson K factor (K_w) defined in Bergamn's method is widely used to characterize fuels [8, 158]:

$$K_w = \frac{1.8{T_b}^{1/3}}{SG}, \quad (104)$$

where T_b is the normal boiling point for a pure component and the MeABP for a mixture. The K_w coefficient was developed to identify the type of molecules in a fuel blend so it is highly related to the chemical family. The boiling point and the SG are indeed a consequence of the strength of the chemical bonds. The MeABP does not respect the previous condition 1 so it cannot substitute the K_w

5.4.1.5 *Air-to-fuel ratio under stoichiometric conditions* AF_s

.

The H/C ratio used in existing methods [8] represents well the hydrocarbon groups but the air-to-fuel ratio under stoichiometric conditions (AF_s) was preferred to consider the oxygen content. It is defined by the global equation of combustion of the generic fuel $C_xH_yO_zN_\alpha$ under stoichiometric conditions and when the combustion is complete and where nitrogen is supposed to react into N_2:

$$C_xH_yO_zN_\alpha + \omega(O_2 + 3.76N_2) \rightarrow xCO_2 + \frac{y}{2}H_2O + (3.76\omega + \frac{\alpha}{2})N_2, \quad (105)$$

where ω is the needed number of moles of oxygen to burn the fuel under stoichiometric condition and is defined as:

$$\omega = x + \frac{y - 2z}{4}. \quad (106)$$

The AF_s depends on the stoichiometric mole number of air which can be calculated from the atomic weight ratio obtained from the atomic weight fractions:

$$AF_s = \frac{1}{Mm_c}\frac{1 + \frac{HC_W\frac{Mm_C}{Mm_H} - 2OC_w\frac{Mm_C}{Mm_O}}{4}(Mm_{O_2} + 3.76Mm_{N_2})}{1 + HC_w + OC_w + NC_w}, \quad (107)$$

where Mm_A is the Mm of atom A and the weight ratio between atom A and carbon, AC_w, is deduced from the atomic mass fractions:

$$AC_w = \frac{y_A}{y_c}, \quad (108)$$

where y_A refers to atom A and y_C refers to carbon.

5.4.1.6 *O/C weight fraction*

The O/C was included to handle the oxygen composition because using the air-to-fuel ratio enabled the oxygen content within the fuel to be considered but relying on the O/C increases the accuracy of the oxygenate prediction. Once the relevant properties are selected, the methods to characterize the properties of the real fuel and of the molecules belonging to the database can be defined.

5.4.2 *Characterization of the properties*

The experimental test methods and the calculations to define the real fuel properties will be presented, followed by the sources and the calculations of the properties included in the database.

5.4.2.1 *Properties of the real fuel*

The experimental characterization of the fuel properties is the only mandatory input to run an existing model to calculate the PIONAOx composition. However, as the model development is based on a given reference fuel, the obtained precision must be calculated depending on the variation of the reference fuel composition. If the model is not yet developed, the measurements of the properties must be coupled to the chemical analysis of the reference fuel. In the present study, the properties were characterized thanks to the ASTM standard test methods listed in Table 22 except for the nitrogen and sulfur fractions that were measured using GC × GC-NCD and GC × GC-SCD at Ghent University. Using a GC × GC to analyze the nitrogen and sulfur content is a special feature of the current work but the model can be run only relying on analysis lead by standardization companies, with GC-FID, GC-NCD, GC-SCD or EA. Depending on the type of fuel, several standard test methods can be applied as, for a light fuel, ASTM D4808 for hydrogen, ASTM D5623 for a sulfur concentration range from 0.1 to 100 mg/kg, ASTM D5762 for a nitrogen level of 40 µg/g to 10 000 µg/g, and ASTM D5622 for an oxygen mass content from 1.0% to 5.0%. ASTM D5291 is not recommended for O, N and S because the results are less accurate.

The MeABP was calculated from the volume average boiling point (VABP) [8] obtained by the volumetric distillation curve measured experimentally according to the standard test method ASTM D86 [103]:

$$\mathrm{VABP} = \frac{T_{10} + T_{30} + T_{50} + T_{70} + T_{90}}{5}, \tag{109}$$

where T_p (expressed in Kelvin) is the temperature at which p% of the fuel is evaporated. The VABP was converted into MeABP [8]:

$$\mathrm{MeABP} = \mathrm{VABP} + \Delta_{\mathrm{Me}}, \tag{110}$$

where the shifting coefficient Δ_{Me} is defined as [8]:

$$\ln(\Delta_{\mathrm{Me}}) = -1.53181 - 0.0128(\mathrm{VAPB} - 273.15)^{0.6667} + 3.646064\mathrm{SL}^{0.333} \tag{111}$$

and SL is the 10-90 slope defined by [8]:

$$SL = \frac{T_{90} - T_{10}}{80}. \tag{112}$$

The experimental methods to measure all the fuel properties are listed in Table 22.

Table 22: Fuel properties and methodologies

Property	Value	Unit	Method
ρ at 15.5°C	796.1	kg/m³	ASTM D4052
ν at 40°C	0.6615	cSt	ASTM D445
C	84.58	%wt/wt	ASTM D5291
H	12.76	%wt/wt	ASTM5291
O	2.34	%wt/wt	ASTM D5622
N	0.26	%wt/wt	GC × GC-NCD
S	0.06	%wt/wt	GC × GC-SCD
n at 20°C	1.4419	/	ASTM D1218
SG	0.7969	/	Equation 4
VGF	1.008	/	Equation 7
K_w	11.412	/	Equation 8
MeABP	144.9	°C	ASTM D86; Equation 14

5.4.2.2 *Properties of the molecules belonging to the database*

The properties of the real fuel were related with the properties of the molecules in the hydrocarbon group. A property database, erected from the library of the software Aspen Properties®, was built to represent each group. This section first lists the molecules included in the software and then cites the formulas to estimate the missing properties. Finally, the properties of each chemical group were plotted to check the distribution over the map.

The Mm, the boiling point, the SG and the refractive index were directly extracted from the database of Aspen Properties®except for the refractive index of 2,4-dimethylheptane, 1,2,3-trimethyl-cyclohexane, 1,2-dimethy-1-pentene, 1,2-dimethyl-1-hexene, 4,6-dimethyl-2-heptene, and 2,5-dimethyl-4-octene. The refractive indices of the last molecules were calculated thanks to the refractive index parameter I [8]:

$$n = \frac{1 + 2I}{(1 - I)^{1/2}}, \tag{113}$$

which can be evaluated with an accuracy of 0.5% for a Mm range from 70 to 300 [8]:

$$I = 2.34310^{-2}\exp(T_b + 2.468SG - 1.026.10^{-3}T_bSG)T_b{}^{0.0572}SG^{-0.72}. \tag{114}$$

All the missing properties were evaluated with Aspen Properties®using the PENG-ROB base property method [25]. The Watson K factor was calculated with equation 104.

Once the database was entirely defined, the property distribution over the boiling point range was plotted to ensure a good separation between

the groups (Figure 51). The Watson factor is known to be dependent on the molecule type, from 9 (aromatics) towards 13 (paraffins). We observe that this property also differentiate the olefins, the naphthenes and the oxygenates. For what concerns the specific gravity, the type of bonds drives the volume taken by the molecules. Conversely to the paraffins, aromatics are characterized by double bonds that shows a strong link between the atoms. Thus, they have a high specific gravity. The oxygenates have a relatively high specific gravity because of the heavy oxygen atom. The n-paraffins and the iso-paraffins have the same raw formula, so they have an equal stoichiometric ratio. This is also the case for the olefins and the naphthenes. The viscosity gravity function is also a good tool to differentiate the molecules. The repartition is very similar than with the specific gravity. The refractive index is useful to differentiate the aromatic and the naphthenes. The O/C helps to identify only the oxygenates as it is the only hydrocarbon class with an O atom. As a conclusion, the differentiation between the groups is good for all the properties, except in the following cases.

1. The iso and normal paraffin share part of their ranges.
2. The refractive index of the oxygenate group overlaps with the iso and normal paraffins.
3. The AF_s of olefins and naphthenes are the same over the boiling point range.
4. The AF_s of iso and normal paraffin are the same over the boiling point range.

These cases are not an issue for almost all the groups because they are well differentiated with at least one property. Nevertheless the differentiation may be difficult between the normal and the iso paraffins.

The pseudo-component method helped to distinguish locally the properties for the first and the second cases and the O/C allowed to estimate the oxygenate content.

This first section described the methods to build the database to create or to run a model. The next part will develop the calculations included in the core of the model.

5.5 MATHEMATICAL MODELS AND RESOLUTION

In this section, we present the formulas to build the pseudo-components – reduced number of theoretical molecules representing a given hydrocarbon group – thanks to a molecule database that characterizes well the molecules in the fuel. Then, the section explains the procedure to approximate the composition of an unconventional fuel thanks to a relation involving its properties measured by standard test methods.

5.5.1 *Pseudo-component definition*

A complex fuel composed of hundreds of molecules can be represented thanks to its pseudo-components. This section develops the equations defining the properties of the pseudo-components.

A pseudo-component is a notional molecule belonging to a hydrocarbon group and characterized by its boiling point. Therefore, each hydrocarbon group in a fuel can be represented by one or several pseudo-components

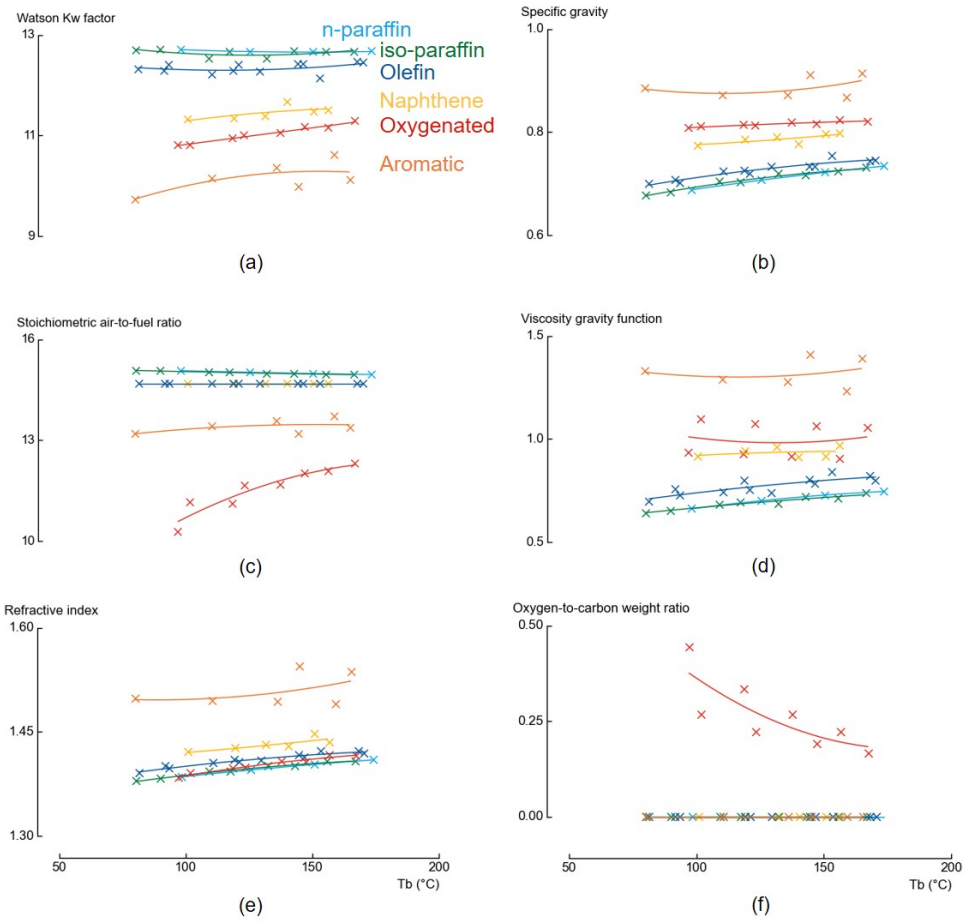

Figure 51: Dependency of the six chosen fuel properties on the hydrocarbon group. The cross refers to the molecules included in the database and the lines are the results of a second order polynomial regression for each hydrocarbon group. We selected a second order polynomial as the properties tend to vary with a power 2 depending on the temperature. Light blue: n-paraffin, green: iso-paraffin, dark blue: olefin, yellow: naphthene, orange: aromatic, red: oxygenate.

depending on the 10-90 slope SL (equation 110). If SL is lower than 0.8, the narrow boiling range hypothesis is respected and one pseudo-component per group is sufficiently accurate to study the fuel. Otherwise, the fuel boiling point range is subdivided and several pseudo-components representing each division must be determined [5]. In the present study, SL = 0.745 so the narrow boiling range is respected. This simple definition allowed to calculate the properties of each hydrocarbon group using only two inputs: the MeABP of the fuel and a database of molecules for each group. The database was used as a basis to define equations for each studied property.

The equations were built from the observation that the correlation coefficients (R) between the calculated properties from a second order polynomial regression and the properties from the database are higher than 0.94, except for the Watson K factor of the 2-methylakane group (R = 0.83). We selected a second order polynomial as the properties tend to vary with a power 2 depending on the temperature. Therefore, the property versus the boiling temperature for a same subgroup of isomers in a chemical group is close to be quadratic. The properties of the pseudo-components were based on a

second order regression. The rules to select the molecules belonging to each hydrocarbon group defined in the first section enabled the different isomers to not be favored during the polynomial regression. Then, the property of the fuel can be calculated with:

$$P_p = \sum_g y_g P_{p,g}, \tag{115}$$

where $P_{p,g}$ is the p-th property of the pseudo-component characterizing the g-th group and y_g is the mass fraction of the g-th group.

The pseudo-components helped to decorrelate the fuel properties according to the different groups. This enabled the creation of the equations linking the fuel properties and the group fractions. The resolution relied on an optimization problem and is described in the next section.

5.5.1.1 *Resolution*

After explaining the benefits of minimizing an optimization problem compared with the linear resolution adopted in conventional methods [8], the details on the minimized objective function are reported.

In the present study, n-paraffin, iso-paraffin and olefin showed very similar ranges of values. Moreover, the boiling point and the properties of the molecular mixtures of each hydrocarbon group in the fuel will not precisely be equals to those of their representative pseudo-component. Because the ranges overlap, these differences of boiling point and properties will propagate an error on the calculated fractions. Consequently, to take into account the inaccuracies due to the differences between the molecular mixtures and the pseudo-components, an optimization problem was solved to introduce a higher flexibility than a simple linear resolution.

If a model already exists for the studied fuel, only one optimization problem must be solved in order to reduce the difference between the p-th property of the real fuel, $P_{rf,p}$, and the p-th property of the mixture of the pseudo-components, P_p. The p-th decision variable was defined as:

$$f_p = \frac{|P_p - P_{rf,p}|}{P_{rf,p}} \tag{116}$$

The properties of the mixture of the pseudo-components P_p were calculated according to equation 115.

Weight coefficients were introduced in the objective function to couple the properties with a relative influence:

$$O_p = \sum_p w_p f_p, \tag{117}$$

where the weight coefficients w_p were equal to a power of 10 because an simple increase by one did not allowed us to observe a significant effect of the weights.

The objective function O_p was reduced thanks to the matlab fmincon function included into the GlobalSearch object coupled with the MultiStart algorithm to run several start points uniformly distributed. Two constraints were also set, the resolution domain [0;1] and:

$$y_p + y_i + y_n + y_a + y_{Ox} = 1 \tag{118}$$

The weights w_p are specific to the studied type of fuel. To build a model suited for a new type of fuel, a second optimization problem was solved which gave the values of w_p. The best set of weights was obtained when the difference between the calculated fuel fractions and the measured fractions of the reference fuel was minimized. The reference fuel must be a good representative of the studied type of fuel in terms of molecules and group fractions. The mathematical formulation of the objective function is:

$$O_g = \sum_g w_g f_g, \tag{119}$$

where the decision variables f_g are defined as the difference between the calculated mass fractions y_g obtained by minimizing the objective function O_p defined by equation 117 and the normalized average value Y_g of the measured fractions of each group g:

$$f_g = |y_g - Y_g| \tag{120}$$

No priority was set such as the weights w_g were all set equal to one. The minimization of O_g gave the weights w_p. The number of starting points defined in the GlobalSearch object was fixed by trial and error when the returned set of weights w_p was persistent.

The entire methodology to develop a model which predicts the PIONAOx composition of an unconventional fuel was proposed. The model depends on two parameters which are the molecule database (Table 21) and the weights defining the objective function (equation 117). Those parameters were defined according to a reference fuel which represents well the type of studied fuel. Some molecules of the database were removed and several set of weights were tested to investigate the achieved accuracy with different parameters. However, although the accuracy was increased when the parameters were tuned with the reference fuel, it may be decreased for the other studied fuel. A high parameter tuning is expected to decrease the maximal variation of composition which is correctly handled. Therefore, the last section aims at estimating which parameters allow to achieve an acceptable accuracy with the reference fuel. The precision of the model with other fuels than the reference one will be investigated in a future study. This will define the maximal composition variation allowed to rely on the same model than the one developed with the reference fuel.

5.6 RESULTS AND DISCUSSION

The model depends on two parameters, the first is a molecule database representing each hydrocarbon group of a reference fuel characterizing the studied type of fuel. The second is the set of weights impacting the reduction of the objective function during the resolution step. The accuracy of the model was investigated for several parameter settings.

5.6.1 *Tuning of the molecule database*

The molecules listed in Table 21 creates an extended database where the isomers are equally represented for each boiling point. However, the molecular configuration depends on the production process such as the type of predominant molecules depends on the boiling point. Tuning the initial

molecule database listed in Table 21 is a way to match the fuel and increase the accuracy of the model. The refinement was performed with respect of the following rules:

1. The selected molecules still cover the PIONAOx groups.

2. The ranges of the hydrocarbon group boiling points must contain the fuel MeABP. For each hydrocarbon group, at least three molecules were selected to rely on a second order polynomial regression.

3. For each property and each group, the plot of the second order polynomial function must be located within the property range of the isomer sub-groups of the original database

To monitor the evolution of the accuracy along the refinement, the molecule tuning scale is defined as:

$$S_m = \frac{n_{refine}}{N_{refine}}, \tag{121}$$

where N_{refine} is the number of molecules removed from the initial molecule database listed in Table 21 to reach the highest accuracy with all the weights equal to one and n_{refine} is the progress variable until N_{refine} and defined by the number of molecules removed to reach the current studied error. The molecule tuning scale evolves according to the number of removed molecules from the initial database.

The molecules were removed in a precise order depending on the following automatic reduction sequence. The molecules were tested per group in the following order: aromatic, oxygenate, naphthene, olefin, iso-paraffin. This order was selected to respect the group repartition order – from higher to lowest and inversely – of half of the studied properties (the K_w, the SG and the VGF) that appears when the properties are plotted (see Figure 51). This avoids a bad interaction between the (n+1)-th removed molecule and the n-th removed one. For instance, the aromatics have only one neighbor group – the oxygenate (Figures 51a, 51b, 51d)) – so these molecules are mostly only impacted by the oxygenates. Therefore, the deletion of an aromatic molecule could be inhibited by the first deletion of an oxygenate without any possible counterbalance by a second group to have a second opportunity to remove the aromatic. No n-paraffin was deleted because only 4 molecules belong to the original database. At each step, the selected molecule is the one whose deletion reduced the most the error of its hydrocarbon group. After one reduction sequence, 9 molecules were removed, reducing the global error (Figure 52).

A group-per-group molecule refinement following this order was obtained: aromatic, naphthene, olefin, iso-paraffin (Table 23). No oxygenates were removed from the original database.

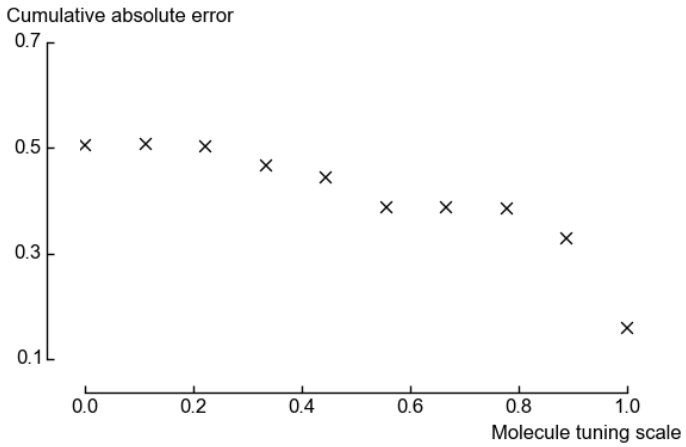

Figure 52: Absolute cumulative error along the molecule refinement.

Table 23: Order of the molecular refinement

Iteration	S_m	Molecule name	Hydrocarbon group
1	0.11	Propylbenzene	Aromatic
2	0.22	Toluene	Aromatic
3	0.33	1,2,3-trimethylcyclohexane	Naphthene
4	0.44	1,1-dimethylcyclohexane	Naphthene
5	0.55	2-methyl-1-heptene	Olefin
6	0.66	2,4-dimethylheptane	iso-paraffin
7	0.77	2,4-dimethyloctane	iso-paraffin
8	0.88	2-methylnonane	iso-paraffin
9	1	2-methyloctane	iso-paraffin

The best accuracy was reached at a molecule tuning scale of one with a cumulative absolute error of 16 % (Figure 52). For each group, the error is further decreased when the confidence interval is considered (ϵ_{CI}<1% except for monoaromatics and n-paraffins for which it is still acceptable, Table 24). The cumulative absolute error reaches 12.6 % when the confidence interval is considered.

Table 24: Estimated fractions Ye (% wt/wt) and absolute errors from confidence interval comparison (ϵ_{CI}, %) at a molecule tuning scale equal to 1.

Chemical group	Y_e (% wt/wt)	ϵ_{CI} (%)
n-paraffin	0.3	4.8
iso-paraffin	11.2	0.4
Olefin	30.1	0
Mononaphthene	13.4	0.5
Monoaromatic	32.1	6.7
Oxygenate	12.8	0.1

Increasing the molecule tuning scale has the benefit to improve the accuracy when the model is being set with the reference fuel. Then, the objective being

to apply this model to another fuel similar to the reference fuel, the accuracy may decrease and the range of applicability of the model could drop due to the differences with the reference fuel. Therefore, to relax this first scale, the second parameter of the model which is the weight allocated to each property in the objective function was also included in a feedback loop.

5.6.2 *Tuning of the weights*

The molecular database is tuned before the weights in order to get a database whose composition match as much as possible with the fuel. Then, the weights allocated to each property can be tuned to reach a better result, the weight tuning scale is defined by:

$$S_w = \frac{\log(w)}{\log(W)}. \tag{122}$$

W is the maximal weight over the whole studied sets of weights and w is the maximal weight of the current set of weights. W is given by the stopping criterion, achieved when the objective function based on the fraction values, O_g, did not decrease more than 1% during three consecutive iterations. This criterion could be strengthened to enhance the accuracy but 1% enabled a good result to be reached within an acceptable computing time. An iteration corresponds to an increase of the maximal weight value 10^M by a factor 10.

The accuracy of the model depending on the weight tuning scale is discussed only for a reduced number of molecule tuning scales. To analyze the effect of improving 0, 1, 2, 3, or 4 hydrocarbon groups, S_m was set equal to 0, 0.22, 0.44, 0.55 and 1 (see Table 23, when S_m is equal to 0.22, 0.44, 0.55 and 1, all the molecules belonging respectively to the aromatic, naphthene, olefin and iso-paraffin hydrocarbon class are removed from the database).

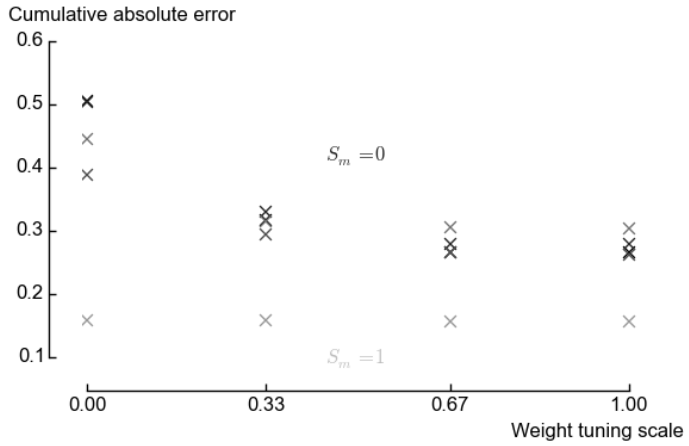

Figure 53: Absolute cumulative error along the weight refinement at a molecule tuning scale equal to 0, 0.22, 0.44, 0.55 and 1 (from darker to lighter grey).

The stopping criteria was respected for all the molecule tuning scales when the maximal weight W was set at 1.10^3. The cumulative absolute error is reduced under this condition for all the molecule databases (Figure 53). The error plunges when the maximal weight evolves from 1 to 10 (weight tuning scale from 0 to 0.33), thus, relying on a maximal weight of 10 could be appropriate. The weights do not have a significant impact when the

best molecule tuning scale ($S_m = 1$) is considered and the error cannot be reduced less than approximately 30% with the other molecule tuning scales. According to the present study, weights are not needed at a molecule tuning scale of 1 because the error and the compositions are constant along the weight tuning scale (Table 25).

Table 25: Calculated fractions (% wt/wt) and cumulated absolute error from confidence interval comparison (ϵ_{CI}, %) at a molecule tuning scale equal to 1, and at a weight tuning scale equal to 0, 0.33, 0.67 and 1.

S_w	P	I	O	N	A	Ox	ϵ_{CI}
0	0.3	11.2	30.1	13.4	32.1	12.8	12.6
0.33	0.0	11.2	30.4	13.5	32.0	12.8	12.7
0.67	0.0	11.4	30.0	13.7	32.0	12.9	12.4
1	0.0	11.4	30.0	13.7	32.0	12.9	12.4

Only the reference fuel is studied in the present chapter. The range of validity of the model can be studied with different compositions. The accuracy of the model depending on the composition depends on the weights and on the database. If the weights and the database are especially fitted for the reference fuel, the accuracy of the model is likely to be impacted with a different composition. Thus, a trade-off would be necessary. Moreover, appropriate weights and database could be used to obtain a good accuracy with different compositions.

The developed methodology has a good accuracy. However, the range of validity of the method probably decreases when the inputs are tuned to reach a high accuracy. Therefore, the range of validity could be studied with an error propagation. The propagation of a variation of the fuel composition on the calculated fraction is an interesting approach. This would complete the current results to find an optimal set of parameters (molecule database and weights) to couple a good range of applicability with a good accuracy. Then, the key parameter between the molecule tuning, the weight tuning, or a combination of both, for achieving good results for a wide range of composition could be determined.

5.7 CONCLUSION

In this chapter, the existing models for predicting the composition of a classical fuel are extended to a model suited for unconventional fuels. As an example, a model for ASR- derived fuels was used as case study. The method relies on the chemical analysis of a reference fuel which characterizes well the unconventional fuel. Once the model is set according to this reference fuel, the chemical analysis is not required anymore and the fuel properties measured according to standard test methods are sufficient. Thereafter, the approximated fuel fractions can be used for several purposes. First, the octane numbers can be estimated thanks to the pseudo-component technique which is relevant as unconventional fuels are often related to constraints (cost, reliability) and are in general produced locally making it hard to perform the same kind of quality control as in a large plan like cooperative fuel research (CFR) tests. Secondly, the unconventional fuel production can be monitored. Lastly, a variation of the fuel characteristics can be explained. Therefore, the developed methodology enables the properties of

an unconventional fuel to be studied during its production, allowing to get retrofitting information, to make technical choices, to study the production stability or to tune the process towards better combustion.

Compared to the existing methods, where a linear system of equations based on two fuel properties is solved to calculate the PNA fractions, this method uses the pseudo-component technique and six properties simultaneously, namely the refractive index (n), the VGF, the K_w, the SG, the AF_s, and the O/C, leading to solve an optimization problem rather than a direct linear system of equation. This method significantly extends the existing methods to less traditional fuels and enables a good estimation of the PIONAOx fuel fractions. The six properties can be easily measured thanks to ASTM standards. The accuracy depends on the parameters of the model and is evaluated comparing the calculated fractions to the confidence intervals of the real fractions estimated from the composition measured with the GC $\times$ GC. The error is low when the model is well-set. For the best estimated composition, the cumulated error of all the groups was evaluated at 12.4%

The estimation of the composition is useful to understand the properties of a fuel. Among others, it is possible to explain how the fuel burns. For instance, the research octane number (RON) and the motor octane number (MON) are two important properties that must be high enough to avoid engine knock and to ensure a high efficiency. Nevertheless, measuring these properties is not always possible. Thus, estimating method exist for conventional fuels. The next chapter develop a new estimating method especially developed for oxygenated fuels.

6

PREDICTION OF THE OCTANE NUMBERS WITH A BAYESIAN INFERENCE APPROACH

The content of this chapter has been published in the following scientific article:

S. Tipler, M. Fürst, Q. Van Haute, F. Contino, and A. Coussement. Prediction of the octane number: A bayesian pseudo-component method. *Energy & Fuels*, 34(10):12598–12605, 2020

6.1 INTRODUCTION

Straight paraffins tend to ignite with a small ignition delay while it is the opposite for aromatics. Thus, the prediction of the composition, as performed in the previous chapter, is useful to get a first insight on the behaviour of a fuel and to know how to change the properties. Nevertheless, relying on properties that express this ignition delay provides quantitative data.

Among all the fuel properties, the research octane number (RON) and the motor octane number (MON) are fundamental. A maximal RON and MON are required to avoid knocking and to optimize the combustion efficiency. The RON and the MON test methods are expensive for a decentralized or small production plant as well as for a project in the design phase because they require a cooperative fuel research (CFR) engine, relatively costly products (n–heptane and iso–octane) and high level of qualification [81, 82]. Nevertheless, unconventional fuels are produced at a small scale, so they are produced with a limited budget and they must be characterized at a cheap price. As a comparison, we estimate the price of an on-site laboratory at 40 000€ while this price would enable the producer to measure the fuel octane numbers twice a week during one year only. It should be noted that additional properties such as the density, the CHO atomic fraction, the distillation curve and the composition would be required as an additional cost. Moreover, the RON and the MON tests require 1L of material which may not be available for fuels in early research stage.

RON and MON measurements can be replaced by one of the many predicting methods available. They differ one another by the input quantities to run the model. The input quantities can either be chemical properties – nuclear magnetic resonance (NMR) data [109, 110], chemical fractions [8, 106], chromatographic data [107, 108] – or physical properties – distillation curves [8, 111], ignition delay time [95, 113].

Among the different methods, the pseudo-component (PC) method is based on the fractions of the hydrocarbon class (n-paraffin, iso-paraffin, naphthene, aromatic) and the distillation cut points. This method, was summarized by Riazi[8]: a PC is characterized by a boiling point which is

equal to the mean average boiling point (MeABP) of a fuel. The method attributes a PC to each hydrocarbon class.

While the pseudo-component method relies on simple input quantities, it has several limitations.

- It does not cover fuels with olefin and oxygenated molecules so it cannot be applied to all of the unconventional fuels [20, 33, 89], hence the method lacks generality.
- Its uncertainty has never been studied.
- It does not differentiate the isomers among each hydrocarbon class. For instance, the iso-paraffins are considered as a blend of 2-methyl-alkane, 3-methyl-alkane, 2,2-dimethyl-alkane and 2,3-dimethyl-alkane in equal proportions.
- It was only presented for the RON, so, no model exist to predict the MON with PCs.

To address these limitations, the current chapter embeds an inductive probabilistic approach based on a Bayesian tuning. This kind of approach has already been used to relate bulk properties and the molecular composition [159].

The pseudo-component method was used in recent publications. For instance, Nguyen et al. [160] proposed a model to predict the viscosity where n-alkane mixtures are represented by a single pseudo-component. Xu et al. [161] predicted binary-interaction parameters of cubic equation state for petroleum fluids represented by pseudo-components. Ramos-Pallares et al. [162] predicted the thermal conductivity of oils characterized into pseudocomponents. Liu et al. [46] extended the pseudocomponent representation to characterize the molecular information of pseudo-components. Bulk properties, including the octane numbers, were accurately estimated even if olefin constituted the fuel. Nevertheless, this method requires a deep characterization of the petroleum fraction as a pseudo-component is characterized every 20K. This requires the n-paraffin, iso-paraffin, olefin, napthene, aromatic (PIONA) analysis of the petroleum product every 20K.

The aim of the current chapter is to formulate a model applicable for gasoline blendstocks mixed with oxygenated molecules and which is able to predict the RON and the MON. The goal includes the characterization of the uncertainty. We focus on gasoline blendstocks mixed with oxygenated molecules. The oxygenated molecule can be composed of up to four carbon atoms and it can be produced via fermentation or gasification [27].

After having described the new Bayesian PC method, the results are discussed and the conclusions are drawn in the last section.

6.2 METHOD

The method section starts with an overview of the original PC method. The original PC method summarized by Riazi attributes a PC to each hydrocarbon class [8]. A PC is characterized by a boiling point which is equal to the MeABP of a fuel. The MeABP depends on the distillation cut points and was defined in section 2.5.4.

An important assumption in the PC method is that the RON of each PC, RON_{pc}, correlates with the MeABP of the fuel. The law between RON_{pc} and MeABP is based on the regression between the boiling point and the octane numbers of pure molecules. In the original PC method, the database of pure

molecules does not take the isomer into account. Specifically, the aromatics are considered as n-alkylbenzenes, the naphthene as n-alkylcyclopentanes and the iso-paraffins as the average between 2-methyl-alkanes, 3-methyl-alkanes, 2,2-dimethylalkanes and 2,3-dimethylalkanes. In the current study, we introduce a correcting factor that modifies the octane number of the PC according to the type of isomer. In the original PC method, a linear blending law by volume relates the RON of the fuel of interest with the RON of each PC:

$$\mathrm{RON}^{*}_{\mathrm{Riazi}} = \left[\mathbf{y_{Riazi}}\right]^{\intercal} \times \mathbf{RON_{pc}}, \tag{123}$$

where $\mathbf{y_{Riazi}}$ is the vector of the volume fractions of the PCs. These volume fractions are equal to the volume fractions of the hydrocarbon classes in the fuel and can be measured by gas chromatography (GC), comprehensive two dimensional gas chromatography (GC × GC) or with a reformulyzer. Note that in the current chapter, the letters in bold refer to vectors and matrices and "×" is the Cartesian product.

Property	Min	Mean	Max
30 Training fuels			
RON	85.8	91.7	99.2
MON	80.8	83.9	88.9
MeABP (°C)	79.3	89.9	101.5
Saturate (%)	57.3	66.0	74.0
Olefin (%)	2.1	4.6	7.8
Aromatic (%)	16.3	21.0	28.9
Oxygenate (%)	2.9	8.4	15.3
15 Test fuels			
RON	86.9	92.0	98.6
MON	81.0	84.0	88.6
MeABP (°C)	80.5	89.4	99.5
Saturate (%)	59.8	64.9	70.2
Olefin (%)	2.2	4.5	7.4
Aromatic (%)	17.0	20.7	27.4
Oxygenate (%)	7.8	9.9	11.6

Table 26: Properties of the 45 BOB-Ox fuels used to train and to test the new method. This table defines the ranges where the model can be applied.

Contrary to the one compiled by Riazi, the proposed method is developed for fuels with olefins and oxygenates. The study of Christensen et al. [27], who highlighted the properties of 77 fuels, offers a lot of experimental data to develop the method. Only 45 out of the 77 fuel are selected. This way of proceeding allows to obtain an equal representation of each oxygenated molecule, thus, achieving a more accurate model. Specifically, for these 45 fuels, three blendstocks for oxygenate blending (BOB) are mixed at three different proportions – at a low (3 to 4.1%), an intermediate (7.9 to 11.6%) and at a high volume fractions (10.6 to 15.3%) – with five oxygenated molecules – 1-propanol, 2-propanol, 1-butanol, 2-butanol, 2-methyl-1-propanol. The 45 fuels are divided in a training set and in a test set. The training set is composed of the low and the high fractions (30 fuels) and the test set is composed of the intermediate fractions (15 fuels). Thus, the model is created with the framing fractions of oxygenates and validated with a fraction which

is in between. The properties of the studied BOB-Ox fuels are reported in Table 26. This Table defines the ranges where the model can be applied.

The method proposed here, based on Bayes law allows to assess the uncertainty, which was not possible with the original PC method. The original Equation 124 is modified with the expectancy of a correcting factor $E(\mathbf{K})$ which is calculated applying Bayes' law. The correcting factor corrects the octane number of each PC according to the type of isomer in the corresponding hydrocarbon class. With the Bayesian PC method, an unbiased estimator of the octane number (ON) is proposed as:

$$ON^* = [\mathbf{y}]^T \times \left([E(\mathbf{K}) \circ \mathbf{ON_{pc}}] \right) + \sigma^*, \tag{124}$$

with σ^* the random error, i.e. an unpredictable error due to the measurement method, and "$\circ$" the Hadamard product.

The modifications adopted to the original equation reported by Riazi [8] are described thereafter.

- $\mathbf{y}$ is the vector of the volume fractions of the four PCs (saturate, olefin, aromatic, oxygenate). Three hydrocarbon classes (n-paraffin, iso-paraffin, naphthene) are merged in a single hydrocarbon class (saturate) because the saturate class constitutes the training data reported by Christensen et al. [27]. Moreover, the olefin and the oxygenate hydrocarbon class are included.

- $\mathbf{ON_{pc}}$ is the vector composed of the octane numbers of the four PCs. The correlations between ON_{pc} and the MeABP are modified to include more isomers than in the original PC method:

$$ON_{pc} = \mathbf{r}^T \times \mathbf{T}, \tag{125}$$

with

$$\mathbf{T} = [{}^{1}_{MeABP}]. \tag{126}$$

The vector $\mathbf{r}$ is composed of the linear regression coefficients between the boiling points and the octane numbers of pure molecules from large databases [8, 25–29]. These databases were completed by measuring the octane numbers of pentan–3–one and heptan–3–one. Relying on ketones as well as alcohol allowed us to propose a general methodology that can be applied to another type of fuel, for generating another model. $\mathbf{r}$ takes into account the evolution of the octane number depending on the boiling point. Nevertheless, the uncertainty on $\mathbf{r}$ does not need to be estimated to calculate the final uncertainty, according to Equation 12. The boiling points and the octane numbers are available in the Appendix C and $\mathbf{r}$ is reported in Table 27.

- In equation 124, $E(\mathbf{K})$ are the expectancies of the correcting factors $\mathbf{K}$ introduced by Bayes' law. The Bayesian method that calibrates the probability density functions (PDFs) of $\mathbf{K}$ is inspired by the work of Josephson et al. [137] With this method, we compute the estimated octane number with an initial guess and we compare the estimation to the measurement. The better is the match between the estimation and

	Saturate	Olefin	Aromatic	Oxygenate
			RON	
Intercept	103.07	112.89	142.14	108.80
Slope	-0.29143	-0.22733	-0.19927	-0.13568
			MON	
Intercept	9.4256	90.794	131.09	91.299
Slope	-0.24124	-0.12941	-0.19675	-0.08470

Table 27: Coefficients (**r**) required for Equation 136. The coefficients were obtained with a linear regression between the octane number and the boiling points of pure molecules from the literature [8, 25–29]. Additional octane number measurements were also lead for pentan–3–one and heptan–3–one (available in the Appendix).

the measurement, the better is the initial guess. When the matching is satisfactory, the initial guess is set as being the right value for the parameters of the model. Below are summarized the calculation steps with a focus on how the work of Josephson et al. is adopted to the current study. If the reader requires more information, the main concepts of the methodology used in the current chapter are explained in depth in the paper of Josephson et al. [137]

According to Bayes' law, the conditional knowledge of the experimental octane number **ON** allows to estimate the correcting factor. When **ON** is known, the PDF of the correcting factor K_i, $f_{K_i|ON}(K_i|\mathbf{ON})$, for the hydrocarbon class i is given by the following proportionality:

$$f_{K_i|ON}(K_i|\mathbf{ON}) \propto f_{K_i}(K_i) f_{ON|K}(\mathbf{ON}|\mathbf{K}). \tag{127}$$

The prior PDF, $f_{K_i}(K_i)$, represents an initial knowledge of the correcting factor. The prior gives the distribution of K_i before any analysis is realized. The distribution of the PDF and the limits where K_i is studied must be defined. As K_i is unknown, we chose an uniform distribution to avoid any preferred choice in the studied range[137]. Thus, we chose a rectangular distribution so that the correcting factor K_i has equal probability across the studied range. Then, the limits where K_i is studied must be defined. As K_i is a priori unknown, the PDF called likelihood ($f_{ON|K}(\mathbf{ON}|\mathbf{K})$) informed us on how far the limits of K_i were from their true value. The likelihood depends on the values of the correcting factors. Thus, changing the limits of K_i changes the shape of the likelihood. When K_i is defined in a wrong range, the value of likelihood tends towards zero. When the prior is defined in the right range, the likelihood tends towards a Gaussian shape because of Equations 128 and 129. Thus, we changed the limits of each K_i iteratively by trial-and-error until getting a well-defined Gaussian shape that described the likelihood. We discretized each K_i simultaneously with a latin hypercube sampling (LHS) procedure and 20 000 samples to balance RAM memory and resolution when visualizing the likelihood.

The likelihood $f_{ON|K}(\mathbf{ON}|\mathbf{K})$ represents the probability to get the experimental octane numbers **ON** with the correcting factors **K**. Concretely, the probability of the likelihood is reduced when the octane number calculated with the chosen parameters does not correspond to experiments. The likelihood is given by the following equation which

combines the probabilities $p\left(ON|ON^*(\mathbf{K})\right)$ for all the experimental ON:

$$f_{\mathbf{ON}|\mathbf{K}}(\mathbf{ON}|\mathbf{K}) = \prod^{n_{exp}} p\left(ON|ON^*(\mathbf{K})\right). \tag{128}$$

$p\left(ON|ON^*(\mathbf{K})\right)$ is the probability of the measured octane number when the estimated octane numbers are defined. The estimated octane numbers are randomly distributed because the parameters **K** were randomly sampled with a LHS procedure. Thus, the octane numbers estimated with the sampled **K** follow a Gaussian shape. This Gaussian is centred at a value equal to the measured octane number when the parameters **K** are correctly chosen.

$$p\left(ON|ON^*(\mathbf{K})\right) = \frac{1}{\sqrt{2\pi\sigma^2}}\exp\left(-\frac{\left(ON - ON^*(\mathbf{K})\right)^2}{2\,\sigma}\right) \tag{129}$$

Equation 129 gives the probability of getting a measured octane number relatively to its estimation. This probability depends on the Gaussian shape, i.e. on the variance σ. The estimation being intrinsically unbiased, this probability depends only on the precision of the experimental measurements. Consequently, the Gaussian shape, i.e. the variance σ, depends on the reproducibility of the ON measurement.

The reproducibility of the ON measurement was published in the ASTM D2699 [81] (RON), ASTM D2700 [82] (MON) and in The Precision of knock rating – 1936-1938 [163] for RON equal to 50, 80, from 90 to 100, 101, 102, 103 and from 104 to 108 and for MON from 80 to 90 and from 102 to 103. The uncertainty has never been characterized in the other ranges so we adopted the worst uncertainty of the surroundings octane numbers. Moreover, we adopted the same reproducibility for low and high MON (below 80 and above 103) than the RON. The uncertainties are summarized in Table 28.

The following procedure explains how to create a new model.

- Initialize the minimal and the maximal values of the correcting factors with a starting guess.
- Create samples for the correcting factors. We relied on 20000 samples generated via LHS.
- For each sample, calculate the octane number with Equation 124. The input parameters, namely the hydrocarbon class fractions and the MeABP are used.
- For each sample, calculate its probability with Equation 129. σ in Equation 129 is calculated with the reproducibility reported in Table 28. The objective parameters, namely, the experimental octane numbers are used.

ON	Half-width	Confidence
	RON	
]0 - 50[	2	95
50	2	99.9
]50 - 90[	2	95
[90 - 100]	0.7	95
]100 - 101]	1	95
]101 - 102]	1.4	95
]102 - 103]	1.7	95
]103 - 104]	2	95
]104 - 120]	3.5	95
	MON	
]0 - 80[	2	95
[80 - 90]	0.9	95
]90 - 103]	2	95
]103 - 120]	3.5	95

Table 28: Confidence interval of the experimental octane numbers (Reproducibility). The level of confidence of the measured octane number is given in the interval = ON $\pm$ half-width.

- Calculate the likelihood with Equation 128.
- Plot the likelihood as a function of the sampled correcting factor to visualize the likelihood.
- Go back to the first step and change the minimal and maximal values of the correcting factor so that the plotted likelihood look like a Gaussian function.
- Once the likelihood looks like a Gaussian function, calculate the expectancy and the variance-covariance matrix of the correcting factors.

6.2.1 *Example*

This section shows how to compute the octane number once the model is created. As an example, we rely on the first fuel of the spreadsheet TestData provided in the Appendix D. We show how to calculate the RON, the MON and their uncertainties. The properties of this fuel are reported in the following table. The MeABP is first calculated with equation 18.

MeABP	80.46
Saturate (%)	66.1
Olefin (%)	7.3
Aromatic (%)	18.1
Oxygenate (%)	8.4

Table 29: Properties of the fuel used as an example.

Then, the octane numbers of the pseudo-components are calculated with Equation 125 with the coefficients from Table 27. The result is reported in the following table.

Thereafter, the expectancy of correcting factors are applied. The expectancies of the correcting factors are reported on Figure 54 for the RON and figure 55 for the MON. The following table reports the result.

	RON_PC	MON_PC
Saturate	79.62	74.85
Olefin	94.60	80.38
Aromatic	126.11	115.26
Oxygenate	97.90	84.48

Table 30: Octane numbers of the pseudo-components.

	RON	MON
Saturate	89.97	90.56
Olefin	-28.38	-45.82
Aromatic	131.15	99.12
Oxygenate	106.71	91.24

Table 31: Corrected octane numbers of the pseudo-components.

Finally, the corrected octane numbers are weighted by the hydrocarbon class fractions (in Table 29) of the fuel of interest to obtain the predicted octane number. The result and the measurement are reported in the following table.

	RON	MON
Estimated	91.1	82.1
Measured	89.9	82.0

Table 32: Estimated octane numbers compared with the measurements.

As showed by Equation 130, the uncertainty depends on the variance-covariance matrix and on the sensitivities. The variance-covariance matrix is reported in Table 34 and Table 35 while the sensitivities are governed by Equation 131.

	RON	MON
Saturate (%)	52.63	49.47
Olefin (%)	6.91	5.87
Aromatic (%)	22.83	20.86
Oxygenate (%)	8.22	7.10

Table 33: Sensitivities

5.4738E-03	-2.1470E-02	-6.2724E-03	-1.3167E-03
-2.1470E-02	1.1514E-01	2.3462E-02	-2.2847E-03
-6.2724E-03	2.3462E-02	7.7526E-03	6.0008E-04
-1.3167E-03	-2.2847E-03	6.0008E-04	5.9258E-03

Table 34: Variance covariance matrix for the RON

Finally, the variance-covariance matrix and the sensitivities give the standard uncertainty, u. The expanded uncertainty at 95%, U, is obtained by multiplying u by 1.96 [19].

Therefore, for the studied fuel, the RON and the MON are evaluated at 95% being equal to 91.10±1.57 and to 82.12±1.60, respectively.

6.5583E-03	-2.7241E-02	-7.7192E-03	-3.0927E-03
-2.7241E-02	1.7442E-01	2.8304E-02	-8.0773E-04
-7.7192E-03	2.8304E-02	1.1941E-02	-1.9105E-03
-3.0927E-03	-8.0773E-04	-1.9105E-03	2.3562E-02

Table 35: Variance covariance matrix for the MON

	RON	MON
u	0.80	0.82
U	1.57	1.60

Table 36: Standard and expanded uncertainty at 95% of confidence interval

6.3 RESULTS AND DISCUSSION

After having reported the values of the correcting factors, this section presents the precision of the method. Finally, it discusses the uncertainty and the sensitivity of the method.

Analysing the correcting factors enables us to understand the role of each hydrocarbon class while the covariances inform us about the interactions between the hydrocarbon classes. Figures 54 and 55 summarize the correcting factors **K** and their covariances for the RON and the MON models, respectively. The expectancies of the correcting factors, which are required in Equation 124 are also reported on Figures 54 and 55.

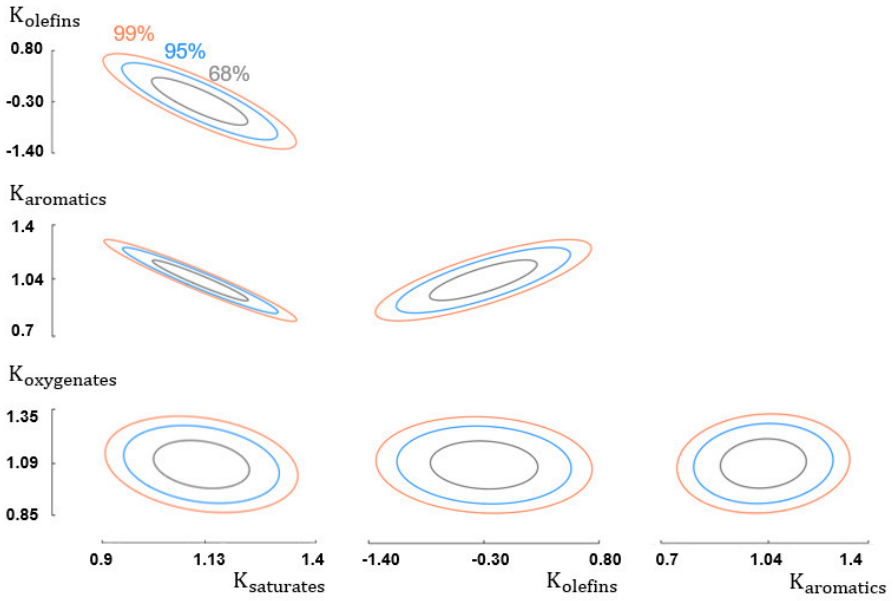

Figure 54: Visual representation of the symmetric variance-covariance matrix of the RON correcting factors. The three variance-covariance error ellipses represent the 99%, 95% and 68% confidence intervals. The ellipses represents the domains where the 20 000 samples of the correcting factors are defined. The directions of the ellipses shows how the correcting factors interact between each others.

The correcting factors of the saturates, the aromatics, and the oxygenates is positive. For the olefins, it can either be positive or negative. Therefore,

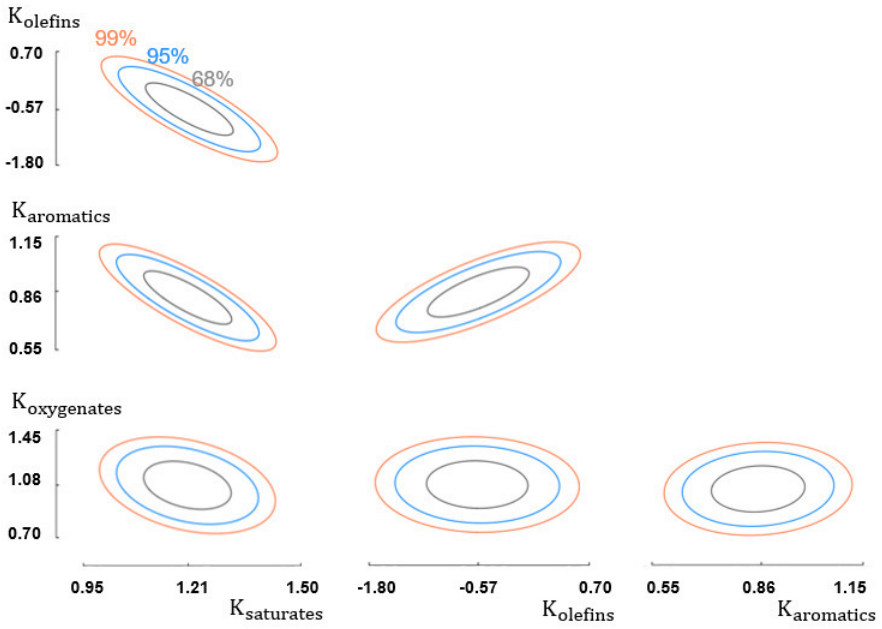

Figure 55: Visual representation of the symmetric variance-covariance matrix of the MON correcting factors. The three variance-covariance error ellipses represent the 99%, 95% and 68% confidence intervals. The ellipses represents the domains where the 20 000 samples of the correcting factors are defined. The directions of the ellipses show how the correcting factors interacts between each others.

the saturates, the aromatics and the oxygenates tend to increase the octane number of the mixture.

The covariances inform us about the interactions between the hydrocarbon classes and the intensity of the covariance, i.e. its slope, shows which interactions are the stronger.

- The oxygenate class exhibits a negligible covariance, so, the oxygenates do not covariate with other classes.
- The saturate class has a negative covariance shared with all the other classes, so, the correcting factors decrease as far as the saturates are concerned. The saturate class counterweights the fuel octane numbers of the other classes. Thus, the saturate class controls the antagonist blending effect [164].
- The covariance between the aromatic and the olefin classes is positive. Thus, an aromatic molecule mixed with an olefin tends to increase the octane numbers. Therefore, the aromatic and the olefin classes control the synergistic blending effect [164].

- The covariance between the aromatic and the olefin with and the saturate class is negative. Thus, the octane number decreases when aromatics and saturates are blended. Therefore, the antagonist blending effect prevails on the synergistic blending effect.
- The covariances are similar between the RON and the MON except for the covariance between the saturates and the aromatics. The dependency between the aromatics and the saturates is higher for the RON. This means that the RON decreases more than the MON when the correcting factor of the saturates increases.

According to Figures 56 and 57, the Bayesian pseudo-component method predicts accurately the octane number for the training and the test fuels, with less than 2% error for all the fuels and less than 1% for most of them. A small bias appear for the RON lower than 88.5. For these values, the RON is slightly over-predicted. The test fuels with a RON lower than 88.5 are the BOB fuels 1 and 2 mixed with 1–butanol. The RON of test fuel BOB 3 mixed with 1–butanol is also over-predicted. Thus, the octane numbers of fuels mixed with 1–butanol tend to be over-predicted. This can be explained by the low octane number of these mixtures, comparing with the other fuels. This difference shows that 1–butanol have a special interaction with gasoline blendstocks. A new model especially fitted for this 1–butanol and similar molecules could be developed after having identified molecules that have the same feature as 1–butanol.

On Figure 56, the new Bayesian PC method is compared with the one reported by Riazi. To lead the calculation, the saturate group was considered as iso-paraffins and the olefins and the oxygenates were neglected. Note that the original PC method would probably give better results without these assumptions while the new model would not be as precise for a different type of fuel than gasoline blendstock for oxygenate blending. The new method gives better results than the original one.

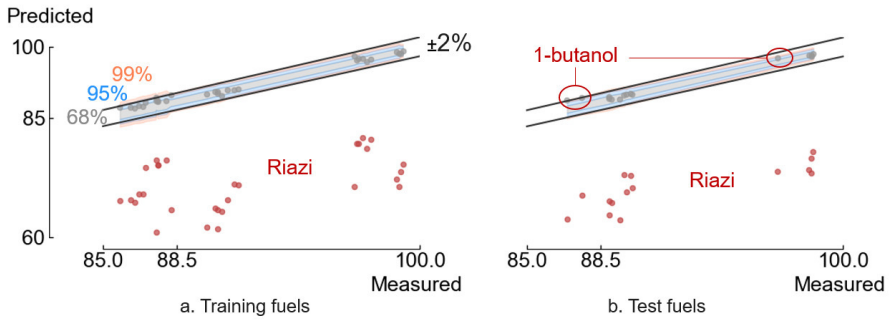

Figure 56: The new Bayesian pseudo-component method gives a very accurate RON prediction for the considered BOB-Ox subpopulation. The 68%, 95% and 99% theoretical confidence intervals are reported as well as a deviation of 2% from the observation. All the points are in accordance with the model uncertainty. The new method is more precise than the original PC method reported by Riazi [8]. Nevertheless, it should be pointed out that the original method was developed for narrow range fractions and for conventional gasoline or naphtas without oxygenates and olefinic compounds. This method may give good results with other fuels while the developed model would not be as precise for a different type of fuel than gasoline blendstock for oxygenate blending.

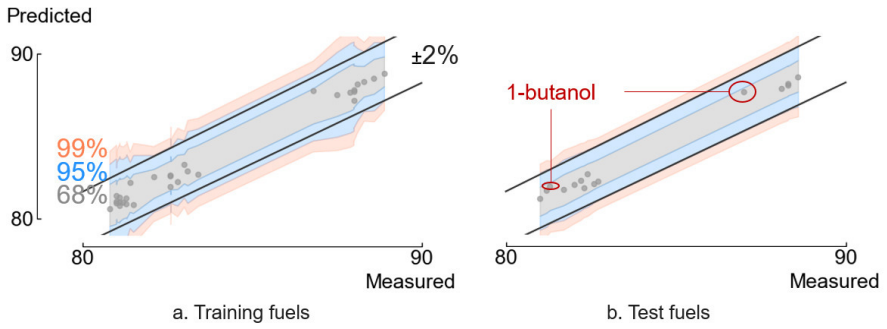

Figure 57: The Bayesian pseudo-component method gives a very accurate MON prediction for the considered BOB-Ox subpopulation. The 68%, 95% and 99% theoretical confidence intervals are reported as well as a deviation of 2% from the observation. All the points are in accordance with the model uncertainty.

Figures 56 and 57 reports also the theoretical uncertainties with a confidence interval of 68%, 95% and 99%. All the experimental points fit within the theoretical model uncertainty. This uncertainty was calculated with the following formula, from the book Evaluation of measurement data — Guide to the expression of uncertainty in measurement [19].

$$u^2 = \mathrm{Var}(\sigma^*) = \sum_{i=1}^{n_{PC}} \left(s_i\right)^2 \mathrm{Var}\left(f_i\right) + 2 \sum_{i=1}^{n_{PC}-1} \sum_{j=i+1}^{n_{PC}} s_i s_j \mathrm{Cov}\left(f_i, f_j\right), \tag{130}$$

where $f_i = f_{K_i|\mathbf{ON}}(K_i|\mathbf{ON})$ is the PDF of the i-the pseudocomponent correcting factor and n_{PC} is the number of pseudo-components.

According to Equation 130, the sensitivities, s_i, indicate which variance of the correcting factor prevails on the combined uncertainty, u.

Owing to Equation 124, the sensitivity for each hydrocarbon class i is given by

$$s_i = \frac{\partial ON^*}{\partial E(K_i)} = y_i ON_{pc_i}. \tag{131}$$

The liquid volume fraction of the fuel hydrocarbon class, y_i, and the octane number of PC i, ON_{pc_i}, govern the sensitivity, s_i. The sensitivities and y_i depend linearly on each others. For instance, the sensitivity $s_{Saturates}$ is the highest because the saturate class constitutes the majority in BOB-Ox fuels (Figure 69). The sensitivity of the saturate group is the highest, so, according to Equation 130, the variance of the correcting factor of the saturates affects the combined uncertainty the most. The sensitivities are sorted in the following ascending order: olefin, oxygenate, aromatic, saturate. Additionally, the octane numbers of the PCs impact this linear trend (Equation 131). Specifically, the octane number of the aromatic pseudo-component is high, thus, it increases the sensitivities of the aromatic class (Figure 69). In contrast, the low octane numbers of the saturate class decreases the sensitivities of the saturate class.

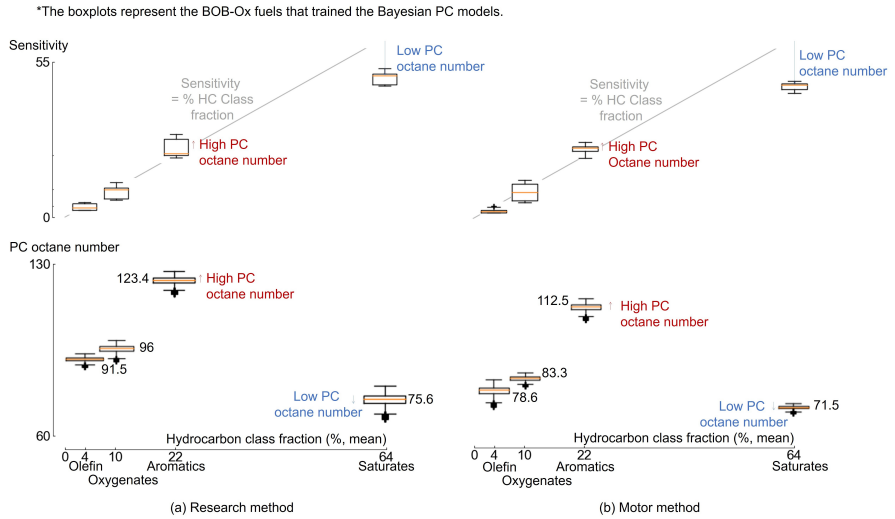

Figure 58: Estimated sensitivities according to the four correcting factors (attributed to Saturates S, Olefins O, Aromatics A and Oxygenates Ox). The estimated octane number is particularly sensitive to the saturate and to the aromatic correcting factors. This is a direct consequence of the higher concentrations of these species, and to the high octane number of the aromatics. The sensitivity is proportional to the hydrocarbon class fraction. This proportionality is impact by the low and the high octane numbers of the PCs.

6.4 CONCLUSION

The current chapter resulted in showing the power of Bayes law to predict the octane numbers.

The method includes an uncertainty quantification and it incorporates the fuel complexity such as the hydrocarbon classes, including olefins and oxygenates, and the types of isomers. Moreover, relying on Bayes' law enabled us to draw the following conclusions for the studied fuels.

- The hydrocarbon class with the higher impact on the uncertainty are sorted in the following ascending order: olefin, oxygenate, aromatic, saturate.
- Compared with the base values of the PCs, of the hydrocarbon classes tend to increase the fuel octane number, except the olefin class.
- The saturate and the aromatic hydrocarbon classes are associated with an antagonist and a synergistic blending effect [164], respectively.

The computational method show that the fuel is governed by high interaction blending effects, particularly when saturates, olefins and aromatics are mixed. These blending effects could be the result of an interaction between the intermediate species playing in the radical pools. This methodology could be used with simple mixtures composed of a reduced number of molecules to identify these kind of interactions and provide information on the chemistry.

The model developed in the current chapter is made to study gasoline blendstock for oxygenated blending mixed with 1–propanol, 2–propanol, 1–butanol, 2–butanol, or 2–methyl–1–propanol (BOB-Ox). The model requires the main hydrocarbon class fractions (Saturate, Olefin, Aromatic, Oxygenate)

and the distillation cut points. It includes the olefin and oxygenate class fractions, so, it is promising for unconventional fuels.

Predicting correctly the octane number is useful to have a rapid insight on a fuel. Nevertheless, it is not a property that enables us to predict how a fuel behave in real conditions. Real conditions during the compression stroke in an engine can be defined by a temperature and pressure profile in time. Under each time step, the auto-ignition delay of a fuel can be defined via its kinetic characteristics. These characteristics depends on the kinetic mechanism which contains the information on the chemical behaviour of the fuel depending on the temperature and pressure. It is noteworthy to remind that the real fuel is not described by its kinetic mechanism due to its complexity. Instead, a surrogate fuel (mixture of 2 to 10 molecules) substitutes the real fuel. The last chapter aims at studying a fuel produced from automotive shredder residues (ASR) in order to define its ignition characteristics and to formulate a surrogate fuel.

7

PREDICTION OF THE OCTANE NUMBERS WITH AN ARTIFICIAL NEURAL NETWORK APPROACH

The content of this chapter will be proposed for publication as: Steven Tipler, Giuseppe D'Alessio, Quentin Van Haute, Francesco Contino, and Axel Coussement. Predicting octane numbers with inexpensive properties relying on principal component analysis and artificial neural network. *To be submitted*

7.1 INTRODUCTION

In the previous chapter, a Bayesian method was developed to predict the research octane number (RON) and the motor octane number (MON) of gasoline blendstocks mixed with an oxygenated molecule. This method has the advantage of being very powerful, in a sense that it can reproduce experimental data very well. Nevertheless, the required input quantities are quite expensive. For instance, this Bayesian method rely on the mean average boiling point (MeABP) and on the saturate, olefin, aromatic, oxygenate (SOAOx) hydrocarbon class fractions. These hydrocarbon class fractions are expensive properties compared to the distillation curve, or to the specific gravity (SG), for example.

In the current chapter, we focus on developing a new octane number predicting method, based on inexpensive input quantities. To proceed, we relied on artificial neural network (ANN) to find the inherent link between the inexpensive properties and the octane numbers of a sample of gasoline blendstocks mixed with an oxygenated molecule. We also apply principal component analysis (PCA) to select an optimal subset of input variables, to work with a reduced number of properties. In the previous chapter, we relied on physical concept to formulate the predicting law. In contrast, we now base our model on machine learning. Then, it will be possible to compare the two methods.

Researchers have already applied ANN to petroleum products. Albahri [116] predicted the octane number of pure molecules based on their chemical composition. Pasadakis [106] applied ANN to predict the RON of gasoline blends from a Greek refinery. To do so, the input data were constituted of the volumetric concentration of the following refinery streams: streams from fluidized catalytic cracking, reforming, isomerization, alkylation, dimersol, butane and Methyl tert-butyl ether (MTBE). Similar work was performed by Doicin et al. [165] to predict the octane numbers of petroleum mixtures. More recently, Ibrahim et al. [166] relied on ANN and PCA to predict the octane numbers based on several chemical features obtained from infrared spectroscopy. Abdul Jameel et al. [109] also predicted the octane numbers based on a chemical analysis, relying for instance on paraffinic CH_3 groups,

paraffinic CH2 groups, paraffinic CH groups, olefinic -CH=CH2 groups, naphthenic CH-CH2 groups, aromatic C-CH groups, and ethanolic OH groups. Kubic et al. [167] estimated the octane numbers of hydrocarbons and oxygenated compounds with an ANN relying on the chemical composition with a group contribution method. vom Lehn et al. [168] also relied on a group contribution method to predict the octane number (ON).

In the available studies from the literature, ANN generally relies on chemical properties, as volume fraction and group contributions, rather than physical properties which tends to be less expensive. Moreover, no prediction models based on inexpensive properties exist for gasoline blendstock mixed with oxygenated molecules. Finally, the methods from the literature predict the ON of pure molecules and of blends of several petroleum fractions, but, no method investigates single petroleum fractions which are not blended.

After having described the method to create the sample of fuels, we list the properties that were investigated. Finally, we detail the PCA and the ANN methods and we conclude with the precision of the created method.

7.2 COMPOSITION OF THE STUDIED FUELS

The studied fuels are gasoline blendstock mixed with an oxygenated molecule. The molecule is one of the following: 1-propanol, 2-propanol, 1-butanol, 2-butanol and 2-methyl-1-propanol. Such alcohol with a high number of carbon atoms can be produced via fermentation or gasification. This type of fuel was studied by Christensen et al. [27]. The studied fuels were simulated, in a sense that their compositions were chosen numerically and their properties were calculated with Aspen Plus and with the available methods from the literature.

Thereafter is explained how the simulated fuels were created.

First, molecules representative of gasoline were selected from the Aspen Plus database. 238 molecules were selected to represent the gasoline blendstock: 9 n-paraffins, 92 iso-paraffins, 83 olefins, 28 naphthenes, 26 aromatics.

Second, the volume fraction of each fuel was calculated. To proceed, the fuel was divided into three layers: the hydrocarbon class (n-paraffin, iso-paraffin, olefin, napthene, aromatic and oxygenate (PIONAOx)), the isomer group, and the mass fraction depending on the carbon number in an isomer group. More information on each layer is described in each of the following paragraphs.

The main hydrocarbon class volume fractions (saturate, olefin, aromatic) were sampled following a latin hypercube sampling (LHS) within the bounds reported in Table 37. These bounds correspond to the Range of applicability of the method developed in the previous chapter to predict the octane numbers of gasoline blendstock mixed with an oxygenated molecule. This range is also the range of applicability of the model developed in the current chapter. Once the saturate, olefin and oxygenate class fractions were sampled, the oxygenate volume fraction was calculated, being 100% subtracted from the sum of the other class fractions. Thereafter, the samples whose oxygenate volume fraction that did not match with the requested bounds (Table 40) were removed. The following approach allowed us to ensure a good distribution of the volume fractions with a small number of samples. We first evaluated by convergence the mean and the standard deviation of the six volume fractions (PIONAOx). From this study, we estimated the minimal number of samples

to reach convergence. Finally, $N_{class}^{Sampling} = 25$ samples were generated in a while loop until reaching the predefined mean and standard deviation.

	S	O	A	Ox
Min	57.3	2.1	16.3	2.9
Max	74.0	7.8	28.9	15.3

Table 37: Limits of the hydrocarbon class fractions of the simulated fuels [27]. For each sample fuel, the oxygenate class is composed of a single molecule among 1-propanol, 2-propanol, 1-butanol, 2-butanol and 2-methyl-propanol. These limits define the ranges where the model can be applied.

Different isomer groups differentiate the molecules with the same molecular weight, but with a different number of methyl substituent. In each hydrocarbon class, a distribution factor defines the percentage of each isomer group. After a convergence study similar to the one realized with the hydrocarbon class layer, $N_{molecule}^{Sampling} = 17$ samples were chosen.

A Gamma distribution drove the molecular weight in each hydrocarbon class, following the method presented by Riazi et al. [8]. The distribution is given by the function:

$$f(x, \alpha, \beta, \eta) = \frac{(x-\eta)^{\alpha-1} e^{-\frac{x-\eta}{\beta}}}{\beta^{\alpha}\Gamma(\alpha)}. \tag{132}$$

Group	η	α		M_{mean}	
		Min	Max	Min	Max
n-paraffin	58	1.5	20	85	115
iso-paraffin	58	1.5	20	82	95
Olefin	70	2.8	10	80	116
Naphthene	70	2	10	80	95
Aromatic	78	2	20	113	128

Table 38: Studied shape and intensity parameters of the gamma function. η is the minimum molecular weight, M_{mean} is the investigated mean molecular weight range and α defines the probability density function shape.

This function requires four input parameters: x, is the molecular weight of a molecule in an hydrocarbon class, the three others, α, β and η, are design parameters that characterize the molecular distribution in each hydrocarbon class. The parameter β can be estimated with the following formula [8]:

$$\beta = \frac{M_{mean} - \eta}{\alpha}. \tag{133}$$

The parameter η is the molecular weight of the lightest molecule in the hydrocarbon class. β depends on the function shape, α, and on the mean molecular weight of the hydrocarbon class, M_{mean}. These two parameters were sampled. Their ranges were defined iteratively with the following procedure.

Sets of 20 parameters were generated iteratively, giving raise to 20 fuels after each iteration. At each iteration corresponds different ranges of mean molecular weight, M_{mean}, and shape parameter, α. For each iteration, the distillation cut points of the 20 fuels were calculated. These cut points

were compared with the experimental distillation cut points published by Christensen et al. [27] (Table 39). This table defines the ranges where the model can be applied. The best correspondence gave the best range of parameters (Table 38). The final sample of fuels was generated with LHS within these ranges. As we did not study the co-variance of the parameters, part of the final fuels did not match with the experimental cut points. These fuels were removed, resulting in $N_{molecule}^{Sampling}$ = 14 out of 20 fuels.

	T5	T10	T30	T50	T70	T90	SL	MeABP
Min	35.85	41.1	58.6	69.9	91.8	163.3	1.21	79.4
Max	62.6	69.8	88.1	103.7	137.25	174.5	1.63	101.5

Table 39: Evaporation characteristics of the studied gasoline blendstocks mixed with an oxygenated molecule [27]. TX refer to the distillation temperature (° C) to get X% evaporated, SL is the 10-90 slope (° C / %v) and MeABP is the mean average boiling point (° C) as defined by Riazi [8]. This table summarizes the ranges where the model can be applied.

The Gamma distribution is continuous over the molecular weight, so, we discretized and integrated the Gamma function depending on the molecular weight of the molecules in the fuel. Moreover, it represents the probability density function of a molecule depending on its molecular weight. Thus, y_k, is given by:

$$y_k = \begin{cases} y_i \frac{r_k}{N_k} \int_{M_k}^{(M_k+M_k^{+1})/2} f(x,\alpha,\beta,\eta)dx \\ \qquad\qquad \text{if } M_k = M_k^{min} \\ y_i \frac{r_k}{N_k} \int_{(M_k+M_k^{-1})/2}^{(M_k+M_k^{+1})/2} f(x,\alpha,\beta,\eta)dx \\ \qquad\qquad \text{if } M_k \in]M_k^{min}; M_k^{max}[\\ y_i \frac{r_k}{N_k} \int_{(M_k+M_k^{-1})/2}^{M_k} f(x,\alpha,\beta,\eta)dx \\ \qquad\qquad \text{if } M_k = M_k^{max}. \end{cases} \tag{134}$$

M_k is the molecular weight of a molecule k. M_k^{-1} and M_k^{+1} are the molecular weights of molecules respectively lighter and heavier than the molecule k. M_k^{min} and M_k^{max} are the minimal and maximal molecular weights in the hydrocarbon class of the molecule k. y_i is the hydrocarbon class volume fraction and r_k is the isomer distribution factor of the molecule k defined in the two previous sections. Several molecules have the same molecular weight in an isomer groups, such as 2-methyl-1-pentene and 4-methyl-1-pentene. Thus, the isomer factor was divided by N_k, which is the number of molecules that shares the same molecular weight with the molecule k in its isomer group.

The number of samples that were simulated is equal to $N_{class}^{Sampling} \times N_{molecule}^{Sampling} \times N_{molecule}^{Sampling} = 5950$.

7.3 PROPERTIES OF THE STUDIED FUELS

The properties of the simulated fuels and their calculation methods were carefully chosen. Fuel properties have been characterized for many years. Then, a lot of calculation methods exist. Among all the available references,

we selected property methods from the *Characterization and Properties of Petroleum Fractions* by Riazi [8], the API *Technical Data Book - Petroleum Refining* [169], and the Peng-Robinson property package from Aspen HYSYS (HYSPR) especially developed for hydrocarbon systems [25]. We investigated the two octane numbers, and 13 thermodynamic, 9 chemical and 7 transport petroleum properties. Some of these 29 properties were calculated with several methods, which results in 41 candidate inputs properties. It is noteworthy that the selected methods are based on a combination of simple properties such as the specific gravity, which is a measure of the density. The selected properties are listed thereafter.

7.3.1 *Thermodynamic properties*

The distillation curve cut points of ASTM D86 at 5, 10, 30, 50, 70 and 90% are the first properties. They were calculated with the HYSYS Peng-Robinson EOS package from Aspen Plus. The MeABP was also calculated and included in the study. The MeABP depends on the distillation cut points and was developed in section 2.5.4.

The critical volume, pressure, temperature, density and compressibility factors were also considered. The following relations were adopted to calculate them from properties that are easily measurable (inexpensive).

The critical volume was calculated with the following formula [8]:

$$V_c = 1.7842 \times 10^{-4} T_b^{2.3829} SG^{-1.683} \tag{135}$$

where V_c is in cm^3/mol and T_b is the MeABP in kelvin. This formula is accurate for lower molecular weights such as gasoline blends.

The critical pressure was calculated with two methods. The first is given by the Riazi-Daubert method:

$$\begin{aligned} Pc = 3.1958 \times 10^5 [\exp(&-8.505 \times 10^{-3} Tb - 4.8014 SG \\ &+5.749 \times 10^{-3} TbSG)] Tb^{4.0844} SG^{4.0846}, \end{aligned} \tag{136}$$

and the second method to calculate the critical pressure is known as the Cavett method:

$$\begin{aligned} \log(P_c) = {} & 1.6675956 + (9.412011 \times 10^{-4})(1.8T_b - 459.67) \\ & -(3.047475 \times 10^{-6})(1.8T_b - 459.67)^2 \\ & -(2.087611 \times 10^{-5})(API)(1.8T_b - 459.67) \\ & +(1.5184103 \times 10^{-9})(1.8T_b - 459.67)^3 \\ & +(1.1047899 \times 10^{-8})(API)(1.8T_b - 459.67)^2 \\ & -(4.8271599 \times 10^{-8})(API^2)(1.8T_b - 459.67) \\ & +(1.3949619 \times 10^{-10})(API^2)(1.8T_b - 459.67)^2. \end{aligned} \tag{137}$$

The critical temperature was calculated also with two methods. The first is the API method[169]:

$$\begin{aligned} T_c = 10.6443 [\exp(&-5.1747 \times 10^{-4} T_b - 0.54444 S + 3.5995 \times 10^{-4} T_b S)] \\ &\times T_b^{0.81067} S^{0.53691}, \end{aligned} \tag{138}$$

and the second is the Cavett method[8]:

$$\begin{aligned} T_c = {} & 426.7062278 + (9.5187183x10^{-1})(1.8Tb - 459.67) \\ & -(6.01889 \times 10^{-4})(1.8T_b - 459.67)^2 \\ & -(4.95625 \times 10^{-3})(API)(1.8Tb - 459.67) \\ & +(2.160588 \times 10^{-7})(1.8Tb - 459.67)^3 \\ & +(2.949718 \times 10^{-6})(API)(1.8T_b - 459.67)^2 \\ & +(1.817311 \times 10^{-8})(API^2)(1.8T_b - 459.67)^2. \end{aligned} \tag{139}$$

The critical density was calculated with:

$$d_c = \frac{M}{V_c} \tag{140}$$

where the critical volume is given by Equation 135. The molecular weight is given by three methods described in the following section dedicated to chemical properties.

The critical compressibility factor is given by the following relation[8]:

$$Z_c = \frac{P_c V_c}{R T_c} \tag{141}$$

with the critical properties calculated with Equations 135, 136 and 138

The acentric factor given by the Lee-Kesler method [8] is also included in the study:

$$\omega = \frac{-\ln(P_c/1.01325) - 5.92714 + 6.09648/T_{br} + 1.28862\ln(T_{br}) - 0.169347T_{br}^6}{15.2518 - 15.6875/T_{br} - 13.4721\ln(T_{br}) + 0.43577T_{br}^6}, \tag{142}$$

with

$$T_{br} = T_b/T_c. \tag{143}$$

The last property of the current section is the Watson K factor:

$$K_w = \frac{(1.8T_b)^{1/3}}{SG} \tag{144}$$

7.3.2 *Chemical properties*

On top of these thermodynamic properties, chemical properties were included. The oxygen-to-carbon and the carbon-to-oxygen ratios, the carbon, hydrogen and oxygen weight ratios were obtained from Aspen Plus by counting the amounts of atoms.

The molecular weight was estimated with three methods. First, the Lee-Kelser method[8]:

$$\begin{aligned} M = {} & -12272.6 + 9486.4SG + (8.3741 - 5.9917SG)T_b \\ & +(1 - 0.77084SG - 0.02058SG^2) \\ & \times(0.7465 - 222.466/Tb)10^7/Tb \\ & +(1 - 0.80882SG + 0.02226SG^2) \\ & \times(0.3228 - 17.335/T_b)10^{12}/T_b^3, \end{aligned} \tag{145}$$

second, the Riazi-Daubert method[8]:

$$M = 1.6607 \times 10^{-4} T_b^{2.1962} SG^{-1.0164}, \tag{146}$$

third, the API method [169]:

$$\begin{aligned} M = {} & 20.486[\exp(1.165 \times 10^{-4} T_b - 7.78712SG \\ & + 1.1582 \times 10^{-3} T_b SG)] T_b^{1.26007} SG^{4.98308}, \end{aligned} \tag{147}$$

Other chemical properties were estimated: the SG, the stoichiometric air-to-fuel ratio, and the aniline point calculated with the API method [169]:

$$AP = -1253.7 - 0.139 MeABP + 107.8 K_w + 868.7 SG, \tag{148}$$

and with the Albahri et al. method [8]:

$$AP = -9805.269 R_i + 711.85761 SG + 9778.7069, \tag{149}$$

with R_i the refractivity intercept defined by:

$$R_i = n - \frac{d}{2} \tag{150}$$

where d and n are respectively the density and the refractive index at 20°C and at 1 atm.

7.3.3 *Transport properties*

Finally, transport properties were included in the study.

The refractive index was calculated with:

$$n = \left(\frac{1 + 2I}{1 - I}\right)^{1/2} \tag{151}$$

where I was calculated with three methods. Firstly with the API method [169]:

$$\begin{aligned} I = {} & 2.266 \times 10^{-2} \exp(3.905 \times 10^{-4} MeABP + 2.468 SG \\ & - 5.704 \times 10^{-4} MeABP\, SG) MeABP^{0.0572} SG^{-0.720}, \end{aligned} \tag{152}$$

secondly with the Riazi-Daubert method [8]:

$$I = 0.3773 T_b^{-0.02269} SG^{0.9182} \tag{153}$$

and last, by the method developed by Riazi and Daubert and included in the API-TDB method [8]:

$$\begin{aligned} I = {} & 2.34348 \times 10^{-2} [\exp(7.029 \times 10^{-4} T_b + 2.468 SG \\ & - 1.0267 \times 10^{-3} T_b SG)] T_b^{0.0572} SG^{-0.720}. \end{aligned} \tag{154}$$

The refractivity intercept, previous defined by Equation 150 was also included.

The m parameter was also considered:

$$m = M(n - 1.475). \tag{155}$$

The liquid and gas thermal conductivity were studied. The liquid thermal conductivity at 20°C was calculated with the API method [169]:

$$k = MeABP^{0.2904} \times (9.961 \times 10^{-3} - 5.364 \times 10^{-6} \times T) \tag{156}$$

and with another method developed by the API group [8]:

$$k = {T_b}^{0.2904} \times (2.551 \times 10^{-2} - 1.982 \times 10^{-5} T) \tag{157}$$

where T and T_b are both in Kelvin.

The gas thermal conductivity was calculated with [8]:

$$k = 1.7307 E (1.8 T_b)^B SG^C \tag{158}$$

with the constants A, B and C defined as:

$$A = \exp(21.87 - 8.07986t + 1.1298t^2 - 0.05309t^3), \tag{159}$$

$$B = -4.13948 + 1.29924t - 0.17813t^2 + 0.00833t^3, \tag{160}$$

$$C = 0.19876 - 0.0312t - 0.00567t^2, \tag{161}$$

and t is a variable such as

$$t = \frac{1.8T - 460}{100}. \tag{162}$$

k is given in W/m.K, and the temperatures T and T_b are in kelvin.

Finally the kinematic viscosity and the viscosity gravity function (VGF) were included in the study. The kinematic viscosity is given by the API method [8]:

$$\begin{aligned}\log(\nu_{38}) =& 4.9371 - 1.94733 K_w + 0.12769 {K_w}^2 \\ &+ 3.2629 \times 10^{-4} API^2 - 1.18246 \times 10^{-2} K_w API \\ &+ \frac{0.171617 {K_w}^2 + 10.9943(API) + 9.50663 \times 10^{-2} (API)^2 - 0.860218 Kw(API)}{API + 50.3642 - 4.78231 K_w}\end{aligned} \tag{163}$$

where API is the API gravity.

The VGF was included, calculated with the following relation:

$$VGF = -1.816 + 3.484 SG - 0.1156 \ln_{38}, \tag{164}$$

with ν_{38} in mm^2/s.

7.3.4 *Octane numbers*

For what concern the octane numbers, the Bayesian pseudo-component (PC) method was adopted. This method was developed in the previous chapter and allowed us to precisely estimate the octane number with an uncertainty lower than 2%.

The predicting law is given by the following formulation:

$$ON^* = [\mathbf{y}]^T \times \left([E(\mathbf{K}) \circ \mathbf{ON_{pc}}] \right) + \sigma^*, \tag{165}$$

with σ^* the random error, i.e. an unpredictable error due to the measurement method, "$\circ$" the Hadamard product and "$\times$" the Cartesian product.

y is the volume fraction of each hydrocarbon class (saturate, olefin, aromatic, oxygenate), $E(\mathbf{K})$ represents a correcting factor which corrects the initial PC method and ON_{pc} are the octane numbers of the PC. More details about these different terms and the calculation method is described in the previous chapter.

7.4 VARIABLE SELECTION AND STRUCTURE OF THE ANN

PCA can be applied to reduce the number of variables (the number of properties in the current study). The main idea behind PCA is to reduce the dimensionality while keeping most information of the initial dataset. Among the 41 studied variables (properties), we selected subgroups of variables relying on PCA to select the principal variables. More information on PCA reduction is available in the literature [136, 170–175]. With PCA, the correlations between the variables are analysed. The idea is to identify the relationship between the variables and to delete redundant information. Mathematically speaking, the distribution of the data is analysed in order to define a new coordinate system where the new directions correspond to the maximal variance. PCA can be separated into 2 steps: 1- centering and scaling, 2- identifying the principal components

First, for multivariate data, i.e., for data with different units, or different range, it is mandatory to center and scale, otherwise the predictive model will not perform well both in the training and testing phase. Centering is done subtracting the mean value, therefore each matrix row can be seen as a fluctuation around the mean. Scaling, is done dividing the centered observation by a factor d_j:

$$\tilde{\mathbf{x}}_j = \frac{(\mathbf{x}_j - \bar{\mathbf{x}}_j)}{d_j}, \tag{166}$$

with d_j the scaling parameter. This scaling parameter depends on the scaling method (Auto scaling, Range scaling, Vast scaling). These scaling methods are accurately described in the literature [136] and in section 3.2.

In the second step, we analyse the covariance matrix as it contains the information of the data. In the current study, we consider a matrix $\mathbf{X}$ of Q variables (Q=41) and n observations (n=5950). With PCA, we project $\mathbf{X}$ onto a rotated basis. This basis is obtained from the eigenvalue decomposition of the covariance matrix:

$$\mathbf{S} = \frac{1}{n-1}\mathbf{X}^T\mathbf{X} = \mathbf{A}\mathbf{L}\mathbf{A}^T, \tag{167}$$

with $\mathbf{A}$ and $\mathbf{L}$ the eigenvectors and eigenvalues of $\mathbf{S}$. From the rotated basis defined by the eigenvectors $\mathbf{A}$, a submatrix $\mathbf{A_q}$ can be extracted. This submatrix is the one whose columns of $\mathbf{A}$ are associated with the largest eigenvalues of $\mathbf{L}$. The original data projected on this basis gives the principal component (PC), $\mathbf{Z_q}$:

$$\mathbf{Z_q} = \mathbf{X}\mathbf{A_q}. \tag{168}$$

An approximate reconstruction of the original dimensional sample can be obtained by inverting Equation 168:

$$\mathbf{X_q} = \mathbf{Z_q}\mathbf{A_q}^T. \tag{169}$$

Then, the retrieved variance compared with the original one can be assessed in terms of a percentage. The retain eigen values ($\lambda_{i=1\ldots q}$) are the biggest while the smallest are deleted ($\lambda_{i=q+1\ldots Q}$) so that the explained variance with q eigen vectors can be defined as:

$$v_q = \frac{\sum_{i=1}^{q}\lambda_i}{\sum_{j=1}^{Q}\lambda_j} \tag{170}$$

To compare the four scaling methods, the dimensionality was based on 8 eigen vectors because they allowed us to explain more than 99% of the variance with the four scaling methods. The number of variables was reduced to 10, 15 and 20 to compare the performance of the ANN with each of these number of variables. It is noteworthy that the Vast method is particularly interesting compared to the other methods because it allows us to reduce the dimensionality even more, with only 4 eigen vectors. This Vast scaling method will be studied apart from the others to test the ANN with the lower dimensions as possible, i.e. 5 properties.

Two variable selection methods were compared: the Procrustes and the B2 methods. The first method is particularly well suited to do a regression such as the creation of an ANN.

The variable selection methods (B2 and Procrustes) are described in section 3.2 and these methods are discussed in [171, 172, 175]. We predefined the number of variables to 10, 15 and 20.

The ANN relates the ON with the inexpensive properties included in the study. More information on the structure of ANN is detailed in Section 3.3. The activation function used are the standard matlab activation functions: sigmoid for the hidden layer, and linear for the last layer. A convergence study was done to determine the size of the hidden layer, starting with 10 and with up to 300 artificial neurons. The scheme of the ANN is drawn on Figure 59. It consists of one input layer, one hidden layer and one output layer, each being composed of a variable number of nodes, 42, 20, 15, 10 (up to 5 for the VAST method) for the input layer and from 10 to 300 for the hidden layer. The output layer is only composed of the two ON. Over the 5950 samples, 70% train the model, 15% are used for validation and 15% for testing.

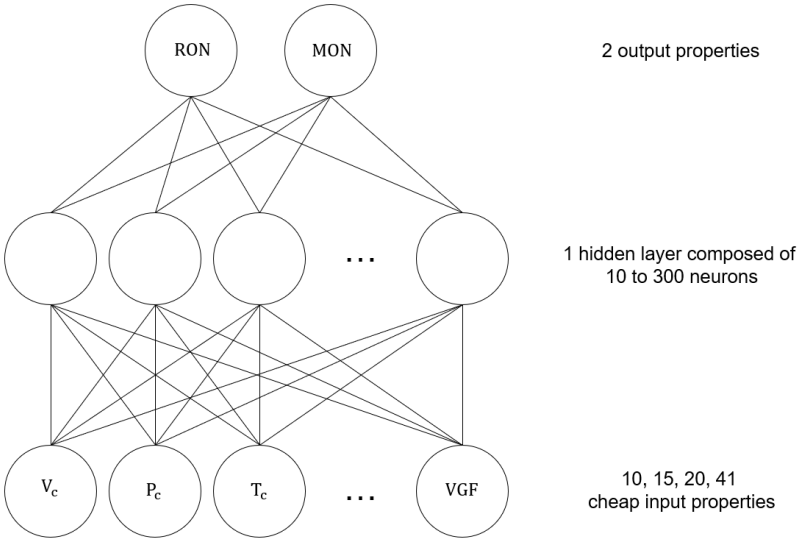

Figure 59: Scheme of the artificial neural network.

7.5 RESULTS

In this section, the different methods are compared. First, the variable selection methods are compared: Procrustes VS B2. Second, the scaling methods are compared: Auto VS Range VS Vast. Third, the size of the hidden layer is discussed. Then, the selected variables are compared with

the best methods and the mean squared error (MSE) obtained with the Vast method and 4 eigen vectors are discussed. Finally, this ANN method is compared with the the Bayesian PC method.

First, the Procrustes and the B2 methods are compared. A selection method has to be selected to do this comparison. We select the Auto method for two reasons showed by the results below: 1- this method allowed us to reach a low MSE, 2- conversely with other methods, the MSE does not fluctuate a lot when the size of the hidden layer increases. The Procrustes and the B2 methods are compared on Figures 60 and 61. The B2 and the Procrustes methods give similar performance. Nevertheless, the fluctuations tend to be higher for the B2 method. Thus, the studies in the current section were done relying on the Procrustes method.

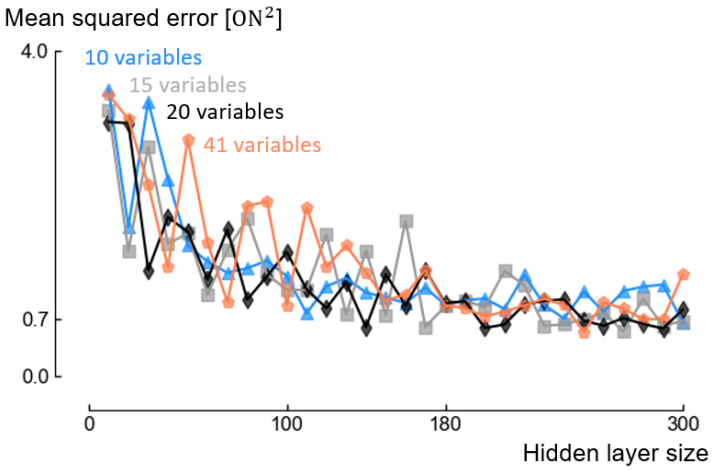

Figure 60: MSE with the Procrustes and the Auto methods. The MSE decreases with the size of the hidden layer. Moreover, the MSE is not impacted when the number of selected variables decreases. Therefore, the Procrustes selection method is appropriate.

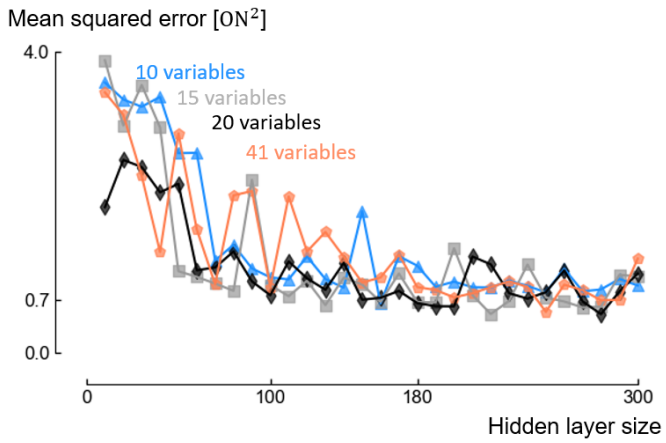

Figure 61: MSE with the B2 and the Auto methods. The MSE decreases with the size of the hidden layer. Moreover, the MSE increases when the number of selected variable decreases. Therefore, the variable selection method B2 is not appropriate.

Second, the scaling methods are compared while the Procrustes method is active. As the variable selection method was previously selected, this com-

parison is done with the lower number of variables, i.e. 10. It is noteworthy that the mean squared error fluctuates with the Vast method. Therefore, the Auto and the Range method are the better to predict the ON.

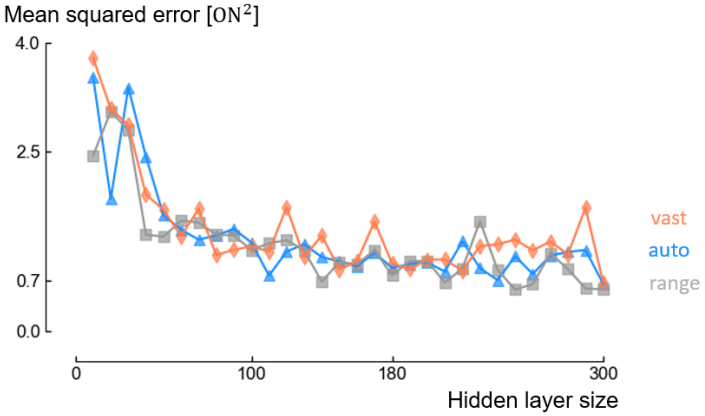

Figure 62: Comparison of the scaling methods.

As showed on Figures 60, 61 and 62, the convergence is reached with at least 100 neurons in the hidden layers. Nevertheless, a high variation is still present with up to 180. Thus, 180 neurons is appropriate.

Then, we compare the selected properties with the best set of methods: Procrustes with the Auto method, and Procrustes with the Range method. The properties shared by the two sets of properties are important. They are the following ones: the temperature at which 10% of the fuel is evaporated, the oxygen weight fraction, the Watson K factor. The carbon ratio is also an important property as it appears in the CH weight fraction and in the OC weight fraction.

Variable selection	Procrustes	Procrustes
Scaling	Auto	Range
Property	T10%	T10%
	O%	T70%
	n (Eq. 151 and 153)	H%
	k (Eq. 157)	O%
	CH%	k (Eq. 158)
	MW (Eq. 147)	OC%
	SG	AP (Eq. 148)
	K_w	K_w
	P_c (Eq. 136)	T_c (Eq. 139)
	Z_c	d_c (Eq. 140 and 147)

Table 40: 10 principal properties with the combination of the best methods.

The correlations between the 10 principal properties obtained with the two best methods are discussed thanks to the analysis of the covariance matrix of the scaled variables. These covariance matrices are represented in Figures 63 and 64. From these figures, we can see that some of the properties listed in Table 40 are correlated within the methods. It shows that similar information are carried by some properties which are not shared between the method.

This is for instance the case for the following properties when the scaling is done with the auto method:

- the hydrogen fraction (range method) and the CH ratio (auto method).

- the oxygen fraction (auto method) and the OC ratio (range method).
- the refractive index (auto method) with d_c (range method).
- k (auto method) with T_c (range method).
- Z_c (auto method) with T_c (range method).

	T10%	T70%	H%	O%	n (Eq. 149 and 151)	k (Eq. 155)	k (Eq. 156)	OC%	CH%	MW (Eq. 145)	SG	AP (Eq. 146)	Kw	Pc (Eq. 134)	Tc (Eq. 137)	dc (Eq. 138 and 145)	Zc
T10%	1.00E+00	4.17E-01	-2.71E-01	9.53E-02	5.24E-01	8.55E-01	-7.73E-01	9.38E-02	-2.12E-01	8.50E-01	5.43E-01	1.17E-01	-1.82E-01	-5.80E-01	8.41E-01	1.93E-01	-8.30E-01
T70%	4.17E-01	1.00E+00	-3.75E-01	-1.56E-01	4.69E-01	7.84E-01	-6.93E-01	-1.59E-01	-4.17E-01	7.82E-01	4.86E-01	1.21E-01	-1.53E-01	-5.43E-01	7.69E-01	1.64E-01	-7.63E-01
H%	-2.71E-01	-3.75E-01	1.00E+00	-6.19E-02	-8.62E-01	-3.68E-01	2.56E-01	-5.39E-02	9.06E-01	-3.03E-01	-8.57E-01	7.42E-01	8.62E-01	-3.31E-01	-5.14E-01	-8.66E-01	1.74E-01
O%	9.53E-02	-1.56E-01	-6.19E-02	1.00E+00	1.74E-01	2.07E-02	1.74E-02	1.00E+00	3.67E-01	4.04E-03	1.71E-01	-1.94E-01	-2.01E-01	1.33E-01	5.94E-02	2.00E-01	2.30E-02
n (Eq. 149 and 151)	5.24E-01	4.69E-01	-8.62E-01	1.74E-01	1.00E+00	6.04E-01	-4.73E-01	1.68E-01	-7.30E-01	5.37E-01	1.00E+00	-6.99E-01	-9.03E-01	1.64E-01	7.45E-01	9.08E-01	-4.06E-01
k (Eq. 155)	8.55E-01	7.84E-01	-3.68E-01	2.07E-02	6.04E-01	1.00E+00	-8.96E-01	1.78E-02	-3.35E-01	9.96E-01	6.26E-01	1.48E-01	-2.02E-01	-6.87E-01	9.82E-01	2.15E-01	-9.73E-01
k (Eq. 156)	-7.73E-01	-6.93E-01	2.56E-01	1.74E-02	-4.73E-01	-8.96E-01	1.00E+00	1.91E-02	2.46E-01	-8.90E-01	-4.94E-01	-2.14E-01	9.90E-02	6.81E-01	-8.59E-01	-1.10E-01	8.81E-01
OC%	9.38E-02	-1.59E-01	-5.39E-02	1.00E+00	1.68E-01	1.78E-02	1.91E-02	1.00E+00	3.74E-01	1.59E-03	1.65E-01	-1.89E-01	-1.95E-01	1.31E-01	5.54E-02	1.93E-01	2.45E-02
CH%	-2.12E-01	-4.17E-01	9.06E-01	3.67E-01	-7.30E-01	-3.35E-01	2.46E-01	3.74E-01	1.00E+00	-2.81E-01	-7.26E-01	6.09E-01	7.18E-01	-2.51E-01	-4.55E-01	-7.22E-01	1.73E-01
MW (Eq. 145)	8.50E-01	7.82E-01	-3.03E-01	4.04E-03	5.37E-01	9.96E-01	-8.90E-01	1.59E-03	-2.81E-01	1.00E+00	5.60E-01	2.27E-01	-1.22E-01	-7.43E-01	9.63E-01	1.36E-01	-9.88E-01
SG	5.43E-01	4.86E-01	-8.57E-01	1.71E-01	1.00E+00	6.26E-01	-4.94E-01	1.65E-01	-7.26E-01	5.60E-01	1.00E+00	-6.79E-01	-8.90E-01	1.37E-01	7.63E-01	8.96E-01	-4.31E-01
AP (Eq. 146)	1.17E-01	1.21E-01	7.42E-01	-1.94E-01	-6.99E-01	1.48E-01	-2.14E-01	-1.89E-01	6.09E-01	2.27E-01	-6.79E-01	1.00E+00	9.39E-01	-8.20E-01	-4.34E-02	-9.34E-01	-3.69E-01
Kw	-1.82E-01	-1.53E-01	8.62E-01	-2.01E-01	-9.03E-01	-2.02E-01	9.90E-02	-1.95E-01	7.18E-01	-1.22E-01	-8.90E-01	9.39E-01	1.00E+00	-5.73E-01	-3.85E-01	-1.00E+00	-2.69E-02
Pc (Eq. 134)	-5.80E-01	-5.43E-01	-3.31E-01	1.33E-01	1.64E-01	-6.87E-01	6.81E-01	1.31E-01	-2.51E-01	-7.43E-01	1.37E-01	-8.20E-01	-5.73E-01	1.00E+00	-5.36E-01	5.61E-01	8.34E-01
Tc (Eq. 137)	8.41E-01	7.69E-01	-5.14E-01	5.94E-02	7.45E-01	9.82E-01	-8.59E-01	5.54E-02	-4.55E-01	9.63E-01	7.63E-01	-4.34E-02	-3.85E-01	-5.36E-01	1.00E+00	3.97E-01	-9.12E-01
dc (Eq. 138 and 145)	1.93E-01	1.64E-01	-8.66E-01	2.00E-01	9.08E-01	2.15E-01	-1.10E-01	1.93E-01	-7.22E-01	1.36E-01	8.96E-01	-9.34E-01	-1.00E+00	5.61E-01	3.97E-01	1.00E+00	1.26E-02
Zc	-8.30E-01	-7.63E-01	1.74E-01	2.30E-02	-4.06E-01	-9.73E-01	8.81E-01	2.45E-02	1.73E-01	-9.88E-01	-4.31E-01	-3.69E-01	-2.69E-02	8.34E-01	-9.12E-01	1.26E-02	1.00E+00

Figure 63: Covariance matrices obtained with all the scaled variables (with the auto method). Only the properties listed from Table 40 are reported. Green refer to high positive correlation (higher than the threshold 0.90. Red refer to high negative correlation (lower than the threshold -0.9), yellow refer to correlations equal to 1 or -1.

A similar study was done for the range method. The higher correlations are find between:

- the hydrogen fraction (range method) with the CH ratio (auto method), the aniline point (range method), the Watson factor (auto and range methods) and d_c (range method).
- the oxygen fraction (auto method) and the OC ratio (range method).
- the aniline point (range method) with the Watson factor (auto and range methods) and d_c (range method).

	T10%	T70%	H%	O%	n (Eq. 149 and 151)	k (Eq. 155)	k (Eq. 156)	OC%	CH%	MW (Eq. 145)	SG	AP (Eq. 146)	Kw	Pc (Eq. 134)	Tc (Eq. 137)	dc (Eq. 138 and 145)	Zc
T10%	3.86E-02	1.73E-02	-1.08E-02	5.26E-03	1.69E-02	2.75E-02	-2.64E-02	5.18E-03	-8.81E-03	2.68E-02	1.75E-02	4.60E-03	-6.64E-03	-1.89E-02	2.71E-02	7.00E-03	-2.58E-02
T70%	1.73E-02	4.46E-02	-1.61E-02	-9.24E-03	1.63E-02	2.71E-02	-2.55E-02	-9.46E-03	-1.86E-02	2.65E-02	1.68E-02	5.11E-03	-6.00E-03	-1.90E-02	2.67E-02	6.37E-03	-2.55E-02
H%	-1.08E-02	-1.61E-02	4.13E-02	-3.53E-03	-2.88E-02	-1.22E-02	9.05E-03	-3.08E-03	3.89E-02	-9.87E-03	-2.85E-02	3.02E-02	3.25E-02	-1.11E-02	-1.72E-02	-3.24E-02	5.60E-03
O%	5.26E-03	-9.24E-03	-3.53E-03	7.89E-02	8.03E-03	9.50E-04	8.51E-04	7.89E-02	2.18E-02	1.82E-04	7.87E-03	-1.09E-02	-1.05E-02	6.18E-03	2.74E-03	1.03E-02	1.02E-03
n (Eq. 149 and 151)	1.69E-02	1.63E-02	-2.88E-02	8.03E-03	2.69E-02	1.62E-02	-1.35E-02	7.73E-03	-2.53E-02	1.41E-02	2.68E-02	-2.30E-02	-2.75E-02	4.46E-03	2.01E-02	2.74E-02	-1.05E-02
k (Eq. 155)	2.75E-02	2.71E-02	-1.22E-02	9.50E-04	1.62E-02	2.67E-02	-2.55E-02	8.17E-04	-1.16E-02	2.61E-02	1.67E-02	4.84E-03	-6.11E-03	-1.86E-02	2.64E-02	6.49E-03	-2.51E-02
k (Eq. 156)	-2.64E-02	-2.55E-02	9.05E-03	8.51E-04	-1.35E-02	-2.55E-02	3.03E-02	9.34E-04	9.05E-03	-2.48E-02	-1.41E-02	-7.46E-03	3.20E-03	1.96E-02	-2.46E-02	-3.54E-03	2.42E-02
OC%	5.18E-03	-9.46E-03	-3.08E-03	7.89E-02	7.73E-03	8.17E-04	9.34E-04	7.89E-02	2.22E-02	7.15E-05	7.57E-03	-1.06E-02	-1.02E-02	6.07E-03	2.56E-03	1.00E-02	1.09E-03
CH%	-8.81E-03	-1.86E-02	3.89E-02	2.18E-02	-2.53E-02	-1.16E-02	9.05E-03	2.22E-02	4.47E-02	-9.53E-03	-2.51E-02	2.58E-02	2.82E-02	-8.80E-03	-1.58E-02	-2.81E-02	5.77E-03
MW (Eq. 145)	2.68E-02	2.65E-02	-9.87E-03	1.82E-04	1.41E-02	2.61E-02	-2.48E-02	7.15E-05	-9.53E-03	2.57E-02	1.47E-02	7.28E-03	-3.61E-03	-1.97E-02	2.53E-02	4.02E-03	-2.50E-02
SG	1.75E-02	1.68E-02	-2.85E-02	7.87E-03	2.68E-02	1.67E-02	-1.41E-02	7.57E-03	-2.51E-02	1.47E-02	2.68E-02	-2.23E-02	-2.70E-02	3.70E-03	2.05E-02	2.70E-02	-1.12E-02
AP (Eq. 146)	4.60E-03	5.11E-03	3.02E-02	-1.09E-02	-2.30E-02	4.84E-03	-7.46E-03	-1.06E-02	2.58E-02	7.28E-03	-2.23E-02	4.01E-02	3.49E-02	-2.72E-02	-1.43E-03	-3.45E-02	-1.17E-02
Kw	-6.64E-03	-6.00E-03	3.25E-02	-1.05E-02	-2.75E-02	-6.11E-03	3.20E-03	-1.02E-02	2.82E-02	-3.61E-03	-2.70E-02	3.49E-02	3.44E-02	-1.76E-02	-1.17E-02	-3.42E-02	-7.89E-04
Pc (Eq. 134)	-1.89E-02	-1.90E-02	-1.11E-02	6.18E-03	4.46E-03	-1.86E-02	1.96E-02	6.07E-03	-8.80E-03	-1.97E-02	3.70E-03	-2.72E-02	-1.76E-02	2.74E-02	-1.46E-02	1.71E-02	2.18E-02
Tc (Eq. 137)	2.71E-02	2.67E-02	-1.72E-02	2.74E-03	2.01E-02	2.64E-02	-2.46E-02	2.56E-03	-1.58E-02	2.53E-02	2.05E-02	-1.43E-03	-1.17E-02	-1.46E-02	2.70E-02	1.20E-02	-2.37E-02
dc (Eq. 138 and 145)	7.00E-03	6.37E-03	-3.24E-02	1.03E-02	2.74E-02	6.49E-03	-3.54E-03	1.00E-02	-2.81E-02	4.02E-03	2.70E-02	-3.45E-02	-3.42E-02	1.71E-02	1.20E-02	3.40E-02	3.67E-04
Zc	-2.58E-02	-2.55E-02	5.60E-03	1.02E-03	-1.05E-02	-2.51E-02	2.42E-02	1.09E-03	5.77E-03	-2.50E-02	-1.12E-02	-1.17E-02	-7.89E-04	2.18E-02	-2.37E-02	3.67E-04	2.50E-02

Figure 64: Covariance matrices obtained with all the scaled variables (with the range method). Only the properties listed from Table 40 are reported. Green refer to high positive correlation (higher than the threshold 0.028. Red refer to high negative correlation (lower than the threshold -0.028).

The Vast method is discussed alone as it is the only scaling method that enables to explain 99% of the variance with only 4 eigen vectors. Unfortunately, the Vast method has a low prediction capability when the number of properties is decreased up to the maximum, i.e. 5 properties (Figure 65).

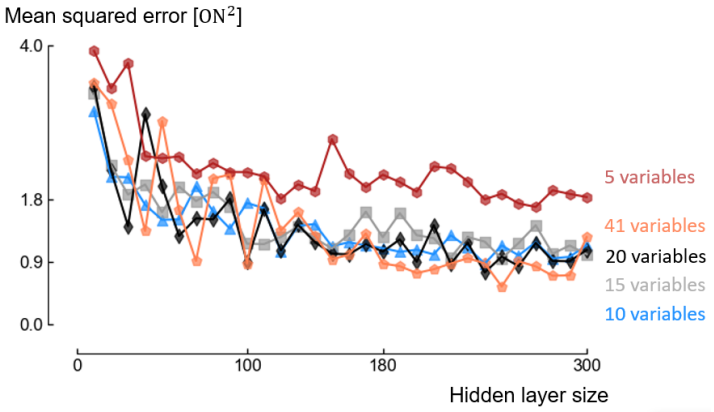

Figure 65: MSE with the Procrustes and the Vast methods with the principal variables selected based on 4 eigen vectors. The MSE decreases with the size of the hidden layer. Moreover, the MSE decreases when only 5 properties are considered. Therefore, the Procrustes selection method is not able to reduce the number of variables to 5.

The estimated octane numbers are plotted against the target octane numbers for the combination of the best methods on Figures 66 and 67. Thanks to this graph, the quality can be assessed by observing the spread over the x=y line. Most of the points reach a precision lower than 2%. The prediction tends to be over-estimated for the low octane numbers and slightly under-estimated for the high octane numbers.

Finally, we compared the method coupling PCA and ANN with the Bayesian PC method. The Bayesian PC method is more precise, with less than 2% of error while some points have more than 2% with the ANN method. Finally, we did a principal component analysis including the hydrocarbon fractions to the 43 previous properties to investigate if relying on PCA captures the physics and retrieve these parameters as principal variables. The results are summarized in Tables 41 and 42. The range method is better at retrieving the physical aspect of the Bayesian PC method. For instance, three properties are retrieved with 9 principal variables against one only for the auto method.

Variable selection	Procrustes
Scaling	Range
9 principal variables	O, A, Ox
15 principal variables	O, A, Ox, MeABP
28 principal variables	S, O, A, Ox, MeABP

Table 41: Number of variables required to retrieve the properties (Saturate S, Olefin O, Aromatic A, Oxygenate Ox, mean average boiling point MeABP) of the Bayesian PC method with the range scaling method.

Variable selection	Procrustes
Scaling	auto
9 principal variables	A
11 principal variables	O, A
17 principal variables	O, A, MeABP
24 principal variables	O, A, Ox, MeABP
35 principal variables	S, O, A, Ox, MeABP

Table 42: Number of variables required to retrieve the properties (Saturate S, Olefin O, Aromatic A, Oxygenate Ox, mean average boiling point MeABP) of the Bayesian PC method with the auto scaling method.

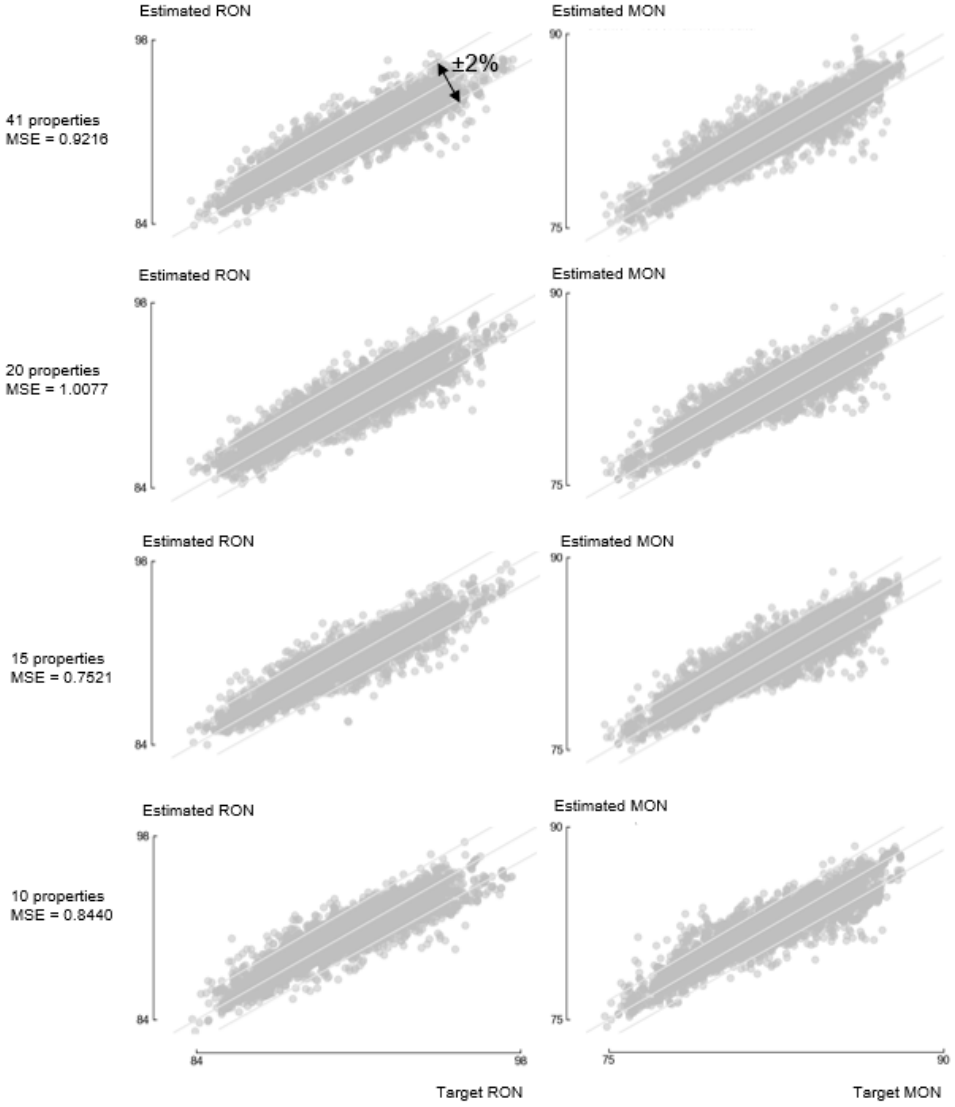

Figure 66: Estimated VS target octane numbers with the Procrustes variable selection method and the Auto scaling method.

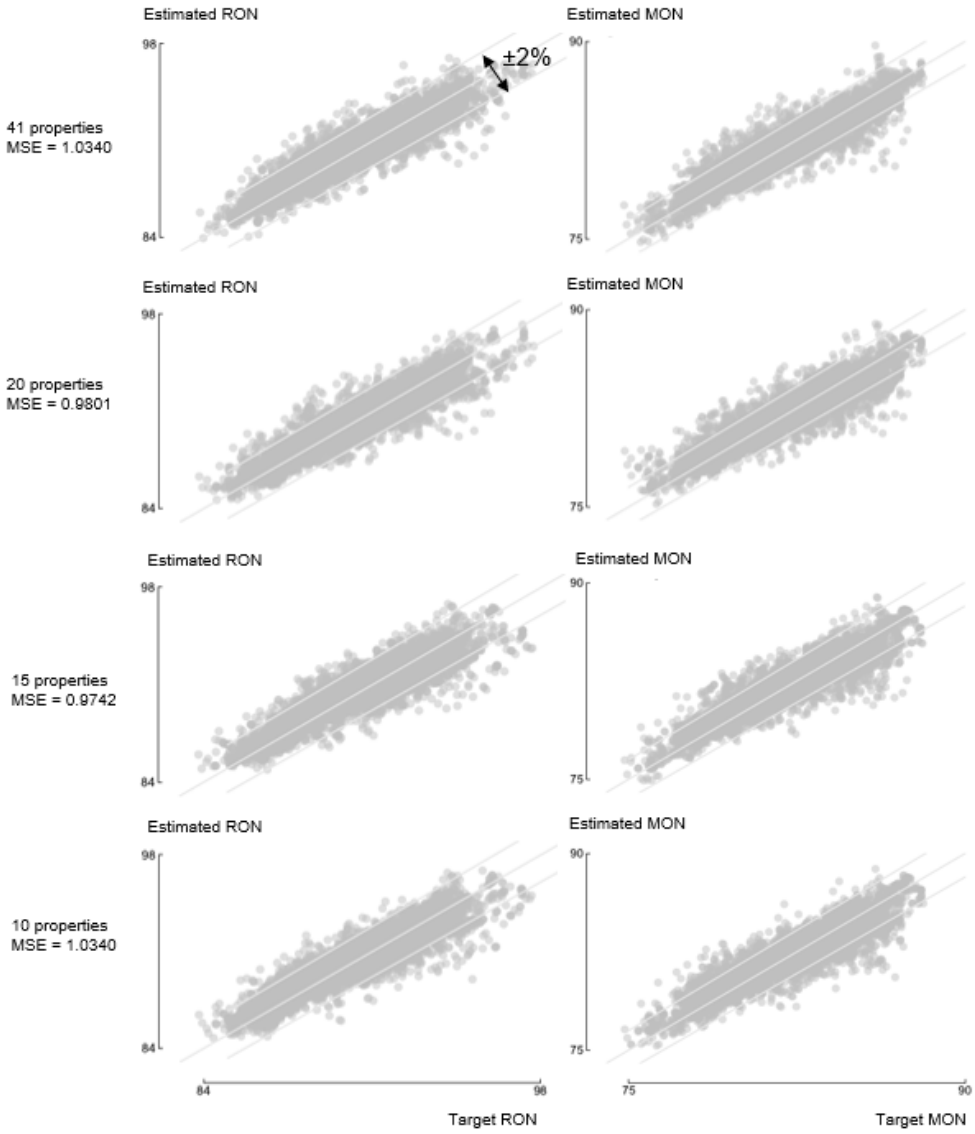

Figure 67: Estimated VS target octane numbers with the Procrustes variable selection method and the Range scaling method.

7.6 CONCLUSION

In the current chapter, a prediction method based on ANN was developed to predict the octane numbers of gasoline blendstocks mixed with a alcohol among 1-propanol, 2-propanol, 1-butanol, 2-butanol and 2-methyl-1-propanol. This kind of heavy alcohol can be produced via fermentation or gasification. The number of input properties was studied, from 10 to 41, with a selection method driven by PCA. A large number of properties were investigated, so, with the results that were collected, the properties useful for ON prediction were identified. It was showed that the number of input properties is not correlated with the size of the hidden layer. Hidden layers of the same size allowed us to reach similar results whatever is the number of input properties. Additionally, as long as the size of the hidden layer of the ANN is big enough, 10 properties predict the octane number accurately.

The 10 properties were calculated only based on the distillation curve, on the atomic content and on the specific gravity.

A new feature from the applied methodology is the usage of PCA to study the principal variables in a fuel blend. This kind of study could be done with the chemical data of fuels obtained with advanced analytical methods such as nuclear magnetic resonance (NMR) or comprehensive two dimensional gas chromatography (GC $\times$ GC).

The current methodology is only applicable for a given type of fuel: a gasoline blendstock mixed with an oxygenated molecule. As prospects, it would be interesting to compare the required properties for ON prediction with another type of fuel. Moreover, an experimental campaign with a large number of fuel would be useful to provide data to validate the current methodology.

8 PREDICTION OF THE AUTO-IGNITION

Part of the content of this chapter has been published in the following scientific article:

S. Tipler, C. S. Mergulhaõ, G. Vanhove, Q. Van Haute, F. Contino, and A. Coussement. Ignition study of an oxygenated and high-alkene light petroleum fraction produced from automotive shredder residues. *Energy and Fuels*, 33(6):5664–5672, 2019

8.1 INTRODUCTION

In the previous two chapters, we predicted the octane number (ON)s. They give important information on the fuel reactivity. Nevertheless, these properties are measured under specific conditions while it would be useful to be able to obtain some ignition characteristics for different conditions. These results could be obtained by the mean of simulations. This would allow us to study if the light fraction from automotive shredder residues (ASR) would not react during the compression stroke under reactivity controlled compression ignition (RCCI) conditions. In fact, as discussed in sections 1.2 and 1.6, ASR fuels coupled with RCCI are an answer to mitigate the environmental impact of fuels produced from ASR.

To do simulations under RCCI conditions, the real fuel must be substituted by a surrogate fuel due to the complexity of the real fuel. Knowing the octane numbers to run a RCCI engine is relevant as the reactivity of the light fraction has to be low enough to ensure that knock does not occur before the heavy fraction injection. Thus, formulating a surrogate fuel for the light fraction requires the knowledge of the octane numbers, as explained in section 2.6.4. Nevertheless, a small quantity of fuel is available, so, the octane numbers cannot be measured.

We propose an alternative which stems from the work from Mehl et al. who related the octane numbers with the ignition delay time (IDT)[176]. Similarly, we propose a new method where the IDTs substitutes the octane numbers as target properties. Thus, the method can be applied if the research octane number (RON), the motor octane number (MON) are unknown.

In this chapter, the work aims at gathering experimental data to later formulate a surrogate, together with addressing the lack of information regarding the reactivity of fuels produced from ASR, which are still uncharted. RCCI-like conditions were investigated in a rapid compression machine (RCM) to measure IDTs, defined as the measured time between the top dead center (TDC) and the maximum pressure derivative value. Studying the auto-ignition delay time of the light-fraction in a RCM is the way to check if the fuel would not ignite before the injection of the high-reactivity fuel for a

specific set of operating conditions. After having described the methodology to characterize the light fraction derived from ASR, its autoignition will be discussed with respect to the temperature and the pressure at TDC to point out the usual and atypical aspects of its ignition characteristics.

This first study will be used as a baseline for formulating a surrogate fuel to perform numerical investigations and is a step forward the reduction of pollutant emissions from waste-derived fuels via advanced combustion modes.

8.2 EXPERIMENTAL SECTION

8.2.1 *Fuel characterization*

Fuel classification is important because similar fuels tend to show similar characteristics while their differences explain their properties and specificities. The studied fuel is known as a light fraction but its composition depends on the raw matter and on the production parameters. The distillation curve was measured according to the ASTM International standards D86 to compare it to the typical classes of fuels: gasoline, naphtha, kerosene or diesel.

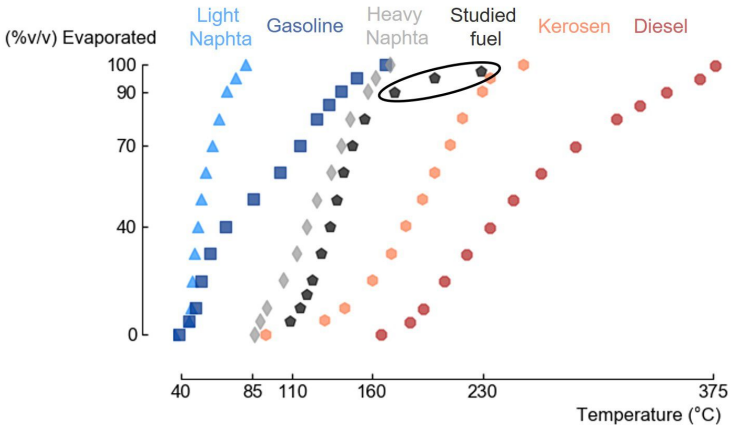

Figure 68: Typical atmospheric distillation ranges of distillation fractions according to the ASTM International D86. The studied fuel is comparable to a heavy naphtha, except for the last 10 volume percent. The distillation curves of the different classes of fuels were published by Chang et al. [13, 14]

The distillation profile almost coincides with the one of a heavy naphtha (see Figure 68), except for the 10 last volume fractions where higher temperatures are required to reach the same evaporation extent. Therefore, the molecules are expected to be longer and more saturated than in a conventional gasoline.

The ONs (RON, ASTM D2699 and MON, ASTM D2700) are important parameters that denote the resistance of a fuel towards end-gas autoignition. They provide information on the fuel reactivity under two conditions and are often used as target properties to formulate a surrogate fuel [30, 85, 86]. ASTM D2699 and D2700 rely on a certified engine but a low volume of fuel was available so it was not possible to measure the octane numbers. Correlations to predict the octane rating from ignition delay times exist [95, 97, 113] but they have never been tested within the ranges of the ASR fuel chemical fraction and could not be applied in the case of this type of

fuel which shows long molecules and high concentrations of olefin, alcohols, ketones and other oxygenates. Therefore these correlations would have lead to an approximated octane index without the knowledge of a confidence interval.

From a kinetic point of view, the difference between the RON and the MON, usually known as the sensitivity, can be assumed to be correlated with the difference in reactivity in the low-temperature and intermediate-temperature ranges [177]. However, comparing measurements of ignition delays with octane number is not straightforward, even though correlations exist [178].

The separation between both these temperature domains is usually associated with the negative temperature coefficient (NTC) behaviour, where the global reactivity towards autoignition decreases as the compressed temperature increases. It is widely accepted that at low temperatures, the reactivity is dominated by chain-branching pathways relying on the addition of O_2 to radicals formed from the parent fuel molecules. In the NTC temperature range, these pathways compete with non-chain branching pathways forming unsaturated species (i.e. an alkene if the fuel is an alkane) [177, 179–181]. The intensity of the NTC, i.e. the slope of the ignition delay according to the compressed temperature under intermediate temperature, is of crucial importance to predict the behaviour of one the light fraction [182]. For this reason, we focused on this temperature region to formulate a surrogate fuel for the light fraction derived from ASR.

The ASR fuel was analyzed at Ghent University with comprehensive two dimensional gas chromatography (GC × GC) coupled with a flame ionization detector and a time of flight-mass spectrometry to obtain the n-paraffin, iso-paraffin, olefin, napthene, aromatic and oxygenate (PIONAOx) distribution [11, 87, 156] (Table 43). The signal of ketones and aromatics overlapped, so a correction was applied to revise the overestimated aromatics and underestimated oxygenates [87]. Other hydrocarbon types identified in minor quantities, namely naphthenaromatics, nitrogenates, diaromatics and sulfurates, have been neglected in the present work. The whole composition is available in Appendix A. The GC × GC revealed only 16.5% of paraffins (normal and iso) in the fuel, where usually, paraffins account for more than 35%. The mean number of carbon atoms was nine for all the groups (C9), except the aromatics (C8) and the oxygenates (C6), whereas gasoline usually exhibit from C7 to C8 molecules. It is noteworthy that the gasoline provided by Haltermann and studied by Lee et al. has a similar composition to the studied fuel where some olefins are basically substituted by paraffins [33] (Table 43).

The elemental composition was measured with an elemental analyzer and GC × GC, associated with a nitrogen chemiluminescence detector and a sulfur chemiluminescence detector [11, 87, 156]. The low hydrogen to carbon ratio (H/C) ratio and the high density of the studied fuel indicate the high quantity of aromatics and saturated compounds, while the high molecular weight – estimated with the Lee-Kesler method [8, 183] – is a consequence of long molecules. The molecular weight uncertainty was estimated based on the literature, as explained thereafter. Riazi compared the errors on the estimated molecular weights of 5 fuels (from 233 to 523 g/mol) [8]. The Lee-Kesler method was particularly accurate for the two fuels with the lowest molecular weights (233g/mol and 267 g/mol estimated with an error of -1.3 g/mol and -0.3g/mol, respectively). Therefore, the uncertainty was estimated to be ±3g/mol. FACE G is the most similar fuel from the recent literature

(%mol/mol)	P	I	O	N	A	Ox
Studied fuel	4.86	11.63	29.61	12.95	24.95	16.00
Overall ranges	[4.80;55.78]	[26.10;83.70]	[0.00;11.20]	[1.50;15.80]	[0.30;33.60]	[0.00;16.80]
FACE A	13.20	83.70	0.40	2.40	0.30	0.00
FACE C	28.60	65.10	0.40	1.50	4.40	0.00
FACE F	4.80	61.00	10.00	15.80	8.40	0.00
FACE G	7.90	38.30	7.90	14.10	31.80	0.00
FACE I	14.00	70.00	7.00	4.00	5.00	0.00
FACE J	31.50	32.40	0.60	2.40	30.60	0.00
HSN	36.70	37.80	0.00	15.00	10.50	0.00
SALN	55.40	35.90	0.00	6.70	1.32	0.00
HG fuel	12.20	26.10	6.30	15.60	22.90	16.80
CG fuel	10.10	31.90	11.20	5.00	33.60	8.20

Table 43: n-paraffin, iso-paraffin, Aromatic, Olefin, Naphthene and Oxygenate (PIONAOx) mole fractions of the studied fuel compared to other light fuels from the literature: Fuels for Advanced Combustion Engine (FACE) A, C, F, G, I and J, a gasoline provided by Haltermann (HG) and other by Coryton (CG), a Saudi Aramco Light Naphtha (SALN), and a Haltermann Straight Naphtha (HSN) [20, 21, 30–33]. Fuels with different features were selected, including atypical fuels, to show the specificities of the studied fuel. HG fuel is the most similar fuel to the studied one with a low paraffin fraction and high olefin and oxygenate fractions.

in terms of properties with a similar HC ratio and a high MW and a high density (Table 44).

	H/C	MW (g/mol)	Density	RON	Sensitivity
Studied fuel	1.80[87]	120 ±3[8, 183]	796.1[184]	–	–
Overall ranges	[1.78;2.34]	[78.40,100.2]	[642,760]	[60.00;97.5]	[-0.1;11.0]
FACE A	2.29	97.80	685.3	83.5	-0.1
FACE C	2.27	97.20	690.5	84.7	1.1
FACE F	2.13	94.80	707.0	94.4	5.6
FACE G	1.83	99.70	760.0	96.8	11.0
FACE I	2.24	95.50	688.0	70.3	0.7
FACE J	1.91	100.2	741.0	70.8	3.0
HSN	2.15	92.41	705.0	60.0	1.7
SALN	2.34	78.40	642.0	64.5	1.0
HG fuel	1.97	88.80	–	91.0	7.6
CG fuel	1.78	90.60	–	97.5	10.9

Table 44: Properties of the studied fuel compared to other light fuels from the literature: Fuels for Advanced Combustion Engine (FACE) A, C, F, G, I and J, a gasoline provided by Haltermann (HG) and other by Coryton (CG), a Saudi Aramco Light Naphtha (SALN), and a Haltermann Straight Naphtha (HSN) [20, 21, 30–33]. Fuels with different features were selected, including atypical fuels, to show the specificities of the studied fuel. FACE G is the most similar fuel to the studied one with a low HC ratio, a high MW but a relatively low density compare to FACE G. The density is reported at 15 °C (kg/m^3).

8.2.2 *Rapid compression machine*

To gain insight on the reactivity of the fuel in both temperature regimes, ignition delays were measured in the ULille RCM, which had been extensively described in previous studies [181, 185, 186]. The RCM is based on a right-angle design in which a moving cam imposes the movement of the

compressing piston, therefore ensuring strictly constant volume of the combustion chamber after the compression, as well as reproducibility of the compression phase. In this study, the volumetric compression ratio was 10.3:1, and the compression time 45 ms. The end of compression time was determined with an optocoupler fixed on the moving piston facing a comb with a 1 mm resolution. A creviced piston is used to mitigate piston corner vortex formation during the compression phase [187], ensuring temperature homogeneity during the ignition delay period. The tests were carried out under pressures ranging from 10 bar to 20 bar at TDC, and at an equivalence ratio of 0.5 to study lean conditions, which is a feature of the RCCI mode. In this mode, the equivalence ratio generally ranges from 0.3 [65–70] to 0.8 [188–190] with a high EGR rate. Measurements for stoichiometric mixtures would not have made sense in the context of RCCI application, while the validity of kinetic mechanisms for very lean mixtures can sometimes be limited. Therefore, an equivalence ratio of 0.5 represents a meaningful compromise.

Figure 69: The rapid compression machine of ULille used to do the experimental campaign.

The compressed temperature is inferred from the measurements of initial temperature and pressure, and compressed pressure using the isentropic law under the adiabatic core assumption. It is varied by changing the composition of the diluent in the mixture, N_2, Ar, and CO_2 being used. Non-reactive mixtures were tested as well.

Despite its globally low molecular weight, the fuel was composed of a small portion of heavy molecules. A GC/MS analysis of the liquid fraction obtained after evaporation at 85°C from 0 to 1.14 kPa revealed molecules with up to 20 carbon atoms.

These molecules can potentially explain the change of slope corresponding to the heaviest in the distillation curve (Figure 68). The fraction of heavy

compounds present in the fuel is likely to be problematic for RCCI application however, the fuel production process is still under development so that the identified heavy molecules will be removed in the future to avoid evaporation and impingement issues. In order to ensure the repeatability of the mixture preparation, the initial liquid volume of fuel, mixture preparation temperature and the evaporation time were kept constant.

The fraction of the fuel that may have been evaporated was estimated but a precise evaporation simulation with Antoine's Equation and Raoult's law cannot be done due to the complexity of the fuel. To circumvent this issue, a confidence interval for the quantity of fuel that was evaporated was estimated. To define a subset of the more volatile molecules that would have been evaporated, the boiling points under atmospheric conditions of the molecules detected by comprehensive two-dimensional chromatography were compared to a predefined limit to estimate if they were likely to evaporate. The indicative threshold was chosen equal to 216 °C, the boiling point of n-dodecane under atmospheric conditions, because this molecule has a boiling point (86 °C at 8.55 torr) of the same order of magnitude as the temperature of the mixing chamber (85 °C at 8.55 torr). Each molecule evaporation being governed by Raoult's law, the fraction that was effectively evaporated is assumed to be between the whole fuel and the sum of the fractions of the molecules that would have been evaporated in the worst case scenario (93.6% in mass).

The fuel heat capacity was estimated based on the molecules identified with GC × GC and considering the molecules that may have not been evaporated according to the subsequent procedure. Each molecule being governed by Raoult's law, the heat capacity of the fuel that was effectively evaporated was assumed to be between the heat capacity of the total fuel and the heat capacity of the mixture where only the more volatile molecules would have been evaporated. For some species, only the raw formula was determined so the maximal and the minimal values were selected from a set of molecules with the same atomic composition to define a confidence interval for the heat capacity of each fuel. As a result, the heat capacity of the evaporated fuel is between those of the reduced and total fuels which defines the confidence interval. The half-width temperature uncertainty was defined based on the two compressed temperatures calculated with the minimal and the maximal values of the specific heat. This uncertainty, resulting of the heat capacity only, remains low (1.5 to 3.5 K) because the mixture heat capacity depends mainly on the oxygen and diluent concentrations.

The final NASA coefficients under low temperatures (0 - 1000K) and the compositions of the studied mixtures defining the minimal and the maximal heat capacities are reported in Appendix B.

The confidence interval is localized between the heat capacity of representative molecules of each hydrocarbon groups (Figure 70). This can be explained by the fact that the PIONAOx is well divided between groups showing a high and a low heat capacity. The influence from aromatics and olefin compensates each other because both classes have similar concentrations, this is also true for ketones and naphthenes. It is noteworthy that the studied fuel shows a rather high heat capacity because two groups out of six, i.e. aromatics and ketones, have a low heat capacity. A simple primary reference fuel (PRF) blend composed of iso-octane and n-heptane would not be able to correctly capture the heat capacity in the studied temperature range. Adding toluene would decrease the heat capacity, therefore a toluene reference fuel (TRF) would not improve the representability of the surrogate.

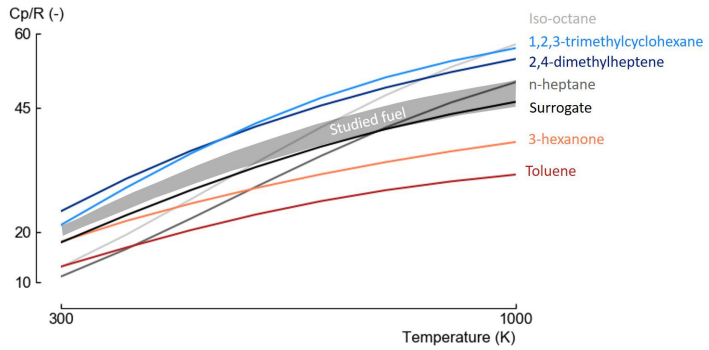

Figure 70: Confidence interval of the studied fuel heat capacity compared to representative molecules for each hydrocarbon group. A surrogate fuel composed of the six plotted molecules blended according to the PIONAOx fraction reported in Table 1 is also considered.

However, a simple surrogate fuel composed of the selected representative molecules blended according to the fuel PIONAOx fraction (Table 43) shows a heat capacity which falls near the confidence interval.

The pressure at TDC was set by controlling the initial pressure of the mixture. The mixtures were prepared using the partial pressure method in a mixture preparation facility heated at 85°C. The theoretical equivalence ratio depends on the atomic mass fractions (measured with an elemental analyzer and GC × GC coupled with a nitrogen chemiluminescence detector and a sulfur chemiluminescence detector [11, 87]), and on the measured partial pressures during the mixture preparation.

The propagation of uncertainty (following the Joint Committee for Guides in Metrology recommendations [19]) leads to the calculation of the accuracy on the equivalence ratio. The atomic mass fractions and the partial pressure standard uncertainties were calculated based on their standard deviations, and the manufacturer's specifications with a rectangular distribution, respectively. A correction factor of 3 was chosen to obtain an estimation at 99% of the confidence interval, defined by the expanded uncertainty. As a result, $u(\phi) = 0.15\%$, so $\phi = 0.5 \pm 0.0045$.

8.3 THEORETICAL CALCULATIONS

In this section, the mathematical developments required to do numerical simulations and to post-process the data are detailed.

First, the calculation of the volume trace of the RCM is detailed. The volume trace is required to do numerical simulations similar to the experiments with a predefined volume trace. The first law of thermodynamics can be written for a close system as the variation of internal energy U equals to the heat and work exchanged by the system.

$$dU = \partial Q + \partial W. \tag{171}$$

The heat term is neglected to follow an approach detailed by Bourgeois et al [191]. The adiabatic core assumption is applied and the losses during the compression are modelled with an additional volume term. Under this assumption, the previous equation can be written as:

$$nC_v dT = -pdV. \tag{172}$$

The only information available is the experimental pressure trace while the volume trace is the quantity of interest. Therefore, the temperature must be removed from this equation, which can be done with the differential form of the perfect gas law:

$$n\bar{R}dT = pdV + Vdp \tag{173}$$

Equation 172 can be written

$$\frac{C_v}{\bar{R}}(Vdp + pdV) = -pdV \tag{174}$$

With $\bar{R} = C_p - C_v$, the previous equation becomes:

$$\frac{dV}{V} = (\frac{\bar{R}}{C_p} - 1)\frac{dp}{p}. \tag{175}$$

The integration of this equation from t_o to t gives:

$$\int_{V_o}^{V} \frac{dV}{V} = \int_{to}^{t} (\frac{\bar{R}}{C_p} - 1)\frac{p'}{p}dt, \tag{176}$$

which can also be written:

$$\log(\frac{V}{V_o}) = \int_{to}^{t} (\frac{\bar{R}}{C_p} - 1)\frac{p'}{p}dt. \tag{177}$$

Finally:

$$V(t) = V_o + \exp\Big(\int_{to}^{t} (\frac{\bar{R}}{C_p} - 1)\frac{p'}{p}dt\Big). \tag{178}$$

he volume trace can then be used in order to do the simulations of RCM in section 7.5.2 and 7.5.3.

Second, the calculation of the temperature in the reaction chamber of the RCM at TDC is detailed.

The compression is supposed to be isentropic, which means that:

$$T^{\gamma}P^{1-\gamma} = C, \tag{179}$$

with C a constant.

The derivative of this equation gives:

$$\frac{dT}{T} = \frac{\gamma-1}{\gamma}\frac{dP}{P}, \tag{180}$$

which can be integrated until the end of the compression:

$$\int_{T0}^{T_{TDC}} \frac{\gamma}{\gamma-1}\frac{dT}{T} = \frac{\ln(P_{TDC})}{P_0}, \tag{181}$$

γ depends on the temperature and can be calculated with the NASA coefficients.

8.4 NUMERICAL SIMULATION

Numerical simulations were carried out to compare the ASR fuel reactivity to two fuels among those identified in Table 44. FACE G shows a high RON (RON = 96.8) and a high sensitivity (s = 7.9) conversely to FACE I (RON = 70.3 and s = 0.7) and their ignition delays are dissimilar [20, 21]. FACE G has a lower reactivity than FACE I. Moreover, they were already tested with the same kinetic mechanism so the just cited fuels were selected to define a frame of reference to discuss the ASR fuel ignition delays. The compositions of FACE G and I surrogates proposed by King Abdullah University of Science and Technology (KAUST) are listed in Table 45.

(%mol/mol)	FGG-KAUST [20]	FGI-KAUST [21]
n-butane	7.6	–
n-Heptane	–	12
2-Methyl butane	9.5	11
2- Methyl hexane	9.8	27
2,2,4-Trimethyl pentane	18	34
1-Hexene	8.1	6
Cyclopentane	15.3	6
1,2,4-Trimethylbenzene	21.1	4
Toluene	10.6	–

Table 45: Composition of the FACE gasoline G and I multi-component surrogates proposed by KAUST.

Simulations of a variable volume batch reactor were carried out with Cantera and the FACE gasoline kinetic mechanism [20]. The volume profile was inferred from the non-reactive pressure profile with an isentropic law assumption as described by Bourgeois et al. [191]. With this method, an additional volume expansion term accounts for the effective heat losses after the end of compression.

Similarly, simulation were carried out with OpenSMOKE++[192] to compare the experimental ignition delays with a sample of surrogate fuels. This comparison aims at defining a surrogate fuel that behave has the real fuel. The surrogate fuels were composed of n-heptane and iso-octane, such mixtures are also known as primary reference fuel (PRF). These two species are included in the Lawrence Livermore detailed mechanism for surrogate gasoline [193]. This mechanism performs well over temperatures and pressures relevant for internal combustion engines. Several PRF were generated following a latin hypercube sampling (LHS) procedure. Then, for each sample, the IDTs at 20 bar from 700 to 875K were calculated. These IDT were compared with the experimental IDT at 20 bar, which allowed us to define an optimal surrogate fuel. Then, the surrogate fuel was validated at 20bar and 10bar thanks to additional simulations. The results are reported in subsection 8.5.3.

8.5 RESULTS AND DISCUSSION

Overall, the results presented below report the investigated conditions, the ignition limits, the NTC zone characteristics, and discuss the fuel ignition.

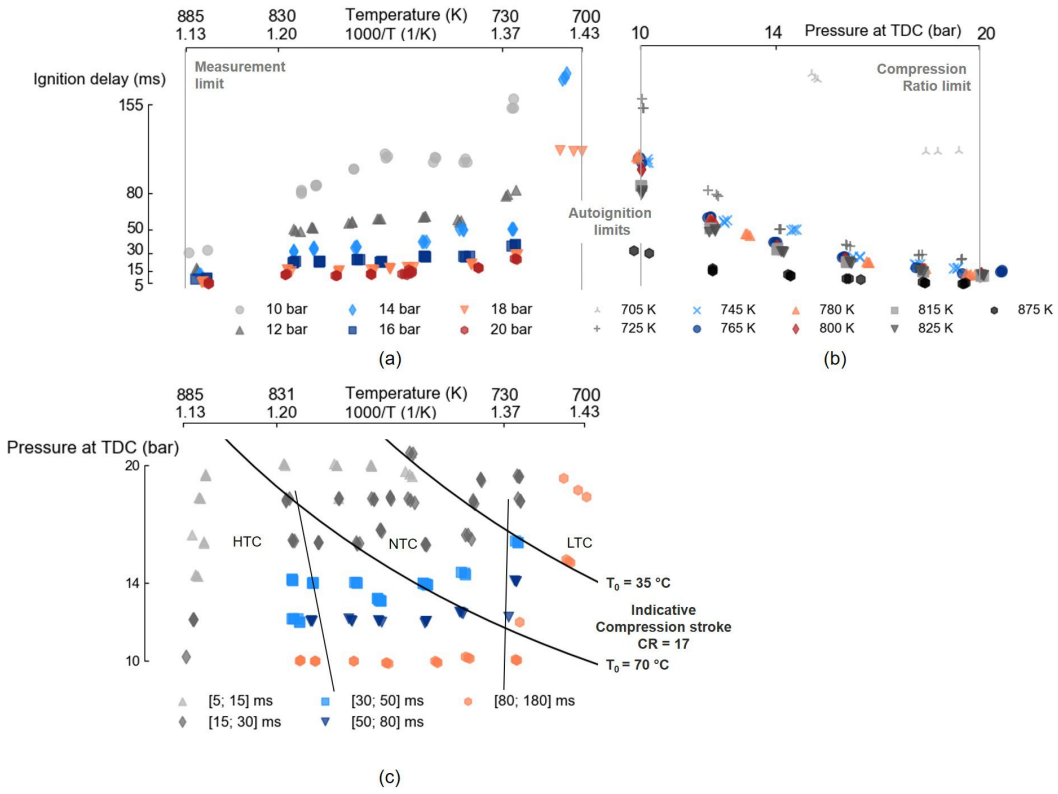

Figure 71: Investigated conditions and measured main-stage IDT. The achieved temperatures were calculated based on the estimated mean value of the heat capacity. The range of investigated conditions is wide as shows panel (c). On the same panel, two illustrative temperature–pressure compression strokes show a range of operating conditions where a meaningful. These indicative lines were obtained by calculating the heat losses as advised by Broekaert et al. [15] and Pochet et al. [16], and the SOC was estimated based on extrapolated ignition delays and the Knock Integral Model (KIM) studied by Shahbakhti et al. [17, 18].

8.5.1 *Ignition delays*

The fuel has a standard behavior governed by the basics of the combustion chemistry under low, intermediate and high temperatures. To cover these conditions jointly with the pressure effect, we tested 10 reactive mixtures (one mixture per temperature) with an equivalence ratio of 0.5 $\pm$0.0045, varying the pressure and the temperature at TDC from 9.8 $\pm$0.4 bar to 21.4 $\pm$0.2 bar and from 705.1 $\pm$1.6 K to 878.4 $\pm$3.5 K, respectively (Figure 71).

Two compression strokes were plotted on Figure 71 panel (c), with two different initial temperatures. These traces show that with a well-chosen compression ratio, the required range of temperatures does not require a stringent preheating system to run under an RCCI engine. Moreover, the studied conditions are relevant and cover the pressure and temperature achieved during an RCCI compression stroke at an equivalence ratio of 0.5.

The lowest investigated temperature and pressure correspond to the ignition limit, while measuring an IDT at higher temperatures or pressures would have lead to very short and unmeasurable IDTs. The measured IDTs (from 5 ms to 155 ms, with a maximum reaching 193.8 ms) show conventional features.

First, the IDTs decrease exponentially when the temperature increases and according to a power law P^n with pressure (Figure 71), with a deviation from Arrhenius behaviour. This deviation corresponds to a temperature zone where the temperature coefficient E/R in the Arrhenius law decreases and can be negative, meaning that the rate at which the reactivity increases with the temperature is reduced. This NTC is a consequence of a competition between two different kinetic pathways, i.e. low temperature chain-branching pathways and intermediate temperature chain-terminating pathways, as described by Battin-Leclerc et al. [194].

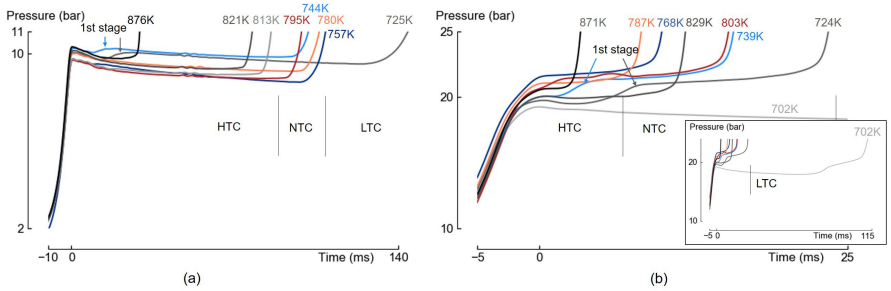

Figure 72: Pressure profiles at 10 bar (9.80 ±0.4 bar) and at 20 bar (19.75 ±0.9 bar). The high temperature chemistry (HTC), NTC and LTC regions were defined according to the changes of slopes on Figure 73.

Second, two-stage ignition was observed between 705K and 750K, where a first pressure rise – also known as first-stage ignition – takes place before the main ignition (Figure 72). Long alkyl-chain molecules can produce keto-hydroperoxides, the chain-branching agents responsible for the appearance of first-stage ignition. The chain-branching pathways of alkanes typically proceed through addition of alkyl radical to O_2, and further isomerization to hydroperoxides, to ultimately yield ketohydroperoxides. By increasing the temperature in this constant volume experiment, the first-stage of ignition promotes reactivity and decreases the total ignition delay.

Third, as the pressure increases, the temperature coefficient increases (Figure 73). This phenomena is explained by the rates of formation and consumption of the intermediates that respectively promotes reactivity in the LTC (hydroperoxides) and in the NTC zones. Intermediate temperature chain branching through decomposition of hydrogen peroxide begins as the temperature reaches the NTC conditions, consequently, the low-temperature reactivity weakens. The extent of the NTC behaviour and associated temperature range is therefore directly correlated to the propensity of a fuel to form hydroperoxides and/or hydrogen peroxide. The decrease of the NTC extent with the pressure that was previously described can be explained by the facilitated decomposition of hydrogen peroxide into two OH radicals under higher pressures [181]. In the chemical equation $H_2O_2(+M) = OH + OH(+M)$, where M is the third body in the reaction expression, any increase in pressure will lead to a significant increase of the reaction rate.

This fuel displays two-stage ignition behaviour, as well as a deviation from Arrhenius law. However, the temperature coefficient, i.e. the slope in the NTC zone, remains positive, probably because of the low paraffin fraction. This has been observed before in the case of alkane/alkene mixtures [195].

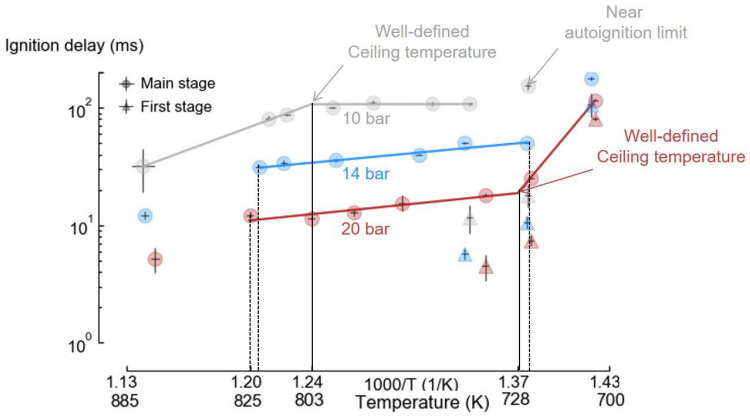

Figure 73: IDTs at an equivalence ratio of 0.5 ±0.0045 for three pressures: 19.75 ±0.9 bar, 14.55 ±0.6 bar, 9.80 ±0.4 bar, and three types of ignition regimes: the high temperature, the negative temperature coefficient, and the low temperature zones. The main and the first-stage ignitions are symbolized by circles and triangles, respectively. The error bars represent the combined uncertainty extended at 95%, taking into account both the repeatability and the Cp uncertainties, and calculated following the Guide to the expression of uncertainty in measurement [19]. The straight lines were drawn when enough data were available to define the limits between the low temperature chemistry (LTC), NTC and HTC regions.

8.5.2 *Atypical behaviour*

In this section, the specificities of the studied fuel reactivity are identified by comparing the ignition delays to two multi-component surrogate fuels proposed by KAUST, i.e. FGG-KAUST and FGI-KAUST. Then, the identified specificities are discussed with regards to the molecular composition. FACE G (surrogate FGG-KAUST) and FACE I (surrogate FGI-KAUST) define a good framework because the first has high ignition delays while the second is a highly reactive gasoline fuel [20, 21].

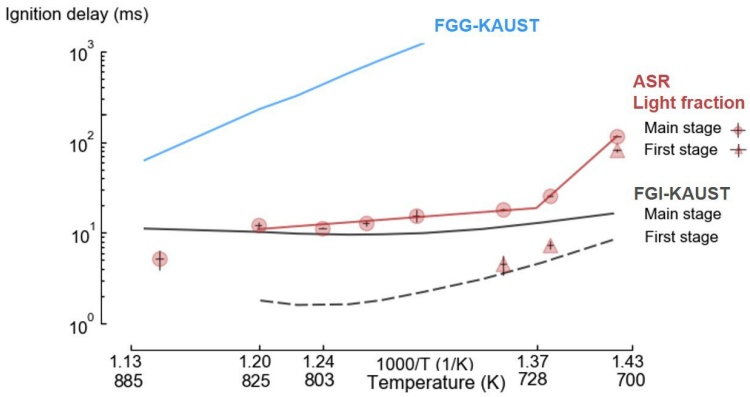

Figure 74: ASR fuel ignition delays at 20 bar and at an equivalence ratio of 0.5, compared to the KAUST surrogate fuels for FACE G and FACE I, i.e. FGG-KAUST and FGI-KAUST [20, 21]. The reactivity in the NTC region is similar to the one of FGI-KAUST.

The following observations show that the studied fuel is characterized by a high reactivity under intermediate temperatures but a very limited one under low temperatures (Figure 74). First, the ASR fuel shows a reactivity of the same order of magnitude (ignition delay of about 10 ms) than the one of FGI-KAUST in the NTC area but it decreases dramatically when the NTC/LTC ceiling temperature is crossed. At low temperature, the autoignition vanishes even if the ignition delay is still relatively low compared to the one of FGG-KAUST (100 ms). Last but not least, conversely to FGI-KAUST, the first stage ignition is only visible when the compressed temperature is lower than 750K, which shows that a small number of low-temperature chain-branching intermediates are formed because they cannot compete with the NTC reaction pathways. The small number of intermediates are consumed by the NTC pathways.

This fuel includes a large olefinic portion (29.61% mol/mol Table 44), molecules that are generally characterized by a low reactivity under low temperatures [196, 197]. 2,4-dimethyl-1-heptene is the olefinic molecule with the higher fraction and is likely to display reaction pathways relevant to alkenes and alkanes because of its double bond yielding a total of 5 allylic H-abstraction sites, as well as its long alkyl chain. Allylic hydroperoxydes are not favorable for addition to O_2 molecules, even though allylic radicals can recombine with HO_2 radicals to form allylic peroxides [198]. The alkylic section of this molecule is branched, which will be detrimental to the internal isomerization of potential RO_2 adducts. To sum up, the long molecule length promotes the reactivity, nevertheless, the limited alkylic isomerization possibilities and the allylic sites limit the low temperature reactivity.

A large portion of aromatics is also present in the fuel with almost 25% mol/mol (Table 44), split into three sub-groups: the toluene, the o-xylene, and the styrene -like groups. Roubaud et al. demonstrated that o-xylene as well as long-chain aromatics react at low temperatures [34] following two-stage ignition, under high pressure conditions. Toluene easily forms the resonance-stabilized benzyl radical, which is an important radical scavenger in the low temperature region [181]. Because all its C-H bonds are either benzenic or vinylic with high bond dissociation energies, styrene is likely to combine ignition resistance characteristics associated with toluene and short-chain alkenes. The studied fuel is characterized by a higher fraction of aromatics belonging to the two groups that do not react in the low temperature region, explaining its low reactivity in this region (Table 46).

Table 46: Distinctive aromatic groups defined by Roubaud et al. [34]

Group	Toluene	o–Xylene	Styrene
Molecules	Toluene 1,3,5–Trimethylbenzene Xylene (m,p)	Ethylbenzene 1,2,3–Trimethylbenzene –	Styrene α–methylstyrene –
Mole fraction (%)	5.72	6.34	8.68

The high aromatic fraction can also explain the high difference of reactivity between the LTC and the NTC. Because of the formation of resonance-stabilized radicals, abstraction of hydrogen by O_2 or HO_2 is favored, facilitating the formation of hydrogen peroxide. Intermediate temperature reactivity is therefore favored, in accordance with the significant octane sensitivity usually observed for these fuels.

Finally, a significant portion of this fuel is composed of a high number of oxygenated molecules (25 molecules and 18 isomers identified). In a previous study, 6.8% of oxygenates had been detected by GC × GC but 16%

were estimated after applying a correction [87]. Ketones represent a large contribution to this group. Short ketones are known to display very low reactivity in the low temperature regime. This is mostly due to the fact that addition to O_2 by radicals originating from these ketones mostly results in HO_2 elimination to yield unsaturated species, the formation of peroxides being difficult [199].

8.5.3 *Formulation of a surrogate fuel*

As explained in section 2.6.4, traditional methods make the octane numbers of a surrogate fuel match with those of the real fuel [132, 133]. In the present study, the octane numbers are not available. According to the literature, the octane numbers can be substituted by the fuel chemical structure (functional groups [134] or carbon types [86]). With both of these two methods, the surrogate fuel must be validated with an additional test in a RCM to reproduce the final application. We propose an alternative where the experimental data from the RCM is directly used to formulate the surrogate fuel. The method is based on matching experimental with simulated IDT for simple mixtures of n-heptane and iso-octane (PRF). We selected such a simple mixture as we observed an interesting linear relationship that has never been exploited before between the ignition delay and the n-heptane concentration. The experimental data are the IDTs at 20 bar and the simulation were conducted under the same operating conditions.

According to the Arrhenius equation, the calculated IDT depends exponentially on the temperature. Specifically:

$$\tau = Ae^{-\frac{E_a}{RT}}, \tag{182}$$

where τ is the ignition delay, A is a pre-exponential factor and $T_a = \frac{E_a}{R}$ is the activation temperature. Relying on the natural logarithm, a linear relation lies in the previous equation:

$$\ln(\tau) = \ln(A) - \frac{T_a}{T}, \tag{183}$$

The pre-exponential factor and the activation temperature depend on the temperature zone (namely the LTC, the NTC and the HTC). In the NTC region, the coefficients A and T_a depend strongly on the concentration of n-heptane as shows Figure 75.

Then, an underlying relation between the coefficients $\ln(A)$ and T_a, and the composition of the PRF exist:

$$\ln(A) = 9.0295 - 67.581x_{n-heptane} \tag{184}$$

$$T_a = 3.6673 - 45.233x_{n-heptane}, \tag{185}$$

These two equations were used to calculate the required n-heptane concentration to obtain an accurate surrogate fuel. With the studied ASR fuel, the parameters $\ln(A)$ and T_a are respectively equal to -2.6485 and -4.1098. Finally, with the two equations 184 and 185, a similar n-heptane concentration was obtained, 17.3 %mol = 15.7 %vol. Thus, a PRF84.3 was defined as a surrogate fuel.

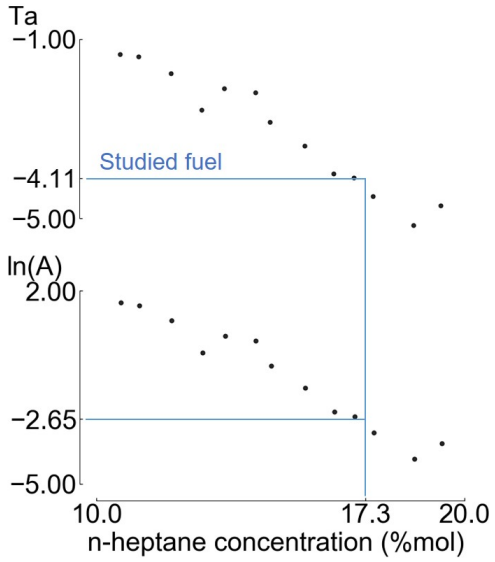

Figure 75: Arrhenius parameters ln(A) and T_a in the NTC region of several PRF according to the n-heptane concentration.

To evaluate the surrogate fuel, the IDTs in the three temperature zones (LTC, NTC and HTC) at 10 bar and at 20 bar (the non-reactive volume profile was not available at 14 bar) were plotted on Figure 76. The surrogate fuel accurately represent the real fuel except for the lowest temperature, whatever is the pressure, and for the highest temperature at 20 bar. The lowest temperature is in the LTC zone where the fuel reactivity is very low, as explained in the previous subsection 8.5.2. This low reactivity is a consequence of the peculiar fuel composition, with large fractions of oxygenated molecules, toluene, styrene and 2,4-dimethyl-1-heptene.

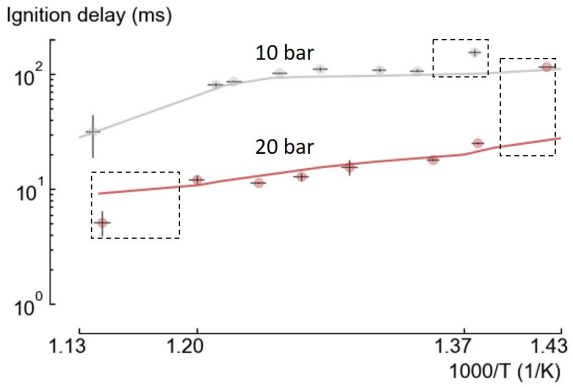

Figure 76: Comparison of the simulated IDT of the ASR surrogate fuel, PRF84.3, at 10 and at 20 bar with the experimental IDT.

8.6 CONCLUSION

The experiments presented in the present chapter provides data under Reactivity Controlled Compression Ignition-like conditions to the combustion

community for a fuel that had not been studied previously in a Rapid Compression Machine. More experimental data for other equivalence ratios, typically 0.3 and 0.8 would provide additional information for operating conditions without exhaust gas recirculation (EGR) and with a high EGR rate. In comparison with RCCI conditions, simulations in a rapid compression machine does not suffer from evaporation issues in theory. Moreover, the fluid dynamic aspects are not considered in the RCM.

The fuel showed common features, such as the decrease of the ignition delay with the pressure and the temperature, except in a negative temperature coefficient (NTC) region ($725 < T < 825$ K). The slope of the NTC region decreases with the pressure and a first stage ignition was detected near the ceiling temperature between the low temperature and the NTC regions. A more specific attribute was observed: a low reactivity under low temperature chemistry (LTC), explained by the major molecules blended: substituted olefin, aromatics with a reactivity comparable with the one of toluene, and oxygenates (ketones, alcohols and benzenoids).

Among the final applications, this study offers a first overview on the reactivity of ASR fuels which, until now, was unknown. A PRF surrogate fuel was formulated and validated although further improvement is possible with additional molecules. The PRF fuel is particularly well suited for the intermediate region but does not capture correctly the reaction under low temperature. This low temperature range is important to correctly estimate the ignition. The surrogate fuel could be improved with additional molecules. Still, relying on the major constituting molecules of the fuel, such as 2,4-dimethyl-1-heptene or long oxygenated molecules, is impossible as they have never been studied in pure form. Such a molecule would be required to propose an accurate surrogate fuel in the low temperature zone. Additionally, molecules with a low reactivity in the low temperature region such as aromatic molecules from the toluene group, ketones or olefins with a high number of substituants would be required. It was showed during the surrogate fuel formulation that the parameters of the Arrhenius law depend linearly on the n-heptane concentration in a PRF mixture. This interesting behaviour was not observed with more complex surrogate fuels such as toluene reference fuel (TRF). Nevertheless, a TRF surrogate fuel could be interested to have a better prediction in the low temperature zone.

As perspective, this study offer the possibility to lead numerical simulations with the surrogate fuel to investigate the potentials of RCCI operating conditions to reduce the pollutants emitted by waste-derived fuels.

9 CONCLUSION

The current thesis extend the existing predicting laws to cover unconventional fuels. Specifically, fuels derived from automotive shredder residues (ASR) are discussed. Coupling these unconventional fuels with advanced combustion modes such as reactivity controlled compression ignition (RCCI) is a way to decrease the produced levels of pollutants. In chapter 4, experimental campaigns with heavy fractions derived from ASR were described and discussed. It was showed that this unconventional fuel behave differently than usual fuels, which can result in the failure of the engine. From this observation, many challenges arise such as:

- Which are the key chemical and physical properties that should be controlled to ensure a safe combustion in a piston engine?
- If the properties cannot be measured at a low cost, are the existing predicting methods applicable for unconventional fuels, and, if not, how can they be adapted?
- To which extent can unconventional fuels be burnt under the RCCI combustion mode?

Unconventional fuels can safely be burnt in an engine as long as their properties are monitored. The current thesis proposes methods to predict the composition and the ignition properties of unconventional fuels. The knowledge of the composition is important as it gives an insight on the fuel properties. The composition explains the behaviour of the fuel, nevertheless, it must be coupled with additional properties such as the octane number (ON) in order to properly assess the fuel reactivity. However, these octane numbers are measured under specific conditions, so, they must be combined with simulations to investigate other operating conditions.

The composition and the octane numbers can be measured with methods that are expensive. Thus, predicting tools must be used instead. In the current thesis, existing prediction methods have been updated to be suitable for unconventional fuels which are oxygenated fuels. First, the composition of an ASR-derived fuel was estimated based on easy-to-quantified properties. Second, the octane number of a gasoline blendstock for oxygenate blending was estimated based on a Bayesian pseudo-component (PC) method. The uncertainty can be evaluated on the fly thanks to the evaluation of the covariance matrix. The uncertainty is lower than 1% for most of the samples and lower than 2% for all of them. The uncertainty is comparable with real measurements in a cooperative fuel research engine. Nevertheless, real measurements are still required to develop predicting models for new fuels. The computational method show that the fuel is governed by high interaction

blending effects, particularly when saturates, olefins and aromatics are mixed. Third, the octane number of the same type of fuel was estimated coupling artificial neural network (ANN) with principal component analysis (PCA). The achieved uncertainty is near 2%. The uncertainty of the predicting models is close to the uncertainty obtained with the real octane number measurements. It is noteworthy that the real measurements are still required to calibrate the models for a new type of fuels. Finally, an ASR-derived fuel was tested in a rapid compression machine (RCM), providing experimental data to the scientific community. This data was also used to formulate a surrogate fuel. The main conclusions of the previous works are summarized thereafter, making the link with the three challenges previously raised.

The ignition timing is a key property which is linked with the hydrocarbon type. For instance, n-paraffins auto-ignite faster than aromatics. Moreover, controlling the hydrocarbon types is required for health issue prevention. For these reasons, the models from the literature to predict the composition were updated to make them suitable for unconventional fuels. With this new model, the prediction of the composition gives accurate results, with a precision of about 12% against 87% with conventional methods. These 87% of error are due to an estimation of only the n-paraffin, napthene and aromatic (PNA) fractions although the fuel is composed of n-paraffin, iso-paraffin, olefin, napthene, aromatic and oxygenate (PIONAOx). More specifically, conventional methods estimated the following composition of the studied light fraction from ASR: P: 31%, N: 45%, A: 24% while the real fuel composition is as follow P: 5.4%, I: 12.2%, O: 30.8%, N: 14.6%, A: 24.4%, Ox: 12.6%. The new method estimates correctly all the fuel fractions except the paraffins. This can be easily explained by the similarity between n-paraffins and iso-paraffins which share very similar properties. Isoparaffins tend to have a much higher ignition delay. For instance, the octane number of n-heptane is zero whereas it is 42.2 for 2-methylhexane. Thus, not being able to dissociate iso and normal paraffins is a real issue.

The second contribution of the current thesis is the development of two models to predict the octane numbers of gasoline blendstocks mixed with an oxygenated molecule (1-propanol, 2-propanol, 1-butanol, 2-butanol, or 2-methyl-1-propanol). The octane numbers are two properties that are linked with the ignition timing. These two models show that statistical and machine learning tools can be applied to hydrocarbon engineering in order to create new models as well as analyse large datasets. For instance, the calibration of a model to predict the ON can provide information on the molecule blended such as their blending characteristics. Another example is the capability of PCA to extract the principal features of a fuel to determine which key properties are linked with the ignition characteristics of the studied fuel. The first model that was created is based on physical data, with the introduction of pseudocomponents to describe the fuel. The second model rely on machine learning tools. It was not possible to retrieve the physical information (mean average boiling points, hydrocarbon class fractions) of the first method with the second one.

Finally, studying the ignition delay in a RCM provides experimental data to characterize the fuel under the RCCI combustion mode. For instance, the light fraction from ASR was showed to have a high ignition delay time (IDT) at low temperatures while the IDT is comparable to other fuels at higher temperatures. An additional result of this study was to show a strong correlation between the n-heptane concentration in a primary reference fuel

(PRF) and the parameters of the Arrhenius law. Thanks to this observation, a PRF surrogate fuel was formulated.

10 DISCUSSION AND PERSPECTIVES

In this chapter, we discuss the limitations of the current thesis and introduce perspectives.

First, identifying a property which allows the separation of the normal and the iso-paraffins would strengthen the method developed to predict the n-paraffin, iso-paraffin, olefin, napthene, aromatic and oxygenate (PIONAOx) composition. Indeed, it was showed that the normal and the iso-paraffins have very similar properties. Additionally to the physical properties, chemical properties were also tested. It was showed that the normal and iso paraffins could not be distinguish, even with nuclear magnetic resonance (NMR) data. Therefore, the normal and the iso-paraffin cannot be separated with a predicting method based on properties.

Secondly, only the properties of the light fractions produced from automotive shredder residues (ASR) were studied. The injection timing could be adapted dynamically depending on the reactivity of the heavy fuel. Nevertheless, methods to predict the composition, the properties, and the ignition characteristics of this heavy fraction could be developed. This heavy fraction would behave similarly to a diesel, so the properties that characterize diesel fuels should be used to characterize the heavy fuel. For instance, a property that would provide important information on how the fuel burns is the cetane number (CN). Relying on principal component analysis (PCA) and artificial neural network (ANN) to update the existing laws to predict the CN would be useful. In addition to the properties studied for the light fraction, properties especially fitted for diesel fuels could be included in the study, for instance, the resin and asphalthene content.

Third, additional experimental campaigns should be carried out. Studying the light fraction in an engine would show how the fuel behave to investigate if the fuel could cause knock. Knocking occurs when the fuel octane number (ON) is too low. It was showed in chapter 8 that a good surrogate for the studied fuel derived from ASR is primary reference fuel (PRF) 84.3 which has a low octane number compared to conventional gasoline. Thus, experimental campaigns are mandatory to study if the fuel is prompt to cause knock. Tests under reactivity controlled compression ignition (RCCI) condition could also be carried out. Relying on a electronic control unit (ECU) fully programmable would allow us to control the combustion timing involved

during the combustion. It would be crucial to determine under which operating conditions the fuel burns.

To determine these operating conditions, simulations could also be performed to study unconventional fuels by the mean of surrogate fuels. The fuel behaviour could be studied depending on the inlet temperature, the compression ratio, the exhaust gas recirculation (EGR) ratio and the equivalence ratio. It would also be interesting to consider some fluctuations in the fuel composition and properties to determine ranges of operating conditions allowing to burn the fuel safely, and with a good efficiency.

Finally, the main limitation is related to the low amount of available fuel. This was due to technical issues which prevent our industrial partner to produce the fuel. The production facility had to be modified several times, which took time. For instance, the process to remove the silica from the fuel had to be implemented. Moreover, the production facility had been damaged. The reactor in which the reaction with NaOH occurs was destroyed during operation. For these reasons only a few quantity of fuel was available. As a consequence, a small number of experiments in piston engine was performed. Moreover, a small number of fuels were available. The methods created in chapters 6 and 7 were developed for gasoline blendstock for oxygenate blending. Similar methods for real ASR-derived fuels could be formulated when enough experimental fuels are available. The current models could be validated or extended for real fuels when enough data would be available. To proceed, the main properties of the fuel would need to be measured: specific gravity, refractive index, kinematic viscosity, distillation curve, CHON atomic fractions.

BIBLIOGRAPHY

[1] Edgar Allan Poe.

[2] IEA. Share of total primary energy demand by fuel, 2010-2019.

[3] Silpa Kaza, Lisa Yao, Perinaz Bhada-Tata, and Frank Van Woerden. *What a waste 2.0: a global snapshot of solid waste management to 2050*. Number 1. 2003.

[4] Europa. End–of–life vehicle statistics, 2016.

[5] InnovaTech. Projet Phoenix - Une magnifique vitrine technologique pour la Wallonie. Technical report, 2013.

[6] Daniel Flowers, William Pitz, Matthew Mcnenly, Mark Havstad, Nick Killingsworth, Marco Mehl, Thomas Piggott, Mani Sarathy, Charlie Westbrook, and Russell Whitesides. Simulation of High Efficiency Clean Combustion Engines and Detailed Chemical Kinetic Mechanisms Development. Technical report, Lawrence Livermore National Laboratory, 2012.

[7] Dhananjay Kumar Srivastava, Avinash Kumar Agarwal, Amitava Datta, and Rakesh Kumar Maurya. *Advances in Internal Combustion Engine Research*. 2018.

[8] M. R. Riazi. *Characterization and Properties of Petroleum Fractions*. ASTM International, 2005.

[9] Juan Daniel Martínez, Neus Puy, Ramón Murillo, Tomás García, María Victoria Navarro, and Ana Maria Mastral. Waste tyre pyrolysis - A review. *Renewable and Sustainable Energy Reviews*, 23:179–213, 2013.

[10] Kevin M. Van Geem, Steven P. Pyl, Marie Françoise Reyniers, Joeri Vercammen, Jan Beens, and Guy B. Marin. On-line analysis of complex hydrocarbon mixtures using comprehensive two-dimensional gas chromatography. 1217(43):6623–6633, 2010.

[11] Thomas Dijkmans, Marko R. Djokic, Kevin M. Van Geem, and Guy B. Marin. Comprehensive compositional analysis of sulfur and nitrogen containing compounds in shale oil using GC×GC – FID/SCD/NCD/TOF-MS. *Fuel*, 140:398–406, 2015.

[12] Christopher M. Bishop. Pattern Recognition and Machine Learning. 2016.

[13] Junseok Chang, Gautam Kalghatgi, Amer Amer, and Yoann Viollet. Enabling high efficiency direct injection engine with naphtha fuel through partially premixed charge compression ignition combustion. In *SAE 2012 World Congress & Exhibition*. SAE International, apr 2012.

[14] Junseok Chang, Yoann Viollet, Amer Amer, and Gautam Kalghatgi. Fuel economy potential of partially premixed compression ignition (ppci) combustion with naphtha fuel. In *SAE/KSAE 2013 International Powertrains, Fuels & Lubricants Meeting*. SAE International, oct 2013.

[15] Stijn Broekaert, Thomas De Cuyper, Kam Chana, Michel De Paepe, and Sebastian Verhelst. Assessment of empirical heat transfer models for a cfr engine operated in hcci mode. In *SAE 2015 World Congress & Exhibition*. SAE International, apr 2015.

[16] Maxime Pochet, Véronique Dias, Hervé Jeanmart, Sebastian Verhelst, and Francesco Contino. Multifuel chp hcci engine towards flexible power-to-fuel: Numerical study of operating range. In *Energy Procedia*, volume 105, pages 1532–1538, 2017. 8th International Conference on Applied Energy, ICAE2016, 8-11 October 2016, Beijing, China.

[17] Mahdi Shahbakhti, Robert Lupul, and Charles Robert Koch. Predicting hcci auto-ignition timing by extending a modified knock-integral method. In *SAE World Congress & Exhibition*. SAE International, apr 2007.

[18] Mahdi Shahbakhti, Robert Lupul, and Charles Robert Koch. Sensitivity analysis & modeling of hcci auto-ignition timing. *IFAC Proceedings Volumes*, 40(10):303–310, 2007. 5th IFAC Symposium on Advances in Automotive Control.

[19] Joint Committee For Guides In Metrology Jcgm. Evaluation of measurement data — Guide to the expression of uncertainty in measurement. *International Organization for Standardization Geneva ISBN*, 50(September):134, 2008.

[20] S. Mani Sarathy, Goutham Kukkadapu, Marco Mehl, Tamour Javed, Ahfaz Ahmed, Nimal Naser, Aniket Tekawade, Graham Kosiba, Mohammed AlAbbad, Eshan Singh, Sungwoo Park, Mariam Al Rashidi, Suk Ho Chung, William L. Roberts, Matthew A. Oehlschlaeger, Chih Jen Sung, and Aamir Farooq. Compositional effects on the ignition of FACE gasolines. *Combustion and Flame*, 169:171–193, 2016.

[21] Tamour Javed, Ahfaz Ahmed, Leonardo Lovisotto, Gani Issayev, Jihad Badra, S. Mani Sarathy, and Aamir Farooq. Ignition studies of two low-octane gasolines. *Combustion and Flame*, 185:152–159, 2017.

[22] N. Nikolaou, C. E. Papadopoulos, I. A. Gaglias, and K. G. Pitarakis. A new non-linear calculation method of isomerisation gasoline research octane number based on gas chromatographic data. *Fuel*, 83(4-5):517–523, 2004.

[23] INFICON. Response Factors for Flame Ionization Detector Operation, 2012.

[24] Keith Schofield Ã. The enigmatic mechanism of the flame ionization detector : Its overlooked implications for fossil fuel combustion modeling. 34:330–350, 2008.

[25] Aspen Technology Inc. *Aspen Physical Property System: Physical Property Methods*. 2013.

[26] American Petroleum Institute. *Knocking Characteristics of Pure Hydrocarbons – Developed Under American Petroleum Institute Research Project 45*. American Society for Testing Materials, 1958.

[27] Earl Christensen, Janet Yanowitz, Matthew Ratcliff, and Robert L. McCormick. Renewable Oxygenate Blending Effects on Gasoline Properties. *Energy & Fuels*, pages 4723–4733, 2011.

[28] Robert L. McCormick, Gina Fioroni, Lisa Fouts, Earl Christensen, Janet Yanowitz, Evgueni Polikarpov, Karl Albrecht, Daniel J. Gaspar, John Gladden, and Anthe George. Selection Criteria and Screening of Potential Biomass-Derived Streams as Fuel Blendstocks for Advanced Spark-Ignition Engines. *SAE International Journal of Fuels and Lubricants*, 10(2):2017–01–0868, 2017.

[29] Thomas Wallner, Andrew Ickes, and Kristina Lawyer. Analytical assessment of c2–c8 alcohols as spark-ignition engine fuels. In *Proceedings of the FISITA 2012 World Automotive Congress*, pages 15–26, Berlin, Heidelberg, 2013. Springer Berlin Heidelberg.

[30] S. Mani Sarathy, Goutham Kukkadapu, Marco Mehl, Weijing Wang, Tamour Javed, Sungwoo Park, Matthew A. Oehlschlaeger, Aamir Farooq, William J. Pitz, and Chih Jen Sung. Ignition of alkane-rich FACE gasoline fuels and their surrogate mixtures. *Proceedings of the Combustion Institute*, 35(1):249–257, 2015.

[31] Tamour Javed, Ehson F. Nasir, Ahfaz Ahmed, Jihad Badra, Khalil Djebbi, Mohamed Beshir, Weiqi Ji, S. Mani Sarathy, and Aamir Farooq. Ignition delay measurements of light naphtha: A fully blended low octane fuel. *Proceedings of the Combustion Institute*, 36(1):315–322, 2017.

[32] Mohammed Alabbad, Gani Issayev, Jihad Badra, Alexander K. Voice, Binod Raj Giri, Khalil Djebbi, Ahfaz Ahmed, S. Mani Sarathy, and Aamir Farooq. Autoignition of straight-run naphtha: A promising fuel for advanced compression ignition engines. *Combustion and Flame*, 189:337–346, 2018.

[33] Changyoul Lee, Ahfaz Ahmed, Ehson F. Nasir, Jihad Badra, Gautam Kalghatgi, S. Mani Sarathy, Henry Curran, and Aamir Farooq. Autoignition characteristics of oxygenated gasolines. *Combustion and Flame*, 186:114–128, 2017.

[34] A. Roubaud, R. Minetti, and L.R. Sochet. Oxidation and combustion of low alkylbenzenes at high pressure: comparative reactivity and auto-ignition. *Combustion and Flame*, 121(3):535 – 541, 2000.

[35] International Energy Agency. World Energy Outlook 2018. Technical report, Paris, 2018.

[36] Maxime Pochet. *Investigation of multi-electrofuel use in Homogeneous-Charge Compression-Ignition engines : an experimental focus on*. PhD thesis, UCLouvain, 2019.

[37] Francesco Di Maria and Marzio Lasagni. On line measurement of the lower heating value of waste and energetic efficiency of an existing waste to energy plant: Identification of uncertainty associated to probes and their influence on the results. *Energy Procedia*, 126:613–620, 2017.

[38] OECD. Electricity generation (indicator). 2020.

[39] IEA. Renewables Information 2019 Overview. *Climate Change 2013 - The Physical Science Basis*, 53(9):1–30, 2019.

[40] Avraam Karagiannidis. *Waste to Energy, Opportunities and Challenges for Developing and Transition Economies*. 2012.

[41] Mufeed Sharholy, Kafeel Ahmad, Gauhar Mahmood, and R. C. Trivedi. Municipal solid waste management in Indian cities - A review. *Waste Management*, 28(2):459–467, 2008.

[42] Rotich K. Henry, Zhao Yongsheng, and Dong Jun. Municipal solid waste management challenges in developing countries - Kenyan case study. *Waste Management*, 26(1):92–100, 2006.

[43] Onur Onel, Alexander M. Niziolek, Faruque M.F. Hasan, and Christodoulos A. Floudas. Municipal solid waste to liquid transportation fuels - Part I: Mathematical modeling of a municipal solid waste gasifier. *Computers and Chemical Engineering*, 71:636–647, 2014.

[44] Ch. Achillas, Ch. Vlachokostas, N. Moussiopoulos, G. Banias, G. Kafetzopoulos, and A. Karagiannidis. Social acceptance for the development of a waste-to-energy plant in an urban area. *Resources, Conservation and Recycling*, 55(9):857 – 863, 2011.

[45] Xiangyu Ren, Yue Che, Kai Yang, and Yun Tao. Risk perception and public acceptance toward a highly protested waste-to-energy facility. *Waste Management*, 48:528 – 539, 2016.

[46] Yong Liu, Yujia Ge, Bo Xia, Caiyun Cui, Xiaoyan Jiang, and Martin Skitmore. Enhancing public acceptance towards waste-to-energy incineration projects: Lessons learned from a case study in china. *Sustainable Cities and Society*, 48:101582, 2019.

[47] European Commission. End-of-life vehicle statistics, 2018.

[48] B.J. Jody and E.J. Daniels. End-of-Life Vehicle Recycling : The State of the Art of Resource Recovery from Shredder Residue. Technical report, Argonne National Lab. (ANL), Argonne, IL (United States), 2006.

[49] R. Cossu and T. Lai. Automotive shredder residue (ASR) management: An overview. *Waste Management*, 45:143–151, 2015.

[50] B J Jody, E J Daniels, C M Duranceau, J A Pomykala, and J S Spangenberger. End-of-life vehicle recycling : state of the art of resource recovery from shredder residue. 2 2011.

[51] Valentina Fortunato, Andreas Giraldo, Mehdi Rouabah, Rabia Nacereddine, Michel Delanaye, and Alessandro Parente. Experimental and numerical investigation of a MILD combustion chamber for micro gas turbine applications. *Energies*, 11(12), 2018.

[52] Abdulkadir Ayanoğlu and Recep Yumrutaş. Production of gasoline and diesel like fuels from waste tire oil by using catalytic pyrolysis. *Energy*, 103:456–468, 2016.

[53] Meng Choung Chiong, Cheng Tung Chong, Jo Han Ng, Su Shiung Lam, Manh Vu Tran, William Woei Fong Chong, Mohammad Nazri Mohd Jaafar, and Agustin Valera-Medina. Liquid biofuels production and emissions performance in gas turbines: A review. *Energy Conversion and Management*, 173(July):640–658, 2018.

[54] Min Tae Kim and Doo Soo Kim. Effect of periodic in situ deposition of silica layer on the long term operation of a micro-gas turbine. *Surface and Coatings Technology*, 206(1):117–123, 2011.

[55] Yuhan Huang, Nic C. Surawski, Yuan Zhuang, John L. Zhou, and Guang Hong. Dual injection: An effective and efficient technology to use renewable fuels in spark ignition engines. *Renewable and Sustainable Energy Reviews*, 143(February):110921, 2021.

[56] Mindaugas Melaika, Gilles Herbillon, and Petter Dahlander. Spark ignition engine performance, standard emissions and particulates using GDI, PFI-CNG and DI-CNG systems. *Fuel*, 293:120454, 2021.

[57] P. Obulesu, R. Siva Kumar, and B. Ramanjaneyulu. A experimental test on 2-stroke spark ignition engine with gasoline and methanol-gasoline blends using brass coated piston. *Materials Today: Proceedings*, 39:590–595, 2020.

[58] Anh Tuan Hoang, Sandro Nižetić, and Aykut I. Ölçer. 2,5-Dimethylfuran (DMF) as a promising biofuel for the spark ignition engine application: A comparative analysis and review. *Fuel*, 285(August 2020), 2021.

[59] Zhenbiao Zhou, Tanmay Kar, Yi Yang, Michael Brear, Jingran Xu, Joshua Lacey, Thomas Leone, James Anderson, Michael Shelby, and Eric Curtis. Mapping K factor variations and its causes in a modern, spark-ignition engine. *Fuel*, 290(August 2020):120012, 2021.

[60] Pavlos Dimitriou and Rahat Javaid. A review of ammonia as a compression ignition engine fuel. *International Journal of Hydrogen Energy*, 45(11):7098–7118, 2020.

[61] Yifeng Wang, Mingfa Yao, Tie Li, Weijing Zhang, and Zunqing Zheng. A parametric study for enabling reactivity controlled compression ignition (RCCI) operation in diesel engines at various engine loads. *Applied Energy*, 175:389–402, 2016.

[62] Anh Tuan Hoang, Sandro Nižetić, Van Viet Pham, Anh Tuan Le, Van Ga Bui, and Van Vang Le. Combustion and emission characteristics of spark and compression ignition engine fueled with 2,5-dimethylfuran (DMF): A comprehensive review. *Fuel*, 288(June 2020), 2021.

[63] M. Mani, G. Nagarajan, and S. Sampath. Characterisation and effect of using waste plastic oil and diesel fuel blends in compression ignition engine. *Energy*, 36(1):212–219, 2011.

[64] Sachin Kumar, R. Prakash, S. Murugan, and R. K. Singh. Performance and emission analysis of blends of waste plastic oil obtained by catalytic pyrolysis of waste HDPE with diesel in a CI engine. *Energy Conversion and Management*, 74:323–331, 2013.

[65] Yanzhao An, Mohammed Jaasim, Vallinayagam Raman, Francisco E. Hernández Pérez, Hong G. Im, and Bengt Johansson. Homogeneous charge compression ignition (HCCI) and partially premixed combustion (PPC) in compression ignition engine with low octane gasoline. *Energy*, 158(X):181–191, 2018.

[66] Francesco Contino, Philippe Dagaut, Fabien Halter, Jean-Baptiste Masurier, Guillaume Dayma, Christine Mounaim-Rousselle, and Fabrice Foucher. Screening method for fuels in homogeneous charge compression ignition engines: application to valeric biofuels. *Energy & Fuels*, page acs.energyfuels.6b02300, 2016.

[67] Subir Bhaduri, Benjamin Berger, Maxime Pochet, Hervé Jeanmart, and Francesco Contino. HCCI engine operated with unscrubbed biomass syngas. *Fuel Processing Technology*, 157:52–58, 2017.

[68] Maxime Pochet, Véronique Dias, Hervé Jeanmart, Sebastian Verhelst, and Francesco Contino. Multifuel CHP HCCI Engine towards Flexible Power-to-fuel: Numerical Study of Operating Range. *Energy Procedia*, 105:1532–1538, 2017.

[69] Maxime Pochet, Véronique Dias, Bruno Moreau, Fabrice Foucher, Hervé Jeanmart, and Francesco Contino. Experimental and numerical study, under LTC conditions, of ammonia ignition delay with and without hydrogen addition. *Proceedings of the Combustion Institute*, 000:1–9, 2018.

[70] Maxime Pochet, Ida Truedsson, Fabrice Foucher, Hervé Jeanmart, and Francesco Contino. Ammonia-hydrogen blends in homogeneous-charge compression-ignition engine. In *13th International Conference on Engines & Vehicles*. SAE International, sep 2017.

[71] Subir S Bhaduri. Experimental Studies on HCCI Combustion of Biomass Syngas Towards Tar Tolerant Operation. 2015.

[72] Yaopeng Li, Ming Jia, Yachao Chang, Maozhao Xie, and Rolf D. Reitz. Towards a comprehensive understanding of the influence of fuel properties on the combustion characteristics of a RCCI (reactivity controlled compression ignition) engine. *Energy*, 99(x):69–82, 2016.

[73] Rolf D. Reitz and Ganesh Duraisamy. Review of high efficiency and clean reactivity controlled compression ignition (RCCI) combustion in internal combustion engines. *Progress in Energy and Combustion Science*, 46:12–71, 2015.

[74] Amin Paykani, Antonio Garcia, Mahdi Shahbakhti, Pourya Rahnama, and Rolf D. Reitz. Reactivity controlled compression ignition engine: Pathways towards commercial viability. *Applied Energy*, 282(PA):116174, 2021.

[75] M Ichikawa, N Nonaka, H Amano, I Takada, and S Ishimori. Proton NMR Analysis of Octne Number for Motor Gasoline: Part IV. *Applied Spectroscopy*, 45(4):637–640, 1991.

[76] M Ichikawa, N Nonaka, H Amano, I Takada, and S Ishimori. Proton NMR Analysis of Octne Number for Motor Gasoline: Part II. *Applied Spectroscopy*, 45(4):637–640, 1991.

[77] Directive 2009/30/ec of the european parliament and of the council. *OJ*, L 140:88–113, 5.6.2009.

[78] Jean-Claude Guibet. *Carburants et moteurs technologies, énergie, environnement Tome 1*. Publications de l'Institut Français du Pétrole. éd. Technip, Paris, nouvelle édition edition, 1997.

[79] Nada Štrumberger, Alen Gospočić, Morh Hvu, and Čedomir Bartulić. Polymeric materials in automobiles. *Promet - Traffic - Traffico*, 17(3):149–160, 2005.

[80] Moinuddin Sarker, Mohammad Mamunor Rashid, Mohammed Molla, and Muhammad Sadikur Rahman. Thermal Conversion of Waste Plastics (HDPE , PP and PS) to Produce Mixture of Hydrocarbons. *American Journal of Environmental Engineering*, 2(5):128–136, 2012.

[81] ASTM International. ASTM D2699-15a, Standard Test Method for Research Octane Number of Spark-Ignition Engine Fuel. 2015.

[82] ASTM International. ASTM D2700-16a, Standard Test Method for Motor Octane Number of Spark-Ignition Engine Fuel. 2016.

[83] William J. Pitz and Charles J. Mueller. Recent progress in the development of diesel surrogate fuels. *Progress in Energy and Combustion Science*, 37(3):330–350, 2011.

[84] Jin Yu, Yiguang Ju, and Xiaolong Gou. Surrogate fuel formulation for oxygenated and hydrocarbon fuels by using the molecular structures and functional groups. *Fuel*, 166:211–218, 2015.

[85] Cécile Pera and Vincent Knop. Methodology to define gasoline surrogates dedicated to auto-ignition in engines. *Fuel*, 96:59–69, 2012.

[86] Ahfaz Ahmed, Gokop Goteng, Vijai S B Shankar, Khalid Al-Qurashi, William L. Roberts, and S. Mani Sarathy. A computational methodology for formulating gasoline surrogate fuels with accurate physical and chemical kinetic properties. *Fuel*, 143:290–300, 2015.

[87] Steven Tipler, Alessandro Parente, Steffen H. Symoens, Marko R. Djokic, Kevin M. Van Geem, Francesco Contino, and Axel Coussement. Prediction of the piona and oxygenate composition of unconventional fuels with the pseudo-component property estimation (pcpe) method. application to an automotive shredder residues-derived gasoline. In *WCX World Congress Experience*. SAE International, apr 2018.

[88] S. Tipler, M. Fürst, Q. Van Haute, F. Contino, and A. Coussement. Prediction of the octane number: A bayesian pseudo-component method. *Energy & Fuels*, 34(10):12598–12605, 2020.

[89] S. Tipler, C. S. Mergulhaõ, G. Vanhove, Q. Van Haute, F. Contino, and A. Coussement. Ignition study of an oxygenated and high-alkene light petroleum fraction produced from automotive shredder residues. *Energy and Fuels*, 33(6):5664–5672, 2019.

[90] Steven Tipler, Giuseppe D'Alessio, Quentin Van Haute, Francesco Contino, and Axel Coussement. Predicting octane numbers with inexpensive properties relying on principal component analysis and artificial neural network. *To be submitted*.

[91] James G. Speight. The Chemistry and Technology of Petroleum. 2006.

[92] Li Robinson, Paul R. Walters, Clifford C. Watt, Murray R Roussis, Stilianos G Briker, Yevgenia Ring, Zbigniew Yang, Hong Xieqing, Wang Chaogang, Xie Zaiting and Esber I. Genquan, Zhu O'Connor, P. Robinson, Paul R. Dolbear, Geofrey E. Gruia, Adrian Mochida, Isao Choi, Ki-Hyouk Cooper, Barry H. Knudsen, Kim G. Song, Chunshan Ma, Xiaoliang Skov, Ebbe R. Dolbear, Geoffrey E. Bingham, F.Ellett Nelson, Douglas E. Shaheen, Eli I. *Practical Advances in Petroleum Processing Volume 1*, volume 1-2. 2012.

[93] Akshat Patil, Arun Patel, and Rajesh Purohit. An overview of Polymeric Materials for Automotive Applications. *Materials Today: Proceedings*, 4(2):3807–3815, 2017.

[94] B Petruson, S Jacobsson, P Pfaffli, A Zitting, and H Frostling. Degradation products of plastics. Polyethylene and styrene-containing thermoplastics–analytical, occupational and toxicologic aspects. *Scand J Work Environ Health*, 8(2):1–60, 1982.

[95] Nimal Naser, Seung Yeon Yang, Gautam Kalghatgi, and Suk Ho Chung. Relating the octane numbers of fuels to ignition delay times measured in an ignition quality tester (IQT). *Fuel*, 187:117–127, 2017.

[96] William R Leppard. The Autoignition Chemistries of Primary Reference Fuels, Olefin/Paraffin Binary Mixtures, and Non-Linear Octane Blending. *SAE Technical Paper*, (922325), 1992.

[97] Nimal Naser, S. Mani Sarathy, and Suk Ho Chung. Ignition delay time sensitivity in ignition quality tester (IQT) and its relation to octane sensitivity. *Fuel*, 233(June):412–419, 2018.

[98] G. T. Kalghatgi. Fuel anti-knock quality-part I. Engine studies. *SAE Technical Papers*, (September 2001), 2001.

[99] G. T. Kalghatgi. Fuel anti-knock quality-part II. Vehicle studies-how relevant is motor octane number (MON) in modern engines? *SAE Technical Papers*, (September 2001), 2001.

[100] ASTM International. ASTM D613. Standard test method for cetane number of diesel oil.

[101] Noel Bezaire, Kapila Wadumesthrige, K. Y. Simon Ng, and Steven O. Salley. Limitations of the use of cetane index for alternative compression ignition engine fuels. *Fuel*, 89(12):3807–3813, 2010.

[102] ASTM International. Standard test method for determination of ignition delay and derived cetane number DCN of diesel fuel oils by combustion in a constant volume chamber.

[103] ASTM International. ASTM D86 - 17, Standard Test Method for Distillation of Petroleum Products and Liquid Fuels at Atmospheric Pressure, 2017.

[104] K.M. Watson and E.F. Nelson. Improved Methods for Approximating Critical and Thermal Properties of Petroleum Fractions. *Industrial and Engineering Chemistry*, 25:880–887, 1933.

[105] Danilo Luiz Flumignan, Fabrício de Oliveira Ferreira, Aristeu Gomes Tininis, and José Eduardo de Oliveira. Multivariate calibrations in gas chromatographic profiles for prediction of several physicochemical parameters of brazilian commercial gasoline. *Chemometrics and Intelligent Laboratory Systems*, 92(1):53 – 60, 2008.

[106] Nikos Pasadakis, Vassilis Gaganis, and Charalambos Foteinopoulos. Octane number prediction for gasoline blends. *Fuel Processing Technology*, 87(6):505 – 509, 2006.

[107] Jaqueline M. de Paulo, José E.M. Barros, and Paulo J.S. Barbeira. A pls regression model using flame spectroscopy emission for determination of octane numbers in gasoline. *Fuel*, 176:216 – 221, 2016.

[108] Don-Min Lee, Dong-Hyun Lee, and In-Ha Hwang. Gasoline quality assessment using fast gas chromatography and partial least-squares regression for the detection of adulterated gasoline. *Energy & Fuels*, 32(10):10556–10562, 2018.

[109] Abdul Gani Abdul Jameel, Vincent Van Oudenhoven, Abdul-Hamid Emwas, and S. Mani Sarathy. Predicting octane number using nuclear magnetic resonance spectroscopy and artificial neural networks. *Energy & Fuels*, 32(5):6309–6329, 2018.

[110] Jeffrey J. Kelly, Clyde H. Barlow, Thomas M. Jinguji, and James B. Callis. Prediction of gasoline octane numbers from near-infrared spectral features in the range 660-1215 nm. *Analytical Chemistry*, 61(4):313–320, 1989.

[111] Gisele Mendes, Helga G. Aleme, and Paulo J.S. Barbeira. Determination of octane numbers in gasoline by distillation curves and partial least squares regression. *Fuel*, 97:131 – 136, 2012.

[112] M.V. Maylin, M.V. Kirgina, E.V. Sviridova, B.V. Sakhnevitch, and E.D. Ivanchina. Calculation of gasoline octane numbers taking into account the reaction interaction of blend components. *Procedia Chemistry*, 10:477 – 484, 2014. XV International Scientific Conference "Chemistry and Chemical Engineering in XXI century" dedicated to Professor L.P. Kulyov.

[113] Jihad A. Badra, Nehal Bokhumseen, Najood Mulla, S. Mani Sarathy, Aamir Farooq, Gautam Kalghatgi, and Patrick Gaillard. A methodology to relate octane numbers of binary and ternary n-heptane, iso-octane and toluene mixtures with simulated ignition delay times. *Fuel*, 160:458–469, 2015.

[114] Neal Morgan, Andrew Smallbone, Amit Bhave, Markus Kraft, Roger Cracknell, and Gautam Kalghatgi. Mapping surrogate gasoline compositions into RON/MON space. *Combustion and Flame*, 157(6):1122–1131, 2010.

[115] Hadeel Solaka Aronsson, Martin Tuner, and Bengt Johansson. Using oxygenated gasoline surrogate compositions to map RON and MON. *SAE Technical Papers*, 1, 2014.

[116] Tareq a. Albahri. Structural Group Contribution Method for Predicting the Octane Number of Pure Hydrocarbon Liquids. *Industrial & Engineering Chemistry Research*, 42(3):657–662, 2003.

[117] Reinhard Meusinger. Gasoline analysis by 1H nuclear magnetic resonance spectroscopy. *Fuel*, 75(10):1235–1243, 1996.

[118] Timothy H. DeFries, Rodney V. Kastrup, and Doren Indritz. Prediction of cetane number by group additivity and carbon-13 Nuclear Magnetic Resonance. *Ind. Eng. Chem. Res*, 26:188–193, 1987.

[119] William L Kubic. A Group Contribution Method for Estimating Cetane and Octane Numbers. Technical report, Los Alamos National Laboratory, 2016.

[120] M. R. Riazi. *Prediction of Thermophisical Properties of Petroleum Fractions*. PhD thesis, Pennsylvania State University, 1979.

[121] M. R. Riazi and T.E. Daubert. Prediction of the Composition of Petroleum Fractions. *Industrial and Engineering Chemistry, Process Design and Development*, 19(2):289–294, 1980.

[122] M. R. Riazi and T.E. Daubert. Prediction of Molecular Type Analysis of Petroleum Fractions and Coal Liquids. *Industrial and Engineering Chemistry, Process Design and Development*, 25(4):1009–1015, 1986.

[123] M. R. Riazi and Y. Roomi. Use of the Refractive Index in the Estimation of Thermophysical Properties of Hydrocarbons and Their Mixtures. *Industrial and Engineering Chemistry Research*, 40(8):1975–1984, 2001.

[124] Abdul Gani Abdul Jameel, Nimal Naser, Abdul Hamid Emwas, and S. Mani Sarathy. Surrogate formulation for diesel and jet fuels using the minimalist functional group (MFG) approach. In *Proceedings of the Combustion Institute*, volume 37, pages 4663–4671. Elsevier Inc., 2019.

[125] R. Vallinayagam, S. Vedharaj, Yanzhao An, Alaaeldin Dawood, Mohammad Izadi Najafabadi, Bart Somers, Junseok Chang, Mani Sarathy, and Bengt Johansson. Compression Ignition of Light Naphtha and Its Multicomponent Surrogate under Partially Premixed Conditions. *SAE Technical Papers*, 2017-Septe(September), 2017.

[126] Peter L. Perez and André L. Boehman. Effects of the chemical structure and composition of surrogate gasoline fuels on homogeneous charge compression ignition combustion in a single-cylinder engine. *Energy and Fuels*, 28(5):3377–3390, 2014.

[127] E. Agbro, A. S. Tomlin, W. Zhang, A. Burluka, F. Mauss, M. Pasternak, A. Alfazazi, and S. M. Sarathy. Chemical Kinetic Modeling Study on the Influence of n-Butanol Blending on the Combustion, Autoignition, and Knock Properties of Gasoline and Its Surrogate in a Spark-Ignition Engine. *Energy and Fuels*, 32(10):10065–10077, 2018.

[128] J. C.G. Andrae. Kinetic Modeling of the Influence of Cyclohexane on the Homogeneous Ignition of a Gasoline Surrogate Fuel. *Energy and Fuels*, 32(3):3975–3984, 2018.

[129] J. C G Andrae and R. A. Head. HCCI experiments with gasoline surrogate fuels modeled by a semidetailed chemical kinetic model. *Combustion and Flame*, 156(4):842–851, 2009.

[130] M. Yahyaoui, N. Djebaïli-Chaumeix, P. Dagaut, C. E. Paillard, and S. Gail. Experimental and modelling study of gasoline surrogate mixtures oxidation in jet stirred reactor and shock tube. *Proceedings of the Combustion Institute*, 31 I:385–391, 2007.

[131] S. Humer, A. Frassoldati, S. Granata, T. Faravelli, E. Ranzi, R. Seiser, and K. Seshadri. Experimental and kinetic modeling study of combustion of JP-8, its surrogates and reference components in laminar nonpremixed flows. *Proceedings of the Combustion Institute*, 31 I:393–400, 2007.

[132] Vincent Knop, Cécile Pera, and Florence Duffour. Validation of a ternary gasoline surrogate in a CAI engine. *Combustion and Flame*, 160(10):2067–2082, 2013.

[133] S. Mani Sarathy, Aamir Farooq, and Gautam T. Kalghatgi. Recent progress in gasoline surrogate fuels. *Progress in Energy and Combustion Science*, 65:67–108, 2018.

[134] Abdul Gani Abdul Jameel, Nimal Naser, Gani Issayev, Jamal Touitou, Manik Kumer Ghosh, Abdul Hamid Emwas, Aamir Farooq, Stephen Dooley, and S. Mani Sarathy. A minimalist functional group (MFG) approach for surrogate fuel formulation. *Combustion and Flame*, 192:250–271, 2018.

[135] Salvatore Iavarone. Uncertainty Quantification for Scale-Bridging Modeling of Multiphase Reactive Flows. 2019.

[136] Alessandro Parente and James C. Sutherland. Principal component analysis of turbulent combustion data: Data pre-processing and manifold sensitivity. *Combustion and Flame*, 160(2):340 – 350, 2013.

[137] Alexander J. Josephson, Neal D. Gaffin, Sean T. Smith, Thomas H. Fletcher, and David O. Lignell. Modeling Soot Oxidation and Gasification with Bayesian Statistics. *Energy and Fuels*, 31(10):11291–11303, 2017.

[138] Andrew Gelman. Bayesian Data Analysis.

[139] John B. Heywood. *Internal combustion engine fundamentals*. 1988.

[140] Joeri De Coster. Dynamic of combustion in high efficiency piston engine using waste - derived fuels engine using waste-derived fuels. 2016.

[141] IFP School. Chapitre 2: Simulation des cycles thermodynamiques dans les moteurs. In *Etude des cycles thermodynamiques des moteurs thermiques et modélisation*. 2007.

[142] ASTM International. ASTM D5134–13, Standard Test Method for Detailed Analysis of Petroleum Naphthas through n–Nonane by Capillary Gas Chromatography, 2013.

[143] ASTM International. ASTM D6729–14, Standard Test Method for Determination of Individual Components in Spark Ignition Engine Fuels by 100–Metre Capillary High Resolution Gas Chromatography, 2014.

[144] ASTM International. ASTM D6730–01(2016), Standard Test Method for Determination of Individual Components in Spark Ignition Engine Fuels by 100–Metre Capillary (with Precolumn) High–Resolution Gas Chromatography, 2016.

[145] ASTM International. ASTM D6733–01(2016), Standard Test Method for Determination of Individual Components in Spark Ignition Engine Fuels by 50–Metre Capillary High Resolution Gas Chromatography, 2016.

[146] ASTM International. ASTM D6839–16, Standard Test Method for Hydrocarbon Types, Oxygenated Compounds, and Benzene in Spark Ignition Engine Fuels by Gas Chromatography, 2016.

[147] Mariel E. Flood, Mary P. Connolly, Michael C. Comiskey, and Amber M. Hupp. Evaluation of single and multi–feedstock biodiesel – diesel blends using GCMS and chemometric methods. *Fuel*, 186:58–67, 2016.

[148] J a Widegren Bruno, T.J. Thermal decomposition kinetics of the aviation fuel Jet-A. *Ind. Eng. Chem. Res.*, 47(13):4342–4348, 2008.

[149] John B. Liu, Zaiyou, Phillips. Comprehensive Two–Dimensional Gas Chromatography using an On–Column Thermal Modulator Interface. *Journal of Chromatographic Science*, 29:227–231, 1991.

[150] Huang Zeng, Fenglou Zou, Eric Lehne, Julian Y. Zuo, and Dan Zhang. Gas Chromatograph Applications in Petroleum Hydrocarbon Fluids. *Advanced Gas Chromatography– Progress in Agricultural, Biomedical and Industrial Applications*, pages 363–388, 2012.

[151] Frédérick Adam, Fabrice Bertoncini, Vincent Coupard, Nadège Charon, Didier Thiébaut, Didier Espinat, and Marie Claire Hennion. Using comprehensive two–dimensional gas chromatography for the analysis of oxygenates in middle distillates. I. Determination of the nature of biodiesels blend in diesel fuel. *Journal of Chromatography A*, 1186(1–2):236–244, 2008.

[152] Ehsan Alborzi, Simon Blakey, Hassan Ghadbeigi, Christophe Pinna, and Christopher Lewis. Investigation of surface deposition in a simulated fuel injector feed arm with sudden expansion/contraction. *Fuel*, 186:534–543, 2016.

[153] Toby Rockstroh, Gareth Floweday, and Andy Yates. Optimisation of synthetic gasoline blend recipes for use in modern charge boosted GDI engines. *Fuel*, 186:800–820, 2016.

[154] Frank Cheng Yu Wang, Kuangnan Qian, and Larry A. Green. GC x MS of diesel: A two–dimensional separation approach. *Analytical Chemistry*, 77(9):2777–2785, 2005.

[155] M.K. Jennerwein, A.C. Sutherland, M. Eschner, T. Gröger, T. Wilharm, and R. Zimmermann. Quantitative analysis of modern fuels derived from middle distillates – The impact of diverse compositions on standard methods evaluated by an offline hyphenation of HPLC-refractive index detection with GC×GC–TOFMS. *Fuel*, 187:16–25, 2017.

[156] Nenad D. Ristic, Marko R. Djokic, Alar Konist, Kevin Van Geem, and Guy B. Marin. Quantitative compositional analysis of Estonian shale oil using comprehensive two dimensional gas chromatography. *Fuel Processing Technology*, 167:241–249, 2017.

[157] ASTM International. UOP990–11, Organic Analysis of Distillate by Comprehensive Two–Dimensional Gas Chromatography with Flame Ionization Detection, 2011.

[158] Tarek Ahmed. *Hydrocarbon Phase Behavior*. Gulf Publishing Company, 1989.

[159] Hua Mei, Zhenlei Wang, and Biao Huang. Molecular-Based Bayesian Regression Model of Petroleum Fractions. *Industrial and Engineering Chemistry Research*, 56(50):14865–14872, 2017.

[160] Thanh Binh Nguyen, Nicolas Riesco, and Velisa Vesovic. Predicting the viscosity of n-alkane liquid mixtures based on molecular description. *Fuel*, 208:363–376, 2017.

[161] Xiaochun Xu, Jean Noël Jaubert, Romain Privat, Pierre Duchet-Suchaux, and Francisco Braña-Mulero. Predicting Binary-Interaction Parameters

of Cubic Equations of State for Petroleum Fluids Containing Pseudo-components. *Industrial and Engineering Chemistry Research*, 54(10):2816–2824, 2015.

[162] F. Ramos-Pallares, F. F. Schoeggl, S. D. Taylor, and H. W. Yarranton. Prediction of thermal conductivity for characterized oils and their fractions using an expanded fluid based model. *Fuel*, 234(April):66–80, 2018.

[163] Donald B. Brooks and Robetta B. Cleaton. The precision of knock rating — 1936-1938: Report from cooperative fuel research committee. *SAE Transactions*, 34:449–456, 1939.

[164] Roland Dauphin, Jerome Obiols, David Serrano, Yann Fenard, Andrea Comandini, Laurie Starck, Guillaume Vanhove, and Nabiha Chaumeix. Using ron synergistic effects to formulate fuels for better fuel economy and lower co2 emissions. In *SAE Technical Paper*. SAE International, 12 2019.

[165] B. Doicin and I. Onutu. Octane Number Estimation Using Neural Networks. *Revista de Chimie*, 65(5):599–602, 2014.

[166] Emad Al Ibrahim and Aamir Farooq. Octane Prediction from Infrared Spectroscopic Data. *Energy & Fuels*, 34:817–826, 2020.

[167] William L. Kubic, Rhodri W. Jenkins, Cameron M. Moore, Troy A. Semelsberger, and Andrew D. Sutton. Artificial Neural Network Based Group Contribution Method for Estimating Cetane and Octane Numbers of Hydrocarbons and Oxygenated Organic Compounds. *Industrial and Engineering Chemistry Research*, 56(42):12236–12245, 2017.

[168] Florian vom Lehn, Benedict Brosius, Rafal Broda, Liming Cai, and Heinz Pitsch. Using machine learning with target-specific feature sets for structure-property relationship modeling of octane numbers and octane sensitivity. *Fuel*, 281(July):118772, 2020.

[169] American Petroleum Institute. Technical Data Book- Petroleum Refining. 1997.

[170] A. Parente, J. C. Sutherland, L. Tognotti, and P. J. Smith. Identification of low-dimensional manifolds in turbulent flames. *Proceedings of the Combustion Institute*, 32 I(1):1579–1586, 2009.

[171] I. T. Jolliffe. Discarding Variables in a Principal Component Analysis. II: Real Data. *Applied Statistics*, 22(1):21, 1973.

[172] W.J. Krzanowski. Selection of Variables to Preserve Multivariate Data Structure, Using Principal Components. *Journal of the Royal Statistical Society. Series C (Applied Statistics)*, 36(1):22–33, 1987.

[173] Axel Coussement, Olivier Gicquel, and Alessandro Parente. MG-local-PCA method for reduced order combustion modeling. *Proceedings of the Combustion Institute*, 34(1):1117–1123, 2013.

[174] Benjamin J. Isaac, Axel Coussement, Olivier Gicquel, Philip J. Smith, and Alessandro Parente. Reduced-order PCA models for chemical reacting flows. *Combustion and Flame*, 161(11):2785–2800, 2014.

[175] Giuseppe D'Alessio, Antonio Attili, Alberto Cuoci, Heinz Pitsch, and Alessandro Parente. Unsupervised data analysis of direct numerical simulation of a turbulent flame via local principal component analysis and procustes analysis. In *International Workshop on Soft Computing Models in Industrial and Environmental Applications*, pages 460–469. Springer, 2020.

[176] M. Mehl, J. Y. Chen, W. J. Pitz, S. M. Sarathy, and C. K. Westbrook. An approach for formulating surrogates for gasoline with application toward a reduced surrogate mechanism for cfd engine modeling. *Energy & Fuels*, 25(11):5215–5223, 2011.

[177] William R. Leppard. The chemical origin of fuel octane sensitivity. In *International Fuels & Lubricants Meeting & Exposition*. SAE International, oct 1990.

[178] Felicite Jarrosson, Yann Fenard, Guillaume Vanhove, and Roland Dauphin. Gasoline and combustion: Relationship between molecular structure and performance. In *SAE Technical Paper*. SAE International, 04 2018.

[179] Judit Zádor, Craig A. Taatjes, and Ravi X. Fernandes. Kinetics of elementary reactions in low-temperature autoignition chemistry. *Progress in Energy and Combustion Science*, 37(4):371 – 421, 2011.

[180] Henry J. Curran. Developing detailed chemical kinetic mechanisms for fuel combustion. *Proceedings of the Combustion Institute*, 2018.

[181] G. Vanhove, G. Petit, and R. Minetti. Experimental study of the kinetic interactions in the low-temperature autoignition of hydrocarbon binary mixtures and a surrogate fuel. *Combustion and Flame*, 145(3):521 – 532, 2006.

[182] Michael D. Boot, Miao Tian, Emiel J.M. Hensen, and S. Mani Sarathy. Impact of fuel molecular structure on auto-ignition behavior – Design rules for future high performance gasolines. *Progress in Energy and Combustion Science*, 60:1–25, 2017.

[183] S. S. Kurtz and A. L. Ward. The Refractivity Intercept and the Specific Refraction Equation of Newton, I: Development of the Refractivity Intercept and Composition with Specific Refraction Equations. *Journal of Franklin Institute*, 222:563–592, 1936.

[184] ASTM International. ASTM D4052 - 18, Standard Test Method for Density, Relative Density, and API Gravity of Liquids by Digital Density Meter. 2018.

[185] Y. Fenard, M.A. Boumehdi, and G. Vanhove. Experimental and kinetic modeling study of 2-methyltetrahydrofuran oxidation under engine-relevant conditions. *Combustion and Flame*, 178:168 – 181, 2017.

[186] S. Scott Goldsborough, Simone Hochgreb, Guillaume Vanhove, Margaret Wooldridge, Henry J Curran, and Chih-Jen Sung. Advances in rapid compression machine studies of low- and intermediate-temperature autoignition phenomena. *Progress in Energy and Combustion Science*, 63:1 – 78, November 2017.

[187] Daeyup Lee and Simone Hochgreb. Rapid compression machines: Heat transfer and suppression of corner vortex. *Combustion and Flame*, 114(3-4):531–545, 1998.

[188] S. V. Khandal, N. R. Banapurmath, and V. N. Gaitonde. Performance studies on homogeneous charge compression ignition (HCCI) engine powered with alternative fuels. *Renewable Energy*, 132(x):683–693, 2019.

[189] Zhi Wang, Haoye Liu, Xiao Ma, Jianxin Wang, Shijin Shuai, and Rolf D. Reitz. Homogeneous charge compression ignition (hcci) combustion of polyoxymethylene dimethyl ethers (pode). *Fuel*, 183:206–213, 2016.

[190] Mina Nishi, Masato Kanehara, and Norimasa Iida. Assessment for innovative combustion on hcci engine by controlling egr ratio and engine speed. *Applied Thermal Engineering*, 99:42–60, 2016.

[191] Nicolas Bourgeois, S Scott Goldsborough, Guillaume Vanhove, Matthieu Duponcheel, Hervé Jeanmart, and Francesco Contino. CFD simulations of Rapid Compression Machines using detailed chemistry : Impact of multi-dimensional effects on the auto-ignition of the iso-octane. *Proceedings of the Combustion Institute*, 36(1):383–391, 2017.

[192] A. Cuoci, A. Frassoldati, T. Faravelli, and E. Ranzi. Opensmoke++: An object-oriented framework for the numerical modeling of reactive systems with detailed kinetic mechanisms. *Computer Physics Communications*, 192:237 – 264, 2015.

[193] Marco Mehl, William J. Pitz, Charles K. Westbrook, and Henry J. Curran. Kinetic modeling of gasoline surrogate components and mixtures under engine conditions. *Proceedings of the Combustion Institute*, 33(1):193 – 200, 2011.

[194] F. Battin-Leclerc. Detailed chemical kinetic models for the low-temperature combustion of hydrocarbons with application to gasoline and diesel fuel surrogates. *Progress in Energy and Combustion Science*, 34(4):440 – 498, 2008.

[195] G. Vanhove, R. Minetti, S. Touchard, R. Fournet, P.A. Glaude, and F. Battin-Leclerc. Experimental and modeling study of the autoignition of 1-hexene/isooctane mixtures at low temperatures. *Combustion and Flame*, 145(1):272 – 281, 2006.

[196] G. Vanhove, M. Ribaucour, and R. Minetti. On the influence of the position of the double bond on the low-temperature chemistry of hexenes. *Proceedings of the Combustion Institute*, 30(1):1065 – 1072, 2005.

[197] Marco Mehl, Guillaume Vanhove, William J. Pitz, and Eliseo Ranzi. Oxidation and combustion of the n-hexene isomers: A wide range kinetic modeling study. *Combustion and Flame*, 155(4):756 – 772, 2008.

[198] C. Franklin Goldsmith, William H. Green, and Stephen J. Klippenstein. Role of o2 + qooh in low-temperature ignition of propane. 1. temperature and pressure dependent rate coefficients. *The Journal of Physical Chemistry A*, 116(13):3325–3346, 2012. PMID: 22250995.

[199] Ultan Burke, Joachim Beeckmann, Wassja A. Kopp, Yasar Uygun, Herbert Olivier, Kai Leonhard, Heinz Pitsch, and K. Alexander Heufer. A comprehensive experimental and kinetic modeling study of butanone. *Combustion and Flame*, 168:296 – 309, 2016.

[200] Miao Tian, Robert L. McCormick, Matthew A. Ratcliff, Jon Luecke, Janet Yanowitz, Pierre Alexandre Glaude, Michel Cuijpers, and Michael D. Boot. Performance of lignin derived compounds as octane boosters. *Fuel*, 189:284–292, 2017.

APPENDIX A: COMPOSITION OF THE ASR LIGHT FRACTION

Molecule	HCgroup	Number id.	Mean molar x	Std. Dev.
2.4-Dimethyl-1-Heptene	Olefin	3	16.49%	0.52%
Styrene	Monoaromatic	3	8.29%	0.24%
Ethylbenzene	Monoaromatic	3	6.61%	0.17%
n-C3 Cyclohexane	Naphthene	3	5.36%	0.61%
Toluene	Monoaromatic	3	5.15%	0.01%
C8 Isoparaffins	Iso-paraffin	3	3.10%	0.18%
C9 Isoparaffins	Iso-paraffin	3	3.00%	0.05%
C3 Benzene	Monoaromatic	3	2.92%	0.08%
Alpha-Methylstyrene	Monoaromatic	3	2.59%	0.06%
Ethyl-cyclohexane	Naphthene	3	2.35%	0.49%
C10 Isoparaffins	Iso-paraffin	3	2.24%	0.13%
Olefins C6	Olefin	3	2.17%	0.17%
Benzene	Monoaromatic	3	2.02%	0.10%
Olefins C8	Olefin	3	1.81%	0.18%
C2 Benzene	Monoaromatic	3	1.78%	0.08%
Olefins C7	Olefin	3	1.67%	0.70%
Olefins C10	Olefin	3	1.44%	0.60%
C12 Olefins	Olefin	3	1.40%	0.04%
Olefins C9	Olefin	3	1.40%	0.09%
C11 Isoparaffins	Iso-paraffin	3	1.25%	0.03%
Nonane	n-Paraffin	3	1.20%	0.10%
C8H18O	Oxygenate	3	1.09%	0.06%
Heptane	n-Paraffin	3	0.92%	0.07%
Decane	n-Paraffin	3	0.87%	0.07%
C5H10O Isomers	Oxygenate	3	0.85%	0.19%
C8 Naphthenics	Naphthene	3	0.81%	0.01%
C3H8O2	Oxygenate	2	0.81%	1.11%
C4 Benzene	Monoaromatic	3	0.76%	0.16%
Octane	n-Paraffin	3	0.74%	0.33%
Aniline	Nitrogen	3	0.69%	0.05%
C4H8O2 Isomers	Oxygenate	2	0.59%	0.17%
1-Pentene	Olefin	3	0.59%	0.11%
C9 Mononaphthenes	Naphthene	3	0.55%	0.05%
1-Pentanol	Oxygenate	3	0.54%	0.22%
C8H12 Naphthenics	Naphthene	3	0.53%	0.07%
C7 Naphthenics	Naphthene	3	0.53%	0.19%
3-Hexanone	Oxygenate	2	0.50%	0.53%
C8H12 Isomers	Naphthene	2	0.49%	0.01%
C7 Isoparaffins	Iso-paraffin	1	0.47%	0.00%
2-Pentene	Olefin	3	0.47%	0.42%
Hexane	n-Paraffin	3	0.46%	0.22%
C6H12O2 Isomers	Oxygenate	3	0.45%	0.19%
n-C4 Cyclohexane	Naphthene	3	0.45%	0.13%
C11 Naphthenics	Naphthene	3	0.42%	0.04%
3-Heptanone	Oxygenate	2	0.42%	0.53%
C11 Olefins	Olefin	3	0.41%	0.09%
C10 Naphthenics	Naphthene	3	0.39%	0.02%
C6H14O	Oxygenate	2	0.39%	0.15%
3-Pentanone	Oxygenate	1	0.37%	0.00%
Undecane	n-Paraffin	3	0.35%	0.01%
2-Methyl-3-Pentanone	Oxygenate	3	0.32%	0.02%

Table 47: Composition of the light fraction from automotive shredder residues (ASR) analyzed by comprehensive two dimensional gas chromatography (GC × GC): 1/3

Molecule	HCgroup	Number id.	Mean molar x	Std. Dev.
D-Limonene	Naphthene	3	0.31%	0.01%
C5 Benzene	Monoaromatic	3	0.30%	0.01%
2-Hexanone	Oxygenate	1	0.29%	0.00%
2-Pentanone	Oxygenate	3	0.29%	0.10%
C15H30 Isomers	Naphthene	3	0.29%	0.01%
Cyclopentanol	Oxygenate	2	0.26%	0.34%
C12 Isoparaffins	Iso-paraffin	3	0.24%	0.01%
C6H12 Isomers	Olefin	3	0.24%	0.03%
Phenol	Oxygenate	3	0.24%	0.03%
n-C5 Cyclohexane	Naphthene	3	0.23%	0.03%
C7H10 Isomers	Naphthenoaromatic	3	0.22%	0.02%
1-Heptyne	Olefin	1	0.22%	0.00%
C7H14O Isomers	Oxygenate	3	0.22%	0.03%
C13 Isoparaffins	Iso-paraffin	3	0.22%	0.02%
6-Dodecene	Olefin	3	0.22%	0.03%
1-Heptene	Olefin	3	0.21%	0.02%
Methylcyclohexane	Naphthene	3	0.20%	0.07%
C7H12O Isomers	Oxygenate	3	0.18%	0.03%
2-Hexanol	Oxygenate	3	0.17%	0.03%
Cyclopentanone	Oxygenate	3	0.16%	0.01%
Dodecane	n-Paraffin	3	0.15%	0.00%
C12 Naphthenics	Naphthene	3	0.15%	0.02%
1-Undecene	Olefin	3	0.15%	0.00%
C6H12O	Oxygenate	2	0.14%	0.01%
Cyclopentanol. 2-Methyl-.Trans-	Oxygenate	1	0.14%	0.00%
C10 Naphthenoaromatics	Naphthenoaromatic	3	0.14%	0.01%
C11 Naphthenoaromatics	Naphthenoaromatic	3	0.14%	0.02%
C10H12 Isomers	Naphthenoaromatic	3	0.13%	0.01%
C8H14O	Oxygenate	3	0.12%	0.10%
C6 Benzene	Monoaromatic	3	0.11%	0.01%
C6H10O Isomers	Oxygenate	3	0.11%	0.02%
C14 Isoparaffins	Iso-paraffin	3	0.10%	0.00%
n-C6 Cyclohexane	Naphthene	3	0.10%	0.01%
1-Dodecene	Olefin	3	0.10%	0.01%
Indane	Naphthenoaromatic	3	0.09%	0.00%
Acetophenone	Oxygenate	3	0.09%	0.02%
Thiophene	Sulfur	1	0.08%	0.00%
1-Hexanol	Oxygenate	1	0.08%	0.00%
1-Propanol	Oxygenate	2	0.08%	0.02%
Tridecane	n-Paraffin	3	0.07%	0.00%
C13 Naphthenics	Naphthene	3	0.07%	0.02%
C6H10O2 Isomers	Oxygenate	3	0.07%	0.01%
C12 Naphthenoaromatics	Naphthenoaromatic	3	0.07%	0.02%
C15H18 Isomers	Naphthenoaromatic	3	0.06%	0.01%
Pentane	n-Paraffin	2	0.06%	0.02%
Methylphenol	Oxygenate	3	0.06%	0.00%
C15 Isoparaffins	Iso-paraffin	3	0.06%	0.00%
C7 Benzene	Monoaromatic	3	0.05%	0.02%
2-Butanone	Oxygenate	2	0.05%	0.01%
1-Tridecene	Olefin	3	0.05%	0.01%
Tetradecane	n-Paraffin	3	0.05%	0.00%
1-Tetradecene	Olefin	3	0.04%	0.00%
Methylaniline	Nitrogen	2	0.04%	0.00%
C6H14O2	Oxygenate	1	0.04%	0.00%
C2 Phenol	Oxygenate	3	0.04%	0.01%
C18 Isoparaffins	Iso-Paraffin	3	0.04%	0.01%
C17H22 Isomers	Naphthenoaromatic	3	0.04%	0.01%
6-Tridecene	Olefin	3	0.04%	0.00%
C18 Olefins	Olefin	3	0.03%	0.00%
Cycloheptanol	Oxygenate	3	0.03%	0.00%
C8H11N Isomers	Nitrogen	3	0.03%	0.02%
C7H10O Isomers	Oxygenate	2	0.03%	0.01%
C8H10O Isomers	Oxygenate	3	0.03%	0.01%
2-Methylpyridine	Nitrogen	3	0.03%	0.02%
Pentadecane	n-Paraffin	3	0.03%	0.00%
C7H16O Isomers	Oxygenate	3	0.03%	0.01%
Indene	Naphthenoaromatic	3	0.02%	0.00%
2-Heptanone	Oxygenate	1	0.02%	0.00%
Hexadecane	n-Paraffin	3	0.02%	0.00%
C14H16 Isomers	Naphthenoaromatic	3	0.02%	0.00%

Table 48: Composition of the light fraction from ASR analyzed by GC × GC: 2/3

Molecule	HCgroup	Number id.	Mean molar x	Std. Dev.
Anisole	Oxygenate	3	0.02%	0.01%
C16 Isoparaffins	Iso-paraffin	3	0.02%	0.00%
C17 Isoparaffins	Iso-paraffin	3	0.02%	0.00%
Aminotoluene	Nitrogen	2	0.02%	0.00%
C14 Naphthenics	Naphthenes	3	0.02%	0.01%
Naphthalene	Diaromatic	3	0.02%	0.01%
n-C7 Cyclohexane	Naphthene	3	0.02%	0.01%
C5H7N Isomers	Nitrogen	3	0.01%	0.01%
N-C8 Cyclohexane	Naphthene	3	0.01%	0.01%
P-Cresol	Oxygenate	2	0.01%	0.00%
C15 Naphthenics	Naphthene	3	0.01%	0.01%
2-Methylbenzofuran	Oxygenate	3	0.01%	0.00%
Heptadecane	n-Paraffin	3	0.01%	0.00%
Benzofuran	Oxygenate	3	0.01%	0.00%
Octadecane	n-Paraffin	3	0.01%	0.00%
4-Ethylphenol	Oxygenate	1	0.01%	0.00%
Xylene (M.P)	Monoaromatic	1	0.01%	0.00%
C19 Isoparaffins	Iso-paraffin	3	0.01%	0.00%
C15 Diaromatics	Diaromatic	3	0.01%	0.00%
C8H12O Isomers	Oxygenate	2	0.01%	0.00%
1-Pentadecene	Olefin	3	0.01%	0.00%
1-Butene. 1-(Methylthio)-	Sulfur	1	0.01%	0.00%
1-Methylnaphthalene	Diaromatic	3	0.01%	0.00%
C18H24 Isomers	Naphthenoaromatic	3	0.00%	0.00%
1-Cyclopentylethanone	Oxygenate	1	0.00%	0.00%
2-Methylnaphthalene	Diaromatic	2	0.00%	0.00%
Icosane	n-Paraffin	3	0.00%	0.00%
1.7-Dimethylnaphthalene	Diaromatic	2	0.00%	0.00%
C9H12O	Oxygenate	3	0.00%	0.00%
Nonadecane	n-Paraffin	3	0.00%	0.00%
C8H9N	Nitrogen	2	0.00%	0.00%
n-C9 Cyclohexane	Naphthene	3	0.00%	0.00%
7-Hexadecene	Olefin	3	0.00%	0.00%
Docosane	n-Paraffin	3	0.00%	0.00%
1-Heptadecene	Olefin	2	0.00%	0.00%
Heneicosane	n-Paraffin	3	0.00%	0.00%
C20 Isoparaffins	Iso-paraffin	3	0.00%	0.00%
C21 Isoparaffins	Iso-paraffin	1	0.00%	0.00%
C22 Isoparaffins	Iso-paraffin	1	0.00%	0.00%
Tricosane	n-Paraffin	1	0.00%	0.00%

Table 49: Composition of the light fraction from ASR analyzed by GC × GC: 3/3

APPENDIX B: NASA COEFFICIENTS

B

Minimal	Mean	Maximal
1.73049265E-01	-9.64285714E-01	2.56862231E-02
7.00388259E-02	8.05804473E-02	7.64351084E-02
-1.14354978E-05	-2.57575758E-05	-3.59795595E-06
-2.51166128E-08	-1.31313131E-08	-4.00610447E-08
1.20279233E-11	7.57575758E-12	1.81294218E-11

Table 50: NASA coefficients of the light fraction from automotive shredder residues (ASR)

APPENDIX C: RESEARCH AND MOTOR OCTANE NUMBERS

Molecule	HC class	Boiling T.(°C)	RON	MON	RON ref.	MON ref.
2,2-Dimethylbutane(D)	Saturate	49.73	91.8	93.4	[26]	[26]
2,3-Dimethylbutane	Saturate	57.98	103.51	94.3	[26]	[26]
2,2-Dimethylpentane	Saturate	79.19	92.8	95.6	[26]	[26]
2,3-Dimethylpentane	Saturate	89.781	91.1	88.5	[26]	[26]
2,4-Dimethylpentane	Saturate	80.494	83.1	83.8	[26]	[26]
3,3-Dimethylpentane	Saturate	86.06	80.8	86.6	[26]	[26]
2,2-Dimethylhexane	Saturate	106.84	72.5	77.4	[26]	[26]
2,3-Dimethylhexane	Saturate	115.61	71.3	78.9	[26]	[26]
2,4-Dimethylhexane	Saturate	109.43	65.2	69.9	[26]	[26]
2,5-Dimethylhexane	Saturate	111.97	55.2	55.7	[26]	[26]
3,3-Dimethylhexane	Saturate	117.73	75.5	83.4	[26]	[26]
3,4-Dimethylhexane	Saturate	115.65	76.3	81.7	[26]	[26]
2,2-Dimethylheptane	Saturate	124.09	50.3	60.5	[26]	[26]
2-Methylbutane	Saturate	27.84	92.3	90.3	[26]	[26]
2-Methylpentane	Saturate	60.26	73.4	73.5	[26]	[26]
3-Methylpentane	Saturate	63.27	74.5	74.3	[26]	[26]
2-Methylhexane	Saturate	90.049	42.4	46.4	[26]	[26]
3-Methylhexane	Saturate	91.85	52	55.8	[26]	[26]
2-Methylheptane	Saturate	117.65	21.7	23.8	[26]	[26]
3-Methylheptane	Saturate	118.93	26.8	35	[26]	[26]
4-Methylheptane	Saturate	117.71	26.7	39	[26]	[26]
n-Butane	Saturate	-0.5	94	89.1	[26]	[26]
n-Pentane	Saturate	36.07	61.8	61.9	[26]	[26]
n-Hexane	Saturate	68.73	24.8	26	[26]	[26]
n-Heptane	Saturate	98.43	0	0	[26]	[26]
2,2,3-Trimethylbutane	Saturate	80.88	112.11	101.32	[26]	[26]
2,2,3-Trimethylpentane	Saturate	99.238	109.61	99.9	[26]	[26]
2,2,4-Trimethylpentane	Saturate	114.77	100	100	[26]	[26]
2,3,3-Trimethylpentane	Saturate	113.47	106.04	99.4	[26]	[26]
2,3,4-Trimethylpentane	Saturate	150.82	102.48	95.9	[26]	[26]
3,3,5-Trimethylheptane	Saturate	160.31	86.4	88.7	[26]	[26]
n-Propylcyclopentane	Saturate	130.96	31.2	28.1	[26]	[26]
n-Butylcyclopentane	Saturate	156.6	-3	-2	[26]	[26]
Methylcyclopentane	Saturate	71.81	91.3	80	[26]	[26]
Ethylcyclopentane	Saturate	103.47	67.2	61.2	[26]	[26]
Methylcyclohexane	Saturate	100.934	74.8	71.1	[26]	[26]
Ethylcyclohexane	Saturate	131.795	45.6	40.8	[26]	[26]
n-Propylcyclohexane	Saturate	156.747	17.8	14	[26]	[26]
Cyclopentane	Saturate	49.25	101.32	85	[26]	[26]
Cycloheptane	Saturate	118.79	38.9	40.8	[26]	[26]
Cyclohexane	Saturate	80.72	83	77.2	[26]	[26]
Ethylcycloheptane	Saturate	164.236	28	30	[26]	[26]
1-Methyl-3-ethylcyclopentane	Saturate	121.177	57.6	59.8	[26]	[26]
iso-Butylcyclopentane	Saturate	148.101	33.4	28.2	[26]	[26]
Isopropylcyclopropane	Saturate	58.314	100.28	88.1	[26]	[26]
Vinylcyclopentane	Saturate	99.198	69.3	54.3	[26]	[26]
Allylcyclopentane	Saturate	126.334	52.1	45.6	[26]	[26]
Isopropenylcyclopropane	Saturate	70.345	94.4	74.9	[26]	[26]
1,3-Dimethylcyclopentane(cis)	Saturate	90.77	79.2	73.1	[26]	[26]
1,3-Dimethylcyclopentane(trans)	Saturate	91.73	80.6	72.6	[26]	[26]
Vinylcyclohexane	Saturate	127	64.3	53.4	[26]	[26]
1,3-Dimethylcyclohexane(cis)	Saturate	120.09	71.7	71	[26]	[26]
1,3-Dimethylcyclohexane(trans)	Saturate	124.46	66.9	64.2	[26]	[26]

Table 51: Boiling points, research octane number (RON) and motor octane number (MON). The boiling points were obtained with Aspen Plus®. 1/4

Molecule	HC class	Boiling T.(°C)	RON	MON	RON ref.	MON ref.
1,4-Dimethylcyclohexane(cis)	Saturate	124.322	67.2	68.2	[26]	[26]
1,4-Dimethylcyclohexane(trans)	Saturate	119.36	68.3	62.2	[26]	[26]
iso-Butylcyclohexane	Saturate	171.3	33.7	28.9	[26]	[26]
1-Methyl-2-n-propylcyclohexane(cis)	Saturate	175.233	30.4	38.8	[26]	[26]
1-Methyl-2-n-propylcyclohexane(trans)	Saturate	175.233	29.4	39.2	[26]	[26]
1,1-Dimethylcyclopentane	Saturate	87.85	92.3	89.3	[26]	[26]
1,1,2,4-Tetramethylcyclopentane	Saturate	128.184	96.2	88	[26]	[26]
1,1,2-Trimethylcyclohexane	Saturate	145.593	95.7	87.7	[26]	[26]
Hydrindan(cis)	Saturate	167.851	70	64.1	[26]	[26]
Pinane	Saturate	167.291	77.7	65.9	[26]	[26]
1-Methyl-4-isopropylcyclohexane(cis)	Saturate	171.514	63.4	62.9	[26]	[26]
1-Methyl-4-isopropylcyclohexane(cis-trans)	Saturate	175.693	62.3	60.5	[26]	[26]
Ethylidenecyclopentane	Saturate	111.874	82.4	66.6	[26]	[26]
Dicyclopropylmethane	Saturate	102.631	95.1	72.1	[26]	[26]
iso-Propylcyclopentane	Saturate	126.43	81.1	76.2	[26]	[26]
Cyclo-octane	Saturate	151.14	69.9	57.8	[26]	[26]
1,3,5-Trimethylcyclohexane(cis)	Saturate	138.734	59.1	56.4	[26]	[26]
1,3,5-Trimethyicyclohexane(trans)	Saturate	140.55	68.5	70.1	[26]	[26]
Ethylidenecyclohexane	Saturate	136.944	83	70.6	[26]	[26]
iso-Propylcyclohexane	Saturate	154.76	62.8	61.1	[26]	[26]
1-Methyl-1-ethylcyclohexane	Saturate	151.907	68.7	76.7	[26]	[26]
Hydrindan(trans)	Saturate	161.076	58.5	48.8	[26]	[26]
sec-Butylcyclohexane	Saturate	179.34	51	55.2	[26]	[26]
1,1,3-Trimethylcyclopentane	Saturate	104.89	87.7	83.5	[26]	[26]
1,2,4-Trimethylcyclopentane(cis,cis,trans)	Saturate	116.73	89.2	79.5	[26]	[26]
1,1-Dimethylcyclohexane	Saturate	119.55	87.3	85.9	[26]	[26]
1,2-Dimethylcyclohexane(cis)	Saturate	129.79	80.9	78.6	[26]	[26]
1,2-Dimethylcyclohexane(trans)	Saturate	123.43	80.9	78.7	[26]	[26]
1,1,3-Trimethylcyclohexane	Saturate	136.63	81.3	82.6	[26]	[26]
1,2,3-Trimethylcyclohexane(cis,trans,cis)	Saturate	143.332	83.4	81	[26]	[26]
1,2,4-Trimethylcyclohexane(cis,trans,trans)	Saturate	143.515	73	74.6	[26]	[26]
1,1,2-Trimethylcyclopropane	Saturate	52.713	110.95	87.8	[26]	[26]
1,1,2,2-Tetramethylcyclopropane	Saturate	75.829	105.27	90.1	[26]	[26]
3-Heptene(cis)	Olefin	95.75	90.2		[26]	
3-Heptene(trans)	Olefin	95.67	89.8	79.3	[26]	[26]
3-Octene(trans)	Olefin	123.3	72.5	68.1	[26]	[26]
4-Octene(trans)	Olefin	122.26	73.3	74.3	[26]	[26]
3-Hexene(trans)	Olefin	67.09	94	80.1	[26]	[26]
1-Pentene	Olefin	30.07	90.9	77.1	[26]	[26]
1-Hexene	Olefin	63.48	76.4	63.4	[26]	[26]
1-Heptene	Olefin	93.64	54.5	50.7	[26]	[26]
1-Octene	Olefin	121.26	28.7	34.7	[26]	[26]
2-Hexene(trans)	Olefin	67.87	92.7	80.8	[26]	[26]
2-Heptene(trans)	Olefin	97.95	73.4	68.8	[26]	[26]
2-Octene	Olefin	130.592	56.3	56.5	[26]	[26]
2,3-Dimethyl-1-butene	Olefin	55.61	101.32	82.8	[26]	[26]
2,3-Dimethyl-1-pentene	Olefin	84.256	99.3	84.2	[26]	[26]
2,4-Dimethyl-1-pentene	Olefin	81.588	99.2	84.6	[26]	[26]
3,4-Dimethyl-1-pentene	Olefin	80.774	98.9	80.9	[26]	[26]
2,3-Dimethyl-1-hexene	Olefin	110.5	96.3	83.6	[26]	[26]
2,3-Dimethyl-2-butene	Olefin	73.2	97.4	80.5	[26]	[26]
2,3-Dimethyl-2-pentene	Olefin	96.485	97.5	80	[26]	[26]
2,4-Dimethyl-2-pentene	Olefin	83.276	100	86	[26]	[26]
3,4-Dimethyl-2-pentene(cis)	Olefin	89.3	96	82.2	[26]	[26]
2,3-Dimethyl-2-hexene	Olefin	121.831	93.1	79.3	[26]	[26]
2,5-Dimethyl-2-hexene	Olefin	112.847	95.2	82.2	[26]	[26]
3-Methyl-2-ethyl-1-butene	Olefin	86.345	97	82	[26]	[26]
2-Methyl-3-ethyl-1-pentene	Olefin	109.238	99.5	85.3	[26]	[26]
2-Methyl-3-ethyl-2-pentene	Olefin	117.077	95.6	82	[26]	[26]
3,3-Dimethyl-1-butene	Olefin	41.247	111.74	93.3	[26]	[26]
3,3-Dimethyl-1-pentene	Olefin	77.112	103.51	86.1	[26]	[26]
4,4-Dimethyl-1-pentene	Olefin	72.495	104.43	85.4	[26]	[26]
4,4-Dimethyl-2-pentene(cis)	Olefin	80.409	105.27	90.2	[26]	[26]
4,4-Dimethyl-2-pentene(trans)	Olefin	76.718	105.27	90.9	[26]	[26]
2,2-Dimethyl-3-hexene(cis)	Olefin	105.421	106.75	88	[26]	[26]
2,2-Dimethyl-3-hexene(trans)	Olefin	100.875	105.27	89	[26]	[26]
2,5-Dimethyl-3-hexene(cis)	Olefin	100.686	103.51	87.5	[26]	[26]
2,5-Dimethyl-3-hexene(trans)	Olefin	102.052	99.8	83.3	[26]	[26]

Table 52: Boiling points, RON and MON. The boiling points were obtained with Aspen Plus®. 2/4

Molecule	HC class	Boiling T.(°C)	RON	MON	RON ref.	MON ref.
5-Methyl-1-hexene	Olefin	85.31	75.5	64	[26]	[26]
2-Methyl-1-heptene	Olefin	119.22	70.2	66.3	[26]	[26]
6-Methyl-1-heptene	Olefin	113.2	63.6	62.6	[26]	[26]
6-Methyl-2-heptene	Olefin	113.228	71.3	65.5	[26]	[26]
3-Methyl-1-pentene	Olefin	54.18	96	81.2	[26]	[26]
4-Methyl-1-pentene	Olefin	53.86	95.7	80.9	[26]	[26]
3-Methyl-1-hexene	Olefin	83.9	82.8	71.5	[26]	[26]
4-Methyl-1-hexene	Olefin	86.73	86.4	74	[26]	[26]
2-Ethyl-1-butene	Olefin	64.67	98.3	79.4	[26]	[26]
3-Ethyl-1-pentene	Olefin	84.11	95.6	81.6	[26]	[26]
3-Ethyl-2-pentene	Olefin	95.851	93.7	80.6	[26]	[26]
5-Methyl-2-hexene(trans)	Olefin	87.381	94.3	81.2	[26]	[26]
2-Methyl-1-butene	Olefin	31.155	102.48	81.9	[26]	[26]
2-Methyl-2-butene	Olefin	38.555	97.3	84.7	[26]	[26]
2-Methyl-1-pentene	Olefin	62.1	94.2	81.5	[26]	[26]
2-Methyl-2-pentene	Olefin	67.3	97.8	83	[26]	[26]
3-Methyl-2-pentene(trans)	Olefin	70.438	97.2	81	[26]	[26]
4-Methyl-2-pentene(cis)	Olefin	56.38	99.7	84.5	[26]	[26]
4-Methyl-2-pentene(trans)	Olefin	58.6	98	82.6	[26]	[26]
2-Methyl-1-hexene	Olefin	91.84	90.7	78.8	[26]	[26]
2-Methyl-2-hexene	Olefin	94.777	92.8	78.9	[26]	[26]
3-Methyl-2-hexene(cis)	Olefin	97.247	92.2	79.9	[26]	[26]
3-Methyl-2-hexene(trans)	Olefin	94.475	91.4	79.4	[26]	[26]
4-Methyl-2-hexene(cis)	Olefin	85.952	98.6		[26]	
4-Methyl-2-hexene(trans)	Olefin	87.598	96.8	83	[26]	[26]
2-Methyl-3-hexene(trans)	Olefin	85.867	97.9	82	[26]	[26]
3-Methyl-3-hexene(cis)	Olefin	95.383	96		[26]	
3-Methyl-3-hexene(trans)	Olefin	93.521	96.4	81.4	[26]	[26]
2-Methyl-2-heptene	Olefin	122.337	83.6	71	[26]	[26]
2-Methyl-3-heptene(trans)	Olefin	113.956	94.4	80.4	[26]	[26]
6-Methyl-3-heptene(trans)	Olefin	113.724	93.4	82	[26]	[26]
2,3,3-Trimethyl-1-butene	Olefin	77.891	105.27	90.5	[26]	[26]
Diisobutylene(J)	Olefin	101.44	105.27	88.6	[26]	[26]
2,3,3-Trimethyl-1-pentene	Olefin	108.212	106.04	85.7	[26]	[26]
2,4,4-Trimethyl-1-pentene	Olefin	101.44	106.04	86.5	[26]	[26]
2,3,4-Trimethyl-2-pentene	Olefin	115.925	96.6	80.9	[26]	[26]
2,4,4-Trimethyl-2-pentene	Olefin	104.91	103.51	86.2	[26]	[26]
3,4,4-Trimethyl-2-pentene	Olefin	111.809	102.48	85.8	[26]	[26]
n-Butylbenzene	Aromatic	183.305	104.43	95.3	[26]	[26]
1,3-Dimethylbenzene	Aromatic	139.12	117.51	115.05	[26]	[26]
1,4-Dimethylbenzene	Aromatic	138.36	116.38	109.61	[26]	[26]
sec-Butylbenzene	Aromatic	173.33	106.75	95.7	[26]	[26]
Indan	Aromatic	177.97	103.51	89.8	[26]	[26]
1-Methyl-2-n-propylbenzene	Aromatic	184.8	103.51	92.2	[26]	[26]
1-Methyl-2-isopropylbenzene	Aromatic	178.18	106.04	96	[26]	[26]
Propenylbenzene(cis)	Aromatic	178.88	104.43	91.7	[26]	[26]
Propenylbenzene(trans)	Aromatic	178.26	104.43	92.1	[26]	[26]
n-Propylbenzene	Aromatic	159.241	110.95	98.7	[26]	[26]
iso-Propylbenzene	Aromatic	152.41	113.11	99.3	[26]	[26]
iso-Butylbenzene	Aromatic	172.79	111.36	98	[26]	[26]
Toluene	Aromatic	110.63	120.10	103.51	[26]	[26]
1-Phenylpentane	Aromatic	205.46	89.2	81.7	[26]	[26]
Ethylbenzene	Aromatic	136.2	107.40	97.9	[26]	[26]
1-Methyl-2-allylbenzene	Aromatic	186.52	98.6	86	[26]	[26]
1-Methyl-2-ethylbenzene	Aromatic	165.18	102.48	92.1	[26]	[26]
Allylbenzene	Aromatic	157.601	102.48	90.9	[26]	[26]
1,2,4-Trimethylbenzene	Aromatic	169.38	110.53	108.01	[26]	[26]
2-Phenylpropene	Aromatic	165.5	113.11	101.32	[26]	[26]
1,2,3-Trimethylbenzene	Aromatic	176.12	105.27	100.81	[26]	[26]

Table 53: Boiling points, RON and MON. The boiling points were obtained with Aspen Plus®. 3/4

Molecule	HC class	Boiling T.(°C)	RON	MON	RON ref.	MON ref.
2-Phenylpentane	Aromatic	191.943	103.51	92.1	[26]	[26]
tert-Amylbenzene	Aromatic	190.553	108.01	96.8	[26]	[26]
1-Methyl-3-ethylbenzene	Aromatic	161.33	112.10	100	[26]	[26]
1,4-Diethylbenzene	Aromatic	183.787	106.04	96.4	[26]	[26]
1,2-Dimethyl-3-ethylbenzene	Aromatic	193.96	104.43	91.9	[26]	[26]
1,3-Dimethyl-4-ethylbenzene	Aromatic	188.44	106.04	95.9	[26]	[26]
1,3-Dimethyl-5-ethylbenzene	Aromatic	183.78	114.80	102.48	[26]	[26]
1,4-Dimethyl-2-ethylbenzene	Aromatic	186.83	106.04	96	[26]	[26]
1-Methyl-3-n-propylbenzene	Aromatic	181.8	112.10	100.55	[26]	[26]
1-Methyl-4-isopropylbenzene	Aromatic	177.13	110.53	97.7	[26]	[26]
1,2,3,4-Tetramethylbenzene	Aromatic	205.04	105.27	100.28	[26]	[26]
1-Phenyl-2-methylpropene	Aromatic	186.904	105.27	91.7	[26]	[26]
Indene	Aromatic	182.62	113.72	106.75	[26]	[26]
1,2,3,4-Tetrahydronaphthalene	Aromatic	207.62	96.4	81.9	[26]	[26]
Cyclopentanone	Oxygenate	130.65	101.32	89.4	[26]	[26]
Cyclohexanone	Oxygenate	153.43	101.32	87.7	[26]	[26]
Methyltert-butylether	Oxygenate	55.05	118.33	101.32	[26]	[26]
Di-iso-propylether	Oxygenate	68.3	102.48	98.9	[26]	[26]
Furan	Oxygenate	31.35	108.582	91.6	[26]	[26]
2-Methylfuran	Oxygenate	64.072	102.48	86.1	[26]	[26]
2,5-Dimethylfuran	Oxygenate	93.618	101.32	88.1	[26]	[26]
Tetrahydrofuran	Oxygenate	65.97	72.9	64.8	[26]	[26]
2-Methyltetrahydrofuran	Oxygenate	79.79	86	73	[26]	[26]
2,5-Dimethyltetrahydrofuran(cis,trans)	Oxygenate	91	92.2	80.2	[26]	[26]
Tetrahydropyran	Oxygenate	88	52.2	35.4	[26]	[26]
Dihydropyran	Oxygenate	85.542	66.5	48.7	[26]	[26]
Ethanol	Oxygenate	78.29	109	90.7	[27]	[27]
n-Propanol	Oxygenate	97.2	104	89	[27]	[27]
n-Butanol	Oxygenate	118.75	98	85	[27]	[27]
n-Pentanol	Oxygenate	137.75	82	76	[29]	[29]
n-Hexanol	Oxygenate	156.75	69.3	64	[29]	[29]
2-Propanol	Oxygenate	82.15	106	99	[27]	[27]
2-Butanol	Oxygenate	99.75	105	93	[27]	[27]
iso-Butanol	Oxygenate	107.66	105	90	[27]	[27]
Pentan-3-one	Oxygenate	101.99	106.8	95.4	[28]	This study
Hexan-3-one	Oxygenate	123.5	101.9	88.5	[28]	[28]
Heptan-3-one	Oxygenate	147.4		88.5		This study
ETBE	Oxygenate	72.8	119	103	[200]	[8]

Table 54: Boiling points, RON and MON. The boiling points were obtained with Aspen Plus®. 4/4

APPENDIX D: TRAINING AND TESTING DATA

D

ID	RON	MON	MeABP(°C)	S	O	A	Ox	Oxygenated molecule
BOB1-2P1	87.5	81	82.52371029	69.9618	7.752	19.1862	3.1	2-propanol
BOB1-2P3	91.4	82.6	79.35169557	63.897	7.08	17.523	11.5	2-propanol
BOB1-1P1	88	81.1	82.57210849	70.034	7.76	19.206	3	1-propanol
BOB1-1P3	91.2	82.1	79.50679638	64.1858	7.112	17.6022	11.1	1-propanol
BOB1-1B1	87	80.8	84.66949948	69.5286	7.704	19.0674	3.7	1-butanol
BOB1-1B3	88.2	81	86.17636867	61.8754	6.856	16.9686	14.3	1-butanol
BOB1-2B1	87.6	81.1	83.76156035	69.6008	7.712	19.0872	3.6	2-butanol
BOB1-2B3	90.9	82.8	82.02932996	62.0198	6.872	17.0082	14.1	2-butanol
BOB1-2M1P1	87.6	81.3	83.4485665	69.3842	7.688	19.0278	3.9	2-methyl-1-propanol
BOB1-2M1P3	90.3	82.6	84.00493223	61.2256	6.784	16.7904	15.2	2-methyl-1-propanol
BOB2-2P1	86.7	81.1	99.49391112	73.8378	4.4574	18.6048	3.1	2-propanol
BOB2-2P3	90.4	83	93.95110815	67.2084	4.0572	16.9344	11.8	2-propanol
BOB2-1P1	86.9	81.3	99.59959503	73.9902	4.4666	18.6432	2.9	1-propanol
BOB2-1P3	90.6	82.6	96.29571438	68.1228	4.1124	17.1648	10.6	1-propanol
BOB2-1B1	85.8	81	101.0355228	73.3806	4.4298	18.4896	3.7	1-butanol
BOB2-1B3	87.5	81.4	99.53858092	65.3034	3.9422	16.4544	14.3	1-butanol
BOB2-2B1	86.3	81.2	100.8267416	73.4568	4.4344	18.5088	3.6	2-butanol
BOB2-2B3	89.9	83.4	97.36529554	65.2272	3.9376	16.4352	14.4	2-butanol
BOB2-2M1P1	86.5	81.5	101.4873982	73.2282	4.4206	18.4512	3.9	2-methyl-1-propanol
BOB2-2M1P3	90.4	83.1	96.96570623	64.6176	3.9008	16.2816	15.2	2-methyl-1-propanol
BOB3-2P1	97.3	88	88.06886478	65.6013	2.4225	28.8762	3.1	2-propanol
BOB3-2P3	99.2	88.9	84.68070648	59.8468	2.21	26.3432	11.6	2-propanol
BOB3-1P1	97.7	87.9	88.78790395	65.669	2.425	28.906	3	1-propanol
BOB3-1P3	99.1	88.3	87.0886414	59.4406	2.195	26.1644	12.2	1-propanol
BOB3-1B1	97	87.5	89.48814278	65.1951	2.4075	28.6974	3.7	1-butanol
BOB3-1B3	96.9	86.8	89.68974616	57.8835	2.1375	25.479	14.5	1-butanol
BOB3-2B1	97.1	88	88.59461091	64.9243	2.3975	28.5782	4.1	2-butanol
BOB3-2B3	98.9	88.6	86.36584819	57.9512	2.14	25.5088	14.4	2-butanol
BOB3-2M1P1	97.5	88	91.01955032	65.0597	2.4025	28.6378	3.9	2-methyl-1-propanol
BOB3-2M1P3	99	88.1	88.05255447	57.3419	2.1175	25.2406	15.3	2-methyl-1-propanol

Table 55: Training data used to formulate the Bayesian pseudo-component (PC) method.

ID	RON	MON	MeABP(°C)	S	O	A	Ox	Oxygenated molecule
BOB1-2P2	89.9	82	80.4566993	66.1352	7.328	18.1368	8.4	2-propanol
BOB1-1P2	89.6	81.7	81.42233611	66.5684	7.376	18.2556	7.8	1-propanol
BOB1-1B2	87.6	81	85.31473991	64.3302	7.128	17.6418	10.9	1-butanol
BOB1-2B2	90	82.3	82.43947087	64.4746	7.144	17.6814	10.7	2-butanol
BOB1-2M1P2	89.7	81.2	83.35329153	64.0414	7.096	17.5626	11.3	2-methyl-1-propanol
BOB2-2P2	88.9	82.4	95.527761	69.7992	4.2136	17.5872	8.4	2-propanol
BOB2-1P2	89	82.2	96.91267019	70.1802	4.2366	17.6832	7.9	1-propanol
BOB2-1B2	86.9	81.3	99.46253877	68.0466	4.1078	17.1456	10.7	1-butanol
BOB2-2B2	88.9	82.7	97.97300198	68.199	4.117	17.184	10.5	2-butanol
BOB2-2M1P2	89.4	82.6	99.02434987	67.5894	4.0802	17.0304	11.3	2-methyl-1-propanol
BOB3-2P2	98.6	88.6	85.53033009	62.2163	2.2975	27.3862	8.1	2-propanol
BOB3-1P2	98.5	88.3	87.22820399	61.8101	2.2825	27.2074	8.7	1-propanol
BOB3-1B2	96.9	87	89.65622866	60.4561	2.2325	26.6114	10.7	1-butanol
BOB3-2B2	98.4	88.3	88.04593674	60.1853	2.2225	26.4922	11.1	2-butanol
BOB3-2M1P2	98.5	88.1	88.8164268	59.8468	2.21	26.3432	11.6	2-methyl-1-propanol

Table 56: Testing data for the Bayesian PC method.